VASCULAR TARGETING IN AN ARTERIOVENOUS MALFORMATION ANIMAL MODEL

Dr Andrew John Gauden

MBBS (Hons), B Med Sci (Hons), MA

A thesis submitted in fulfilment of the requirements for the degree of Doctor of Philosophy at the Faculty of Medicine and Health Sciences, Department of Clinical Medicine, Macquarie University

July 2018

This thesis is dedicated to those individuals and their families that have suffered as a result of brain arteriovenous malformations and their consequences.

Table of Contents

Table of Contents 3
Table of Figures 7
Table of Tables 8
Abbreviations 9
Summary 12
Declaration of Originality 13
Publications and Presentations 14
Acknowledgements 17
Overview 20
Chapter 1 Literature Review 23
1.1 Arteriovenous malformations 23
1.1.1 Definition and Overview 23
1.1.2 Epidemiology 27
1.1.3 Presenting Symptoms 28
1.1.4 Incidence of Haemorrhage 29
1.1.5 Haemorrhage risk factors 30
1.1.6 Limitations of Haemorrhage Risk Assessments 31
1.1.7 Morbidity and Mortality 31
1.1.8 Pathogenesis 32
1.1.9 Treatments 35
1.2 Vascular targeting 46
1.2.1 Overview and Historical Context 47
1.2.2 Vascular targeting agents in malignancy 53
1.2.3 Vascular targeting in AVMs 54
1.3 Arteriovenous Malformation Endothelium Structure 55
1.3.1 Light Microscopic Features 55
1.3.2 Ultrastructure 57
1.3.3 Molecular Structure 58
1.4 Changes to Arteriovenous Malformations Post-Radiation 63
1.4.1 Light Microscopy 64
1.4.2 Ultrastructural Changes 66
1.4.3 Molecular changes 68
1.5 Animal Models of AVM Research for testing AVM vascular targeting 73
1.5.1 Surgical AVM Animal Models 73

1.5.2 Transgenic Animal Models 81
1.5.3 Summary 86
Hypothesis and Aims 87
Chapter 2 Methods 88
2.1 Animal Model 88
2.2 Radiosurgery 91
2.3 Angiography 93
2.4 Sacrifice and Perfusion 94
2.5 Haematoxylin and Eosin Stain 95
2.6 Martius Scarlet Blue Stain 95
2.7 Annexin V/Thrombin Conjugate 96
2.7.1 Rationale 96
2.7.2 Conjugate Formation 97
2.7.3 Conjugation Verification 98
2.7.4 Thrombin Activity 102
2.8 Outcomes and Statistical Analysis 102
Chapter 3 Annexin V/Thrombin Conjugate Optimisation 104
3.1 Background 104
3.2 Hypothesis 106
3.3 Aim of this chapter 106
3.4 Methods 107
3.4.1 Methods – Dose Estimation – *In Vitro* Dose Response Study ("Slide Rocking Test") 107
3.4.2 Methods– Rat animal model 109
3.5 Results 113
3.5.1 Results - Dose Estimation – In Vitro Dose Response Study ("Slide Rocking Test"). 113
3.5.2 Results – Rat animal model 118
3.6 Discussion 123
3.6.1 Discussion – Dose Estimation – *In Vitro* Dose Response Study ("Slide Rocking Test") 123
3.6.2 Discussion - Dose Escalation Test 1 – In Vivo Dose Response - AVM Naïve Animals 124
3.6.3 Discussion – Dose Escalation Test 2 – In Vivo Dose Response AVM Animals 126
3.7 Conclusion 128
Chapter 4 Vascular targeting of PS in the AVM animal model 129
4.1 Background 129

4.2 Hypothesis 129
4.3 Aims 129
4.4 Methods 129
4.4.1 Conjugate administration 129
4.5 Results 133
4.5.1 Animal treatment allocations 133
4.5.2 Angiographic Outcomes 133
4.5.3 Flow Measurement 139
4.5.4 Histological outcomes 142
4.6 Discussion 152
4.7 Conclusion 157
Chapter 5 Dose Modification Increases Targeting Selectivity 159
5.1 Background 159
5.2 Hypothesis 159
5.3 Aims 159
5.4 Methods 160
5.4.1 Treatment Groups 160
5.4.2 Conjugate Administration 160
5.4.3 Outcome Measures 161
5.5 Results 161
5.5.1 Overview 161
5.5.2 Angiographic Outcomes 161
5.5.3 Histological outcomes 165
5.6 Discussion 174
5.7 Conclusion 176
Chapter 6 Preliminary validation of novel radiation-induced vascular targets 177
6.1 Background 177
6.2 Aims 179
6.3 Methods 179
6.3.1 Animal Model 179
6.3.2 Cryosectioning and immunostaining 179
6.3.3 Animal Model and GKS for in vivo fluorescent optical imaging 181
6.3.4 Near-infrared (NIR) dye preparation and NIR fluorescence optical *in vivo* imaging 183
6.4 Results 185
6.4.1 Immunolocalisation of PDC-E2 in rat AVM nidus in response to radiation 185

6.4.2 Immunolocalisation of CD166 in rat AVM nidus in response to radiation 187
6.4.3 Results of *in vivo* imaging for PDCE2 189
6.5 Discussion 191
6.6 Conclusion 194
Chapter 7 General Discussions and Future Directions 195
7.1 Overview 195
7.2 PS and Other targets 196
7.3 Conjugate Targeting Agent and Effector 200
7.4 Translation from animal model to the clinic 202
7.5 Conclusion 203
References 204
Appendix 1 – Ethics 229

Table of Figures

Figure 1-1 A diagrammatic representation of an AVM 24
Figure 1-2 Multiplanar MRI demonstrating a high-grade left-sided thalamic AVM.....25
Figure 2-1 Formation of arteriovenous malformation animal performed in a Sprague-Dawley rat 90
Figure 2-2 Radiosurgery administered to the animals using a Leksell Gamma Knife.....92
Figure 2-3 Coumassie gel analysis of annexin V/thrombin conjugate and components.....100
Figure 2-4 Repeat Coumassie gel analysis of annexin V/thrombin conjugate and components.101
Figure 3-1 Graph of time to flow cessation.....115
Figure 3-2 Graph of time to visible clot to flow cessation 116
Figure 3-3 Mean percentage of thrombosed vessels present on nidus tissue of model AVM. ...120
Figure 3-4 MSB stain of left EJV.....121
Figure 3-5 MSB stain of AVM nidus vessel following irradiation and annexin V thrombin conjugate administration.....122
Figure 4-1 Separation of treatment groups. 131
Figure 4-2 Digitally-subtracted-angiogram of a sham-GKS, saline-injected animal.....135
Figure 4-3 Angiogram of a GKS conjugate treated animal.....136
Figure 4-4 Digitally-subtracted-angiogram of a GKS-conjugate treated animal 137
Figure 4-5 Number of animals with occluded angiogram compared to patent vessels.....138
Figure 4-6 Graphs of flow in the left external jugular vein.....140
Figure 4-7 Graphs of flow in the left distal common carotid 141
Figure 4-8 Graph of number of animals with left EJV thrombus vs patent 143
Figure 4-9 H and E stained axial section of a left EJV.....144
Figure 4-10 Graph of number of animals with large nidus vessel intraluminal thrombus.....147
Figure 4-11 H and E stained sections from large nidus vessels 148
Figure 4-12 Graph of number of animals with nidus microvessel intraluminal thrombus.....150
Figure 4-13 H and E stain of microvessels of the AVM nidus of a GKS, thrombin treated animal 151
Figure 5-1 Digitally-subtracted angiogram of GKS with double 1/2-dose conjugate-treated animal 163
Figure 5-2 Numbers of animals with occluded/stenosed vs patent angiogram in 1/2-dose and 2× 1/2 dose conjugate groups. 164
Figure 5-3 Numbers of animal with external jugular vein (EJV) thrombus in 1/2-dose and 2× 1/2-dose conjugate groups. 166
Figure 5-4 H and E stain of left external jugular vein (LEJV). 167
Figure 5-5 Number of animals with large vessel thrombi in 1/2-dose and 2×1/2-dose conjugate groups 169
Figure 5-6 H and E stain of large AVM nidus vessels. 170
Figure 5-7 Number of animals with micro vessel thrombus in 1/2-dose and 2× 1/2-dose conjugate groups.....172
Figure 5-8 H and E stain of nidus microvessels in a GKS 2×1/2-dose conjugate treated animal. 173
Figure 6-1 CT planning images for GKS in AVM naive animals.....182
Figure 6-2 SDS-PAGE gel of PDCE-2 antibody conjugate for use in in vivo imaging 184
Figure 6-3 Immunohistochemical localisation of PDCE2 in the rat AVM 186
Figure 6-4 Immunohistochemical localisation of CD166 in the rat AVM.....188
Figure 6-5 In vivo near-infrared fluorescent optical imaging of PDCE2 expression.....190

Table of Tables

Table 1-1 Potential tumour vessel markers for ligand-directed vascular targeting agents.....50
Table 1-2 Treatment-effective payloads used in vascular targeting.....52
Table 3-1 Time to visible clot and flow cessation in rocking slide test. 114

Abbreviations

ALK1	Activin receptor-like kinase 1
ANPT	Angiopoietin
APA	Ascending pharyngeal artery
ARUBA	Randomized Trial of Unruptured Brain AVMs
AVM	Arteriovenous malformation
AVMs	Arteriovenous malformations
BBB	Blood brain barrier
bFGF	Basic fibroblast growth factor
CA4DP	Combrestatin A4 disodium phosphate
CAMs	Cellular adhesion molecules
CCA	Common carotid artery
CI	Confidence intervals
CNS	Central nervous system
DNA	Deoxyribonucleic acid
DOL	Degree of labelling
ECA	External carotid artery
ECs	Endothelial cells
EJV	External jugular vein
ENG	Endoglin
ERK	Extracellular signal-regulated kinase
GKS	Gamma knife radiosurgery
H and E	Haematoxylin and Eosin
HHT	Hereditary haemorrhagic telangiectasia
ICAM-1	Intercellular adhesion molecule-1
Ig	Immunoglobulin
IL	Interleukin
KI	Karlsson index
KRAS	Kirsten Ras oncogene
LD50	Lethal dose
LINAC	Linear accelerator

MAPK	Mitogen-activated protein kinase
MCA	Middle cerebral artery
MEK	MAPK/ERK kinase
MGP	Matrix Gla protein
MMP9	Matrix metalloprotease 9
MSB	Martius Scarlet Blue
MW	Molecular weight
OPBI	Obliteration prediction index
PCR	Polymerase chain reaction
PDCE2	Pyruvate-dehydrogenase complex E2 subunit
PDCN	Perinidal dilated capillary network
PDGF	Platelet-derived growth factor
PECAM-1	Platelet endothelial cell adhesion molecule-1
PET	Positron emission tomography
PS	Phosphatidylserine
RAS	Ras oncogene
RBGS	Radiosurgery-Based Grading System
RM	Rete mirabile
SD	Standard deviation
SMA	Smooth muscle antigen
SMAα	Smooth muscle actin-alpha
SRS	Stereotactic radiosurgery
SSS	Superior sagittal sinus
STA	Superficial temporal artery
TF	Tissue factor
tTF	Truncated tissue factor
TGFα	Transforming growth factor alpha
TGF-β	Transforming growth factor beta
TM	Thrombomodulin
VCAM-1	Vascular cell adhesion molecule-1
VEGF	Vascular endothelial growth factor
VLA-4	Very late activation antigen-4

vWF	von Willibrand’s factor

Summary

Brain arteriovenous malformations (AVMs) pose a significant lifetime risk of haemorrhagic stroke that preferentially affects children and young adults. Despite the current available treatments of surgical excision, approximately one third of AVMs have no effective treatment. It is therefore important that newer treatment modalities are identified. A treatment that has shown some promise in cancer is vascular targeting. This method may provide an alternative treatment for AVMs without affecting surrounding normal brain vasculature.

Previous work has identified phosphatidylserine (PS) as a potential target that is increased in the endothelium following radiation exposure. It is hypothesised that treatment of AVMs with gamma knife radiosurgery (GKS) and using a vascular targeting agent to deliver a pro-thrombotic compound can cause localised thrombosis and vessel occlusion within AVM vessels.

Using a rat animal model, a novel vascular targeting conjugate was formed from the protein annexin V and thrombin to target PS. On assessment of the conjugate, AVM occlusion occurred in 75% of conjugate-treated animals with similar rates of flow cessation noted in the GKS and non GKS treated groups. These findings were noted both with angiographic occlusion and histological evidence of large and small vessel thrombus formation.

On reducing the dose to half the dose per weight per animal and administering it in a multiple dose treatment regimen a statistically significant proportion of animals had evidence of AVM occlusion in only irradiated animals, suggesting effectiveness of sensitising AVMs with focussed irradiation.

This research has demonstrated a significant association between use of the vascular targeting annexin V/thrombin conjugate and thrombosis of AVM vessels both radiologically and histologically. This technique and the use of radiation sensitisation may demonstrate a potential new treatment for AVMs. This finding is the first of its kind in the treatment of AVMs and with further development may become an alternative treatment modality for previously untreatable lesions.

Declaration of Originality

I acknowledge that the work presented in this thesis is my original research work. I declare that the content of this thesis has not been presented to any other institution for any award. To the best of my knowledge no material from this thesis has been previously published or written by another person, except where due acknowledgements are made.

This work was carried out with ethical approval from the Macquarie University Animal Ethics Committee (protocols 2014/035, 2015/026 and 2017/18).

Dr Andrew John Gauden

July 2018

Publications arising from this thesis

Gauden, AJ, Lee, VS, McRobb, LS, Zhao, Z, Grau, GE, Subramanian, S, Moutrie V, Stoodley MA. "Vascular targeting of phosphatidylserine causing occlusion in an arteriovenous malformation animal model" (In preparation)

Subramanian, S, Ugoya, SO, Zhao, Z, McRobb, LS, Grau, GE, Combes, V, Inglis, DW, Gauden AJ, Lee, VS, Moutrie, V, Santos, ED, Stoodley MA. "Stable thrombus formation on irradiated microvascular endothelial cells under pulsatile flow: pre-testing an annexin V-thrombin conjugate for treatment of brain arteriovenous malformations" (Thrombosis Research 167 (2018) 104-112)

McRobb, LS, McKay, MJ, Gauden, AJ, Lee, VS, Subramanian, S, Thomas, SG, Wiedmann, M, Moutrie, V, Grace, M, Zhao, Z, Molloy, MP, Stoodley MA. "Radiation-stimulated markers on the endothelial surface provide potential vascular targets in brain arteriovenous malformations" (Submitted: Radiation Research 6/7/2018)

Conference Presentations and Posters

"Dose modification of annexin V/thrombin conjugate is effective in causing selective occlusion of gamma knife radiosurgery sensitised arteriovenous malformations" Neurosurgical Society of Australasia Annual Scientific Meeting 2018, Gold Coast, Australia – Oral Presentation

"Vascular targeting of phosphatidylserine causing thrombotic occlusion in an arteriovenous malformation animal model" Gauden A.J., Subramanian, S., Moutrie, V., Zhao, Z., McRobb, L., Stoodley, M.A., Australia and New Zealand Association of Neurologists Annual Scientific Meeting, June 2018 – Poster Presentation

"Vascular targeting causing thrombosis in an arteriovenous malformation animal model" American Association of Neurological Surgeons Annual Scientific Meeting, Cerebrovascular Scientific Section Meeting, New Orleans, LA, USA April/May 2018 – Oral Presentation

"Ligand vascular targeting of phosphatidylserine translocation causing thrombosis in an arteriovenous malformation animal model" Encourage Seminar for Early Career Researchers, Macquarie University, Sydney Australia October 2017 – Oral Presentation

"Ligand vascular targeting of phosphatidylserine translocation in an arteriovenous malformation animal model" Gauden A.J., Subramanian, S., Moutrie, V., Zhao, Z., McRobb, L., Stoodley, M.A., Australasian Vascular Biology Society Annual Scientific Meeting, Sunshine Coast, Queensland, Sept 2017 – Poster Presentation

"Vascular targeting causing thrombosis in an arteriovenous malformation rat model" Neurosurgical Society of Australasia Annual Scientific Meeting 2017, Adelaide, South Australia, Australia August 2017 – Oral Presentation

"Radiation sensitisation with vascular targeting in an arteriovenous malformation animal model" Innovations in Radiation Applications 2017, University of Wollongong, Wollongong, New South Wales, Australia April 2017 – Oral Presentation

Awards

Finalist 2018 Peter Leech Memorial Prize for Neurosurgical Society of Australasia (Final pending)

Winner of Cerebrovascular Section- Best Basic Scientific Paper – American Association of Neurological Surgeons and Congress of Neurological Surgeons 2018, New Orleans, LA, USA

Finalist 2017 Peter Leech Memorial Prize for Neurosurgical Society of Australasia

Scholarships for Research

2015-2017 Avant Doctor in Training – Full-time Research Scholarship

2015-2018 National Health and Medical Research Council Research Scholarship for Clinician

Acknowledgements

My PhD has been an amazing enriching experience allowing me to further develop my interest in basic science research in neurosurgery. This experience has also enhanced my clinical training in neurosurgery and has confirmed my plan to embark upon a mixed academic and clinical career in the future. None of this body of work would have been possible without the contribution of several people.

I would like to acknowledge the financial support during my candidature from the Avant Doctor in Training Scholarship and the National Health and Medical Research Council Clinical research scholarship. Without the funds from these bodies none of this research would be possible.

I would first like to thank my supervisor and friend Professor Marcus Stoodley. Without Marcus' initial research in arteriovenous malformation vascular targeting of which this project is based upon none of these results would be possible. Marcus has been involved in all aspects of this research, in the generation of the research concepts as well as the direction of the experiments and the writing of this thesis. Marcus Stoodley has also provided many of the original images used in this research and these have been duly acknowledged.

I also thank Marcus for fostering my interest in research and giving me the opportunity to complete this PhD. This break in my clinical training has deepened my understanding of medical research techniques and of clinical neurosurgery. I hope to continue this work in collaboration with Professor Stoodley and his team in the future.

None of this work would have been possible without the patience and hard work of my co-supervisor Dr Lucinda McRobb. Lucinda was always available for advice and allowing me to discuss ideas and clarify issues concerning this research. Her kindness and patience were particularly important when I began this research and eased my transition from clinician to researcher.

I would also like to thank Professor Michael Morgan, my other co-supervisor. His extensive clinical work in arteriovenous malformations provide much of the background clinical context for this research. His work and achievements in vascular neurosurgery and that of other vascular neurosurgeons in helping individuals suffering from these conditions provided me with the desire to research in this area and hopefully to work as a vascular neurosurgeon in the future.

I also acknowledge Ms Vivienne Lee with thanks for her vital work in the surgical procedures and assistance with the animal work and for advice with much of the laboratory procedures. Her patience in dealing with a 'clinician researcher' with minimal laboratory experience is to be commended.

I would also like to acknowledge the work by Vaughan Moutrie and the services of Genesis Cancer Care at the Macquarie University Hospital in assisting with the imaging, planning and delivery of the Gamma Knife Radiosurgery to animals. His patience and availability on many evenings over the two years allowed us to complete this research.

I thank the rest of the Macquarie University Arteriovenous Malformation Research Group Sinduja Subramanian and Dr Zhenjun Zhao as well as the remaining members of the Neurosurgery research group. The opportunity to regularly present my research to experienced individuals allowed me to develop this project and address many of my methodological questions.

My parents, Stan and Eve have provided support for all my academic work from my undergraduate medical degree through to this PhD journey. I thank them for their patience, encouragement and support. Without them and my sisters Ruth and Katarina I would never have achieved the success I have with medical training, neurosurgical clinical training and my foundations in clinical research. I could not imagine embarking on this undertaking without their support.

Finally, I would like to thank my fiancée Christine Burdick. Her patience and love over the long hours of laboratory work and thesis writing provided me with the pillar of support to complete this PhD. Our relationship has stood firm amongst the stress that came with this undertaking. Christine has been involved in every step of this research and in the conception of this thesis and I am grateful for the sacrifices that she has made to enable me to have this opportunity. I look forward to our new lives together as a married couple.

Although many individuals have contributed to the research at concept level as well as its execution, the work enclosed is mine as is the responsibility for any errors or omissions.

Overview

Brain arteriovenous malformations (AVMs) pose a significant lifetime risk of haemorrhagic stroke that preferentially affects children and young adults. Despite the current available treatments of surgical excision, endovascular embolization and radiosurgery, approximately one third of AVMs are deep and large and have no effective treatment available or are treatable with an unacceptable degree of risk. It is therefore important that newer treatment modalities are identified.

A treatment that has shown some promise in cancer is vascular targeting. This method consists of the identification of differentiating molecular targets that are expressed on the surface of the endothelium and targeting these with a protein or antibody to deliver a treatment-effective payload. This method would provide an alternative method to treat an AVM without affecting surrounding normal brain vasculature.

The challenge in developing such a treatment is identifying a target that is only present in pathological AVM vessels. To date there is no marker that differentiates AVM endothelial cells from normal systemic endothelium. It is hypothesised that by causing endothelial damage with radiosurgery that molecular changes can be induced on the surface of the endothelium. Previous work has identified phosphatidylserine (PS) as one of these markers externalised on the plasma membrane of the endothelium in AVMs that have undergone treatment with focused irradiation and has suggested this as a potential target. It is hypothesised that treatment of AVMs with gamma knife radiosurgery (GKS) and using a vascular targeting agent to deliver a pro-thrombotic compound we can cause localised thrombosis and vessel occlusion within AVM vessels.

In order to study AVM treatments, it is necessary to use an *in vivo* model that is both financially affordable and analogous to human brain AVMs anatomically, haemodynamically, histologically and ultrastucturally. Historically, many AVM models have been proposed ranging from small

and large surgical animal models and transgenic mouse models, each with its own limitations. One model that has been used in AVM vascular targeting research is formed by performing an end-to-side anastomosis of the external jugular vein (EJV) to the common carotid artery (CCA) in a rat. The resultant arteriovenous fistula has been demonstrated to be closely analogous to human brain AVMs.

Using this model, a novel vascular targeting conjugate was formed from the protein annexin V and thrombin to target the previously identified target of PS. Initial dose escalation studies were performed using these AVMs and treatment of the AVM with a dose of focused radiation of 20 Gy using a Leksell Gamma Knife. At 3 weeks following GKS, a dose of the conjugate was administered intravenously. Histological evidence of small vessel thrombus formation was identified, and a maximal safe dose of the conjugate established.

On a larger scale assessment of the conjugate, AVM occlusion occurred in 75% of conjugate-treated animals with similar rates of flow cessation noted in the GKS-treated and the sham-GKS treated groups. These findings were noted both with angiographic occlusion and histological evidence of large and small vessel thrombus formation.

It was postulated that the reason for the lack of difference of conjugate efficacy between GKS and non-GKS treated animals was due to baseline PS translocation previously identified in non-irradiated AVM animals. It was hypothesised that with dose modification the selectiveness of the annexin V/thrombin conjugate may be improved. On reducing the dose to half the dose per weight per animal and administering it in a multiple dose treatment regimen a statistically significant proportion of animals had evidence of AVM occlusion in only irradiated animals, suggesting effectiveness of sensitising AVMs with focussed irradiation.

It is possible that an alternative target may be a more effective and safer alternative to PS and may result in improved thrombus formation with a lack of off-target binding and thrombus formation beyond the AVM. Preliminary work was completed using immunohistochemistry in harvested AVM samples and suggested that other targets such as the E2 subunit of the pyruvate-

dehydrogenase complex (PDCE2) may warrant further investigation. Pilot work was completed to examine *in vivo* imaging of PDCE2 in irradiated AVM naïve animals.

This research has demonstrated a significant association between use of the vascular targeting annexin V/thrombin conjugate and thrombosis of AVM vessels both radiologically and histologically. This technique and the use of radiation sensitisation may demonstrate a potential new treatment for AVMs. This finding is the first of its kind in the treatment of AVMs and with further development may become an alternative treatment modality for previously untreatable AVMs.

Chapter 1 Literature Review

1.1 Arteriovenous malformations

1.1.1 Definition and Overview

Brain arteriovenous malformations (AVMs) are defined as complex networks of abnormal arteries and veins that directly connect without the usual intervening capillary bed (Figure 1-1, Figure 1-2)[1]. These were first described by Steinheil in 1895 [2]. These lesions differ in structure and morphology from other brain vascular malformations including vein of Galen malformations, and dural arteriovenous fistulae.

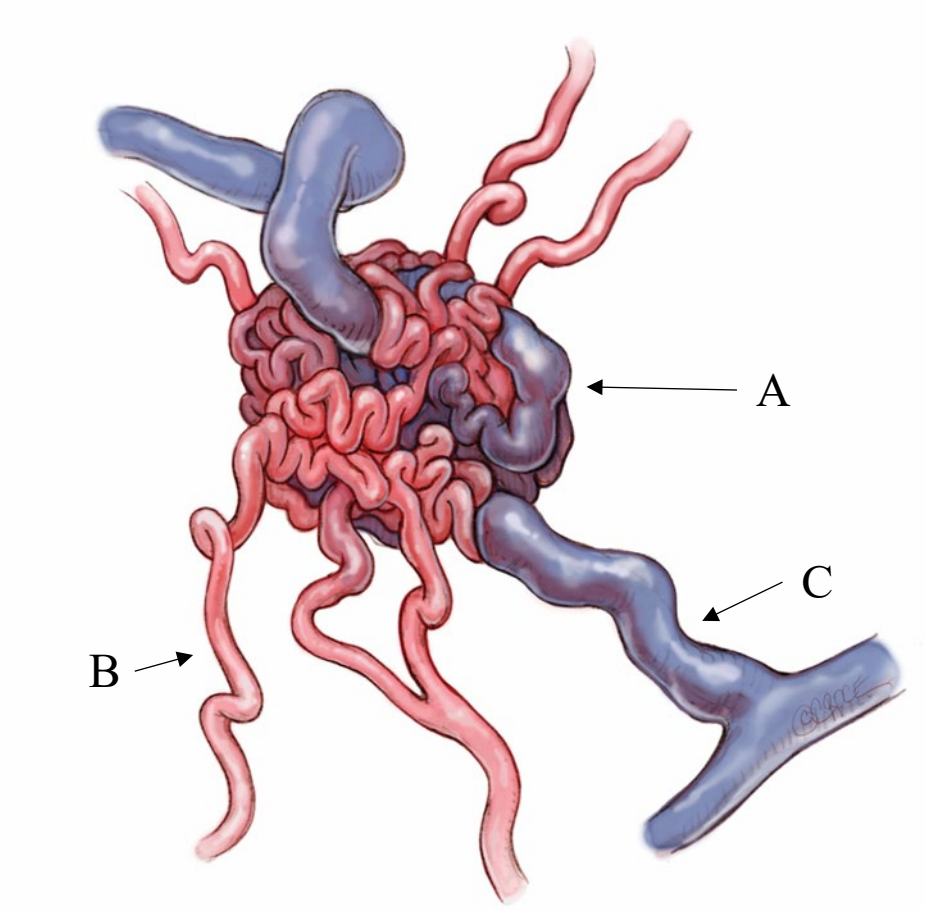

Figure 1-1 A diagrammatic representation of an AVM as a direct communication between the arterial and venous systems. This demonstrates the structures of the nidus (A), the feeding arteries (B) and draining vein (C) which feature in later discussions. Figure courtesy of Professor Marcus Stoodley

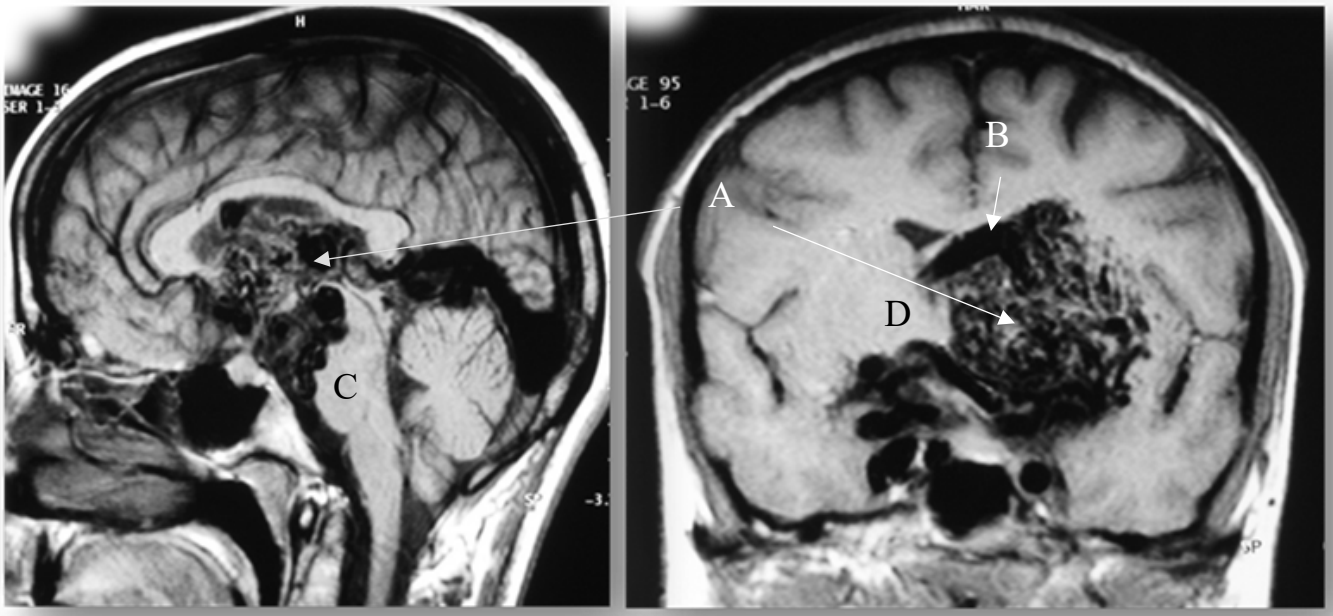

Figure 1-2 Multiplanar MRI demonstrating a high-grade left-sided thalamic AVM. The AVM is located within the left thalamus with deep venous drainage. A denotes the AVM nidus and B demonstrated an enlarged draining vein (similar to Figure 1-1). C denotes the brain stem and D denotes the normal contralateral thalamus. Figure courtesy of Professor Marcus Stoodley.

A classification and definition of AVMs was formulated originally by McCormick and colleagues [3, 4]. They described a cerebral vascular lesion with particular histological characteristics, presence of intervening brain parenchyma, and the presence of surrounding gliosis in the adjacent neural tissue [5, 6]. This definition has been refined more recently by the American Association of Neurological Surgeons, the Congress of Neurological Surgeons and the American Academy of Neurology. An AVM is now defined as including a distinct fistulous connection between arterial and venous circulations possessing both muscular and elastic laminae. This definition also includes a description of afferent arteries communicating with draining veins distinct from other vascular malformations [7]. AVMs are generally sporadic, although they do appear in association with a number of different disorders such as hereditary haemorrhagic telangiectasia (HHT) [1].

1.1.2 Epidemiology

It is difficult to obtain an accurate measure of AVM incidence and prevalence. Obtaining accurate AVM incidence and prevalence is difficult because all epidemiological studies have included only those patients that were symptomatic. This underestimates the true incidence and prevalence, missing those cases that are initially clinically asymptomatic. It has been suggested that to be strictly accurate a term of "rate of detection" should be used in the setting of AVMs [1].

To date only few studies have attempted to answer these questions and currently there are no population-based prevalence data on brain AVMs [1]. Six population-based studies have investigated the incidence of AVMs in the setting of both symptomatic and incidentally diagnosed pathology [8-15]. These studies have examined the incidence in Nordic, North American, Western European, Asian, and Middle-Eastern settings and report a total of 2167 AVM cases [1, 8, 9, 11-13, 15-18].

The first study to examine the incidence of AVMs was a retrospective analysis conducted by Brown and colleagues during the period 1985 to 1992, examining residents from Olmsted County, Minnesota, who had presented to the Mayo Clinic for management [9, 10]. The authors determined an incidence of 2.05 cases per 100,000 population per year (95% Confidence Intervals (CI) 1.46 – 2.64) and an age- and sex-adjusted incidence of 0.82 cases of haemorrhage per 100,000 population per year (95% CI 0.46 – 1.19) [9, 10]. A similar result was noted in the study by Jessurun et al. who conducted an 11 year retrospective review in the Dutch Antilles from 1980 to 1990 [13]. This study identified 1.1 cases per 100,00 population years of new diagnoses of symptomatic AVMs [13]. However, it should be noted that this population may not be useful to identify a true estimate of incidence as the population studied was relatively confined with a known high prevalence of HTT in the region (which comprise 35% of the study's AVM population), a genetic condition with a known increased risk of AVM development. Therefore, it is possible that this study overestimates the true incidence of sporadic AVMs [1, 13].

A Swedish study by Hillman was conducted over an 11 year period and identified 135 cases between 1989 and 1999 [12]. This provided an estimation of incidence of 1.24 cases per 100,000 population years with a proposed incidence of haemorrhage of 0.84 cases per 100,00 population years [12]. The interim results of a large-scale prospective multicentre study, the New York Islands Arteriovenous Malformation Study, were published in 2003 revealing 284 new diagnoses of AVM in patients residing on Manhattan Island, Staten Island, or Long Island [14]. This suggests an incidence of 1.34 cases per 100, 000 population per year and of haemorrhagic presentation of 0.51 per 100,000 [14]. Al-Shahi and colleagues examined the incidence of AVM in a Scottish setting from 1999 to 2000 and have suggested similar incidence rates of 1.12 cases per 100,00 population per year (95% CI 0.90 – 1.37) and a rate of haemorrhagic presentation of 0.51 population per year (95% CI 0.37 – 0.69) [8]. The most recent study of brain AVM incidence was conducted in Northern California from 1995 to 2004. The incidence was reported as 1.42 cases per 100,000 population per year (95% CI 1.20 – 1.57) and a first haemorrhagic presentation of 0.70 (95% CI 0.62 – 0.83) [11]. Assessing the recent literature therefore reveals an incidence of 1.12 – 1.42 cases per 100,000 population per year and of these cases, 38 – 68% presented with haemorrhage [1].

Although the geographic variations in AVM incidence would suggest that there may be underlying genetic, socioeconomic or environmental factors may be implicated in AVM pathogenesis or diagnosis, as yet no specific environmental or epidemiological risk factors have been identified [19]. The one exception to this is essential hypertension, although further work is needed to better understand its importance [19, 20].

1.1.3 Presenting Symptoms

Brain AVMs most commonly present during adulthood at a mean age of presentation of approximately 40 years [19, 20]. A large scale multi-centre study of 1289 patients reported a mean age at diagnosis of 31.2 years (95% CI 30.2 – 32.2 years) [17]. Subsequent statistical analysis of this data set has suggested that there is a high degree of geographic variability in the ages, which

may suggest a genetic predisposition associated with AVMs in association with such conditions as HHT.

A systematic review of nine large population-based studies of brain AVMs examined the common presentations of AVMs. The most common initial presenting feature of AVMs was haemorrhage in approximately 50% of cases [1, 15, 17]. The second most common presenting symptom is that of seizures, in approximately 30% of cases. Headaches as a result of AVMs are only reported in two case series at a rate of 5 – 14% [1]. Variations are noted in geographic distribution with Nordic countries reporting an initial haemorrhage rate of 71%, compared to 42% and 52% for North American and Western Europe, respectively. A first presentation with seizures is noted more commonly (31%), in patients in Western Europe and the Middle East, compared to a significantly lower proportion (19%), in patients in Nordic countries and North America [1]. This geographic variability, although likely partly due to regional differences in diagnostic medical practices and institution bias, could also reflect a different genetic subtype of disease or proportion of HHT within the populations.

1.1.4 Incidence of Haemorrhage

An important aspect of AVM epidemiology is the risk of haemorrhage and the factors that influence this risk. Patient and lesion factors have been investigated [16, 20-27]. Historical studies made attempts to examine the risk of haemorrhage in brain AVMs and estimated the risk to be less than 5% [21, 26, 27]. However, it should also be noted that even at this early period, it was noted that there was a high degree of heterogeneity in haemorrhagic events and outcomes [26-28]. More recent data on haemorrhage rates can be drawn from two meta-analyses that have examined all existing natural history studies and large database cohorts [20, 29]. Gross et al. concluded that from the higher quality population-based studies the overall risk of AVM annual rupture is 3% with ruptured AVMs having a risk of 4.5% per annum and unruptured AVMs a risk of 2.2% [22]. Kim et al. examined data gathered from four large AVM cohorts and suggest a similar risk profile with an overall annual risk of haemorrhage of 3.0%, with ruptured AVMs having a risk of 4.5%

and unruptured AVMs a risk of 2.3% per annum [29]. This would suggest that annual risk of rupture for an unruptured AVM is 2 to 3% and of ruptured AVMs of 4.5% per annum.

1.1.5 Haemorrhage risk factors

The meta-analyses by Gross et al. and Kim et al. provide the most current assessment of risk factors associated with haemorrhage. Both studies suggest an initial haemorrhage was the most prominent risk factor associated with subsequent haemorrhagic events [20, 28, 29]. Gross et al. noted that architectural risk factors of a deep location of the lesion, exclusive deep venous drainage and the presence of associated nidal or feeding artery aneurysms were associated with an increased risk of haemorrhage [22]. This finding, however, was not noted in the study by Kim et al., although a non-significant association between deep venous drainage patterns and risk of haemorrhage was noted [29]. In addition, both studies found a slight increased risk of haemorrhage amongst women [20, 29]. Although not found in these studies, earlier research suggested that small AVM size may predispose to an increased risk of haemorrhage from a theory suggesting that feeding arteries in these lesions may have a higher intraluminal pressure [24, 25, 30-33]. This finding is not supported by the more recent literature [20, 28]. Other risks have in the past been attributed to ethnicity, smoking, family history and pharmacological anticoagulation but they are unlikely to be significant [30].

Increasing age has been noted to be positively correlated with increased haemorrhage risk. The study by Kim et al. demonstrated that with each decade of life the risk of haemorrhage of a known brain AVM increased by approximately one third [29]. In earlier prospective studies, both population cohort and randomised studies, this risk has been quantified as an annual risk of 1–2% per annum [8, 19]. It is important to note that these data are exclusively for unruptured AVMs. Due to the increased risk post haemorrhage, few AVMs are observed without any intervention following a haemorrhagic event [20, 25, 28, 30, 34]. Following this assumption of an annual risk of haemorrhage that increases with age, attempts have been made to quantify life-long risk using

the annual rupture risk and patient life expectancy. Two such formulae have been proposed [35-37]:

$$\text{Rupture risk} = 1 - (\text{risk of no haemorrhage})^{(\text{life expectancy})}$$

OR Rupture risk = 105 – patient age

Although these methods that are proposed only provide a crude estimate of risk of haemorrhage, they do highlight that there is a significant lifelong risk of haemorrhage of brain AVMs. Particularly in the setting of children and young adults, this will mean that most individuals will undergo a haemorrhagic event during their life time if left untreated. It would then follow, that in younger patients it is important to consider intervention to eliminate the risk of haemorrhage and its consequences.

1.1.6 Limitations of Haemorrhage Risk Assessments

There remain significant limitations regarding the current available natural history studies. The majority of studied AVMs in the literature have been identified because they are symptomatic (either due to haemorrhage or from seizures). This therefore calls into question the applicability of the findings of these studies in the setting of true incidental diagnoses of AVMs and may overestimate the risk of haemorrhage for these lesions [30]. It should also be noted that patients who appear to be at a higher risk of haemorrhage because of noted risk factors would be more aggressively treated than those individuals with lower risk lesions. This could potentially underestimate the risk associated with an observation treatment approach [30].

1.1.7 Morbidity and Mortality

Similar difficulties are encountered when interrogating the natural history literature to ascertain the magnitude that haemorrhagic events have on mortality and morbidity of the patient. Due to the high degree of heterogeneity in both study design and results it is unlikely that an accurate

assessment of the true impact of these lesions is possible [22]. In fact, in earlier studies, death as a result of an initial haemorrhage ranged widely from 4% to 29% [40]. Other studies have suggested that the risk of severe neurological morbidity and mortality from a single haemorrhagic event is as high as 35% and 29%, respectively [23]. Despite the variability in outcomes in what is both a heterogeneous population and body of literature, it is clear that brain AVM haemorrhagic events are a source of considerable neurological morbidity and mortality [21, 24, 34]. This impact has prompted a search in the neurosurgical community for an appropriate form of treatment to prevent intracranial haemorrhage in these patients.

1.1.8 Pathogenesis

The causative event and the pathogenesis of brain AVMs remain unknown. The study of the aetiology and pathogenesis of these lesions is difficult as a mature AVM is most likely the result of a complex series of genetic pathways and environmental conditions following a yet unknown inciting event that may have happened many decades prior to presentation.

To date, no diagnostic marker proteins have been identified for AVMs. Recent literature has suggested that AVMs may result from a series of changes in DNA methylation and histone modification of genes concerned with vascular development in addition to aberrant modifications of the genome of endothelial cells that result in the vascular phenotype that is regarded as a mature AVM [39]. Further recent work using DNA sequencing of AVM samples has identified mutations in the KRAS pathway and has led to proposed alternative DNA mechanisms in AVM pathogenesis [40, 41].

Historically, these lesions were considered to be congenital, however, this has more recently been challenged by the report of AVMs recurring following complete surgical resection [42-48]. Furthermore, there is a suggestion from case reports that AVMs may not be congenital but may occur de novo following events such as trauma or ischaemic insult [49-51].

AVMs are lesions that are highly dynamic and in the case of children, exhibit features of rapid growth, remodelling and regression. This suggests a genetic cause of AVMs. Two approaches

have been utilised to identify the genetic basis of pathogenesis. The first method is in family linkage analysis in patients with a confirmed diagnosis of an AVM and the second method involves the analysis of defective genetic changes using AVM samples post resection [54]. Assessment of family cohorts with inherited congenital AVMs is possible in conditions such as HHT, Wyburn-Mason syndrome and Sturge-Weber syndrome [39, 53, 54]. Although these conditions provide easy access to familial cohorts for assessment, it has been suggested that the pathogenesis and behaviour of these AVMs may be different to sporadic AVMs and may signify a different pathological process [55].

In these analyses, AVMs have been associated with aberrant molecular signalling in the angiogenesis pathway. Single nucleotide polymorphisms in several genes that have been linked to angiogenesis and inflammation have been implicated and reviewed [55, 56]. In the setting of HHT, mutations in the genes of endoglin (*ENG*) and activin receptor-like kinase 1 (*ALK1*) have been noted to predispose to aberrant signalling in the transforming growth factor beta (TGF-β) pathway [57]. In addition to TGF-β, studies have demonstrated that genes that encode for angiopoietins (ANGPT1 and ANGPT2) and their receptor TIE-2 have an important role in vascular stability and angiogenesis and abnormalities in this system have been associated with AVMs [58].

Although the genetic link is well substantiated, until recently, no data have convincingly supported a genetic link in sporadic, non-familial AVMs. Recent DNA sequencing studies on sporadic non-familial AVMs have examined the role of the Kirsten Ras oncogene (KRAS) pathway in AVM pathogenesis. These studies identified *KRAS* mutations in approximately 50% of tissue samples harvested from human AVMs [42]. This involvement of the RAS–mitogen-activated protein kinase (MAPK) pathway has been validated in other "high-flow" vascular abnormalities [41, 59-62]. This finding of *KRAS* mutations specific to endothelial cells (ECs) has suggested that dysregulation of ECs is a key feature of AVM pathogenesis. These mutations are well known to drive strong constitutive MAPK–extracellular signal-regulated kinase (ERK) signalling [63], and are important in tumourigenesis [64]. Further research has suggested that in the *in vitro* setting

inhibition of the MAPK–ERK pathway has the potential to reverse the abnormal endothelial phenotypes [42]. This may carry clinical implications in AVM treatment using pharmacological agents such as small molecule MAPK/ERK kinase (MEK) inhibitors, which are used in cancer research [65, 66].

Haemodynamic parameters may also be involved in the pathogenesis of AVMs. Illi et al. have demonstrated a connection between haemodynamic forces and environmental modulators in the exposure of ECs to shear stress that resulted in chromatin modifications and change in gene expression [67]. It has been speculated that the altered haemodynamic forces may be a critical epigenetic regulator and direct the development of the endothelial cells [68]. It has also been postulated that in the setting of brain AVMs, cerebral haemodynamic flow changes such as haemorrhage, ischaemia and seizures may be implicated closely in AVM pathogenesis [39, 69, 70].

Vascular remodelling has been demonstrated to be induced by the specific haemodynamic parameters of blood pressure and wall shear stress. Immense wall shear stress and circumferential strain in AVM feeders have been described and the subsequent increase in expression of certain factors including matrix metalloprotease 9 (MMP9), platelet-derived growth factor (PDGF), and vascular endothelial growth factor (VEGF); all of which have been implicated in the process of vascular remodelling [71-75]. Studies using a deficient ALK1 mouse model have suggested that changes in wall shear stress induces a higher expression of VEGF that subsequently leads to the formation of distended vessels within the mouse brain. The vascular morphological features that resulted in these mouse models appear to be structurally very similar to brain AVM vessels in humans [39, 76, 77]. Current literature supports the theory that changes in haemodynamic flow in the junction of AVM blood vessels could result in changes in the epigenetic mediators that could ultimately lead to the development of a mature AVM [39]. Endothelial dysfunction has been reported to occur following disturbed shear stress and altered haemodynamic forces at areas of branching arteries and curvatures of blood vessels [80]. Additionally, disrupted shear and

oscillatory haemodynamic pressure have been implicated in the activation of several atherogenic genes within endothelial cells and thus may promote atherosclerosis [81]. From these reports, it would seem to be likely that epigenetic factors from haemodynamic changes could be involved in the development of AVMs.

The common pathway for AVM formation and subsequent rupture seems to involve an inflammatory reaction within the walls of the AVM that is triggered by a combination of haemodynamic stress with associated genetic factors [55].

In summary, the pathogenesis of AVMs remains poorly understood and despite significant research in this area no specific markers have been established [39]. In the setting of HHT, polymorphisms in the TGF-β receptor complex have been implicated in AVM formation [53, 54]. It has been postulated that sporadic, non-HHT, associated AVMs, may be the result of a combination of genetic and epigenetic factors from haemodynamic derangements. Previous pathogenesis theories have hypothesised that AVM formation requires stimuli to endothelial cells in the form of either transcription factors or associated metabolites within endothelial cells [39].

Regardless of these theories, the pathogenesis remains poorly understood and in the absence of markers, or an understanding of the development of these lesions, there is currently no method to prevent or improve early diagnosis AVMs. Until significant advances are made in the field of pathogenesis it is important to improve the efficacy of treatment of mature AVMs.

1.1.9 Treatments

The goal of management in AVMs is to exclude the vessels from circulation either through surgery, endovascular embolisation or radiosurgery, and to prevent haemorrhage. Ideally, any treatment should achieve this without associated neurological morbidity or mortality [28, 80, 81].

Treatment of AVMs has recently fallen under scrutiny with the publication of the Randomized Trial of Unruptured Brain AVMs (ARUBA) trial [21]. This prospective randomised study assessed 223 patients with unruptured brain AVMs and randomised them to either interventional therapy or

to conservative medical management. The trial was ceased prematurely (at a mean follow-up of 33.3 months) due to a statistically significant higher risk of stroke or death in the interventional group than the conservative medical management (hazard ratio 0.27, 95% CI 0.14-0.54) [21].

Interpretation of the ARUBA results might suggest that observation would be a more appropriate management strategy than intervention for brain AVMs. However, there are several important criticisms that should be noted about this study. Despite the conclusion from the ARUBA study, this finding is based on a study that was only of 33.3-month duration. Given that the risk of haemorrhage from a brain AVM is one that is life-long this duration of study was insufficient to effectively answer the question of treatment effect on reduction of haemorrhage risk and haemorrhage outcome [28, 81].

This study was fundamentally flawed from the outset. It would almost be inconceivable that the treated group would be better off than the non-treated observed group in the short-term. After all, the treatment of AVMs is directed at the prevention of the life-long risk of rupture. It is therefore not unexpected that the patients having an intervention would have a risk of complication and potential poorer short-term outcome in comparison with the observed group. Although observation does carry a degree of risk for each patient, it is important to determine the projected reduction in haemorrhage risk that a patient could be subjected to over the course of their life and compare this to the risk of treatment-related morbidity. Furthermore, the ARUBA study, although assessing all standard AVM interventions, did not resemble usual practice, as most patients in the interventional arm underwent endovascular embolisation. This does not resemble usual practice in AVM treatment where only a minute proportion of AVMs are able to be cured via endovascular embolisation. Despite the results and conclusion proposed in ARUBA, it is generally accepted that interventions, where possible, are indicated in AVMs to prevent lifelong haemorrhage risk [83]. Established treatments of AVMs include microsurgical resection, radiosurgery and endovascular embolisation.

1.1.9.1 Microsurgical Resection

Microsurgical resection of AVMs remains the current gold standard treatment due to its immediate cure. Like the alternative treatments it is important to quantify the risk of treatment-related morbidity and mortality and to compare that to the potential reduction in the risk of AVM haemorrhage. The most widespread surgical risk assessment system is the six-grade Spetzler–Martin system [84]. This system stratifies the expected surgical outcomes based on size of the nidus (<3cm = 1 point, 3–6 cm = 2 points, >6cm = 3 points), location (in eloquent brain = 1 point, in non-eloquent brain = 0 points), and the pattern of venous drainage (deep venous drainage = 1 point, no deep venous drainage = 0 points) [84]. Spetzler et al. also describes a grade VI AVM which is described as large diffuse AVMs that are distributed throughout critical eloquent locations. In these cases, death following surgical resection is unavoidable and they are regarded as "inoperable" [84]. This scale has been externally validated [83], and on evaluation of its use, AVMs have now been stratified into three groups of surgical risk, including those AVMs where surgical resection is possible [86]:

1. Low surgical risk (Spetzler–Martin grade I-II)
2. Intermediate surgical risk (Spetzler–Martin grade III)
3. High surgical risk (Spetzler–Martin grade IV–V)

Based on these categories, Spetzler et al. recommended surgical management for low-risk lesions and multimodality treatment for AVMs in the intermediate risk group utilising radiosurgery or endovascular treatment as adjuncts. In the case of high-risk lesions, observation is the usual recommended treatment approach apart from patients with recurrent haemorrhage, progressive neurological deficits, or seizures related to the AVM that are refractory to medical treatment [85].

The Spetzler–Martin system has been criticised for its assessment of the intermediate-risk group (Spetzler–Martin grade III). This group of AVMs encompasses the largest and most heterogeneous of the five groupings. Congar et al. have proposed that the grade III lesions encompass four different types of AVMs: small AVMs with deep venous drainage in eloquent

areas (S1V1E1), medium-sized AVMs with deep venous drainage (S2V0E1), and larger AVMs in non-eloquent regions without deep venous drainage (S3V0E0) [30]. Following this criticism, research has been completed to differentiate among these groups and to propose a threshold between low-risk and high-risk AVMs [86, 87]. Lawton et al. demonstrated that the S1V1E1 subtype has a risk of surgical morbidity similar to Spetzler–Martin grade I and II lesions. The S2V1E0 group appears to have a surgical risk that is similar to the earlier published risks for Spetzler–Martin grade III. In contrast to these other groups, the S2V0E1 subtype appears to have a higher risk of surgical morbidity that is comparable to the Spetzler–Martin grade IV and V AVMs and microsurgical resection is not recommended. The final group of S3V0E0 subtype is uncommon and the risk of surgical morbidity is not well understood [88].

Further criticism of the Spetzler–Martin system has been raised due to the absence of patient characteristics and the haemorrhage status of the AVM. It has been noted that microsurgical resection is facilitated in the setting of haemorrhage with a reduced degree of surgical morbidity [88]. The character of the AVM nidus has also been noted to affect surgical morbidity, a lesion with a diffuse nidus and deep arterial feeders conveys a higher risk [89]. Lawton et al. examined these criticisms and proposed a supplementary grading system as an addition to the established Spetzler–Martin scale [90]. This scale comprises a 10-point scale awarded for age (<15 = 1 point; 15–40 = 2 points; >40 = 3 points), appearance of the nidus (diffuse = 1 point; compact = 0 points), and presence or absence of haemorrhage (haemorrhage = 0; no haemorrhage = 1). The points awarded for these categories are then added to the standard Spetzler–Martin grade [90]. This supplementary scale incorporates age as a surrogate marker for a patient health status.

This scale has been externally validated and this has demonstrated its superiority over the traditional Spetzler–Martin scale [93]. The Supplementary scale provides a quantification of surgical risk of stable or improved neurologic status against the risk of neurological deficit or mortality. The rates of poor outcomes were proposed by Lawton et al. to be as follows: Grades 2–3, 0%; grade 4. ~9%; grade 5, ~21%; grade 6, ~27%; and grades 7–10, ~40–60% [90]. From these

rates, it can be deduced that in the case of patients with AVMs of grades 2–6, surgery is a valid option due to the relatively low risk of perioperative morbidity and mortality, whereas, in the case of grades 7–10, observation would be recommended as a more appropriate treatment option [28, 90].

An alternative scale to assess surgical risk in AVMs was reported by the University of Toronto Brain AVM Study Group [92]. Following publication of their patient series the authors propose a scale composed of nine points assessing the three separate criteria of: eloquence (4 points); diffuseness (3 points); and deep venous drainage (3 points). From the published series Spears et al. propose four different risk groups based on the scale and the probability of sustaining an early disabling neurological deficit. The risk groups are as follows [92]:

- 0–2 points → Low risk = 1.8%
- 3–5 points → Moderate risk = 17.4%
- 6–7 points → High risk = 31.6%
- >7 points → Very high risk = 52.9% [92]

Assessment of this surgical risk tool has demonstrated that the University of Toronto grading scale has a higher predictive ability (area under receiver operating characteristic [ROC] curve = 0.79) than the 10-point Supplemented Spetzler–Martin scale (area under ROC curve = 0.78) and the original Spetzler–Martin scale (area under ROC curve = 0.69) [28, 82, 92]. Despite this, the University of Toronto scale has yet to gain widespread usage.

Both scales highlight that despite the success of microsurgical resection there is still a subset of patients where resection is either not possible or carries an unacceptable degree of risk. It is difficult to quantify exactly how many AVMs are considered too high risk for surgical resection due to the inherent selection bias present in many published series. One series from a specialist cerebrovascular centre has proposed that approximately 5% of cases referred for surgery were considered inoperable due to the high perioperative risk associated with the AVMs [95]. This

number most likely underestimates the true figure in average neurosurgical practice. This further highlights the importance of finding alternative approaches to treat AVMs.

1.1.9.2 Stereotactic Radiosurgery

Stereotactic radiosurgery (SRS) is a well-established treatment for a subset of brain AVMs. Published series have demonstrated cure with successful obliteration of an AVM at a rate of 80% in select cases after a latency period of 1 to 3 years with an acceptably low risk of periprocedural morbidity [94-108].

Treatment with SRS differs significantly from surgical resection, both in mechanism and the associated procedural risks. SRS lacks the instantaneous outcome that occurs with microsurgical resection with occlusion of an AVM occurring over a period of years. Importantly, during this latency period a risk of haemorrhage persists [30]. In addition, there are risks associated with radiation toxicity. Appraising the morbidity risk of SRS in the treatment of brain AVMs requires analysis of specific patient and AVM characteristics. Scales that assess microsurgical risk such as the Supplemented Spetzler–Martin Scale are not effective predictors of patient outcome following SRS [109-111]. This is not unexpected as the Spetzler–Martin grading system is not sensitive to important radiosurgical parameters that impact the obliteration rate such as AVM volume and specific location. This is particularly important in AVMs located within deep structures such as the thalamus or brainstem where radiation-related complications due to injury to critical adjacent neurological structures are more likely than in hemispheric AVMs [112, 113].

Initial methods proposed included the use of the Karlsson index (KI) index as a method to predict obliteration following AVM radiosurgery [116], and the obliteration prediction index (OPI) as a method to estimate the probability of AVM obliteration in individual patients [117]. Although these methods demonstrate a correlation with AVM obliteration, they do not assess the risk of radiation toxicity-related complications against the radiation dose. In addition, the KI and the OPI are methods based on radiation dosimetry at the time of treatment and are not based on patient or AVM characteristics.

With these limitations in mind, a risk assessment score has been developed and named the Radiosurgery-Based Grading System (RBGS) in 2002 [111]. This method predicts the probability of nidus obliteration and periprocedural morbidity following a single-session treatment using SRS. The predictive variables identified were AVM volume (cm^3), patient age, and AVM location. The formula for the AVM score is [111]:

AVM score = (0.1) (AVM volume) + (0.02) (patient age) + (0.3) (AVM location)

AVM volume is calculated using preoperative MRI assessment. Location is assigned a value of 0 for a frontal or temporal lesion, a value of 1 for parietal, occipital, cerebellar, intraventricular, or corpus callosal lesion, and a value of 2 for lesions located within the basal ganglia, thalamus or brainstem. Using this formula and assessing a study population from a different institution, Pollock and Flickinger noted that 100% of patients with a score ≤1 had an excellent outcome, whereas in patients with a score >2 only 39% had an excellent outcome. In this study an excellent outcome was defined as a patient having complete nidus obliteration with no new or worsening neurological deficit [111].

The RGBS has been externally validated in studies using both GKS and linear-accelerator-based SRS and in both adult and paediatric settings [101, 116-123]. More recently, Pollock and Flickinger re-evaluated the RBGS and further simplified the complex three-tiered location variable by assigning 1 point for AVM's located within the basal ganglia, thalamus, or brainstem and 0 points for all other locations. This revised formula is as follows [126]:

AVM score = (0.1) (AVM volume) + (0.02) (patient age) + (0.5) (AVM location)

This simplified version of the RGBS has also been externally validated and no change in the accuracy of predicting periprocedural morbidity was noted in the setting of either GKS or linear accelerator (LINAC) based systems [124-126].

In 2013 an alternative grading system, the Virginia radiosurgery AVM scale, was proposed [129]. This scale purported to address the complexity of the RGBS formula and create a more clinically usable system. This scale was based on 3 variables and assessed on a 4-point scale. AVM volume (cm^3) was assessed with a score of 0 for <2 cm^3, 1 point for 2 to 4 cm^3, and 2 points for AVM's >4 cm^3. Location was determined in a similar manner to the Spetzler–Martin scale with an eloquent lesion assigned 1 point and non-eloquent AVMs assigned 0 points. In addition to these variables a history of haemorrhage was assigned 1 point and the absence of haemorrhage as 0 points. From these variables, the Virginia group stratified AVMs into 4 groups with reducing probability of favourable outcome [129]:

- Score 1 → 79% chance of favourable outcome
- Score 2 → 70% chance of favourable outcome
- Score 3 → 48% chance of favourable outcome
- Score 4 → 39 % chance of favourable outcome

Since publication of this grading system, the group from the University of Virginia has internally validated their scoring system [128-130], however, no external validation of this score has been published [30].

These scales highlight the limitations of AVM radiosurgery. The principal cause for treatment failure is the volume and morphology of the AVM and difficulties delivering an adequate radiation dose to the whole AVM [116]. Furthermore, the technical limitations of dose planning and the previous reliance on two-dimensional angiography as preoperative imaging has the potential to

leave portions of AVM outside the planned radiosurgical treatment volume [101, 131-133]. Although newer dose delivery techniques incorporating conformal dose planning and staged treatments of complex AVMs maximise the chance of obliteration, larger AVMs still pose a significant treatment challenge for radiosurgery [134].

Radiosurgery has a different risk profile to either microsurgery or endovascular embolisation. Radiosurgery for AVMs can sometimes induce unwanted radiation injury in surrounding normal brain tissue in the form of brain necrosis [112, 113, 134-138]. Imaging studies have demonstrated changes in surrounding brain in approximately 30% of patients that appears to be dependent on treatment volume and dose administered [112, 134-137]. A model has been proposed aiming to predict the development of radiation necrosis from radiosurgery, but its development has been complicated from the dramatic variability of necrosis from location and volume of dose [114].

It has been suggested that radiosurgery for AVMs may increase the risk of haemorrhage during the first 12 months following treatment [139, 140]. Other studies have proposed that radiosurgery reduces the risk of haemorrhage even if incompletely obliterated as demonstrated on follow-up angiography [143]. A recent retrospective observational study of 531 patients undergoing radiosurgery with GKS has suggested that the risk of haemorrhage was significantly reduced following treatment even before the presence of angiographic evidence of obliteration [144]. Other studies have supported this finding and suggested that the increased risk of haemorrhage previously observed may be related to other AVM factors such as size of nidus, volume and applied single dose of radiation [143, 144]. Further prospective data are required to understand the true impact of radiosurgery on the risk of AVM haemorrhage.

Other less frequent complications of AVM radiosurgery have been reported, including arterial stenosis [147], occlusive hyperaemia [148], diffuse white matter ischaemia [149], and delayed cyst formation [107, 148-153].

In summary, AVMs of small to moderate size may be successfully treated with radiosurgery. This can require a period of up to 3 years, during which the patient is still subject to a risk of

haemorrhage. In addition, proposed AVM radiosurgery scoring systems demonstrate the different risk profile included in this treatment compared to microsurgical techniques and that even with newer radiosurgical techniques a subset of AVMs remain untreatable. To provide comprehensive and effective treatments to all AVMs, improvements in current treatments or new treatment modalities are required.

1.1.9.3 Endovascular embolisation

The role of endovascular embolisation in the treatment of AVMs is poorly understood and it is currently generally used as an adjunctive treatment in conjunction with SRS or microsurgery [30]. This may be due to its historical low rates of obliteration with early reports of endovascular treatment reporting an obliteration rate of 13% [156]. More recent studies have suggested higher embolisation rates of the order of 50.3% to 90.6% [155-157]. These smaller series suggest that endovascular treatment may be more effective with small to medium superficial AVMs with a compact nidus, a small number of accessible feeding arteries within the same vascular territory, and easily delineated draining veins [159]. These results suggest that similar to SRS, endovascular embolisation may only be effective in achieving curative embolisation in a small subset of AVMs rather than AVMs in general [159]. In addition, embolisation may have a role in reducing AVM grade, making an AVM more amenable to microsurgical resection or SRS [30]. This technique, however, is only available in specialised centres and is not always technically possible due to difficult locations of the nidus or significant vessel tortuosity [160].

Early risk assessments of endovascular embolisation of AVMs were based on the Spetzler-Martin surgical risk grading scale. Similar to SRS, due to the technical differences of endovascular treatments and the different risk profiles, the applicability of this grading scale to endovascular techniques is questionable [159, 160]. In 2001, Willinsky proposed a 6−point scale based on the angioarchitecture of small AVMs [163]. This scale is graded based on the type of nidus (fistula = 0 points, <1 cm nidus = 1 point, 1−3 cm nidus = 2 points), type of feeding arteries (cortical = 0, perforator or choroidal = 1), and the number of feeding arteries (single = 0, multiple = 1).

Subsequent validation of this scale has found that AVMs with more simple angioarchitecture (0−2 points) were more likely to be cured with embolisation with a low risk of permanent morbidity (2.5%) [163].

A second scale has been proposed by Feliciano et al. based on a review of existing AVM endovascular literature. They suggest a 5−point scale based on the number of feeding vessels (<3 vessels = 1 point, 3−5 vessels = 2 points, and >5 vessels = 3 points), eloquent location (eloquent location = 1 point, non-eloquent location = 0 points), and the presence of an arteriovenous fistula (no AVF = 0 points, AVF = 1 point) [164]. Despite the extensive review of the literature this proposal scale is based upon, it has yet to be validated in the clinical setting [30].

In addition to aiming for cure of the AVM, embolisation may have a role in multimodality treatment of AVMs. In select circumstances embolisation can be used in a preprocedural setting to decrease blood flow through an AVM or by occluding deep arterial feeders that may be difficult to approach surgically, thereby facilitating safer surgical resection. Embolisation can also be used to facilitate SRS through the reduction of the volume of the nidus and this is thought to improve the likelihood of successful AVM obliteration with SRS. Endovascular treatment of AVMs has also had success in alleviating the progressive neurological deficit associated with the vascular 'steal' phenomenon that has been reported with AVMs with a high-flow arteriovenous shunt [28, 85, 163-165]. Although these alternative goals of endovascular treatment of AVMs may have some merit, there is currently a lack of larger scale evidence supporting its use in the literature. Further analysis is necessary to better determine the role of endovascular embolisation in the treatment of AVMs. In addition, there is a suggestion that over-embolisation of AVM feeding vessels can result in an enlargement of deep white matter feeding vessels and this may result in an increase in the technical complexity of microsurgical resection or may also precipitate premature rupture and haemorrhage [30].

Similar to SRS and microsurgical resection, endovascular embolisation has its limitations and appears to be only successful in a small subset of cases [166-168]. The success rate may improve

with newer modalities and treatment techniques, but, currently each case needs to be assessed on an individual basis [171]. The AVMs that are not successfully treated with endovascular embolisation include larger AVMs with diffuse architecture, eloquent location and multiple complex arterial feeders [170, 171]. These endovascularly-challenging AVMs share many similarities with those that cannot be successfully treated with either SRS or microsurgical resection. This highlights that despite current treatment modalities, there are AVMs that lack an effective treatment and remain a significant risk of haemorrhage.

1.1.9.4 Limitations of Available Treatments

It is generally accepted that AVMs require treatment, where possible, to eliminate the life-long risk of rupture. The available treatments of microsurgical resection, radiosurgery and endovascular embolisation have some success with treating AVMs, however, AVMs have variable characteristics that may render a treatment ineffective or only successful with an unacceptable risk of morbidity and mortality. In the case of large high-grade AVMs, over 90% have no effective treatment [85]. New developments in either modality may improve current treatment efficiency, but they are unlikely to improve the efficacy of the treatment sufficiently to be able to treat these lesions. It is clear that because of these limitations newer treatment modalities are required.

1.2 Vascular targeting

An alternative treatment that may be effective in AVMs is vascular targeting. Vascular targeting is a method by which a differentiating target is identified that is presented on the luminal surface of the endothelium. Such a target is ideally only present in pathological vessels and not in normal vasculature. An antibody or protein is then administered to bind to that location. The protein is conjugated to a treatment-effective payload that activates in the pathological area exhibiting the target.

Such a treatment is attractive for AVMs as it may provide a medical alternative treatment that does not carry the invasive risks associated with the surgical access requirements of microsurgical resection or the endovascular embolisation. Such a treatment may also provide an alternative to

radiosurgery. Furthermore, if a target could be identified that is expressed only in the nidus and not present elsewhere systemically, it would allow treatment without harming normal brain vasculature or the draining vein and prevent an associated infarct.

The section below provides a general discussion on the development of vascular targeting techniques, with reference to the previous work in cancer research.

1.2.1 Overview and Historical Context

The concepts behind vascular targeting agents were first described by Denekamp as a potential cancer therapy during the 1980s [172-174]. In this research Denekamp observed that physical obstruction of the vasculature of solid tumours led to tumour regression in a murine model and further postulated that through vascular targeting it might be possible to cause vessel occlusion pharmacologically [172, 173]. This hypothesis was subsequently validated using a toxin targeted by an antibody specific for tumour blood vessels ultimately resulting in tumour regression in an animal model [175-177]. Further work has suggested that anti-tubulin drugs demonstrate vascular targeting activity [178, 179].

Vascular targeting differs conceptually from anti-angiogenic agents, which are also commonly used in the treatment of malignancy. Anti-angiogenic agents prevent the formation of new blood vessels rather than targeting existing established vasculature [176]. Animal model studies have also suggested that vascular targeting therapies appear to be more active in larger experimental tumours with established vasculature [180]. Furthermore, vascular targeting has been shown to cause a characteristic pattern of central necrosis with relative preservation of the periphery, possibly due to the larger vessels preferentially targeted and the high interstitial pressure in these lesions that results in vascular collapse [176]. This preferential targeting of larger vessels of vascular targeting lends itself to the targeting of established vessels within AVMs.

Current vascular targeting agents may be divided into two categories based on their mechanism of action: biologics and small-molecule agents. Both of these agents are designed to target

vasculature and, in the case of cancer-based treatment cause acute vascular collapse leading to tumour necrosis [183].

Biologic agents or ligand-directed agents include antibodies and peptides that are used to target selective differences on the luminal surface of the endothelium and deliver a therapeutic payload to the endothelium such as a toxin, pro-coagulant or pro-apoptotic effector. This effector agent would then, within minutes of systemic administration of the compound, initiate a sequence of events that ultimately would lead to blood vessel occlusion and ischaemia of the region of targeted endothelium.

The second category of small molecule vascular targeting agents includes compounds that do not specifically localise to changes within the endothelium. These agents achieve their targeting through exploitation of known physiological differences between normal and pathological endothelium. In the case of cancer research these differences in tumour vessel endothelium include their increased proliferation rate, permeability, and reliance on a tubulin cytoskeleton to maintain cell shape [172, 182, 183].

1.2.1.1 Ligand-directed vascular targeting agents

The proposed strategy behind ligand-directed vascular targeting techniques is to use ligands to bind selectively to a component of pathologic blood vessels that is not present on normal vessels, to then selectively target and cause vessel occlusion. These ligand-directed compounds are composed of both a targeting and an effector component that are usually linked with chemical cross-linkers or peptide bonds. The targeting component is usually an antibody or peptide that binds selectively to a marker that is upregulated or present on pathological endothelium compared to normal tissue endothelium.

In the setting of malignancy, several molecules have been identified for use in tumour neovasculature. Growth factors such as VEGF-A have been used to target growth factor receptors overexpressed in tumour vasculature and have been used in conjugates with diphtheria toxin, and gelonin. Other molecules include those involved in angiogenesis and vascular remodelling, cell

adhesion molecules induced by inflammatory mediators such as interleukin (IL)-1, and molecules associated with pro-thrombotic changes occurring on the luminal surface of vascular endothelium [186]. Examples of potential targets for ligand-directed treatments include endoglin [187, 188], vascular endothelial growth factor (VEGF) [189, 190], αv-integrins [191, 192], the fibronectin EDB domain [191], and prostate-specific antigen [194]. Other potential tumour vessel markers are included in Table 1-1. One potential target for AVM targeted treatment that has been demonstrated in targeted tumour treatment as well as previous animal model AVM work is phosphatidylserine (PS) [193].

Table 1-1 A list of potential tumour vessel markers for ligand-directed vascular targeting agents [176]

Class	Examples
Angiogenesis/vascular remodelling	Vascular endothelial growth factor-*a* receptors
	Vascular endothelial growth factor: receptor complexes
	$\alpha_v\beta_3$ integrin
	Prostate specific membrane antigen
	CD44-related antigen (TES-23)
	Fibronectin ED-B domain
	Collagen IV HUIV26 epitope
	Endoglin
	Endosialin
	MMP2, MMP9
Cell adhesion	Vascular cell adhesion protein-1
	E-selectin
Pro-thrombotic change	Phosphatidylserine
	Tissue factor
Infiltrating leukocyte-acquired	Eosinophil peroxidase

The treatment-effective payloads connected to the targeting agent include compounds that either induce thrombosis directly, kill ECs to cause thrombosis indirectly, redirect host immune systems to attack targeted vasculature, or to cause physical changes in ECs that ultimately cause blockage of tumour vessels [176]. Table 1-2 lists potential effector molecules used in vascular targeting research.

Table 1-2 A list of categories and specific treatment-effective payloads used in vascular targeting [176]

Class	**Examples**
Coagulation-inducing proteins	Tissue factor
Toxins	Diphtheria toxin
	Ricin
	Gelonin
Cytotoxic agents	Doxorubicin
	Neocarzinostatin
Cytokines	Interleukin-2
	Interleukin-12
	Tumour necrosis factor-α
Apoptosis-induction	*RAF-1* gene
	Mitochondrial-membrane disrupting peptide
Radioisotopes	Iodine-131
	Actinium-225
	Bismuth-213
Liposomally encapsulated effectors	Arabinofuranosylcytosine derivative

1.2.1.2 Small molecule vascular targeting agents

Small molecule vascular targeting agents differ in their mechanism of action to ligand-directed vascular targeting agents. These agents do not specifically localise to tumour endothelium but aim to exploit structural differences between pathological endothelium compared to normal endothelium such as the enhanced permeation and retention effect common to tumour vasculature [196]. The more common small molecule targeting agents used to date include microtubule destabilising agents or cytokine inducers. Microtubule destabilising agents aim to disrupt rapidly proliferating and immature endothelial cells based on their reliance on their tubulin cytoskeleton to maintain cell structure. These agents are known to have both anti-mitotic or anti-vascular effects that result in reduced tumour blood flow [195]. In earlier tumour vascular targeting studies, the anti-vascular activity was only observed at a dose close to the maximum tolerated dose, whereas direct tumour cell cytotoxicity via mitotic arrest appeared to be the dominant mode of action. The early tubulin targeting studies using colchicine and vinca alkaloids (vincristine and vinblastine) appeared to only have a narrow therapeutic window and only caused vascular shutdown at near-toxic doses in preclinical tumour models [178, 196, 197]. More recently developed microtubule destabilising agents, (combrestatin A4 disodium phosphate [CA4DP], ZD6126 and AVE8062A) appear to induce anti-vascular changes at doses that are less than 1/10 of the maximum tolerated dose [198-204].

1.2.2 Vascular targeting agents in malignancy

Vascular targeting in cancer is an attractive treatment alternative primarily because tumour vasculature may represent a perfect target for the development of ligand-based treatments. This is because of the accessibility of the endothelium and the differences between pathological vessels with those of the normal endothelium. A number of vascular targeting agents have reached evaluation in clinical studies in solid tumours including CA4DP [205, 206], AVE8062, ZD6126, and DMXAA.

CA4DP, a compound isolated from the South African *Combretum caffrum* tree, is one of the more studied vascular targeting agents and is a tubulin-binding agent that is similar to colchicine in

structure [176]. The mechanism by which this is achieved is through inhibition of tubulin polymerisation through binding to a site on the tubulin molecule [209]. This compound has been examined in the experimental tumour setting and has been able to cause vascular damage that results in haemorrhagic necrosis occurring after 1 hour of treatment and subsequent retardation of tumour growth in solid tumour models [198, 201, 208, 209]. Other small-molecule targeting agents have been examined in the cancer setting and include Oxi 4503 [212], AVE8062 [195], ZD6126 [200], and TZT-1029 [211, 212].

Vascular targeting in cancer treatment has also been explored using ligand-directed vascular targeting agents [176]. A wide variety of potential targets have been examined in the setting of cancer vascular targeting. A significant proportion of this work concerning PS has been completed by Thorpe et al. [213]. PS is a phospholipid that ordinarily is located on the inner leaflet of the phospholipid membrane. Under certain conditions such as platelet activation, apoptosis, and tumour endothelial proliferation, PS translocates to the external surface [213, 214]. Thorpe's group targeted PS with the use of annexin V and monoclonal antibodies in the oncological setting [213]. Although all of the work to date has been completed in the setting of cancer vascular targeting, recent work has identified PS externalisation in the AVM setting [193].

1.2.3 Vascular targeting in AVMs

Vascular targeting is an attractive alternative treatment for AVMs. Due to the vascular nature of AVMs and the aim of any AVM treatment to occlude the arteriovenous flow, a vascular targeting treatment is an attractive treatment alternative. To achieve such an effect, such a treatment would have to identify a differentiating molecular feature of AVM vasculature from normal brain vasculature and combine a compound to recognise those changes and use it to deliver a pro-thrombotic treatment-effective payload. If this target was present in adjacent normal arterial feeders or the draining vein there would potentially be a risk of causing brain infarction or precipitate a haemorrhage due to vein occlusion. Therefore ligand-directed vascular targeting is an attractive treatment for AVM treatment.

Previous work has demonstrated rapid, small-vessel thrombus formation in irradiated vessels in an animal model using a non-ligand method of vascular targeting of PS with co-administration of tissue factor and lipopolysaccharide [215, 216]. This method of non-ligand vascular targeting of PS has also been described in the cancer research setting [219]. These techniques require the presence of externally located PS as a tissue factor cofactor, to initiate the thrombotic cascade [216-218]. Although the results of these studies are promising, as yet, no method has demonstrated thrombus formation or angiographic evidence of occlusion using vascular targeting. In addition, the toxicities associated with lipopolysaccharides prevent direct translation to the treatment of human AVMs.

The challenge in developing AVM treatments remains the identification of targets that differentiate the AVM nidus from adjacent normal brain vasculature and the AVM draining vein as well as other systemic vessels. While in the setting of cancer vascular targeting these differentiating factors of tumour vessels are known, it is necessary to better understand AVM endothelial structure to identify a potential differentiating factor.

1.3 Arteriovenous Malformation Endothelium Structure

1.3.1 Light Microscopic Features

Many historical studies have assessed the light microscopic features of the AVM nidus [3, 4, 219-224]. McCormick classified the gross anatomical features of large AVMs as a “bag of worms”, with great dilated and thickened venous channels forming a wedge-shaped mass that extends from the superficial leptomeninges deep into the parenchyma. The vessels vary in size and appearance and may be associated with calcification [3, 4, 225, 226]. The overlying meninges are often described as thickened and opacified [3, 4].

Microscopically, the nidus is described as extremely variable and complex with vessels ranging from well differentiated arteries and veins to malformed, thick and thin-walled, hyalinised vessels that do not conform to either arterial or venous appearance [3]. Segmental dilations of the hyalinised vessels are often observed [229, 230]. Large irregular nodules of hyalinised intima and

smooth muscle often project into the vessel lumen resembling ‘endothelial cushions’ [230, 231]. Amyloid-like material has also been reported within the vessel walls [230, 231]. Ossification of the AVM has also been reported in historical studies but is believed to be uncommon [234]. The surrounding brain parenchyma degenerates [235], and surrounding haemosiderin within this tissue indicating past haemorrhage is commonly present [3, 4].

Although the microscopic appearance of the nidus is well accepted, only in more recent publications is the appearance of the perinidal tissue described [234, 235]. The historical studies of perinidal vessels are very limited. Early descriptions of the vessels by Hamby describe the nidal vessels as both convoluted and straight and the peripheral small vessels as plexal in arrangement [222]. Arterioles, venules, and capillaries were identified in the perinidal brain tissue [3, 220, 223, 236]. Abnormal vessels have also been described with no direct connection to nidus [3, 220].

More recent research has assessed the perinidal structure using a computer-assisted, three-dimensional reconstruction method [234, 237, 238]. This technique demonstrated that the perinidal intraparenchymal small vessels form an irregular dilated blood vessel network. This network was identified as perinidal capillaries communicating with arterioles branching from feeding arteries, with venules connecting to draining veins from the nidus, and with arterioles and venules branching directly from the nidal wall. This network was defined by Sato et al. as the perinidal dilated capillary network (PDCN) [236]. This network was noted to be fed by arterioles branching from feeding arteries and small vessels branching from nidal vessel walls and was drained by venules connected to the draining vein or to normal venules in normal brain parenchyma.

The basic structure of the capillaries in the PDCN is normal but the calibres of the vessels are variable and range from 30 to 300 micrometres, 10 to 25 times normal [236]. The authors theorise that PDCN is a dilated vascular network with its origin in the capillary network adjacent to the nidal border of AVMs. The PDCN may not function as a capillary network, but rather mimic tiny AVMs in which the blood flow extends rapidly to the surrounding area via multiple connecting vessels. This proposed network may explain the difficulty in achieving haemostasis within the

AVM perinidal tissue and the risk of haemorrhage in the early postoperative period [234, 239-241].

1.3.2 Ultrastructure

The ultrastructure of AVMs has been assessed in the literature and features have been noted that differentiate them from normal central nervous system (CNS) vasculature [242, 243]. The AVM nidus has been assessed using transmission electron microscopy of AVM tissue that has been microsurgically harvested from patients and compared to normal control cerebral tissue obtained from patients undergoing surgery for epilepsy [245].

The feeding vessels of AVMs have been demonstrated to be identical to normal brain vasculature with an intact basal lamina, tunica intima, and adventitia. The nidal vessels, however, were vastly different to normal CNS vasculature and were associated with an underlying matrix of disorganised collagen bundles with associated smooth muscle [245]. Intact pericytes and smooth muscle cells were also noted in both normal vasculature and AVM tissue and did not appear abnormal. AVM ECs have been noted to be disrupted and abnormal with preservation of the underlying subendothelium, however, these cases may be due to surgical manipulation, electrocautery injury, or preoperative embolisation.

The ultrastructure of perinidal AVM vessels has also been assessed in a similar assessment of resected AVM specimens. Perinidal capillaries were observed to have abnormal ultrastructure of the blood-brain barrier (BBB). The vessels were observed to have absent basement membranes and astrocytic foot processes [245]. This finding has been noted in other resected AVMs with chronic steal related to the malformation [244].

Perinidal ECs have differences to normal CNS ECs. Perinidal ECs have been noted to have fenestrations, a feature that is absent in normal CNS ECs. These fenestrations are 60 to 70 nm in diameter and form an alternative route for diffusion and may signify an absence of the BBB [244]. A proportion of perinidal ECs demonstrate signs of necrosis and apoptosis, which leads to activation of death-associated protein 3, caspase 4, and tumour necrosis factor, and upregulation

of cellular adhesion molecules [245]. This apoptotic process may cause gaps in the vessel wall and allow for extravasation of red blood cells into the surrounding brain. This absence of the BBB may contribute to surrounding haemorrhage from AVMs and associated gliosis and haemosiderin. It may also partly explain the immediate postoperative risk of haemorrhage from AVM resection margins and the possible recurrence of inadequately treated AVMs.

1.3.3 Molecular Structure

It is difficult to assess the molecular structure of true AVMs as all harvested samples in the human setting have undergone surgical resection with thermal injury from diathermy, and, in some cases, they have undergone alternative treatments that may confound results. Additionally, a number of these studies lack an appropriate control tissue for comparison. Future PET imaging may assist in determining the presence or absence of a particular molecule. Some prior animal experimental and human immunohistochemical work has demonstrated that cerebral AVMs exhibit different histological and antigenic properties when compared to brain and systemic endothelium [246-248].

Structural proteins in AVMs are expressed differently to normal brain vasculature. The proteins, fibronectin and laminin, were demonstrated to be expressed in a greater proportion in the AVM subendothelia than control vessels or cavernous malformations, with more laminin expressed in comparison to fibronectin [249]. Fibronectin and laminin are structural proteins that are normally found in basement membranes of normal vascular beds in varying quantities [250-253]. The function of these proteins is thought to be to sustain the structural integrity of the vessel wall by providing a place to anchor endothelial cells to the internal elastic lamina and smooth muscle layers [250, 251, 254-256]. Fibronectin and laminin have also been implicated in angiogenesis and have been noted in varying quantities at different maturation steps [251, 252, 256].

Collagen IV has also been identified in AVMs and has been located within the subendothelial layer [248, 249]. Collagen IV is one of the most abundant matrix proteins located within the normal endothelial basement membrane [259]. Collagen IV has also been identified in the extracellular matrix of newly growing vascular beds from the initial commencement of angiogenesis and

reaches maximal expression in the late maturation phase [252, 253]. It has therefore been suggested that the high expression of collagen IV may support a theory that AVMs are at a stage of angiogenic maturity.

Smooth muscle alpha-actin (SMAα) has also been identified in the tunica media of AVMs to a moderate degree and less than in cavernous malformation endothelium [258]. SMAα is an isomer of α-actin and is normally found synthesised in myoepithelial cells, pericytes, and myofibroblasts [261]. It is found mainly in the smooth muscles as part of the molecular structure of microtubules. It functions as part of the contractile system of the blood vessel wall. It has been suggested that SMAα is a marker of more immature vascular malformations and this is the reason that it is found preferentially in cavernous malformations and not AVMs [249].

AVMs have also been noted to express the three main angiogenic growth factors. This is not unexpected as the features of AVMs reflect a continuing angiogenic process [249, 260, 261]. VEGF has been demonstrated in AVMs in high amounts in both the endothelium and subendothelial region. This is in line with current AVM research and supports the fact that the endothelium is the ultimate target cell for the actions of VEGF [249]. Similar to VEGF, basic fibroblast growth factor (bFGF) has been identified in the perivascular tissue and media of AVMs. This zone of perinidal tissue signifies the interacting area between the surrounding gliotic cells and the adventitia of the abnormal AVM vessels [264]. It has been postulated that the source of bFGF is modified glial cells and fibroblasts of the adventitia within the perivascular tissue [263, 264]. Transforming growth factor alpha (TGFα) has also been identified in high concentration in the endothelial and perivascular layers [249]. TGFα expression within the endothelium of AVMs overlaps the distribution of VEGF. It has been postulated that the angiogenic response of TGFα may be mediated via the upregulation of VEGF [265, 266].

The identification of vascular growth factors has been well validated in other resected AVM studies [267-270]. In addition to the AVM tissue, the presence of these angiogenic factors, except for VEGF, was noted in surrounding brain tissue presumably produced by modified glial cells.

These growth factors support the hypothesis that AVMs arise from a disorder of angiogenesis, however, it is unlikely that they have a specific relationship to vessel type or the clinical behaviour of the lesion [249, 267, 271]. Furthermore, although these targets have been identified within AVM tissue, they are ubiquitously present systemically and in surrounding brain making these molecules non-differentiating targets and not useful in developing a therapeutic intervention.

Pro-thrombotic molecules have also been identified in AVMs in larger proportions than in normal brain tissue. They may assist in the contribution to the vascular shift of the coagulation balance towards a pro-thrombotic state. Immunohistochemical evidence from resected AVMs suggest that some of these compounds are increased. A uniform distribution of increased expression of von Willibrand's factor (vWF) has been demonstrated in non-irradiated AVMs [246, 248]. vWF is a high molecular weight glycoprotein that plays a critical role in haemostasis by interacting with platelet membrane receptors [272, 273]. The endothelial anti-coagulant thrombomodulin (TM) has also been noted in AVM endothelium. TM is an important anti-coagulant and binds to thrombin and the resultant thrombin-TM complex activates the anticoagulant, protein C [274-276]. To date no thrombotic molecule has been demonstrated to be increased in AVMs compared to normal vessels [246].

Tissue factor (TF) has also been demonstrated to be increased in AVM tissue [277]. TF is a transmembrane receptor for Factor VII/VIIa and is constitutively expressed by cells surrounding blood vessels, but not on the endothelium. Damage to the vessel wall can result in exposure of TF on underlying cells or substratum or can induce TF production in the endothelium [280]. Once the TF/Factor VII/VIIa complex is formed it is a key initiator of the coagulation cascade via the extrinsic pathway. This procoagulant substance is normally prevented from inappropriate activation of the clotting cascade due to the physical separation from the blood stream and its circulating ligand by the intact endothelium [281]. Studies of resected AVM samples have demonstrated increased TF upregulation within the adventitia and perivascular region, but no increase within the endothelium [280]. Although these three thrombotic compounds have been

identified in AVM vessels, they have also been demonstrated in normal, non-AVM cerebral vessels [246]. The thrombotic molecules do not, therefore, provide a useful differentiating feature for the development of future treatments in untreated AVMs.

Several inflammatory markers have also been identified in resected AVM tissues. This is not unexpected as inflammatory proteins are likely to be implicated in the development of AVM vasculature as well as in AVM response to various insults such as hypoxia, embolization and radiation treatment [247, 281]. The molecule CD31, or platelet endothelial cell adhesion molecule 1 (PECAM-1), has been identified with high expression within the endothelial layer of AVMs as well as that of normal brain endothelium. CD31 is a transmembrane glycoprotein that has multiple functions in various physiologic and pathologic pathways including leukocyte detachment, platelet activation, T-cell activation, angiogenesis, atherosclerosis, and maintenance of vascular integrity [282-286].

Other selectins, a group of inflammatory proteins have also been identified in AVMs. These proteins are a family of transmembrane glycoproteins that are important inflammatory mediators by facilitating leukocyte rolling and adhesion in addition to platelet adhesion to the endothelium. E-selectin was not noted in normal brain vasculature but was significantly upregulated in AVMs relative to normal vessels. Further increase of endothelial E-selectin was noted in AVMs that had been embolised [247]. E-selectin (or CD62E) is a cellular adhesion molecule and similar to others in the family it mediates the rolling of leukocytes along the endothelium at sites of inflammation [287, 288]. It has functional roles in granulocyte rolling [291], and stable adhesion of leukocytes to microvascular endothelium [292] that overlap with the functions of another adhesion molecule, P-selectin (CD62P) [291].

P-selectin was demonstrated in moderate to strong expression within the endothelium of AVMs as well as normal cerebral arteries. In addition, many AVMs demonstrated faint staining within the subendothelium [292, 293]. P-selectin is a mediator of adhesion for leukocytes and is normally expressed in activated platelets and endothelial cells [294-296]. Although in the setting of the

endothelium, P-selectin has been clearly demonstrated to be involved in leukocyte and platelet rolling [297, 298], its role in platelets is less clear. It has been postulated that P-selectin may have a role in haemostasis regulation [299, 300], and a direct function in activated platelet scavenging [301, 302].

The cellular adhesion molecules (CAMs) were assessed in a study examining post-surgical AVM specimens [247, 303]. Vascular cell adhesion molecule-1 (VCAM-1) or CD106 expression has not been noted in normal cerebral vascular tissue but has been identified in AVM endothelium. Expression was further increased in those AVMs that had undergone preoperative embolisation [247]. VCAM-1 is a member of the immunoglobulin gene superfamily that mediates leukocyte binding to the endothelial cell through its interaction with its integrin counter-receptor, very late activation antigen-4 (VLA-4) [304-306]. VLA-4 is selectively distributed on monocytes and lymphocytes but not neutrophils. Therefore VCAM-1 has a specific role in mediating mononuclear leukocyte-selective adhesion [306-310].

Intercellular adhesion molecule-1 (ICAM-1, or CD54) upregulation was noted in AVM tissue, similar to VCAM-1. Faint expression was noted in one specimen of non-AVM brain vasculature with the other samples not demonstrating upregulation [247]. ICAM-1 is a single-chain membrane glycoprotein that in addition to endothelium is expressed on cells of the monocyte-macrophage lineage, B lymphocytes, plasma cells, and on both memory and activated T lymphocytes [311]. ICAM-1, similar to VCAM-1, plays a critical role in leukocyte adhesion during the inflammatory process [311]. In addition, ICAM-1 is also involved in leukocyte-endothelial cell interaction and cell differentiation [314]. Both cellular adhesion molecules (VCAM-1 and ICAM-1) were demonstrated using *in vivo* imaging within an extracranial AVM rat animal model [313-316]. It is clear that inflammatory molecules are upregulated in AVMs and may implicate inflammation in AVM pathogenesis.

There is evidence to suggest that the endothelium of AVMs possesses different molecular properties than normal cerebral vasculature. Unfortunately, however, to date there is no

sufficiently differentiating target that would allow the development of a vascular targeting technique. In order to develop an effective targeting technique for AVM treatment it is necessary to then develop a method to create the presentation of targets through evoking changes in the endothelium.

1.4 Changes to Arteriovenous Malformations Post-Radiation

Although differences have been observed in AVMs with reference to normal systemic and cerebral vasculature, these differences are not unique to AVMs. If a targeted treatment were to be developed that would treat AVMs in isolation to normal vessels a differentiating target would need to be identified.

In cancer vascular targeting research, cell injury has been noted to cause certain molecular changes in tumour vascular endothelium [319]. Further research has suggested that the effect of vascular targeting agents may be enhanced through the use of radiation therapy to enhance the therapeutic effect [205]. Furthermore, other research has suggested that it is the damage to tumour endothelial cells themselves that may determine the tumour response to radiation therapy [318]. It is possible that through inducing cell injury with the application of radiation to the AVM, changes in the endothelium may result in the presentation of potential targets that could then be exploited with a vascular targeting technique.

Radiosurgery through such techniques as GKS, is an attractive method to cause localised cell injury because of its ability to target abnormal AVM vessels with high precision and would prevent the targeting of normal brain vasculature and the draining vein. Standard radiosurgery is believed to cause AVM vessel occlusion through a combination of endothelial dysfunction, smooth muscle cell proliferation, fibrosis and thrombosis [319-322]. It is important to consider the changes that occur within AVMs following radiation insult to better understand the changes and potentially exploit these differences with vascular targeting. This section will aim to discuss the current understanding of post radiation changes in AVMs, at the light microscopy level but also at the ultrastructural and molecular levels.

1.4.1 Light Microscopy

The histopathological effects of radiosurgery have been well examined in the literature through observation of irradiated AVM tissue samples at the light microscopy level in human settings [319-324], and also in AVM animal models [242, 325]. Radiation-treated AVMs demonstrate a number of changes that appear to be progressive, and ultimately result in vessel-wall thickening with stenosis or obliteration of the vessel lumen [321]. Due to the limited samples and the lack of standard post radiosurgery time points it is difficult to be certain of histopathological changes in the human brain AVM setting.

Initial damage to the vessel appears as injury to the endothelium or subendothelial region. The endothelium becomes denuded or is disrupted and separated from the underlying connective tissue. The intima demonstrates spaces that are infiltrated by leukocytes with deposition of proteinaceous material. These spaces are theorised to be the result of fluid leakage across the damaged endothelium into the intima. Early infiltration and proliferation of spindle cells has also been observed [326].

Following intimal damage, there is proliferation of intimal smooth muscle cells. These appear around the vessel wall circumference and result in concentric or eccentric narrowing of the vessel lumen. There are also variable degrees of thickening of the tunica media and adventitia and in some cases the entire vessel wall thickness has been observed to have a “neoproliferative” appearance. The spindle cells located within the intima and vessel wall stain positively for SMA, and negative for factor VIII–related antigen and have been identified as myofibroblasts [257]. These myofibroblasts have been implicated in the vessel wall proliferation, vessel lumen narrowing and ultimate occlusion of AVM vessels [320, 322, 323].

In later stages following radiosurgery there is progressive cellular degeneration and increased extracellular matrix density. Cellular degeneration was noted through evidence of nuclear pyknosis, decreased cell number and ultimately the loss of SMA immunoreactivity [319, 320, 322]. The extracellular matrix demonstrates increased density and hyaline change. There is

deposition of dense fibrillar collagen which replaces the type IV collagen noted in the previous phase. End-stage vessels demonstrate complete obliteration of the vessel lumen with a uniform dense hyalinisation of the vessel. There is a loss of cellularity and there are few remaining nuclei. Not uncommonly, some end-stage vessels contain one or multiple small endothelial-lined lumina containing erythrocytes within the vessel wall [319-321].

Animal studies have been used to replicate AVMs and to observe the changes post-radiation. Although these studies have the added advantage of being able to assess the temporal quality of post radiation changes, the resemblance to human AVMs may be variable and whether they completely reflect the behaviour of a human AVM is unclear.

Radiation changes were described using the linear accelerator system in a swine model created from the rete mirabile (RM) [325]. This study aimed to examine the effects of serial doses of radiation from 20 to 90 Gy and followed the animals for a period of 7 months. De Salle et al. identified intimal hyperplasia and progressive thickening of the vessel wall that ultimately led to occlusion of the vascular lumen and thrombosis after 2 months. They also identified a direct dose response with higher doses of radiation, over 50 Gy, leading toward vessel occlusion [325].

Other animal studies have examined the effects of radiosurgery on normal, non-AVM vessels. The first of these examined the effects of GKS on the basilar artery of a cat [329]. This study administered high doses of GKS of 100 to 300 Gy and observed the animal's survival. Histological evidence of intimal hyperplasia was observed with surrounding hypertrophy of the tunica and dose-related fibrosis of the surrounding adventitia. Similar to other studies significant injury to the endothelium was observed [329].

A similar animal model of GKS was conducted in a rat model, treating the anterior cerebral artery with doses of radiation up to 100 Gy and observation up to 20 months [330]. Similar arterial wall thickening was observed in these animals with intimal proliferation. Occlusion was only observed in 1 animal in the highest dose group of 100 Gy [330].

More recently, using a rat animal model proposed by Yassari et al. [329], Kashba et al. examined the effect of GKS in an extra-cranial model AVM [326]. This study examined the effects of a marginal dose of 20 Gy administered to the model AVM. Histological changes were only observed in irradiated animals at 6 or 12 weeks following the radiation dose. The vessel walls were thickened with luminal narrowing. The endothelium in these animals remained intact. No changes were observed at the 1, 3, 7 or 21 day time points [330].

These animal studies demonstrate similar histological changes to the reported effects of radiation in human AVMs, including perivascular fibrosis, subendothelial proliferation, and luminal narrowing [242, 281, 319]. Further work with animal models may be useful in better understanding the early effects of radiation as it is not currently possible to obtain histological samples from humans.

These histopathological changes exhibit clear differences from non-irradiated AVM vessels. It can be postulated that these changes may be reflected both at the ultrastructural level and molecular level. The evidence of endothelial injury may indicate changes of surface protein expression of the endothelial cells that may provide a potential differentiating target for new AVM treatments.

1.4.2 Ultrastructural Changes

Post radiation changes in AVMs have also been observed at the ultrastructural level in a number of surgically-resected human specimens [243, 281, 330].

A study of resected irradiated AVM specimens substantiated the findings of light microscopy studies [283]. Endothelial cell damage was observed with occlusion or partial occlusion of AVM vessels. The ECs showed degenerative nuclear changes and a loss of cellularity. EC death was also observed in irradiated vessels and was found to be directly related to the time lapsed from radiosurgery dose with samples collected 64 months following radiation having more dead ECs than at 48 or 33 months. Similar to the light microscopy studies, hyalinisation of the vessel wall matrix was observed [283].

Neoproliferation of smooth muscle cells has also been confirmed on ultrastructural studies within the tunica media of AVM vessels following radiation. These smooth muscle cells show increased amounts of proliferating microfilaments, large numbers of glycogen particles, and surface vesicles within the cytoplasm. Weibel-Palade bodies have also been identified in smooth muscle cells that have been re-endothelialised [283]. This finding of Weibel-Palade bodies in smooth muscle cells may signify that the smooth muscle cells have a protein storage and secretion function and point to a wider role for vascular smooth muscle cells in vessels having undergone radiation injury [283].

A small scale study of resected irradiated AVM tissue examined the ultrastructural characteristics of the spindle cell population with electron microscopy [332]. These cells had features of typical fibroblasts with ovoid nuclei and a smooth contour with surrounding cisterns of endoplasmic reticulum within the cytoplasm. These cells were surrounded by extensive bundles of collagen fibres located within the extracellular matrix. Other cell types were also noted with similar nuclear morphology to the spindle cells with abundant intracytoplasmic filaments and sometimes prominent nucleoli. A number of modified fibroblasts were noted with folds and indentations on the nuclear contour [332]. These degenerative fibroblasts have been observed in other ultrastructural studies [283]. These cells have a fibrillary system within the cytoplasm that is attached to the extracellular layer of basement membrane. These cells and fibres resemble smooth muscle cells and resemble the contractile myofibroblasts [332]. Due to the limitations of sample acquisition and restricted time points, human AVM ultrastructural studies are limited in providing information regarding post radiation changes over time. In particular, the early ultrastructural changes occurring within an AVM in the days to weeks following the radiation remain unknown. To date no animal study has examined AVM changes following radiation at the ultrastructural level.

Similar to the studies examining light microscopic changes in irradiated AVMs, the ultrastructural changes demonstrate clear changes within both the endothelium and the surrounding tunica media and adventitia. These differences may signify the presence of underlying molecular differences

associated with these structural changes that be exploited in the development of targeted AVM therapies.

1.4.3 Molecular changes

It is important in the development of a vascular targeting technique, to identify molecular differences that can discriminate between abnormal and normal endothelial cells. Identification of such a target in AVMs is challenging particularly as the only differentiating factors in non-irradiated lesions are associated with a pro-angiogenic phenotype [331, 332], or pro-inflammatory cellular adhesion molecules [246, 247, 303], and both are expressed elsewhere systemically in normal non-AVM vessels. In addition, untreated AVM endothelial cells have been noted to be similar to normal endothelial cells [313].

From the histopathological and ultrastructural changes observed in human AVMs treated with radiation it can be postulated that changes must occur at the molecular level. Due to the difficulty in obtaining human AVM samples in the early phase following irradiation, animal models must be relied upon to provide information regarding the molecular changes that occur within the endothelium.

The molecular changes in endothelium have been noted in a number of post radiation models. Early studies using a murine brain endothelial cell line subjected the cells to a single dose of 25 Gy of ionising radiation from a linear accelerator. Expression of pro-inflammatory and thrombotic molecules such as E-Selectin, TF and TM were noted using immunofluorescence techniques [333]. The apoptotic phospholipid, PS, is well established in the literature to translocate to the external surface of the endothelium following radiation treatment [317, 334]. Furthermore, early vascular targeting studies have demonstrated rapid vessel occlusion with the use of a non-ligand targeted approach of PS in an irradiated AVM model [215, 216]. Further studies using animal AVM models have examined the radiation-induced upregulation of the cellular adhesion molecules VCAM-1, ICAM-1 and E-selectin [246, 247].

More recent research has examined the molecular changes using *in vitro* and *in vivo* biotin labelling [326, 335]. These molecules will be considered in further detail below both in terms of the evidence supporting their upregulation following radiation and their potential utility for the development of a targeted therapy for AVMs.

1.4.3.1 Phosphatidylserine

PS is one of the four main phospholipids that is located within the plasma membrane of mammalian cells [338]. PS is ubiquitous amongst all cells and has functions in cell signalling, haemostasis, thrombosis and apoptosis [218, 336-338]. In quiescent cells it has been noted to be almost exclusively located on the cytoplasmic side of the membrane with the outer layer being primarily composed of phosphatidylcholine and sphingomyelin [336, 339, 340]. This normal level of asymmetry is maintained through an ATP-dependent process involving aminophospholipid translocase, which is responsible for the inward movement of aminophospholipids [5, 218, 341]. Importantly, PS is absent from the external surface of vascular endothelial cells in normal tissues suggesting that if an inducing event could be used it may externalise and present itself as a potential target [344].

In response to cellular injury and other conditions, PS can translocate to the external surface where it is involved in phagocytosis and in activation of the coagulation cascade [5, 220, 345]. Induction and externalisation of PS has been noted under various conditions using *in vitro* modelling by hypoxia/reoxygenation, thrombin, acidity, inflammatory cytokines, and hydrogen peroxide [344]. In the case of normal viable cells, PS exposure triggered by surface events cause an influx of Ca^{2+} into the cells [346]. This increase of intracellular Ca^{2+} activates the enzyme scramblase [346], and simultaneously inhibits aminophospholipid translocase [348]. The overall effect of this is to tip the balance in favour of externalisation of PS in the phospholipid membrane [344].

In vivo studies have demonstrated PS translocation to the external leaflet of the phospholipid membrane following irradiation of a rat AVM model following a single dose of 15 Gy administered via GKS [193, 313]. This difference between the irradiated and non-irradiated

animals was noted at 3 weeks following radiation and reached statistical significance at day 84. This area of translocation was found to be localised specifically to the AVM region. In addition, this study noted a baseline level of PS translocation was present in the non-irradiated animals suggesting that PS translocation may occur due to the change in haemodynamics within the arterialised vein of the model AVM [193]. These findings suggest that with the aid of sensitising radiosurgery, PS may be a suitable candidate target for a vascular targeting AVM agent.

1.4.3.2 ICAM -1, VCAM-1

ICAM-1 and VCAM-1 are endothelial cellular adhesion molecules that belong to the immunoglobulin (Ig) superfamily. These molecules play a critical role in acute and chronic inflammation by mediating the adhesion of leukocytes and subsequent leukocyte recruitment [343-345]. VCAM-1 has been noted to be an important modulator of specific lymphocyte and monocyte trafficking, different to ICAM-1 [346]. Evidence suggests that the degree of leukocyte recruitment increases with extent of ICAM-1 and VCAM-1 expression on the surface of endothelial cells [346]. ICAM-1 has been demonstrated to be constitutively expressed on surface endothelium in cultured endothelial cells of both human and murine sources. This has been observed also in the case of VCAM-1, although, to a much-reduced extent [347, 348]. Although they are widespread, the magnitude and kinetics of expression of these cellular adhesion molecules have been noted to vary in an organ and stimulus-specific manner [343, 349].

Radiation has been noted to upregulate cellular adhesion molecules within the endothelial membrane including ICAM-1 and VCAM-1 both in the *in vitro* and *in vivo* settings [346, 350-354]. ICAM-1 expression has been demonstrated to increase in various different organ settings in response to radiation, and in particular in human cerebral endothelial cells [355]. Furthermore, blockade of ICAM-1 in these models has diminished leukocyte infiltration in the hours or days following irradiation. Despite this finding, this molecule has been demonstrated to be upregulated in the later periods following radiation and its function at these time points remains unclear [356, 357]. The role of VCAM-1 in radiation-induced leukocyte recruitment is less clear although it has

been suggested to be an important modulator of lymphocyte and monocyte trafficking [353]. Investigations involving human dermal endothelial cells and human umbilical vein endothelial cells have revealed varying patterns of expression [353, 356, 358]. Later time points have also been assessed in the setting of thoracic irradiation and VCAM-1 has been noted to be upregulated at a later time point after ICAM-1 and remained elevated 1 week after irradiation. Despite this upregulation the function of VCAM-1 in these late time points following irradiation remains undetermined [346].

Both these adhesion molecules have been used to some effect in vascular targeting in multiple contexts [174, 194, 359], including the treatment of malignancy in the setting of Hodgkin's lymphoma [365], the endothelial delivery of anti-thrombotic agents [366], and for targeting of areas of inflammation [367]. Although these findings demonstrate the upregulation of both ICAM-1 and VCAM-1 in these settings spanning the pulmonary, gastrointestinal and general vascular systems and some success in the use of these settings in vascular targeting treatments, they do not demonstrate upregulation in irradiated AVMs.

The upregulation of these inflammatory markers in the AVM setting has been explored both in the setting of *in vitro* brain microvascular endothelial cells and in *in vivo* work using an AVM animal model [313]. The endothelial cells demonstrated an increase in both ICAM-1 and VCAM-1 following exposure to 15 to 25 Gy of irradiation compared to no upregulation in the non-irradiated and 5 Gy irradiated groups. In the *in vivo* setting upregulation of both inflammatory markers was noted irrespective of radiation status due to an elevated baseline expression within the abnormal AVM vessels [313]. This finding from the *in vivo* study suggests that although upregulation was identified it was not identified selectively in the irradiated sample and that due to the ubiquitous nature of these inflammatory markers, they would be unlikely candidates for the development of a vascular targeting technique for AVMs.

1.4.3.3 E – Selectin

E-selectin is a protein of the endothelial cell adhesion molecule family, similar to ICAM-1, VCAM-1 and P-selectin. Similar to the above proteins these molecules play a key role in mediating neutrophil adhesion to endothelial cells [355, 363].

Research that examines the expression of E-selectin following irradiation on cultured endothelium has had varied results [355]. One group has noted up-regulation of E-selectin in human umbilical vein endothelial cell culture occurring within 4 hours of irradiation [356, 364]. A further group has suggested conflicting results of an upregulation occurring within 48 hours using dermal endothelial cells [365]. In the case of human ECs, E-selectin is upregulated at 72 hours after irradiation [355]. It has also been postulated that these adhesion molecules may be further upregulated at even later times, although, unfortunately the current *in vitro* studies have confined their time points to below 72 hours following irradiation and this remains unknown [356, 364-366].

Initial research performed on AVM surgical samples established upregulation of E selectin from 15 human AVM samples. It was also noted that pre-operative embolisation appeared to be associated with an increase in its expression [83, 249, 360][83, 249, 361][83, 249, 361][83, 249, 361][83, 249, 361][83, 249, 361][83, 249, 360][83, 249, 359][83, 249, 358][83, 249, 358][83, 249, 358][83, 249, 357][83, 249, 357][82, 248, 356][81, 247, 355][247, 355, 367]. Although this work suggested the presence of the inflammatory molecule in AVM endothelium it did not establish whether the molecule increased expression following irradiation.

More recent research has noted E-selectin upregulation at 24 hours following irradiation of endothelium with a pattern of expression that was membranous in distribution [305]. Although a statistically significant difference was noted between non-irradiated and irradiated endothelial cell lines, a moderate expression was also noted in normal endothelium [333]. It appears that there is a great degree of variability of the time to upregulation. Although these findings would need to be validated in an *in vivo* model, the high variability (and ubiquitous distribution of adhesion

molecules as a whole) of distribution suggests against the use of E-selectin as a potential target for a vascular targeting treatment method for AVMs.

1.4.3.4 Other targets

Other potential radiation-stimulated targets have been identified using biotinylation for labelling and enrichment of surface molecules for downstream proteomic analysis [326, 335]. These potential novel targets may be more appropriate for a vascular targeting technique. Of particular interest are normally intracellular proteins that appear to become exposed on the endothelial cell surface in response to radiation. They may make highly discriminatory targets and be useful for further work in vascular targeting in AVMs. These will be discussed further in Chapter 6.

1.5 Animal Models of AVM Research for testing AVM vascular targeting

In order to understand the development of brain AVMs and to develop a targeted treatment to cause occlusion it is necessary to develop a model that is closely analogous to the human brain counterpart. Such a model would need to be reproducible and to closely mimic the characteristics of an AVM at both macroscopic and microscopic levels and to mimic the AVM phenotype including enlarged dysplastic vessels, arterialised veins and arteriovenous shunting. Currently, there are two approaches to the development of an animal model, the first to surgically create an arteriovenous fistula and the second using a transgenic animal model using HHT mutations in the endoglin (*ENG*) or activin-like kinase 1 (*ALK1*) genes. A recent systematic review has assessed the reported animal models in both of these examples [372].

1.5.1 Surgical AVM Animal Models

In addition to the model used in the research reported here, seven different surgically formed types were noted in addition to transgenic animal models [372].

1.5.1.1 The Carotid-Jugular Fistula Model

This model was first proposed by Spetzler et al. to explain the phenomenon of adjacent brain tissue swelling and haemorrhage following excision of the AVM. This model was created by forming a

surgical carotid-jugular fistula in cats by anastomosing the rostral end of the common carotid artery (CCA) to the caudal end of the external jugular vein (EJV) with ligation of the remaining vessel stumps. This model aimed to create non-infarction cerebral hypoperfusion by retrograde drainage of the circle of Willis through the formed anastomosis [373]. The model was used in research on cerebral blood flow but was not successful in clarifying the cause or mechanism of adjacent tissue vessel injury [369-371].

Following the lack of success with this model, a modified fistula model was proposed by Morgan et al. in rats. In this example an end-to-end anastomosis of both rostral ends of the CCA and the EJV was performed on the right side and the caudal ends of both vessels and the ipsilateral external carotid artery (ECA) were ligated. This resulted in an arteriovenous fistula between the circle of Willis and the right transverse sinus [377]. This model has been validated for use in examining the normal perfusion pressure breakthrough phenomenon [244, 373, 374], as well as testing of the hypothesis the intracerebral, extracellular norepinephrine relationship to cerebral blood flow levels [380], and the effect of ionising radiation on the blood-stolen parenchyma of hypoperfused brain tissue [376].

A further modification of this model was developed by Bederson et al. to examine the effect of high blood flow and mass effect of AVM lesions and the potential obstruction of venous outflow. This rat model was a similar carotid-to-jugular fistula model and was achieved by a proximal CCA-to-distal EJV anastomosis with contralateral EJV occlusion [382]. The creation of this model resulted in increased torcular pressure and decreased systematic pressure which resulted after one week in venous infarction, subarachnoid haemorrhage, and severe cerebral oedema [382]. From these results, Hai et al. developed a more moderate model of chronic cerebral hypoperfusion with an end-to-side anastomosis between the EHV and CCA on the right side with ligations of bilateral ECAs and the left vein draining the transverse sinus [383]. This particular model has been validated in investigating the normal perfusion pressure breakthrough phenomenon [379, 380].

Larger animal models have been proposed for use in the carotid-jugular fistula model including primates. In these cases the primates were found to be difficult to handle, expensive to create and had complex ethical concerns for their use in research [386]. It is generally accepted that a rodent fistula model is preferable due to their reproducibility and economic viability. Although the fistula resulted in whole brain or hemispheric brain haemodynamic changes, it did not result in regional haemodynamic changes that were similar to parenchymal AVMs.

1.5.1.2 Intracranial Arteriovenous Fistulae

In order to create parenchymal haemodynamic changes and larger animal models were proposed. Numazawa et al. proposed a canine model, because of the larger brain for use in surgical procedures and also because the physiology and haemodynamic aspects of the canine brain were similar to human brains. In this model following a craniotomy a fistula was created by a femoral venous graft with an end-to-side anastomosis of a cortical branch of the middle cerebral artery (MCA) to the superior sagittal sinus (SSS) [387]. This fistula model markedly decreased regional cerebral blood flow within the MCA territory but not in other vascular territories. Re-occlusion of the shunt restored normal patterns of cerebral blood flow within 15 minutes. Despite the effectiveness of this model it was an acute model and the procedure to form the fistula was complex and difficult to reproduce effectively [372].

The main criticism of both intracranial and extracranial arteriovenous fistula models was that the animal models did not have a real AVM nidus. These models were focussed more on the haemodynamic and pathophysiological changes caused by an AVM to adjacent brain parenchyma and not the creation of an AVM itself [372].

1.5.1.3 The Rete Mirabile as a model AVM

The carotid RM that is present in both swine and bovine sources, (and other artiodactyl animals including sheep, goat, oxen and cats) is a unique vascular structure comprised of a tangle of microarteries and arterioles that is located at the site of termination of the ascending pharyngeal

artery (APA) as it enters the cranial base. The RM is located on two sides associated with each carotid artery and connects across the midline. It is supplied by small collateral arteries to ultimately form the internal carotid arteries. During the 1980s, it was proposed that the RM could be used in swine models to resemble an AVM nidus. This technique was used to investigate the efficacy of embolisation and single-dose radiation treatments due to its morphological similarities to an AVM nidus [325, 383-385]. Despite the morphological similarities between AVMs and the RM, they lacked the same haemodynamic characteristics as an AVM nidus is an arteriovenous system compared to the arterioarterial system of the RM. This absence of an arteriovenous pressure gradient is a significant criticism of this model.

This criticism was addressed by Chaloupka et al. who produced a high flow arteriovenous shunt in a swine RM model by inserting a needle through the orbit to create a direct communication between the RM and the surrounding cavernous sinus, effectively creating a carotid-cavernous fistula. The haemodynamic changes of this model were effectively demonstrated with angiography cannulating the APA and demonstrating rapid filling of the RM, cavernous sinus and basilar sinus [391]. Despite this improvement of the model, the intraorbital insertion of a needle gave rise to significant orbital complications and spontaneous occlusion of the arteriovenous shunt which limited its use to only short-term experimental research.

Massoud et al. developed an improvement on the swine RM AVM model by surgical formation of a side-to-side arteriovenous fistula between the CCA and the EJV with ligation of the CCA proximal to the fistula on the right side [387]. Angiography performed in this model demonstrates a pattern that is morphologically similar to an AVM with feeding arteries (the APA), the nidus (bilateral RM), and draining vein (the right APA down to the fistula). This morphological appearance was further validated with haemodynamic measurements and the model was able to be preserved for up to 180 days. Histological assessment of a model after formation revealed transmural changes of the nidus vessels that closely resembled the histopathologic features of AVMs [393]. This model has been well validated in studies examining the haemodynamic

changes of AVMs as well as investigations into embolisation therapy and radiosurgery [389-395]. This model has been modified slightly in other studies and a higher pressure gradient was achieved which was closer to the values found in human AVMs and resulted in a reduced rate of spontaneous thrombosis in the RM [292, 396].

This model, in theory is transferrable for use in other artiodactyl animals that have similar structures of carotid RM, however, the majority of work is confined to swine and this remains unknown. A small-scale feasibility study has been conducted in sheep. The vascular structure of the RM differs in sheep compared to swine. A sheep AVM model was able to be formed by performing a side-to-side anastomosis of the CCA and the EJV with ligations of the vein above and the artery below [295]. On angiography the morphological features appeared to mimic human AVM's, however, this model has yet to be validated. The sheep model is a simple and cost-effective model and may be adopted in future AVM research.

1.5.1.4 Extracranial Venous Plexus as the AVM Nidus

In 2004 Yassari et al. described formation of a rat model AVM by ligating the left EJV at the confluence of the subclavian vein and performing an end-to-side anastomosis of the EJV to the CCA [329]. The rodent setting is an attractive option due to the venous anatomy of the rat and the simplicity of the anastomosis when compared to other animal models. By anastomosing the caudal end of the EJV to the CCA. The retrograde blood flow along the jugular then splits into several smaller branches that resemble the small branches of an AVM nidus. These branches then coalesce to form the sigmoid and transverse sinuses which resemble an AVM draining vein. In this model, flow can be assessed from the 'feeding' artery and arterialised vein. The entire system can also be assessed with a formal angiogram performed by cannulating the femoral artery [142, 216].

This particular AVM model differs from previously described models. The location of the created AVM nidus remains constant and with technical training the surgical creation of the model AVM is reproducible. The technical considerations of this model are further elaborated in Chapter 2 (Section 2.1).

This model has been validated extensively and has been shown to have similarities to the human brain AVM counterpart [280]. This study examined the haemodynamic and histological characteristics of both the animal model as well as human brain AVMs. From this study these similarities have been confirmed at the histological and ultrastructural level where the similarities included the heterogeneity of the vessel size and wall thickness. The arterialised venous vessels also demonstrated an increase in collagen deposition, splitting of the elastic lamina, multiple layers, and the formation of endothelial cushions. Also present was evidence of immature features of the endothelial cells including numerous filopodia on the luminal surface, fenestrated processes, lysosomes, cytoplasmic vesicles and vacuoles on the endothelial lining [280].

From a haemodynamic perspective, this rat model had increased blood flow rates within the arterialised vein in a linear fashion to a maximum flow rate at 42 days following fistula creation. Although these findings were not able to be compared to flow data from human AVM samples, the observed morphological changes at that same time point were postulated to be caused by the high flow rates and associated shear stress [280].

Using this model, a number of studies using immunofluorescence have established an increase in endothelial expression of inflammatory markers such as P- and E-selectin, ICAM-1, VCAM-1 and PECAM-1 [247], and thrombotic molecules such as vWF and thrombomodulin [246]. Using similar immunofluorescence techniques and *in vivo* imaging, endothelial expression of inflammatory markers has also been identified in this rat AVM model [303, 313]. Although no direct comparison exists, this evidence would suggest that the molecular expression of a number of these targets is shared between human brain AVMs and our extracranial rat model AVM.

Despite the validation of this model it has a number of limitations. Although the venous drainage of the model does extend intracranially, this model is extracranial with the arterialised vein and nidus all located in the neck. Although there have been morphological similarities noted with brain AVMs it is not known whether there may be endothelial molecular differences that differentiate AVMs located intracranially versus the extracranial AVMs. Although there are

haemodynamic components of our model that resemble an AVM, this model is still an arteriovenous fistula model and due to the uncertain pathogenesis of AVMs it may not signify a true AVM.

Some authors propose that the human AVM endothelial phenotype is the result of a congenital abnormality and not a secondary response [58, 397, 398]. More recent data supports a genetic role in pathogenesis and has implicated *KRAS* mutations causing increased ERK activity and increased expression of genes implicated in angiogenesis and Notch signalling that may give rise to the AVM endothelial phenotype [41, 399]. Other authors propose that these phenotypic differences of AVM endothelium are rather the result of a secondary response to the increased flow through a congenitally-formed arteriovenous fistula. These secondary responses are hypothesised to result from the production of growth factors in response the wall shear stress caused by the fistula [405]. These different theories could potentially result in the presentation of different molecular targets and could complicate the development of a vascular targeting technique that is transferrable to the human brain AVM setting. In the model used in the work reported here, the arteriovenous fistula is surgically (and not congenitally) formed, and the formation of the AVM follows as a secondary effect. This process would favour the latter theory on AVM pathogenesis and not the former [280].

1.5.1.5 AVM-Like Lesion Derived from Implants

Both the models with simulated nidi may share morphological characteristics with human AVMs, however, they are not AVMs located within the brain parenchyma. Pietila et al. have attempted to address these criticisms through their method of inducing an AVM lesion within a canine brain. In this example a vascular bypass was formed between the MCA and the SSS through the interposition of a superficial temporal artery (STA) segment. This was achieved by taking a muscle graft supplied by the interposed vessel segment and implanting it in the blood-stolen brain area from the arteriovenous shunt [406]. Angiography performed after a 6-month period demonstrates the morphology of an AVM with a feeding artery (the STA segment near the MCA), and the dilated draining vein (the STA segment near the SSS). Between these two structures

AVM-like lesions with newly developed vessels were observed surrounding the implanted muscle. This concept of using a pedicle muscle graft as a stimulus for inducing the formation of intracerebral AVM-like lesions was derived from the use of indirect revascularisation procedures performed in Moyamoya disease.

Histological assessment of this model has demonstrated some features that resemble the appearance of AVMs in humans including thickening and fibrosis of the draining vein wall, neovascularization, vascular proliferation, and surrounding brain tissues with signs of ischaemia and haemorrhage. This model may be useful in understanding the pathogenesis of AVMs but is limited due to the surgical technology required for its performance [372].

1.5.1.6 Xenograft Arteriovenous Fistula

This model was created to better understand the mechanism by which radiosurgery achieves obliteration of the AVM nidus and to assist in the development of pharmacological therapies to improve the radiosurgery's occlusive effects. In this model a segment of main arteries was harvested from transgenic mice and interposed between the caudal end of the CCA and the rostral end of the EJV in immune-deficient nude rats [402]. The arterial graft was not a true AVM nidus; however, it shared some haemodynamic features of an AVM with a low resistance and high flow. The decision was made to use a murine donor due to accessible transgenic mice but due to the small size of the animals homotransplantation was not possible and rats were chosen as a receptor for the implantation.

This model has been validated and has been used to investigate the effect of radiation treatment on arteriovenous fistulae. A distinct radiation arteriopathy was observed in the graft that resembled the radiation arteriopathy observed in human AVM specimens that had undergone radiation treatment. A further study has used these implanted fistulae to detect radiation responses in *ENG* and eNOS knockout transgenic fistulae [403]. Despite the validation of this model, its overall angiographic patency was only 50%. In addition, research is limited to a time period of 4 months

for the transplanted tissues to retain their phenotypes due to rejection reactions. These considerations limit the use of this model in AVM research [372].

1.5.1.7 Rat Cornea with Human AVM tissues

A further model has proposed that by transplanting human AVM tissues into the corneal micropocket of rats, the angiogenic activity of the implanted tissues could result in the formation of an AVM [404]. The added advantage of this model is that angiogenic activity could be repeatedly measured by assessing microvessel counts and VEGF expression. Using this model, the implanted AVM tissues demonstrated the highest angiogenesis compared to other cerebrovascular disorders, which suggested that AVM nidi were more likely to be active and progressively growing. It was also noted that AVMs that have been previously treated with embolisation were noted to have the highest angiogenic activity [405]. This may suggest why AVM recurrence after embolisation is more common. This method has demonstrated to be of some use in evaluation of molecular mechanisms of the neovascularisation process over time. Despite this utility, this model does not share the same haemodynamic and complete morphological aspects of human mature AVMs which limits its use in AVM research.

1.5.2 Transgenic Animal Models

Brain AVMs are a common phenotype in patients with the inherited condition HHT. The two main subtypes of this include HHT1 caused by loss-of-function mutations in the gene *ENG*, a type III transforming TGFβ coreceptor, and HHT2, caused by mutations in the gene *ALK1*, a type I TGFβ signalling receptor. These conditions are attractive for use to generate an AVM as the prevalence of brain AVMs in HHT1 is 1000 times more likely than the general population, and in HHT2 it is 100 times higher [411]. This high propensity of HHT mutations to cause the phenotypic brain AVM with its large dysplastic, tangled vessels and arteriovenous shunting provides an attractive option for a transgenic animal model to aid translation to the human setting.

Knockout mutation of *ALK1* with splice-site blocking morpholino resulted in a spectrum of morphologic and functional defects with AVM lesions in zebrafish embryos but no reproducible formation of brain AVMs [412].

Early studies examined a transgenic murine model with homozygous deletion of either *ALK1* or *ENG*. This resulted in death in gestation in both examples [408-411]. Further work examined both *ENG* and *ALK1* haploinsufficient mice. These mice did develop vascular lesions in a variety of organs, however spontaneous brain AVMs were only present in a very modest proportion of *ENG* mice and minimal in the *ALK1* mice [57, 412].

Xu et al. reported a transgenic murine model and were able to demonstrate that VEGF stimulation in adult *ALK1* or *ENG* heterozygous mice causes capillary level vascular abnormalities within the brain but not at the macroscopic level [413-416]. In these examples, the AVM-like capillary dysplasia was noted to be more pronounced in the haploinsufficient *ENG* mice than the *ALK1* animals. In addition, increased cerebral perfusion caused by intraventricular administration of hydralazine or nicardipine after the VEGF delivery promoted capillary dysplasia in the *ALK1* mice. These studies, although useful in creating AVM-like microvascular dysplasia were not successful in creating a model that could become a direct model for the disease. This model is useful because the finding of the combination of deletion with VEGF stimulation suggests a response-to-injury cause for AVMs [421]. Following the use of vectors expressing both Cre and VEGF and injecting directly into the basal ganglia of $ALK1^{2LoxP/2LoxP}$ and $ENG^{2LoxP/2LoxP}$ mice the group was able to produce AVM lesions within the adult mouse brain [417, 418]. In this model the cerebrovascular AVM-like lesions were noted to be more severe in the $ALK1^{2LoxP/2LoxP}$ group due to the more effective gene deletion, in contrast to their earlier publications. These transgenic models are promising for examining AVM pathogenesis as well as potentially the development of medical therapies to slow AVM progression and stabilise rupture-prone abnormal vasculature.

The use of the conditional knockout technique with the Cre/LoxP recombination system has also been used to delete both *ALK1* alleles in adult mice using a tamoxifen inducible Cre. This model

has had some success in creating arteriovenous fistula formation and spontaneous haemorrhage, however, the lesions have been confined to the lung, gastrointestinal tract and the uterus and not in the brain [419]. This model has also been attempted in conditional *ENG* deletion mice, which were able to create microvessel abnormalities mimicking a nidus but not the complete AVM features that were described in the paper by Walker et al. [420].

Transgenic models have also been proposed with HHT gene deletions in restricted cell groups. Antenatal deletion of both *ALK1* allelles in restricted endothelial cells has been noted to cause severe, fatal visceral AVMs [421]. A more moderate conditional deletion of *ALK1* in endothelial cells in adult mice was noted to cause multiple site AVM formation within the gastrointestinal tract, lung, around ear-tag wounds as well as within the brain area that had been injected with VEGF expressing vectors. In this case the mice died in 6 to 13 days due to haemorrhage and anaemia [422]. The phenotype observed in these animals was similar to the phenotype observed in animals with global *ALK1* deletion [419]. Similar to endothelial specific deletion of *ALK1*, specific deletion of *ENG* resulted in endothelial proliferation and AVM formation within the neonatal retina and venous hypertrophy within the adult skin when induced by mechanical and VEGF stimulation [423]. Also similar to *ALK1* this model was not successful in generating a brain AVM.

Milton et al. was successful in creating a mouse model with spontaneous brain AVM formation within the brain and spinal cord through deletion of *ALK1* within the embryo by SM22-Cre, which was expressed in smooth muscle cells, endothelial cells, and in some other cell types in various organs [429]. Although most of the mice developed a phenotype with paralysis or death from internal haemorrhage during the first 15 weeks of life, a subset survived this period and had much reduced mortality despite carrying multiple AVMs. A similar model was produced by Choi et al. with spontaneous onset AVMs in $ENG^{2LoxP/2LoxP}$ with SM22-Cre expressed mice. In this example, AVMs developed throughout the central nervous system and gastrointestinal tract with most mice dying prior to 6 weeks [420]. These models may assist with investigation into the pathophysiology

of AVM rupture, however, due to the high mortality and cost associated with them they will have limited use in treatment development.

Despite the promising nature of these HHT-based transgenic models, the use of a HHT model is problematic. The condition carries a reduced spontaneous rupture rate and therefore a reduced risk when compared to the spontaneous counterparts. This may resemble a change in the haemodynamics of the lesion and potentially a different molecular expression on the AVM endothelium. Use of such a model may not assist in translation to the human sporadic AVM setting. In addition, the variable location of the formed brain AVM introduces a level of difficulty in assessing the AVM and in using radiosurgery in a reproducible manner. Finally, the use of a murine animal model provides a level of technical difficulty in performing angiographic assessment of the AVM due to the small size of the vessels and difficulties imaging the AVM intracranially. These difficulties are not present in the surgically formed AVM animal model elaborated above.

Other non-HHT related genes involved in angiogenesis have been proposed for use in a transgenic AVM model. Pathways essential in vascular development and remodelling have been proposed such as the Notch signalling pathway, which was noted to be upregulated in human AVMs [425]. Both Notch loss-of-function and gain-of-function mutations have been trialled in zebrafish and mouse embryos and have been noted to impair vascular development and give rise to arteriovenous shunting. This suggests that Notch activity is critical in the process of angiogenesis [426-428]. A model of postnatal overexpression of constitutively active Notch4 within the endothelium by the tetracycline-regulatory system was able to elicit arteriovenous shunting within the brain, and gene suppression of this reverses the AVM progression. Investigation of this model demonstrated AVM formation from pre-existing microvessels in size of capillaries, without smooth muscle coverage but with high blood flow. This mechanism resembles that of AVM pathogenesis [429]. Similar to Notch4, endothelial expression of constitutively active Notch1 gave rise to AVM formations within the neonatal mouse brain, and in the adult mouse it caused other AVM's and not the brain

[428, 429]. These models suggest that the Notch pathway may be implicated in AVM pathogenesis.

Matrix Gla protein (MGP) has also been implicated in AVM pathogenesis and may be a potential for a transgenic AVM model. MGP is a bone morphogenetic protein (BMP) inhibitor. Increased BMP activity in case of MGP deficiency has been noted to induce the expression of ALK1 and ultimately increased expression of the Notch ligands Jagged 1 and Jagged 2, which cause an increase in Notch activity. The absence of MGP in mice has been noted to cause enlargement of cerebral vessels with direct arteriovenous connections in homozygous deleted mice but not in heterozygous animals. Reduction of Jagged expression by crossing MGP homozygous deleted animals with Jagged deficient mice normalised endothelial differentiation and prevented AVM formation [430]. A similar model involving deletion of endothelial *Rbpj*, a Notch signalling mediator, was noted to result in AVM-like abnormalities in the postnatal mouse brain, including AV shunting and enlarged tortuous vessels. Adult deletion of the same gene did not result in brain AVM formation [431]. These models suggest a congenital pathogenesis of AVMs and may provide an alternative animal model to the HHT mutations *ALK1* and *ENG*.

Transgenic models have demonstrated cerebrovascular abnormalities, AVM formation and spontaneous haemorrhage occurring spontaneously in both directly or conditionally deleted at both antenatal and postnatal stages. In most cases the mouse models demonstrated only minimal cerebral vascular lesions or obvious AVM formation outside the brain. Although these lesions provide simulation of AVM formation, they lack reproducibility and uniformity in lesion maturation, size and location. Focal angiogenic stimulation based on HHT deficiency may help to create adult onset models with mature AVMs that may be suitable for research in both AVM mechanism and therapeutic studies. Further work is still needed to create a transgenic model that is reproducible and uniform.

1.5.3 Summary

Current AVM models are varied and include both surgically formed artificial AVMs as well as AVMs formed from manipulation of angiogenesis-related genes. An ideal AVM model would be one that shares the same anatomical, physiological, biological and clinical features that human AVMs have. Currently, even with the transgenic models, we are not able to reproduce the clinical AVM effectively and much of the pathogenesis of AVMs remains poorly understood. In spite of these limitations, the two models proposed by Yassari et al. and Lawton et al. of extracranial venous plexus and a transgenic HHT mouse model provide the most useful current AVM animal models. The model proposed by Yassari et al., although extracranial and a surgically created fistula, is reproducible and well validated for use in investigation of an AVM vascular targeting technique.

Hypothesis and Aims

Through the use of a ligand targeting technique, a pro-thrombotic compound can be delivered to AVM vessels to cause thrombosis and occlusion of the AVM.

The overall aims of this research were:

- To assess the thrombotic effect of combined radiosurgery and vascular targeting of PS on AVM vasculature in an animal model;
- To test the efficacy and safety of our vascular targeting agent, a conjugate of annexin V and thrombin.

The specific aims of this research were:

1. To assess the safety and optimum dose of the novel vascular targeting conjugate annexin V/thrombin (Chapter 3);
2. To assess the thrombotic effect of the annexin V/thrombin conjugate angiographically and histologically in both irradiated and non-irradiated model AVMs (Chapters 4 and 5);
3. To use immunohistochemistry techniques and preliminary *in vivo* optical fluorescent imaging to investigate alternative vascular targets (Chapter 6).

All the studies involving the rat animal model were approved by the Macquarie University Animal Ethics Committee (Ethics record numbers 2014/035, 2015/026 and 2018/018). Sprague-Dawley rats were used at 5 – 6 weeks of age with a weight range of 200 – 250 g. A surgical arteriovenous fistula was created between the CCA and EJV in line with previous descriptions of the model [329]. Anaesthesia was induced using inhalational isoflurane with initial induction dose at 5% with O_2 at 0.2 L/min and maintenance isoflurane dose at 2%. Preoperative analgesia was administered to each animal via a subcutaneous injection of Carprofen (50 mg/mL at 5mg/kg) and 5 mL of sterile normal saline was administered via an intraperitoneal injection.

The rat was placed supine with the neck extended and supported by a gauze neck rest positioned transversely. The anterior neck was shaved and swabbed with iodine antiseptic solution. After sterile draping, a linear midline incision was performed with an 11-blade scalpel extending superiorly from the manubrium to a point inferior to the most anterior point of the mandible. The subcutaneous tissue and investing fascia were opened anteriorly and divided with surgical scissors and self-retaining retractors were placed.

The left CCA and the left EJV were exposed under sterile conditions using the aid of an operating microscope (Pentero, Zeiss). The left CCA was exposed and dissected free of the accompanying internal jugular vein and vagus nerve. The anterior belly of the omohyoid muscle was divided to expose the length of the CCA. Division of the ansa cervicalis was performed to aid mobilisation of the CCA. The left EJV was ligated with a 10-0 monofilament nylon suture (Ethilon, Ethicon) at the point of union with the left subclavian vein to form the left brachiocephalic vein. Coagulation of the side tributaries of the EJV was performed and specific care was taken to preserve the EJV and manipulate the vessel minimally. The left CCA was then isolated between 2 small temporary aneurysm clips and a 2 mm long arteriotomy was performed with the aid of 10-0 nylon suture to transfix the vessel and a curved pair of microscissors. An end-to-side anastomosis

of the caudal segment of EJV to the CCA with 10-0 nylon suture was performed in a continuous manner (Figure 2-1). This surgical arterio-venous fistula model was based on earlier work and creates a feeding artery (CCA), arterialised vein (EJV), a nidus (branches of EJV), and a draining vein (sigmoid and transverse sinus) [280, 324, 329].

This model has been shown to be morphologically similar to the human AVM vessels [329]. Histologically, the presence of thickened walls, splitting of the elastic lamina, thickened endothelial layers, endothelial cushions, absence of tight junctions, loss of endothelial continuity, endothelial-subendothelial adherent junctions, and luminally directed filopodia have been noted and demonstrated to be similar to the histology of resected human AVMs [280]. In addition to morphological similarities, this model has been demonstrated to be similar to the human brain counterpart from a haemodynamic, ultrastructural and molecular perspective [280, 329].

Following surgical formation of the AVM, the temporary aneurysm clips were removed, beginning with the EJV and proceeding with the distal and proximal CCA. Care was taken to confirm the pulsatility of flow within the anastomosed EJV. Slight massaging of the anastomosis was performed to ascertain whether any thrombus had formed within the EJV. If thrombus had formed, the anastomosis was deemed non-viable, the aneurysm clips were re-applied, and the sutures were removed. If the intima was intact, a second attempt at anastomosis was performed.

Wound closure was performed with 4-0 braided undyed Vicryl (Polyglactin 910) absorbable suture with a continuous suture (Ethicon). Animals were observed until fully recovered from the anaesthetic and were observed twice daily for 48 hours and daily for 1 week following surgery. If signs of distress were observed in animals, post-procedure analgesia was administered (Bupranorphine – Temgesic® 0.01 – 0.05 mg/kg). In line with previous studies, a period of 6 weeks was considered appropriate for AVM maturation from a haemodynamic perspective to achieve maximum flow rates through the anastomosed left EJV [280].

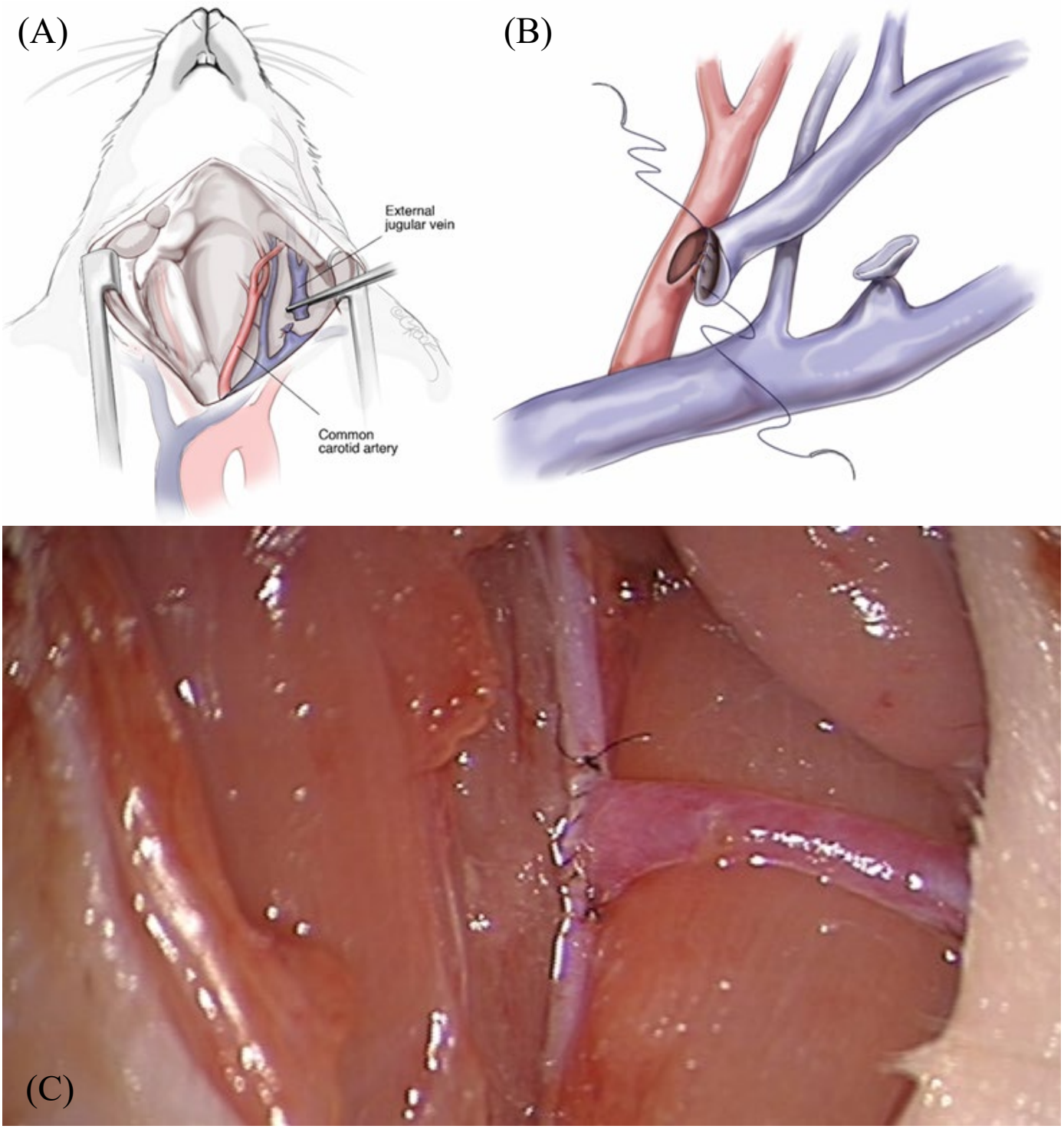

Figure 2-1 Formation of arteriovenous malformation animal performed in a Sprague-Dawley rat. This was achieved by ligating the caudal end of the external jugular vein and performing an end-to-side anastomosis to the common carotid artery (A, B). An intraoperative photo of the final anastomosis is also demonstrated (C) (A and B: Artists images courtesy of Professor Marcus Stoodley. C – original intraoperative image obtained by thesis author).

2.2 Radiosurgery

Radiosurgery was performed after a 6-week period of maturation of the AVM. This was in line with the period noted in earlier studies to cause a maximal change in haemodynamics within the arterialised vein [280]. Animals underwent anaesthesia using an intraperitoneal injection of ketamine (75 mg/kg), and medotomidine (0.5 mg/kg). Adequate anaesthesia was confirmed by pinching the hind paw at the interphalangeal joint and observing for paw withdrawal.

Following anaesthesia, animals were secured in a specially constructed stereotactic frame that was designed to be compatible with the Leksell Gamma Knife stereotactic frame connections. Axial full-body CT scan was performed with 3D reconstruction. The reconstructed CT was used to localise the AVM. Dose planning was performed with a spherical shape with a diameter of 1 cm and centred on the model AVM. A marginal dose of 20 Gy was planned and care was taken to make sure the 50% isodose line did not breach the medial wall of the trachea or oesophagus. This was to prevent post procedural tracheal inflammation and airway compromise. This method has been previously outlined [432]. The planning of the GKS treatment was performed with the aid of Macquarie University Hospital radiation physicists (Moutrie, V).

GKS treatment was performed using a Leksell Gamma Knife (Elekta Instruments, Stockholm, Sweden) at Macquarie University Hospital (Sydney, Australia) (Figure 2-2). The treatment field was planned to cover a larger area of the anastomosis and arterialised EJV to preserve dose homogeneity over the entire arterialised vessel. Following reversal of anaesthesia with atipamezole, (150 µL), via a subcutaneous injection, the animals were closely monitored for evidence of airway compromise and early radiation toxicities. The animals were observed for 1 to 2 hours following reversal of the anaesthetic to determine airway patency and appropriate recovery from the anaesthetic. Postoperative care was performed with twice daily reviews for 48 hours and then daily for a period of 1 week following GKS. Animals had their weight recorded daily and were fed with dietary supplements if weight loss was noted.

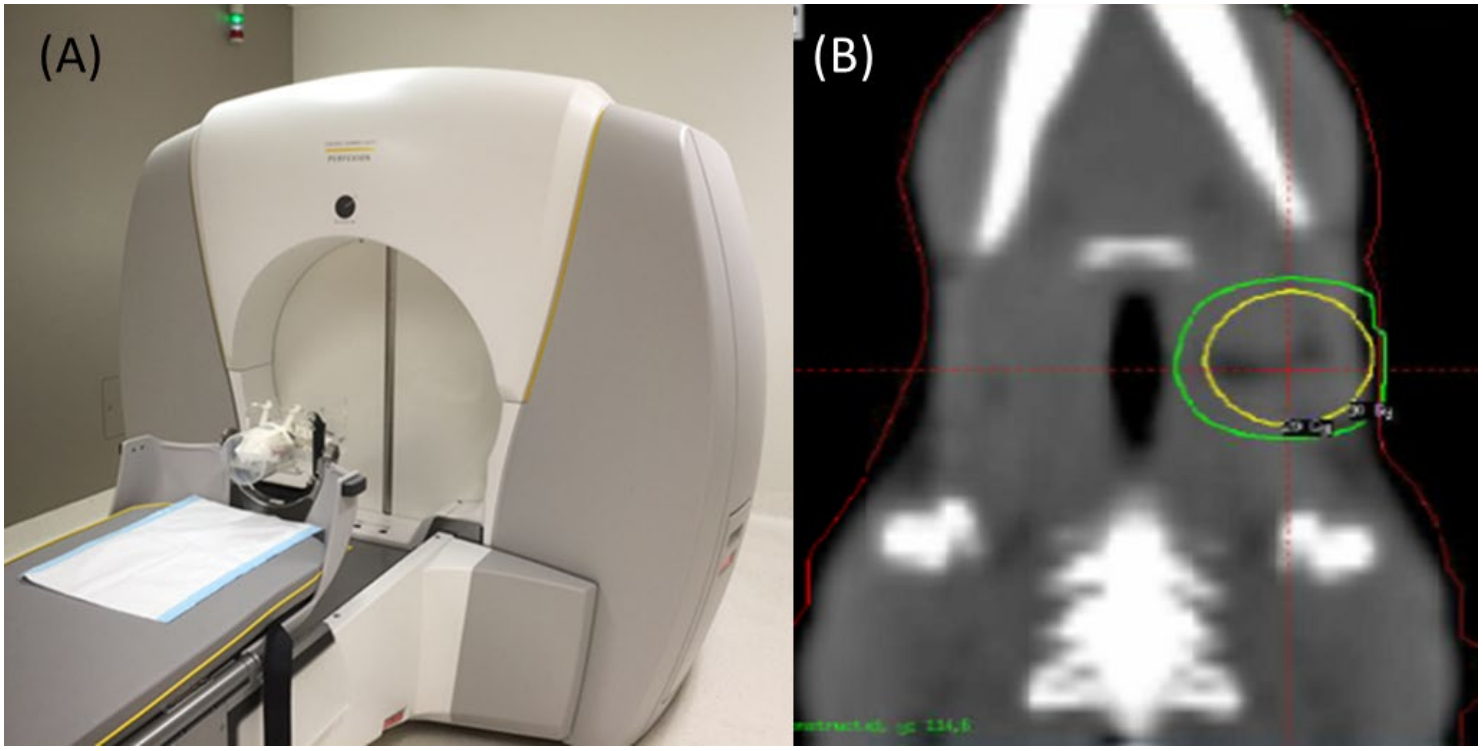

Figure 2-2 Radiosurgery administered to the animals using a Leksell Gamma Knife. Following intraperitoneal administration of anaesthesia, the animals underwent CT planning and gamma knife radiosurgery using a Leksell Gamma Knife (A). A marginal dose of 20 Gy was administered to the model AVM with care not to breach the tracheal mucosa medially (B) (A, B Original images, A obtained by thesis author and B obtained from Leksell Gamma Knife CT planning Software)

Sham GKS was also performed in the comparison animals at the same time points as the GKS animals. Animals undergoing sham GKS underwent intraperitoneal sedation with ketamine and medetomidine using the same dose and method as the GKS animals. Following confirmation of sedation, the animals were monitored for 30 minutes and then the reversal agent atipamezole was administered. The animals were monitored for 1 hour following anaesthetic to confirm appropriate recovery. Animals were reviewed 24 hours following the sedation for sham GKS.

2.3 Angiography

After 3 – 4 weeks following intravenous administration of conjugate, thrombin or saline, the animals underwent an inhalation general anaesthetic using 2 – 3% isoflurane in 0.2 L/min of O_2. Using an operating microscope, the left femoral and iliac artery were exposed. The distal femoral artery was ligated with a 4-0 silk suture (Ethicon). An arteriotomy was performed and a Progreat 2.4 French 130 cm hydrophylic catheter (Terumo) was passed in a retrograde fashion along the external iliac artery to the arch of aorta and the left CCA was cannulated. The catheter was then passed to the point of anastomosis of the EJV under fluoroscopic guidance.

After confirmation of the position of the catheter, approximately 1 mL of Urografin® 76% (Amidotrizoate meglumine 660 mg/mL; Sodium amidotrizoate 100 mg/mL) (Bayer Australia Ltd) was administered and a digital subtraction angiogram was performed. The angiogram was recorded in an AP projection with animal positioned supine and both fore paws secured to the side of the animal with tape. Continuous screening was used, commencing at the time of injection and ceased once the contrast had left the left EJV and fistula region. Following retraction of the catheter the femoral artery was ligated.

The video of the subtracted angiogram was recorded. In addition, a peak opacified image was also recorded to demonstrate the flow of contrast from the proximal CCA to the final emptying into the right brachiocephalic vein. The diameter of the EJV immediately distal to the anastomosis site was recorded and also at the curve superiorly toward the sigmoid sinus. If a stenotic area was

noted on the angiogram the percentage of stenosis was estimated using the image intensifier software.

2.4 Sacrifice and Perfusion

Following the angiogram, the midline anterior wound was reopened, and the anastomosis was exposed on the left side and the right EJV and CCA were also exposed. Blood flow measurement was then performed for the proximal and distal left CCA and the anastomosed left EJV as well as the contralateral right CCA and right EJV using a Doppler flowmeter. Circumferential perivascular flow probes (Transonic Systems) were used in a size to match the specific size of the vessel. The probes were connected to a transit time perivascular flowmeter (TS420, Transonic Systems). Average measurements were recorded over a 5-minute period of monitoring and recorded in mL/min. After blood flow measurement, a photograph was taken of the anastomosis using the operating microscope.

After reconfirmation of the animal being completely anaesthetised, the animals underwent a midline laparotomy and sternotomy with intracardiac perfusion with 200 mL of phosphate-buffered saline with 5000 IU of unfractionated heparin and 400 mL of 4% paraformaldehyde/phosphate-buffered saline was performed. The apex of the heart was accessed with a blunt-tip needle and passed through the left ventricle to the proximal aorta. The insertion point was clamped, and perfusion commenced.

The right atrium was then incised with scissors to allow for egress of the perfusant. After perfusion, the surgical anastomosis was exposed and samples were taken from the left proximal CCA, distal CCA, the anastomosed EJV and the AVM nidal tissue from the anastomosis point to the base of skull. The right sided CCA and EJV were also harvested for comparison reasons. The tissue was post-fixed in 4% paraformaldehyde/phosphate-buffered saline for 48 hours and then transferred to 80% ethanol. Following tissue processing (Leica Tissue Processor), the tissue was embedded in paraffin wax. The tissue was then cut in 5-micron thickness slices (10-micron

thickness for nidus tissue) and stained with haematoxylin and eosin (H and E). If uncertainty was raised regarding presence of a thrombus, a Martius-Scarlet-Blue (MSB) stain was performed.

2.5 Haematoxylin and Eosin Stain

Assessment of the AVM tissue was performed using a standard H and E staining protocol. Tissue segment slides were placed in a 60-degree Celsius drying oven for 30 minutes prior to commencing the staining process. The slides were rehydrated using 3 pots of 100% Xylene for 1 minute each and then 3 pots of 100% ethanol for 1 minute each. The slides were then washed in distilled H_2O in 2 pots for 2 minutes each.

Tissues were then stained in haemotoxylin solution (Stain number, 1.05174.0500, Merck, Australia) for 5 minutes and then rinsed in tap water until the solution cleared. The slides were then stained in lithium carbonate solution (Lithium carbonate saturated solution in 500 mL tap water), for 1 minute and washed in tap water for 5 minutes. The tissue was then stained in Eosin Y Solution (Stain number, 1.02439.0500, Merck, Australia) for 3 minutes.

Dehydration of the tissue segments was then performed with washing the tissue in three sequential pots of 100% ethanol solution for 1 minute each and then in three pots of Xylene solution for 1 minute each. Coverslips were then mounted with Ultramount resin solution (Trajan Scientific and Medical, Australia) and allowed to dry for 24 hours until viewed.

2.6 Martius Scarlet Blue Stain

The Martius Scarlet Blue (MSB) stain is a specific stain for collagen, fibrin, erythrocytes, nuclei and muscle morphology [438]. This stain was used in cases where the presence of thrombus within the AVM nidus and feeding vessels was uncertain. The slides were warmed and hydrated in an identical method to the H and E stain.

Following hydration, the slides were placed in pre-warmed Bouin's fixative (Merck, Australia), in a sealed container at 60 degrees Celsius for 1 hour. The slides were then washed in running tap water. Slides were stained with Celestine blue (Merck, Australia) for 8 minutes. The tissue slides

were then stained in fresh Weigert's iron haemotoxylin solution (Merck, Australia) for 5 minutes. Slides were washed in running tap water for 5 minutes and rinsed quickly in 95% ethanol solution.

The slides were stained in Martius yellow 85% solution (Merck, Australia) for 3 minutes and washed in running tap water. The slides were then stained in brilliant crystal scarlet solution (Merck, Australia) for 15 minutes and immersed in 1% phosphotungstic acid for 10 minutes with running tap water used to clear the slide following each stain. The slides were then stained with 0.5% soluble blue (aniline blue) (Merck, Australia) solution for 16 minutes prior to being washed in running tap water for 5 minutes. Slides were then dehydrated and mounted in an identical method to the H and E stain method.

2.7 Annexin V/Thrombin Conjugate

2.7.1 Rationale

From earlier work there is evidence to suggest that in response to GKS, PS translocation occurs within the endothelium in the Yassari et al. rat AVM model [329]. Although, a baseline level of translocation was observed in the non-irradiated group, the animals undergoing radiation developed an increase in PS translocation in the model AVM at 3 weeks post irradiation that became statistically significant [193]. PS presents itself as an attractive target for the development of a vascular targeting technique. Annexin V, as has been already described, is a protein that binds with a high affinity to PS and would be a possible targeting agent for PS. Thrombin, or factor IIA, is a pro-thrombotic compound that acts to convert a number of factors within the coagulation cascade including factor XI to Xia, VIII to VIIIa, V to Va, XIII to XIIIa and fibrinogen to fibrin [434, 435]. In addition to interacting with these factors, thrombin also promotes platelet activation and aggregation via activation of protease-activated receptors on the platelet membrane [435, 436]. These features would make the use of thrombin an attractive pro-thrombotic compound. The combination of the protein annexin V and thrombin would both recognise the translocated PS within the model AVM and if bound to thrombin cause targeted thrombus formation within that area.

2.7.2 Conjugate Formation

To conjugate annexin V and thrombin, a Lys-to-Lys Protein conjugation system was used (Click Chemistry Tools, USA). The conjugations between the proteins are formed by an inverse-electron demand Diels-Alder cycloaddition reaction between trans-cyclooctene (TCO) and tetrazine (Tz) functional groups, a biorthogonal clock reaction characterised by high kinetics ($k > 800\ M^{-1}s^{-1}$) and selectivity. The Tz/TCO reaction pair is a powerful catalyst-free protein-protein bioconjugation. The fast kinetics of this conjugation enable fast conjugation times of 30 – 60 minutes of lysine containing proteins to each other even at low concentrations of 5 – 10 mM concentrations with > 99% conversion of the limiting protein. Other attractive features of this conjugation technique include long-term stability of the functional groups.

Human recombinant annexin V was used (eBioscience, Austria) and reconstituted in distilled water to achieve a concentration of 1 mg/mL. Human thrombin was used (Prospec, Israel) at 3.46 mg/mL in a solution of 50 mM sodium Citrate, 0.2 M NaCl and 0.1% PEG-8000 with a pH of 6.5. Prior to commencement of the conjugation process the thrombin was diluted to a solution of 2 mg/mL using sterile water.

BupH in PBS (phosphate-buffered saline) was dissolved into 500 mL of ultrapure water and a pH of 7.5 was confirmed. Desalting spin columns (Zeba™ Spin Columns – Click Chemistry Tools, Arizona, USA) were washed three times with the BupH solution in a centrifuge at 1,500 x g for 2 minutes. After this, the thrombin and annexin V were added to separate columns (300 µL each) and were washed through the columns at the same settings.

In line with standard calculations for the conjugation provided by Click Chemistry, the volume of dimethyl sulfoxide (DMSO) added to the labelling components of tetrazine and TCO-PEG2-NHS was determined, with 89.15 µL of DMSO added to TCO-PEG2-NHS and 120.6 µL of DMSO added to tetrazine (after later conjugation trials the amount of DMSO was halved in order to maximise the conjugation process). The labelling agents were vortexed for 2 minutes to confirm complete reconstitution of the stored substance. After complete reconstitution of the labelling

agents, 5 µL per 100 µL of each labelling agent was added to annexin V and thrombin (tetrazine added to annexin V and TCO-PEG2-NHS to thrombin). The tubes were vortexed for 10 seconds and were stored at room temperature for 1 hour.

The labelled thrombin and annexin V were passed through two new washed desalting spin columns in a similar method to that previously described. Following this, the annexin V and thrombin were combined and stored at room temperature for 1 hour. Following conjugation, the combined annexin V/thrombin was stored at 4 degrees Celsius if used immediately and if longer storage was required at -80 degrees Celsius. Prior to administration of annexin V/thrombin conjugate a formal BCA Protein Assay (Thermo Fisher Scientific, Australia) was performed to confirm the concentration prior to dose calculations per animal weight. The method used was supplied with the product.

To prevent any theoretical loss of thrombin activity and prothrombotic therapeutic benefit the conjugate was formed the same day as it was administered to the animals. This negated any need to determine loss of thrombin activity during conjugate storage.

2.7.3 Conjugation Verification

To confirm full conjugation of the labelled proteins a gel electrophoresis was run using a standard Western analysis method. Approximately 1 – 2 µL of sample conjugate, free annexin V and free thrombin was obtained and added to 5 – 6 µL of sample buffer (NUPAGE system, supplier Life Technologies) with 2 – 3 µL of sample reducing agent (10×, NUPAGE). The sample tubes were mixed and centrifuged briefly. They were then heated to 70 degrees Celsius for 15 minutes and then placed on ice for 5 minutes prior to centrifuging and then loading onto the gel.

A standard gel was used (10% Bis-Tris, 10-lane, 1.5 mm – 37 µL loading volume) and this was soaked in Novex MOPS/SDS transfer buffer for 20-30 minutes. The gel apparatus was then assembled and filled with 1 × MOPS-SDS running buffer. The wells were cleared, and a pre-stained protein ladder was positioned in wells on each side of the samples (15 µL per well). The

unit was surrounded with ice and run at 200V for approximately 1 hour or until adequate separation of the ladder was observed. Following this, the gel was removed and soaked in transfer buffer for approximately 20 minutes and stained in Coomassie G250 stain (Thermo Fisher Scientific, Australia) for approximately 1 hour before imaging.

Using this method, the ratios of free annexin V (Molecular weight (MW) ~36 kDa) or thrombin (MW ~37 kDa) to conjugate (MW ≥60-70 kDa) were observed and an estimate of conjugation was determined. Initial conjugate trials demonstrated high amounts of components that had similar molecular weights (~35 kDa) to Annexin V and thrombin and only a small amount of higher molecular weight sample at 60 to 80 kDa (Figure 2-3). The conjugation method was reviewed and a decision to double the concentration of TCO and tetrazine prior to adding to each compound was made. The subsequent gel demonstrates only negligible amounts of protein within the band occupied by the free annexin V and thrombin (30-40 kDa range) (Figure 2-4). There is a wider band of high MW ranging above 80 kDa that is highly suggestive of increased conjugation following the modification of the conjugation method.

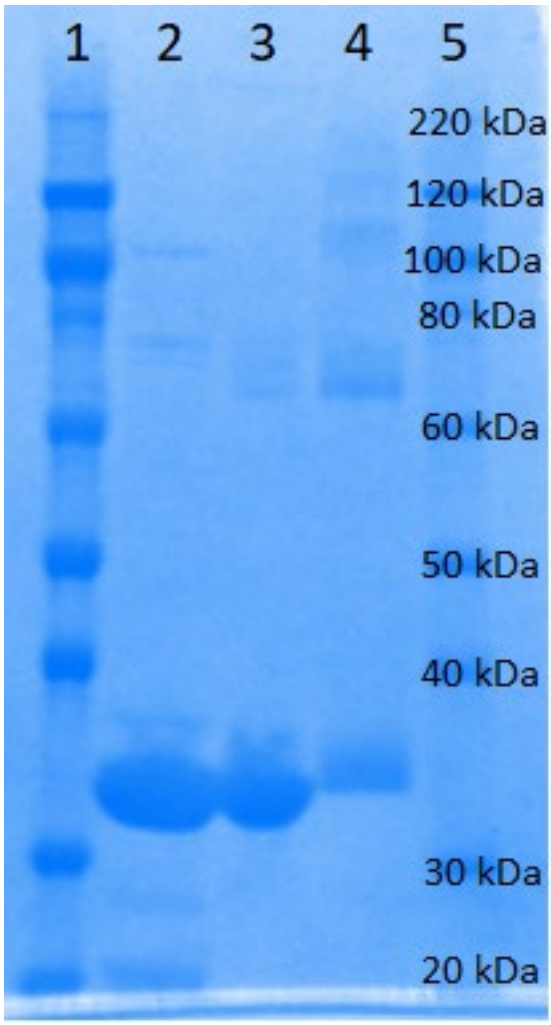

Figure 2-3 Coumassie gel analysis of annexin V/thrombin conjugate and components. Initial gel with conjugate demonstrating in lanes 1 and 4 the protein standard. Lane 2 contains annexin V and lane 3 contains unconjugated thrombin. Lane 4 contains the annexin V and thrombin conjugate.

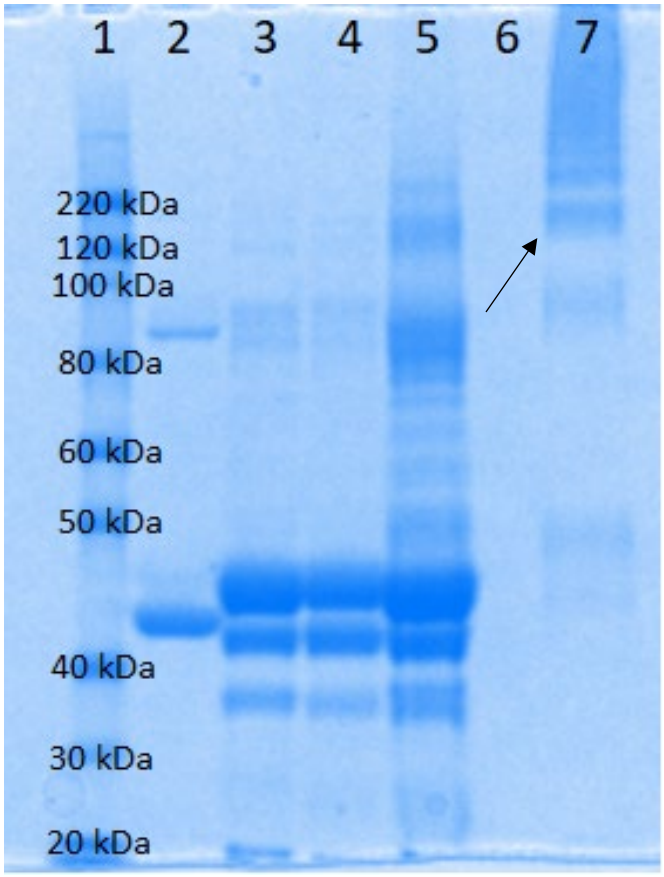

Figure 2-4 Repeat Coumassie gel analysis of annexin V/thrombin conjugate and components. The standard was placed in lane 1. Lane 2 contains free thrombin and Lanes 3 and 4 contain two different sources of annexin V. Lane 5 contains the conjugate demonstrated in the previous figure. Lane 6 is a blank control lane and lane 7 contains conjugate made after the modifications demonstrates almost no small MW components suggesting high amounts of conjugation (arrow).

2.7.4 Thrombin Activity

It was postulated that due to the conjugation process it was possible that a loss of thrombin activity could occur. As such a thrombin activity assay was performed on the formed conjugate using a standard thrombin activity assay (SensoLyte® Thrombin Activity Assay, Supplier Click Chemistry, USA). This assay is performed using a novel internally quenched 5-FAM/QXL® 520 FRET substrate for thrombin. Thrombin cleaves the FRET substrate into two separate fragments which results in the release of %-FAM fluorescence which can be monitored at excitation/emission at 490 nm/520 nm. This thrombin activity assay has been well validated in the literature [437-440]. A standard protocol was used in line with the product comparing the created annexin V thrombin conjugate against the thrombin in serial dilutions of thrombin substrate and fluorescence standard.

Assessment of thrombin activity revealed a fluorescent activity of the annexin V/thrombin conjugate to be a mean value of 1100 at 2 µg/µL and 550 at 1 µg/µL. At a near equivalent concentration of thrombin at 1.6 µg/mL the fluorescence level was recorded as 4700. This would equate to the thrombin activity of the annexin V/thrombin conjugate to be 23% of thrombin at a near equivalent concentration. This would suggest a loss of approximately 77% of thrombin activity through the conjugation process.

2.8 Outcomes and Statistical Analysis

Primary outcomes included angiogram results detailing presence of EJV occlusion or regions of stenosis. Histology was assessed for evidence of thrombus formation within both large vessels and microvessels. Large vessels were defined as those exhibiting evidence of muscularis propria. The EJV was sectioned and assessed for evidence of luminal thrombus. This outcome measure is discussed in further detail in later chapters. Statistical analysis was performed using Fisher exact test and Chi^2 test and 95% confidence intervals were calculated with a Wilson score interval, continuous variables were assessed with a Student's t test (GraphPad Online calculator – GraphPad Quick Calcs Web site https://www.graphpad.com/quickcalcs, Graphpad Prism 8.2 version for

Windows, GraphPad Software, La Jolla California USA, IBM SPSS Statistics for Windows, Version 25.0, SPSS Inc. Chicago, USA).

Chapter 3 Annexin V/Thrombin Conjugate Optimisation

3.1 Background

The use of the Yassari et al. AVM model [329], is well established within the Macquarie University AVM research group and has been validated for AVM research [280, 324]. This model has been used to search for potential targets and to test pro-thrombotic vascular targeting treatments in AVMs [193, 246, 247, 303, 313]. Prior work established the presence of PS translocated to the external membrane of the endothelium in the AVM model in response to radiation [193] and it has thus been postulated that with sensitising radiosurgery PS may be a potential target in irradiated AVMs. Having identified PS as a potential target in AVMs, creation of an appropriate PS-targeting, pro-thrombotic conjugate involves consideration and testing of the ligand or antibody used to selectively target the PS molecule as well as the nature of the thrombotic effector molecule.

A number of potential targeting agents to recognise PS translocation were considered. The protein annexin V has been postulated as a potential targeting agent for PS. Annexin V (or annexin A5) is a protein of 45 kDa molecular weight that is encoded by the gene located on chromosome 4q26-g28 [446], and is a protein that binds with a high affinity to PS in a calcium-dependent manner [447]. The function of annexin V is believed to be anti-thrombotic through binding to PS and preventing its interaction with TF [448], and binding of Factors VIIa and Va to PS [449]. Annexin V has also been proposed to downregulate the cellular surface expression of TF [445].

Annexin V is used extensively in the research setting in fluorescent labelling of apoptotic cells in experimental research [451], and also in a radiolabelled recombinant form that has been trialled in the human setting of molecular imaging of apoptotic cells *in vivo* [447]. In addition to investigation and treatment evaluation, annexin V has been proposed as a PS targeting, drug delivery agent [447]. This has been shown in *in vitro* cell studies in the setting of pancreatic cancer [448], and breast cancer [449, 450]. Annexin V has also been postulated as a therapeutic agent in inflammatory conditions such as atherosclerosis and systemic lupus erythematosus [451, 452].

Because of the high affinity binding to our proposed target, PS, annexin V may be an effective targeting agent for irradiated AVMs.

Tissue factor has been used previously as the treatment-effective payload in non-liganded vascular targeting and shown to be successful in causing small-vessel thrombus formation in irradiated animals but was unable to induce large vessel thrombus formation [215, 216]. Other studies have used truncated TF as a pro-thrombotic agent in vascular targeting in cancer studies [191, 217, 312, 360, 453, 454], where other non-PS tumour targets were investigated. However, it was considered whether the combination of PS targeting and TF as effector molecule may be appropriate for this study. It has been demonstrated that the downstream effect of annexin V binding at PS is to inhibit the coagulation cascade and thrombin formation from prothrombin, through the internalisation of TF at the endothelial surface through endocytosis [448]. Hence, TF may not be appropriate for use specifically with the annexin V ligand. The use of thrombin as the active effector molecule precludes the need for TF presence and activation and hence would be hypothesised to promote platelet activation and fibrin formation within the AVM vessels even if TF were to be internalised by annexin V binding. The theory is that radiation would provide the other essential pro-coagulant surfaces i.e. downregulation of the endothelial anti-coagulant – TM [333], that allows thrombin to have pro-coagulant effects [246]. Hence thrombin was considered for use in this series of studies.

Due to the pro-thrombotic nature of the conjugate and the need to administer the compound intravenously, there is a theoretical risk of systemic thrombus formation due to the externalised PS located outside the AVM or propagation of thrombus causing thromboembolic events. Furthermore, there are no data concerning a lethal dose in rats via the intravenous route of administration. The use of the surgical AVM model proposed by Yassari et al. and the use of GKS is both time consuming and costly [329]. It is therefore important to establish an estimate of maximum safe dose in non-AVM animals prior to conducting experiments with the animal model. Rats without AVM creation provide a useful alternative subject with which to conduct dose escalation studies and determine a safe dose and assess for systemic complications of

thromboembolic events. In addition, it was postulated that by using harvested rat blood and testing the annexin V/thrombin conjugate and free thrombin *in vitro,* that this would provide an estimate for a safe maximum dose of conjugate for use in the rat animal model. In this chapter, preliminary *in vitro* and *in vivo* studies are described to establish a maximal dose of conjugate that would not induce systemic toxicity.

Preliminary work has demonstrated the presence of PS externalised in the endothelium of the AVM animal model. Although this was also noted in non-irradiated animals, there was an increase in PS translocation that began at 3 weeks following irradiation and became more significant with time [193]. Earlier work established that fibrosis and thrombosis of vessels was noted in irradiated vessels at periods greater than 4 weeks following irradiation (unpublished data). Because of this, the time point of annexin V/thrombin conjugate administration was established at 3 weeks following irradiation of the model AVM.

This work was designed to identify both a safe dose threshold and an optimal starting dose for the targeting agent. Once this suitable dose could be identified then a larger scale assessment of the treatment effect of the conjugate could be undertaken. Earlier unpublished work established a dose of 0.384 mg/kg based on research of the maximum safe dose of thrombin in rats and humans [455-457](H. Bandi, unpublished data). Despite this, no dose escalation studies have been performed using the annexin V/thrombin conjugate. These experiments will estimate a suitable dose of conjugate initially with *in vitro* testing and progress to *in vivo* administration in both AVM naïve animals before finally examining dose escalation in the AVM animal model.

3.2 Hypothesis

There is a threshold dose of annexin V/thrombin conjugate that if exceeded will result in systemic thrombosis.

3.3 Aim of this chapter

To establish a maximum safe dose of annexin V/Thrombin for *in vivo* studies in the AVM model.

3.4 Methods

3.4.1 Methods – Dose Estimation – *In Vitro* Dose Response Study ("Slide Rocking Test")

In order to assess the effect of the annexin V/thrombin in an expensive AVM animal model, it is preferable to obtain an estimate of the safe dose before proceeding to further experiments. The use of clot-based assays and citrated plasma or blood are well established in clinical haematology [463]. The citrate prevents clot formation within harvested blood and must be reversed with the administration of calcium chloride and magnesium chloride. The method below is a simple adaptation of these methods in an attempt to obtain an estimate of the ideal dose of our annexin V/thrombin conjugate for further research.

To compare the thrombotic effect of the conjugate it was necessary to compare the times to clot formation with both thrombin, as a positive control, and saline as a negative control on harvested rat blood. The aim of this experiment was to identify a dose threshold when annexin V/thrombin conjugate did not increase clot formation within the harvested blood above that of the saline solution.

Ethics approval was obtained from the Macquarie University Animal Care and Ethics Committee (Sydney, Australia; AEC reference no. 2014/035) for the use of rat blood in these *in vitro* experiments. Animals used primarily for other experimental purposes (e.g. surgical training of AVM anastomosis technique) were obtained just prior to final sacrifice for extraction of blood in the interests of minimising animal use according to the code of practice. Rat blood was harvested via cardiac puncture from Sprague Dawley rats using a 21-gauge needle and 10 mL syringe. Approximately 10 – 15 mL was routinely harvested from a single animal. The blood was stored immediately in three 5 mL tubes, each containing 0.5 mL of buffered sodium citrate solution (0.109 M) to prevent coagulation until ready for the coagulation test when $CaCl_2$ and $MgCl_2$ were added to reverse the action of sodium citrate.

To assess the time to thrombus formation of the annexin V/thrombin Conjugate, three separate experimental groups were used:

1) Human thrombin (Prospec, Israel) (3.41 mg/mL – Specific thrombin activity 3026 NIH Units/mg) –in a 1:200 dilution in 0.9% NaCl solution);
2) Annexin V/thrombin conjugate (as created in Chapter 2, Section 2.7) (1mg/mL (1.47 mL saline (0.9% NaCl with 0.05 mL annexin V/thrombin 1.5 mg/mL (approximately 1:100 dilution));
3) Saline (0.9% NaCl solution)

The choice of dilutions was based on estimated concentration of thrombin in both human thrombin and in the annexin V/thrombin conjugate. The two samples aim to have an approximate similar thrombin concentration of 0.02 mg/mL (the concentration of annexin V solution was 0.05 mg/mL). While this does not take into account the potential loss of thrombin activity that was noted with the conjugate formation, it provides an estimate for future dose escalation studies with the animal model.

Once the conjugates and thrombin were prepared for testing and immediately before assaying, a volume of µL of $MgCl_2$ (75mM) and CaCL2 (37.5mM) was added to the blood in a 1:2 ratio with 250 µL added per 500 µL of citrated blood. This was in order to reverse the clotting inhibition effect provided by the sodium citrate solution added at the time of blood harvest.

Then, a volume of 500 µL of re-activated blood was added to a glass slide with a graduated pipette and after commencement of slide movement on a laboratory rocker, varying doses of annexin V/thrombin conjugate were added in 5, 10, 25 and 50 µL volumes from the diluted conjugate stock. This was to simulate serial dilutions of 1×, 2×, 5× and 10× dilutions. The volumes were matched with the diluted thrombin and saline solutions. Slides were run simultaneously at each dose/volume with thrombin/conjugate/saline and were observed for continuous flow of blood and visible clot formation. Outcomes recorded included the time to visible clot (seconds) and time to cessation of blood flow (seconds).

3.4.2 Methods– Rat animal model

3.4.2.1 Methods - Dose Escalation Test 1 – In Vivo Dose Response - AVM Naïve Animals

The results provided by the previous *in vitro* experiment provided an estimate regarding the ideal dose of the annexin V/thrombin conjugate. The pro-thrombotic conjugate still provides a risk of systemic thrombus formation and potential disseminated intravascular coagulation. It is therefore necessary to examine the systemic pro-thrombotic effect of the conjugate in the animal model prior to its large-scale assessment. This experiment was designed to examine the systemic effect of the conjugate in AVM naïve animals in a dose escalation to provide a baseline safe dose to be used in animals with AVM formation having undergone radiosurgery.

Ethics approval was obtained from the Macquarie University Animal Care and Ethics Committee (Sydney, Australia; AEC reference no. 2015/026). Sprague-Dawley rats were used at weights 250 – 350 grams at 5 – 8 weeks of age. The animals underwent inhalational anaesthetic with isoflurane in the same manner as is described in Chapter 2 however did not undergo AVM creation or GKS (Sections 2.2). Following confirmation of adequate anaesthesia by pinching the hind-paw, the animals underwent tail vein injection with a 25-gauge cannula and a 1 mL needle (Terumo) and administration of annexin V/thrombin conjugate.

The conjugate dose was administered in a 400 µL volume of 0.9% sterile saline, over 1 minute and the cannula was immediately flushed with 200 µL of sterile saline solution. The animals were observed under anaesthetic for 5 minutes and then recovered for 1 hour following dosage administration. The animals were observed daily for 72 hours following injection and weekly for evidence of weight loss or acute thrombotic event that may result in death or disability.

Four separate dosage groups were established in response to the results from the *in vitro* clotting test, with 1 rat allocated to each as follow:

- Dose 1 – 1× – 0.14 mg/kg of annexin V/thrombin Conjugate
- Dose 2 – 2× – 0.28 mg/kg of annexin V/thrombin Conjugate

- Dose 3 – 4× – 0.56 mg/kg of annexin V/thrombin Conjugate
- Dose 4 – 8× – 1.1 mg/kg of annexin V/thrombin Conjugate

The inclusion of the 0.14 mg/kg was based on initial *in vitro* studies and earlier unpublished research (H. Bandi, unpublished research). Although these data suggested that pro-coagulant action of the conjugate increased with increasing concentrations of pro-thrombotic conjugate an *in vivo* threshold dose remains unknown and this was the reason for the increasing dose-doubling treatment groups.

At 2 – 3 weeks following conjugate injection each animal underwent standard isoflurane inhalational anaesthetic and was perfused with PBS and 4% Paraformaldehyde/PBS Solution as per Chapter 2 (Section 2.4). After perfusion, samples of solid organs (liver, lung, brain, and kidney) were harvested and placed in 4% Paraformaldehyde/PBS Solution for 48 hours before undergoing tissue processing as per Chapter 2 (Section 2.4 to 2.6). Following tissue processing and embedding in paraffin wax, 5-micron thickness slices were cut from each sample. Tissue was stained with H and E stain and MSB stain as per Chapter 2 (Sections 2.5 and 2.6) and assessed for thrombus formation.

Outcomes assessed included death, including recording of details if animal had a major event during the injection and in the immediate postoperative phase. In addition, tissue samples were examined by two independent researchers and evidence of thrombotic lesions was documented. The tissue samples were compared to known positive thrombus controls from samples of traumatised liver taken from AVM training animals at time of sacrifice (Ethics number 2014/035).

3.4.2.2 Methods – Dose Escalation Test 2 – In Vivo Dose Response AVM Animals

The previous work established a potential threshold dose of annexin V/thrombin conjugate for use in AVM naïve animals. The distribution of PS is known to be different in animals where an AVM has been surgically formed [193]. It is therefore necessary to determine a similar threshold dose

(and potential therapeutic dose) for AVM animals. This experiment was performed to determine this threshold in animals where AVMs have been surgically formed.

Ethics approval was obtained from the Macquarie University Animal Care and Ethics Committee (Sydney, Australia; AEC reference no. 2015/026). Sprague-Dawley rats were used weighing 200 – 250 g. Standard AVM formation in line with the model by Yassari et al. [329], was performed (Chapter 2 Section 2.1). Following AVM formation, the animals were monitored twice daily for 48 hours and then daily for 1 week.

After a 6-week period of maturation in line with the published model the animals underwent GKS. A marginal dose of 20 Gy was administered to the model AVM. Detailed general methods of anaesthesia, positioning, and GKS are recorded earlier in this thesis (Chapter 2-Methods, Section 2.2).

At 3 weeks following radiosurgery, in line with the *in vivo* research by Raoufi Rad et al. [313], the animals underwent inhalation isoflurane anaesthesia and intravenous tail vein injection of annexin V/thrombin using the method reported in the previous experiment with AVM naïve animals.

From the earlier dose escalation study in AVM naïve animals, a safe dose range was established from 0.14 mg/kg to 1.2 mg/kg. Due to the absence of systemic thromboembolic disease or fatal events, and other unpublished studies (H. Bandi), a baseline dose in line with this research was established at 0.384 mg/kg. In addition to the baseline dose group, two sequential doubling treatment groups were included. The treatment groups were as follows with three animals per treatment group:

- Dose 1 – 1× – 0.38 mg/kg
- Dose 2 – 2× – 0.77 mg/kg
- Dose 3 – 4× – 1.5 mg/kg

Standard post-injection observation was performed in line with the previous experiment. At 3 – 4 weeks following intravenous conjugate injection the animals underwent isoflurane inhalational anaesthetic and the AVM was exposed and inspected.

The animals were then perfused using the standard protocol already described. In addition to solid organ samples, the AVM nidus and major branches were harvested including the proximal left CCA, the distal left CCA, the horizontal segment of the left EJV, and for comparison control vessels, the right CCA and the right EJV (Section 2.4). The distal segment of the left EJV and small venous branches was harvested with the surrounding tributaries and fat was also harvested. The tissue was post-fixed in 4% paraformaldehyde solution for 48 hours and then in 80% ethanol. The tissue was then processed as described (Sections 2.4, 2.5, 2.6).

The tissues were cut and processed with both H and E and MSB stains (Sections 2.5 and 2.6). Microscopy was performed with two independent researchers. Outcomes included evidence of thrombus within the solid organs and the major vessels involved with the AVM nidus (proximal CCA, distal CCA, and left EJV). The nidus tissue was also assessed for evidence of small and large vessel thrombi. Five representative high-power fields (10×) were taken and the proportion of thrombosed vessels against the total vessel count was recorded. Thrombi were classified as either microvessel or large vessel thrombi. Large vessels were determined by the presence of a muscularis mucosa.

3.5 Results

3.5.1 Results - Dose Estimation – In Vitro Dose Response Study (“Slide Rocking Test”)

The addition of human thrombin to the rat blood caused accelerated clotting times and was abandoned at lower doses due to the minimal change in clot formation time observed (Table 3-1). For the annexin V/thrombin conjugate, clotting times increased above thrombin and approached that of the saline group especially at the lower doses. At doses greater than 25 µL (0.0, the annexin V/thrombin clotting times approached that of thrombin (Table 3-1 Time to visible clot and flow cessation in rocking slide test. Figure 3-1). A similar relationship was observed when assessing the time to visible clots in the blood samples (Figure 3-2).

Table 3-1 Time to visible clot and flow cessation in rocking slide test.

	Saline		Thrombin		Annexin V/Thrombin	
Thrombin dose (µg)	Time to clot (secs)	Time to flow cessation (secs)	Time to clot (secs)	Time to flow cessation (secs)	Time to clot (secs)	Time to flow cessation (secs)
1	310	290	255	150	255	195
0.5	300	300	210	120	210	180
0.2	642	615	120	115	320	463
0.1	644	624	167	155	540	523
0.02	290	235	*	*	290	235
0.02-rpt	292	268	*	*	292	268

** denotes absence of thrombin results, due to the minimal change in clotting time for thrombin, this group was abandoned for the lower volume tests of 2 µL and used as a comparison from earlier doses.*

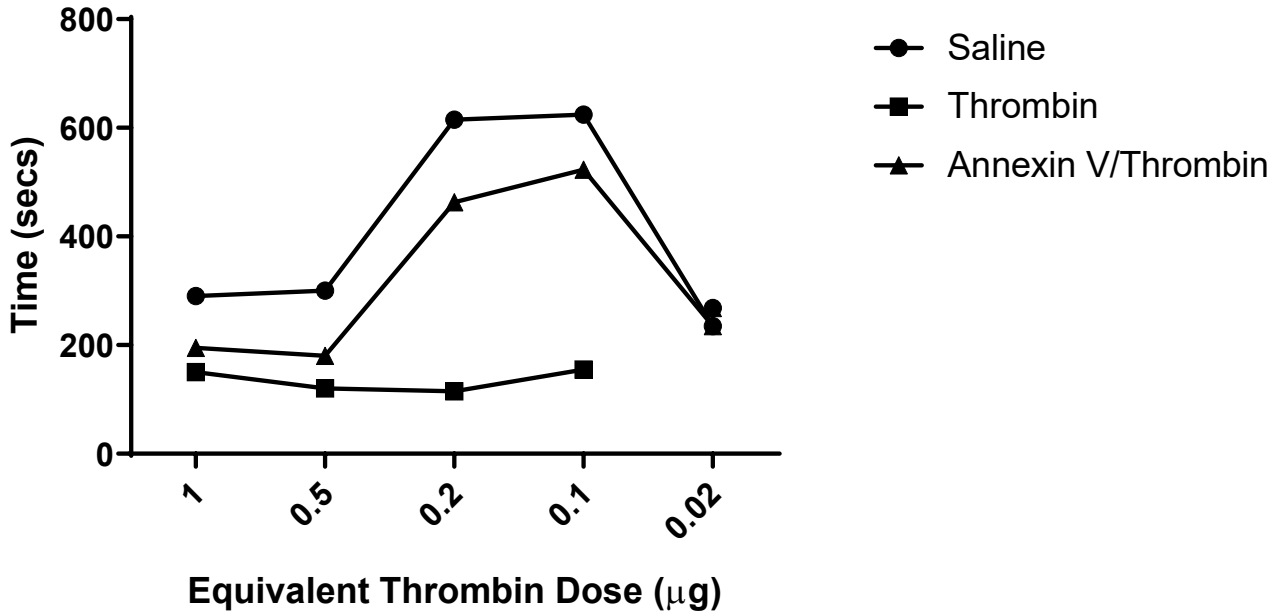

Figure 3-1 Graph of time to flow cessation for serial doses of saline, thrombin, and annexin V/thrombin. Although small sample size, this graph demonstrates that time to cessation of flow of annexin V/thrombin conjugate approaches the value of an equivalent dose of thrombin.

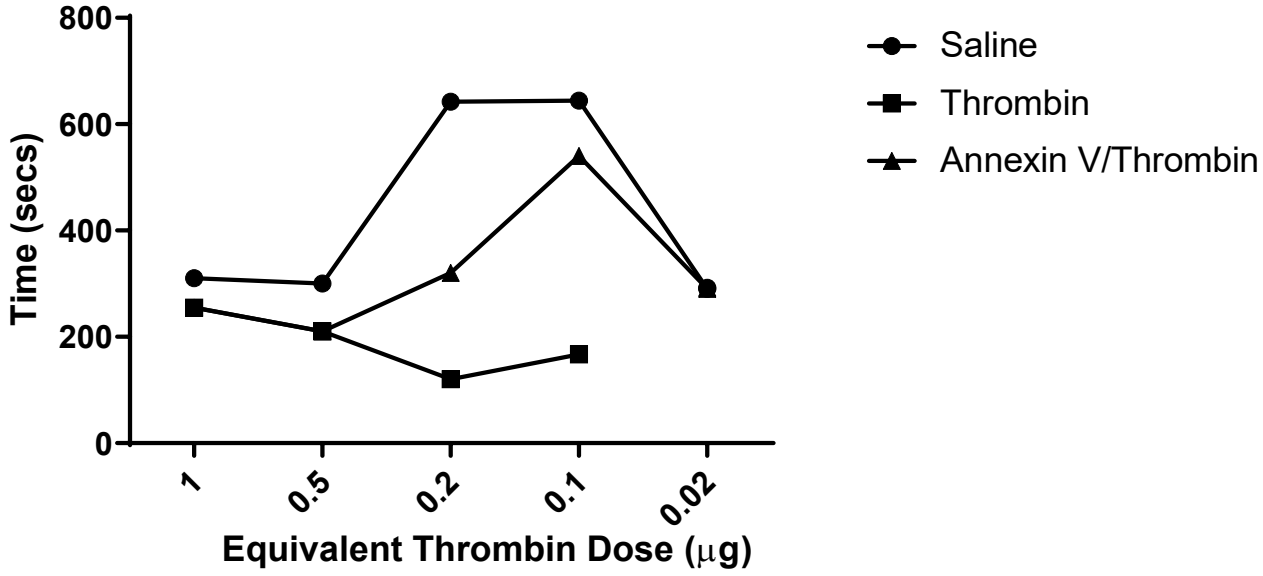

Figure 3-2 Graph of time to visible clot to flow cessation for serial doses of saline, thrombin, and annexin V/thrombin. Similar to Figure 3-1 this demonstrates that the dose of annexin V/thrombin conjugate approaches an equivalent dose of thrombin.

Thrombosis, thromboembolic events and disseminated intravascular coagulation are all recognised complications of increased intravascular thrombin activity [462]. Although this is based on activity of thrombin and not necessarily the concentration or dose of free thrombin it is necessary to establish a safe dose for dose escalation studies *in vivo*.

Thrombosis, thromboembolic events and disseminated intravascular coagulation are all recognised complications of increased intravascular thrombin activity [462]. Although this is based on activity of thrombin and not necessarily the concentration or dose of free thrombin it is necessary to establish a safe dose for dose escalation studies *in vivo*.

The results proposed in this experiment suggested that a threshold exists where if a certain annexin V/thrombin conjugate dose is exceeded; spontaneous intravascular thrombus formation could occur. Therefore, the threshold dose group was 2 µL of 0.05 mg/mL of annexin V/thrombin conjugate. This translates to a dose of 0.0001 mg of annexin V/thrombin conjugate per 500 µL of rat blood as an upper threshold for conjugate administration in animals.

A number of estimates of rat blood volume have been proposed in the literature. The general consensus in earlier work is that rat blood volume equates to approximately 7% of body weight [464]. This value has been derived from simultaneous measurements of plasma volume and red blood cell volume [465, 466]. Other research has suggested that this method of calculating rat blood volume may be an inaccurate measurement as younger rats have been demonstrated to have a larger blood volume relative to their body weight than older rats [460, 461]. The animals undergoing intravenous injection of conjugate in later experiments were planned to be performed at the same time at the same animal age and at similar body weights. The dose of conjugate was therefore established using the 7% body weight calculations and was determined to be 0.14 mg/kg.

3.5.2 Results – Rat animal model

3.4.2.1 Results - Dose Escalation Test 1 – In Vivo Dose Response - AVM Naïve Animals

Earlier work from the *in vitro* test established a safe theoretical threshold dose of 0.14 mg/kg of annexin V/thrombin conjugate. All 4 animals underwent intravenous tail vein injection of annexin V/thrombin conjugate as described. All animals tolerated conjugate injection with no sign of cardiorespiratory complications and recovery was uneventful. No fatal complications were noted in the 72-hour recovery period for all animals. All animals continued to make incremental weight gains from time of injection to sacrifice and perfusion.

Microscopic assessment of all solid organs, (brain, liver, lung, and kidney), did not reveal any evidence of thromboembolic disease on either H and E or MSB stain.

3.4.2.1.1 Discussion

The dose range of 0.14 mg/kg to 1.1 mg/kg appears to be safe for administration in AVM naïve animals and did not cause demonstrable thrombus formation or evidence of fatal thrombotic event or disseminated intravascular coagulation. These findings will need to be validated on a larger scale and in the setting of animals with formed AVMs, and also in animals undergoing focussed irradiation treatment. This pilot study provides evidence of safety to proceed to further dose escalation studies in animals with AVMs.

3.5.2.2 Results – Dose Escalation Test 2 – In Vivo Dose Response AVM Animals

3.5.2.2.1 Overview

Nine animals underwent the treatment protocol with three animals per dose group. All animals underwent AVM creation surgery with no complications. Three animals (one per treatment group) died during the GKS treatment phase of the experiment. On post-mortem inspection, the formed AVM appeared patent and the cause of death appeared to be secondary to retroperitoneal great vessel injury and haemorrhage from the intraperitoneal administration of the anaesthetic.

Both animals in the highest dose group (4× dose group) developed immediate signs of cardiorespiratory instability with agonal breathing. One animal died as a direct consequence of the conjugate injection. The cause of death is presumed to have been an acute thrombotic event. Despite performing a post-mortem and harvesting and inspection of the AVM tissue and solid organs no evidence of acute thromboembolic complication was noted.

3.5.2.2.2 Histological Assessment

Evidence of microvessel thrombi were present in all animals' nidus tissue. All large vessels appeared patent and transverse sections of left EJV, proximal CCA and distal CCA were patent. Similar rates of microvessel thrombi were observed in all three dosage groups with an average of 32% of microvessels thrombosed in the Dose A group (0.38 mg/kg), 22% in the Dose B group (0.77 mg/kg), and 18.4% of vessels in the Dose C group (1.5 mg/kg) (Figure 3-3). Differences between the mean proportions of thrombosed vessels in the treatment groups were not statistically significant.

No histological evidence of thrombi in either macro or microvessels was found on microscopic assessment of all of the solid organs in both H and E and MSB stains (Figure 3-4, 3-5)

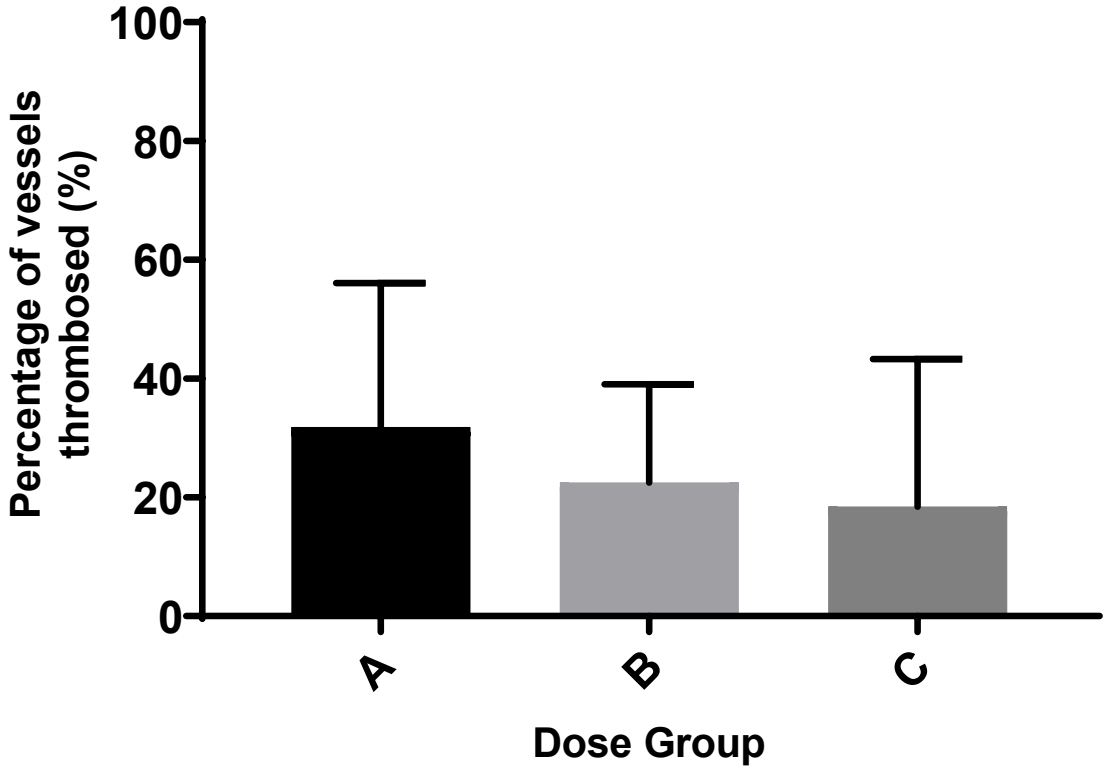

Figure 3-3 Mean percentage of thrombosed vessels present on nidus tissue over five representative high-power fields (10×) with sequential doubled dose groups. An average of 32% of microvessels thrombosed in the Dose A group (0.38 mg/kg), 22% in the Dose B group (0.77 mg/kg), and 18.4% of vessels in the Dose C group (1.5 mg/kg). The differences between the treatment groups was not statistically significant (Student's t test – Graphpad Prism 8.2 version for Windows, GraphPad Software, La Jolla California USA)

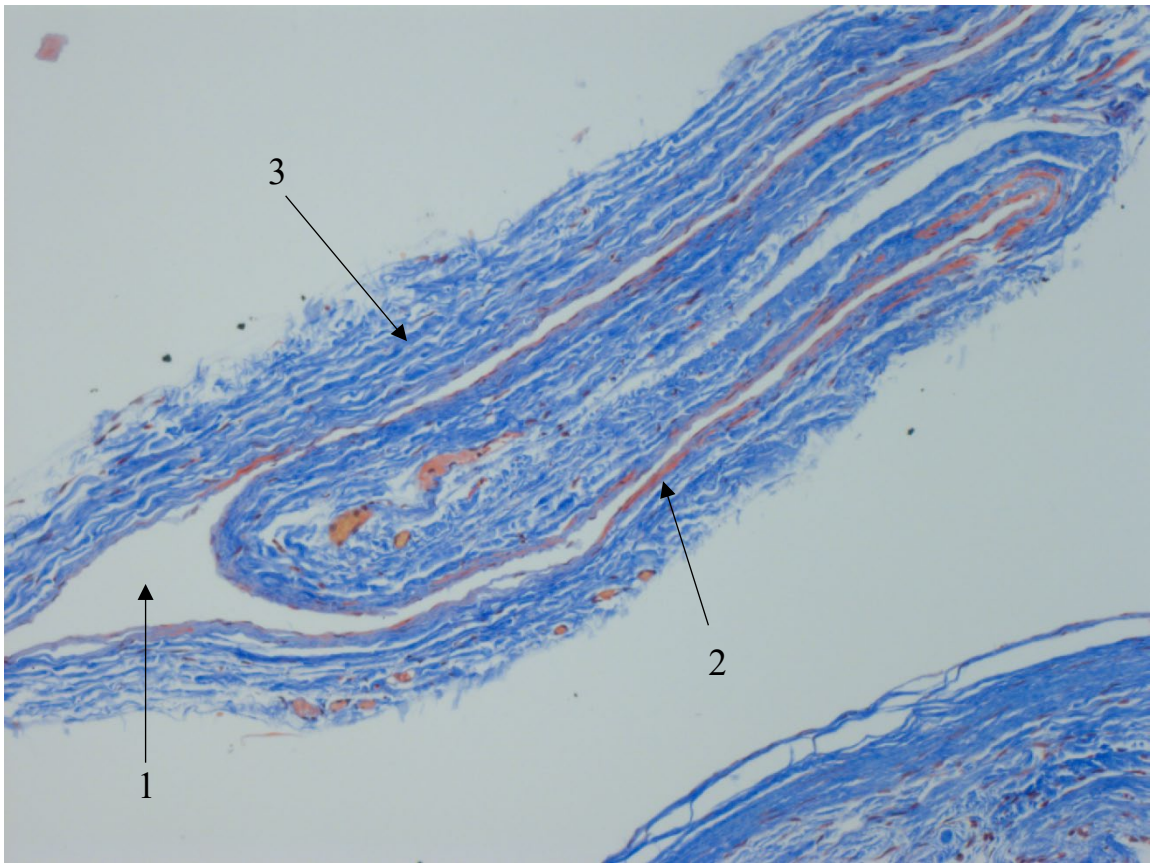

Figure 3-4 MSB stain of left EJV of an animal treated with GKS and 0.38 mg/kg of annexin V thrombin conjugate. This sample does not demonstrate any evidence of thrombus formation. This image demonstrates complete patency of the vessel and no evidence of thrombus (denoted as red on an MSB stain. 1 demonstrates the vessel lumen which was patent. 2 demonstrates the vessel endothelium and 3 denotes the tunica media of the vessel.

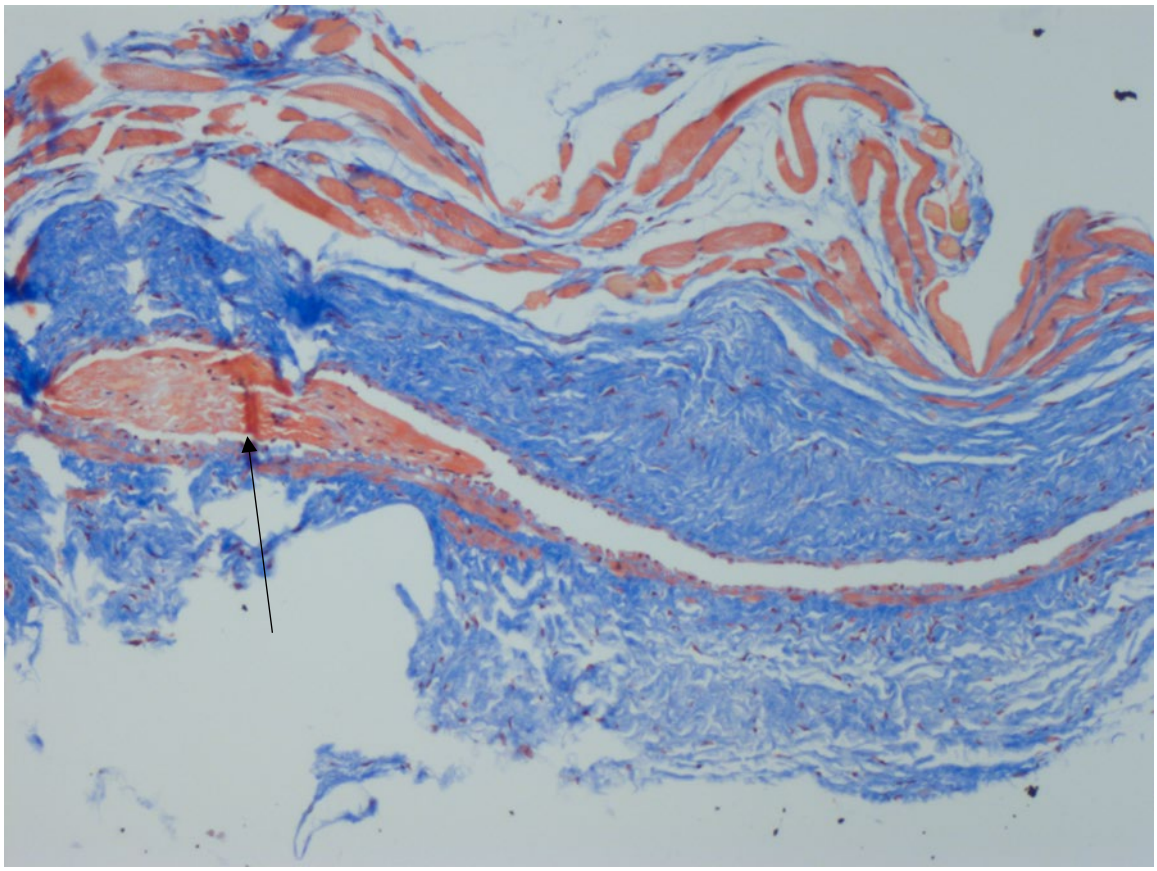

Figure 3-5 MSB stain of AVM nidus tissue with a sample of the EJV in an animal treated with GKS and annexin V thrombin conjugate administration at 0.77 mg/kg. This slide demonstrates thrombus formation within the vessel lumen appearing as red on an MSB stain. The organised thrombus is denoted by the arrow.

3.6 Discussion

3.6.1 Discussion – Dose Estimation – *In Vitro* Dose Response Study ("Slide Rocking Test")

The *in vitro* testing performed in this chapter was an initial attempt to establish a baseline dose of annexin V/thrombin conjugate that will not cause systemic thrombus formation and the potentially fatal side effects associated with this. This is important to establish prior to assessing conjugate efficacy in the AVM animal model. A search of the literature could not identify any data detailing the lethal dose (LD50) of human thrombin if administered via intravascular means. This necessitated a cautious approach to determining a starting dose of the annexin V/thrombin conjugate when commencing dosage studies. Earlier studies established a dose of 0.384 mg/kg based on limited available data on toxicity of human thrombin (H. Bandi, unpublished data).

It was found that the relationship between decreasing dose of annexin V/thrombin and increase in clotting times was not directly linear, as may have been expected. This was evidenced by the 2 µL group, which had a time to clotting that approached the thrombin treatment group. This may have been due to varying concentrations of citrate, $CaCl_2$, and rat blood or other inaccuracies introduced by the method. Despite this inaccuracy, the clotting times of annexin V/thrombin conjugate group did approach the clotting times of the saline control group.

It is important to acknowledge that there are significant limitations of this experiment. The rat blood slide model is not a true physiological model and lacks the surrounding vascular endothelial structure and normal haemodynamic flow that could give rise to systemic thrombosis. It also eliminates the surrounding endothelium that could, in theory, present externalised PS for the annexin V to bind to and result in thrombus formation. In addition, this study was only performed on a small scale (in part due to the limited available rat blood that was harvested). The experiment was intended to be only a rough estimate for further studies to be performed using an *in vivo* animal model. Furthermore, the estimate of thrombin activity in this example is based on concentration and not thrombin activity.

Finally, this study did not attempt to assess either the targeting effect of the conjugate or its effect to cause thrombosis with an irradiated AVM. This experiment aimed only to estimate a maximal safe dose of conjugate for use in the animal model.

3.6.2 Discussion - Dose Escalation Test 1 – In Vivo Dose Response - AVM Naïve Animals

The dose-escalation study in AVM naïve animals provides an estimate of a baseline safe dose of annexin V/thrombin conjugate for use in later dose escalation studies. It was postulated that this baseline dose would not cause systemic thrombus formation if administered intravenously in an animal model. Further work is needed to better estimate the safest effective dose prior to large stale assessment of the conjugate in the animal model.

This study provides further safety information regarding the annexin V/thrombin conjugate and examines thromboembolic complications following intravenous dose escalation. The optimum dose of administration of annexin V/thrombin for use in the AVM model is as yet unknown and these data will help in providing information for use in dose escalation studies within the AVM rat model.

The results of this experiment suggest that in the dose ranges from 0.14 mg/kg to 1.1 mg/kg lethal complications from annexin V/thrombin conjugate injection such as disseminated intravascular coagulopathy are not high. Furthermore, within the limits of the study there was no evidence of extensive systemic thrombosis in the solid organs assessed. This would suggest that in the dose range assessed it would be safe to proceed to use these in the AVM model. These results cover the dose used in earlier studies of 0.3 mg/kg, in which no lethal thromboembolic complications were recorded (H. Bandi, unpublished data).

Although it would seem that the annexin V/thrombin conjugate is safe in the above dose range, the biodistribution and pharmacokinetics of the novel conjugate remain unknown. Furthermore, although PS translocation was noted in the AVM model, the systemic distribution of externalised PS in the rat AVM model remains unknown. These difficulties have been acknowledged in radiolabelled technetium/annexin V, where high uptake in the liver and kidneys presented a

challenge for their imaging techniques [469]. Other reports have also highlighted the internalisation of annexin V in cells exhibiting PS translocation [447]. Although this latter quality may be useful for cancer vascular targeting, our proposed vascular targeting treatment relies on the conjugate to bind to endothelial membrane and allow the active component, thrombin, to activate thrombus formation in the intravascular space. Within our study limitations, we did not observe any evidence of thrombus formation elsewhere, particularly within the liver or kidney to suggest inappropriate uptake of annexin V/thrombin conjugate. This risk of off-target effects remains a concern in the development of a treatment in the human setting. Although no systemic thrombus was noted, an alternative effector compound to be considered is truncated tissue factor (tTF) that may have a more favourable side effect profile. This consideration is discussed further in Chapter 7 and remains an issue that will need to be addressed prior to translation to human trials.

The examination of dose escalation in the rat model, also has limitations. The sample size is small with N=1 per treatment group. The histological assessment of solid organs provides a general overview of common sites of thromboembolic disease. Due to the size of the tissue, and the preliminary nature of this study, it was not possible to harvest and section entire organs and only a representative sample of each organ was processed. It is possible in our assessment of the tissue the thromboembolic segments of the tissue were not included within our representative samples.

In addition, the process of perfusion involves the pumping of approximately 700 mL of PBS and paraformaldehyde through the animals' vascular system at 25 mL per minute. It is possible that with the force and volume of this perfusion that more friable thrombi will be disrupted and not be deducted in the histological samples. This may underestimate the degree of systemic thromboembolic disease caused by the conjugate injection. Despite these limitations, this study is a pilot small-scale study and the results do suggest a safe dose range to proceed to dose escalation studies of the conjugate in animals with a formed AVM.

3.6.3 Discussion – Dose Escalation Test 2 – In Vivo Dose Response AVM Animals

The rat AVM model study examines a dose escalation study of annexin V/thrombin in the setting of a rat AVM model and GKS. This was the first trial of annexin V/thrombin conjugate administration at the time point 3 weeks post GKS [193]. This pilot study was arranged to establish an optimal dose of conjugate for a larger scale assessment of conjugate efficacy.

The results of the experiment suggest that there was a similar thrombotic effect on the microvasculature of all 3 treatment groups. This would suggest a pro-thrombotic effect in our irradiated AVM model although further verification is required with appropriate comparison control groups. A trend was observed that suggested higher rates of nidus microvessel thrombi formation favouring the lower dose group was noted but this was not statistically significant.

The injection related death and the cardiorespiratory instability that was observed in the highest dose group suggests that annexin V/thrombin conjugate administered at that dose level carries the risk of a potential fatal thromboembolic event or haemorrhage from disseminated intravascular coagulopathy. From this information it would be reasonable to assume that either the Dose A or Dose B group would be a safer alternative dose for larger scale assessment of the conjugate.

This experiment has a number of important limitations that must be taken into consideration when interpreting its results. The absence of appropriate control groups in the form of saline and thrombin injection and sham GKS groups makes it difficult to determine the true effect of the annexin V/thrombin conjugate. These treatment groups were also not included in the earlier studies trialling the conjugate assessment (H. Bandi, unpublished data). In a larger scale assessment, it would be important to include such comparison control groups.

The small sample size in each treatment was complicated by one animal sustaining a lethal complication in each treatment group reducing each group to two animals. This may introduce selection bias and provide an inaccurate measurement of the degree of thromboembolic disease caused by the annexin V/thrombin conjugate. Furthermore, due to the injection related death in the highest dose group the animal was not sacrificed at 2 – 3 weeks following injection and

therefore may not have had sufficient time to develop AVM thrombus that was stable enough to not be dislodged in the perfusion process. This may have underestimated the degree of thromboembolic disease in the highest dose group.

The histological outcomes are difficult to interpret in this study. The tissue included in the nidus histological section is highly varied, containing adipose tissue, skeletal muscle, submandibular gland in conjunction with the distal arterialised EJV and its tributaries. The varied nature of the tissue makes it difficult to identify a representative high-power field with a significant proportion of vessels. This may introduce selection bias when assessing the proportion of microvessels thrombosed. Alternative measurements have been proposed in the literature using immunohistochemical methods to detect thrombi with an anti-fibrin antibody [465, 466]. Due to the varied nature of the nidus tissue and different distribution of vasculature, even with the aid of immunofluorescence it is difficult to quantify the level of thrombus formation within the nidus. Future experiments should focus on differentiating between macro and microvessels and a binary outcome of thrombi formation vs patent vessels on consultation of the entire nidus may be easier to interpret and analyse.

Although the reliance on histological outcomes alone for evidence of the conjugate effect provides good information regarding small vessel thrombosis, it does not provide evidence of the degree of occlusion of the larger arterialised vessels distal to the anastomosed left EJV. In the clinical setting, evidence of AVM occlusion is provided by formal digital subtraction angiography. Previous research examining the use of soluble tissue factor and lipopolysaccharide in the Yassari AVM model used formal angiography as an outcome for the vascular targeting treatment. To date, however, no vascular targeting treatment has demonstrated angiographic flow abnormalities [217]. For our model to demonstrate treatment efficacy that is translatable to the human clinical setting it will need to demonstrate large vessel occlusive disease significant enough to cause stenosis or occlusion of the model AVM.

3.7 Conclusion

This study has demonstrated evidence of thrombus formation within our AVM model in a similar proportion in all dosage groups. This suggests that treatment with GKS and annexin V/thrombin conjugate may be successful in causing small vessel thrombus formation, but no thrombus was detected in the larger arterialised EJV. In addition, a dosage threshold has been demonstrated at 1.5 mg/kg, which, if exceeded may result in fatal thrombosis. Within the limitations of the current dose escalation study, the maximum safe dose of annexin V/thrombin conjugate is determined to be 0.77 mg/kg. Further work is needed to validate these results on a larger scale and to include comparison control groups in the form of thrombin and saline and GKS and sham GKS arms. The addition of alternative outcome measures in the form of angiography and flow measurements may assist in providing a more accurate outcome measure of the thrombotic effect of our conjugate and assist translation to the human setting.

Chapter 4 Vascular targeting of PS in the AVM animal model

4.1 Background

Vascular targeting in AVMs has been successful in causing microvessel thrombus formation with tissue factor and lipopolysaccharide [217], and more recently in unpublished data with the novel annexin V/thrombin conjugate (H. Bandi, unpublished). In these preliminary dose response studies, there are promising data to suggest that use of radiosurgery to increase PS translocation prior to the administration of the annexin V/thrombin conjugate may cause thrombosis in AVM vessels. As yet, however, no large vessel thrombus formation or angiographic abnormalities have been demonstrated. Also, no study has compared the use of annexin V/thrombin conjugate against appropriate control groups and its use in non-irradiated animals. Further work is needed to determine the extent of the pro-thrombotic effect of targeting of PS translocation after radiation with an annexin V/thrombin conjugate.

4.2 Hypothesis

GKS sensitisation and the vascular targeting agent (annexin V/thrombin conjugate) will cause thrombus formation in the model AVM in comparison to control treatment groups.

4.3 Aims

- To test the efficacy and safety of the vascular targeting agent, a conjugate of annexin V and thrombin.
- To use the AVM animal model to assess the thrombotic effect of combined radiosurgery and vascular targeting of PS on AVM vasculature.

4.4 Methods

4.4.1 Conjugate administration

The animals underwent the same protocol for AVM creation and GKS as previously described (Section 2.1 and 2.2). This included initial AVM surgical formation, and, after a period of 6 weeks

of maturation, the animals underwent GKS (or sham GKS) with a marginal dose of 20 Gy administered to the model AVM.

At 3 weeks following GKS or sham GKS treatment, the animals underwent injection of saline or pro-thrombotic agent (thrombin alone, or annexin V/thrombin conjugate). This timing was used in line with the previous dose escalation studies (Chapter 3) and the prior *in vivo* research that noted an increase in PS externalisation in our AVM model from 3 weeks after radiosurgery [193].

The animals underwent inhalation anaesthetic with isoflurane and a dose of 0.77 mg/kg of conjugate was administered via an intravenous tail vein injection in a volume of 400 µL over a 1-minute time period. The dose of 0.77 mg/kg was established from the results of the previous dose escalation studies as the highest maximum safe dose of conjugate. Each administration of conjugate (or thrombin or saline) was followed by a flush of 200 µL of normal saline (0.9% sodium chloride).

In order to assess the efficacy of the annexin V/thrombin conjugate, 6 treatment groups were included to examine the effect of the conjugate in GKS and sham GKS groups (Figure 4-1). Control groups were also included of saline and unconjugated thrombin. There were 8 animals per treatment arm (n=8).

Animals administered saline underwent an identical treatment protocol to the conjugate-treated animals with the exception that instead of conjugate dose, an intravenous injection of 400 µL of sterile normal saline (0.9% NaCl) was administered followed by a bolus of 200 µL of saline.

Thrombin dosage was calculated to be of an equivalent thrombin activity to the annexin V/thrombin conjugate, as assessed by the thrombin activity assay (Chapter 2, Section 2.7.4). Therefore, to achieve an activity of 23% of thrombin at an equivalent concentration, the dose per weight of thrombin was calculated to be 0.18 mg/kg. This was distributed into a volume of 400 µL of normal saline and injected over 1 min, followed by a 200 µL bolus, in an identical method to the conjugate injection.

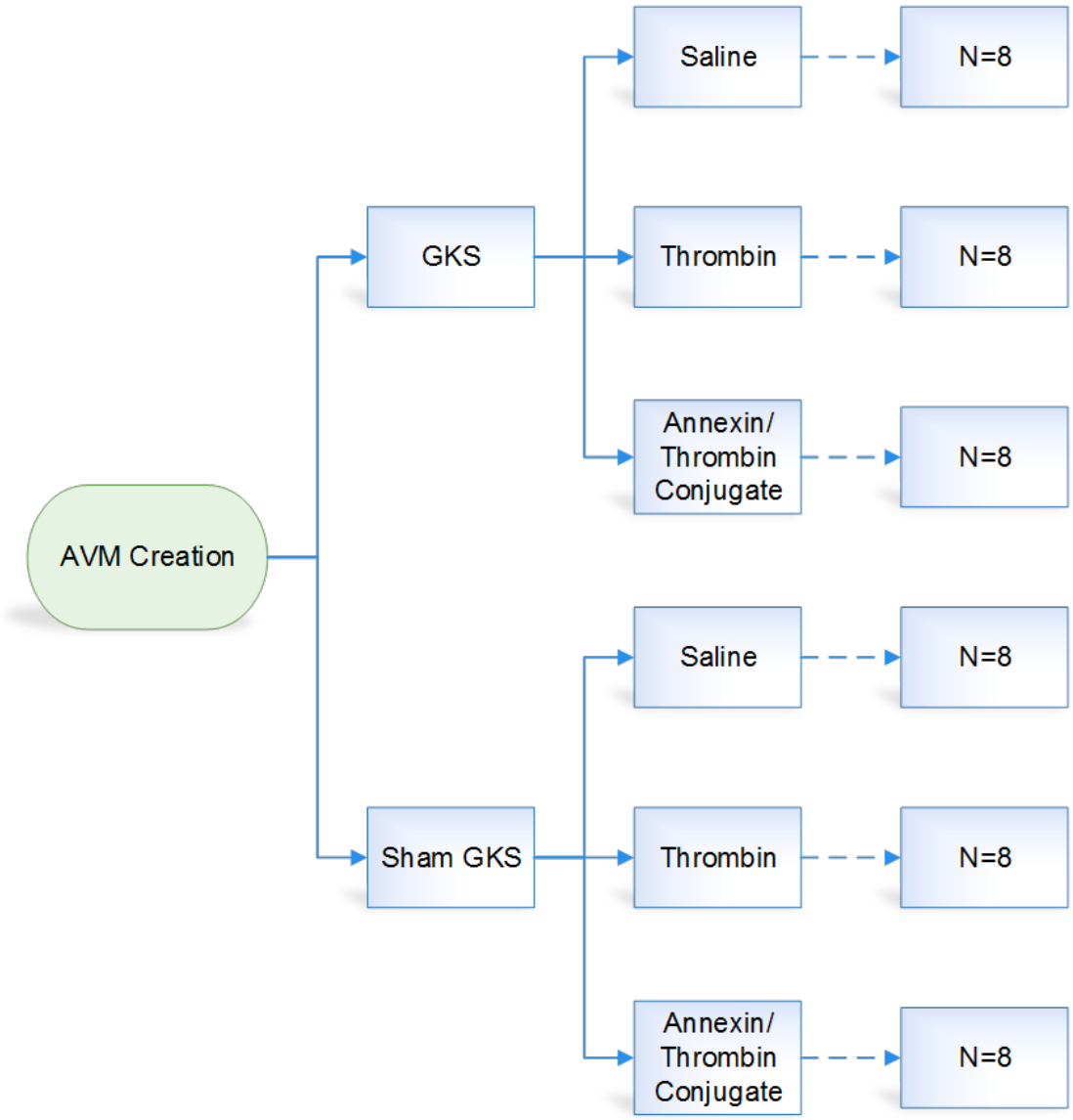

Figure 4-1 Separation of treatment groups. This demonstrates the 6 treatment arms of the planned study examining both with and without GKS and the conjugate compared to control arms of thrombin and 0.9% sodium chloride. The initial plan was for n=8 for each treatment arm to allow for optimum comparison within financial and ethical constraints.

At 3 – 4 weeks following prothrombotic conjugate or saline administration, the animals underwent a further inhalation anaesthetic and the AVM was exposed and inspected. Measurement of flow was performed with the Transonic circumferential Doppler probe in line with the methods recorded in Chapter 2 (Section 2.4). Flow was measured from the proximal CCA, distal CCA, left EJV and the comparison sides of right CCA and right EJV. Flow was recorded as an average over a 5-minute period in mL/min.

An angiogram was performed in line with the method described in Chapter 2 (Section 2.3). Following the angiogram, each animal underwent standard perfusion as previously described and sections were taken from the proximal and distal CCA, the left and right EJV and the right CCA. The model AVM nidus was harvested, and solid organs were similarly harvested in line with the previous methods (brain, liver, lung, and kidney).

Following standard tissue processing the tissues underwent H and E staining (Section 2.4) and if, on microscopy a thrombus was suspected, then an MSB stain was performed (Section 2.5).

Primary outcomes included angiographic patency and flow assessment (Section 2.3). Flow was observed from the point of anastomosis in a retrograde fashion through the EJV to the sigmoid sinus intracranially and ultimately draining into the contralateral right brachiocephalic vein. Angiography was recorded as negative if a normal flow was observed along the EJV to the sigmoid sinus with no evidence of stenosis or occlusion. A positive angiogram was defined as one that had stenosis or occlusion of the EJV after the anastomosis point. Particular attention was given to the horizontal first segment of the EJV which was the segment that was targeted with GKS.

Secondary histological outcomes were also recorded. The tissues assessed included the main vessels including transverse sections of proximal CCA, distal CCA, left EJV and the contralateral comparison vessels right CCA and right EJV. The AVM nidus was also assessed for evidence of thrombus formation. In line with the challenges experienced in assessing the thrombotic effect in the previous chapter, it was decided that a binary outcome would be the presence or absence of thrombus within the horizontal EJV, large nidus vessels, (defined as those vessels with a

muscularis propria), and microvessel thrombi, (small vessels without a muscularis propria, including capillaries, arterioles and venules). No continuous variable of histological thrombi was recorded. Although the animals had their solid organs harvested similar to the previous study, due to the absence of systemic thrombi in both of our dose response studies these were not assessed.

4.5 Results

4.5.1 Animal treatment allocations

Following injection with thrombin, one animal died within 2 – 3 minutes of the injection. Due to time course and immediate cardiorespiratory instability that was observed prior to the animal's expiration, the death was believed to be as a result of a thromboembolic event although no direct cause of death was apparent on post-mortem.

Eight animals underwent sham-GSK with full-dose conjugate treatment, and 11 animals were treated in the GKS/full-dose conjugate arm. Although an attempt was made to include eight animals per treatment arm, the procedure to perform the angiogram was technically demanding and in a number of cases required aborting of the procedure for urgent perfusion due to the risk of the animal exsanguinating prior to perfusion. This has meant that in some cases the numbers per treatment groups did not equal the n=8 that was originally planned.

4.5.2 Angiographic Outcomes

No animals in the saline or thrombin arms demonstrated any angiographic evidence of impairment or occlusion of the model AVM irrespective of radiation exposure (Figure 4-2), (95% CI: for sham saline and GKS saline, 0 – 32%; for sham thrombin, 0 – 43%; and for GKS thrombin, 0 – 35%). Evidence of impairment or occlusion of flow on angiogram was observed in 75% of animals (n=8; 95% CI: 41 – 93%) undergoing sham-GKS with conjugate and 63% of animals (n=8; 95% CI: 31 – 86%) in the GKS with conjugate group (Figure 4-3, Figure 4-4,Figure 4-5). Both the sham-GKS and GKS groups with conjugate had a statistically significant increase in animals with occlusion or impairment when compared to the control arms (p=0.007 and p=0.02, respectively) (Figure 4-5). The slight trend favouring angiographic

abnormality in the sham-GKS conjugate group over the GKS conjugate group was not statistically significant (p=1.0).

In addition to occlusion of the EJV, three conjugate-treated animals demonstrated evidence of a distal occlusion of the EJV beyond the anastomosis (Figure 4-4). In these animals the venous drainage pattern was different from the control animals where rather than draining intracranially, the contrast drained preferentially via an anomalous venous tributary to the left subclavian vein. This venous drainage pattern may have implications when considering the assessment of flow in the model AVM.

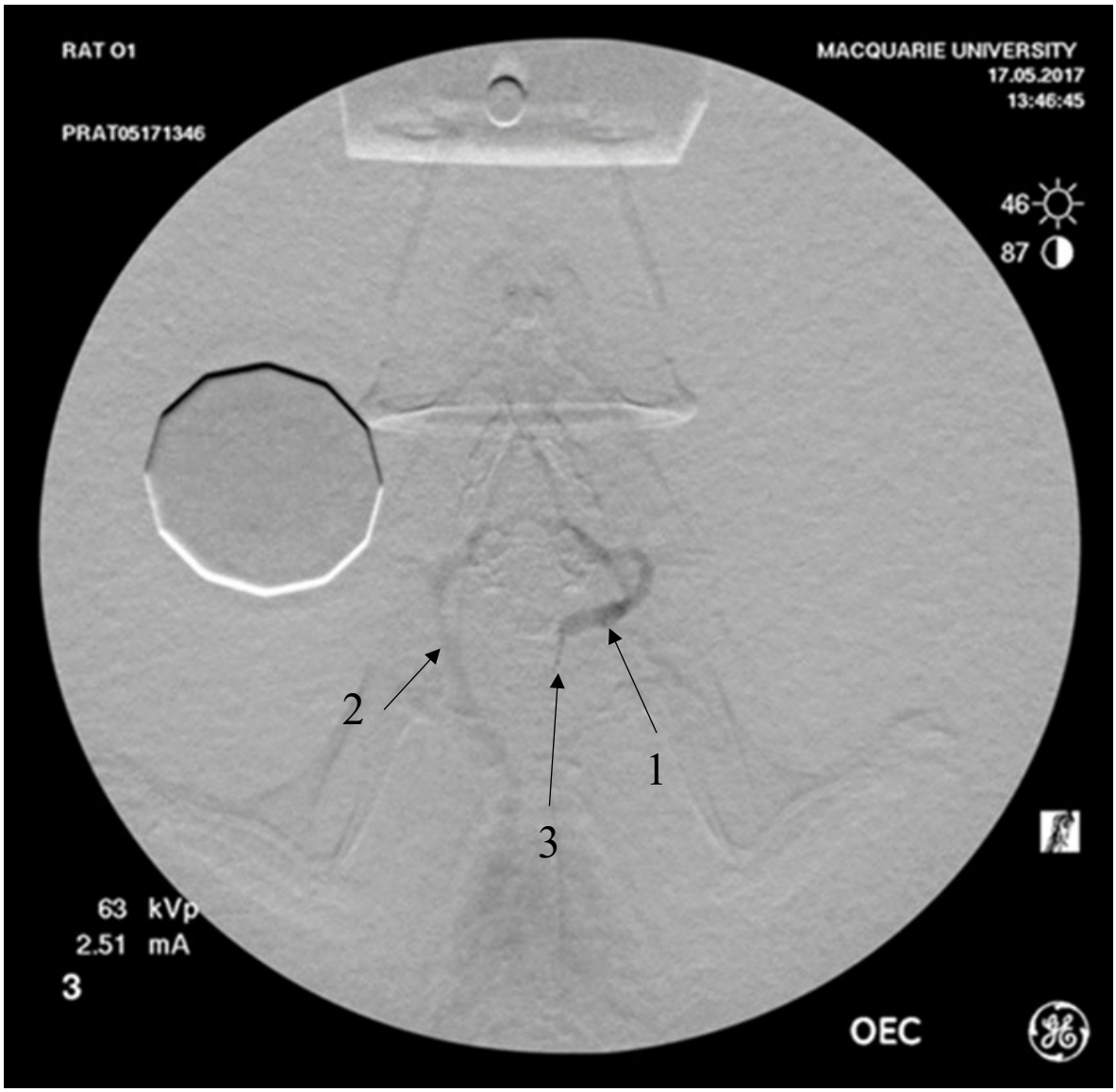

Figure 4-2 Digitally-subtracted-angiogram of a sham-GKS, saline-injected animal. The tip of the angiogram catheter is located at the point of anastomosis within the lumen of the CCA. It demonstrates patency of the anastomosed EJV (1) and flow of contrast from the proximal CCA (3) along the vein ultimately draining into the contralateral EJV (2) (Original image).

Figure 4-3 Digitally-subtracted angiogram of a GKS conjugate treated animal. The full angiogram (above) and the enlarged image (below) are included). Similar to Figure 4-2 the tip of the catheter is within the CCA at the point of anastomosis. This angiogram demonstrates a near-90% stenosis caused by a calcified thrombus within the horizontal segment of the left EJV (denoted by A and the arrow), occurring within our previously planned treatment field. B denotes the more distal left EJV, C the contralateral draining right EJV and D the tip of the catheter and the proximal left CCA (Original image).

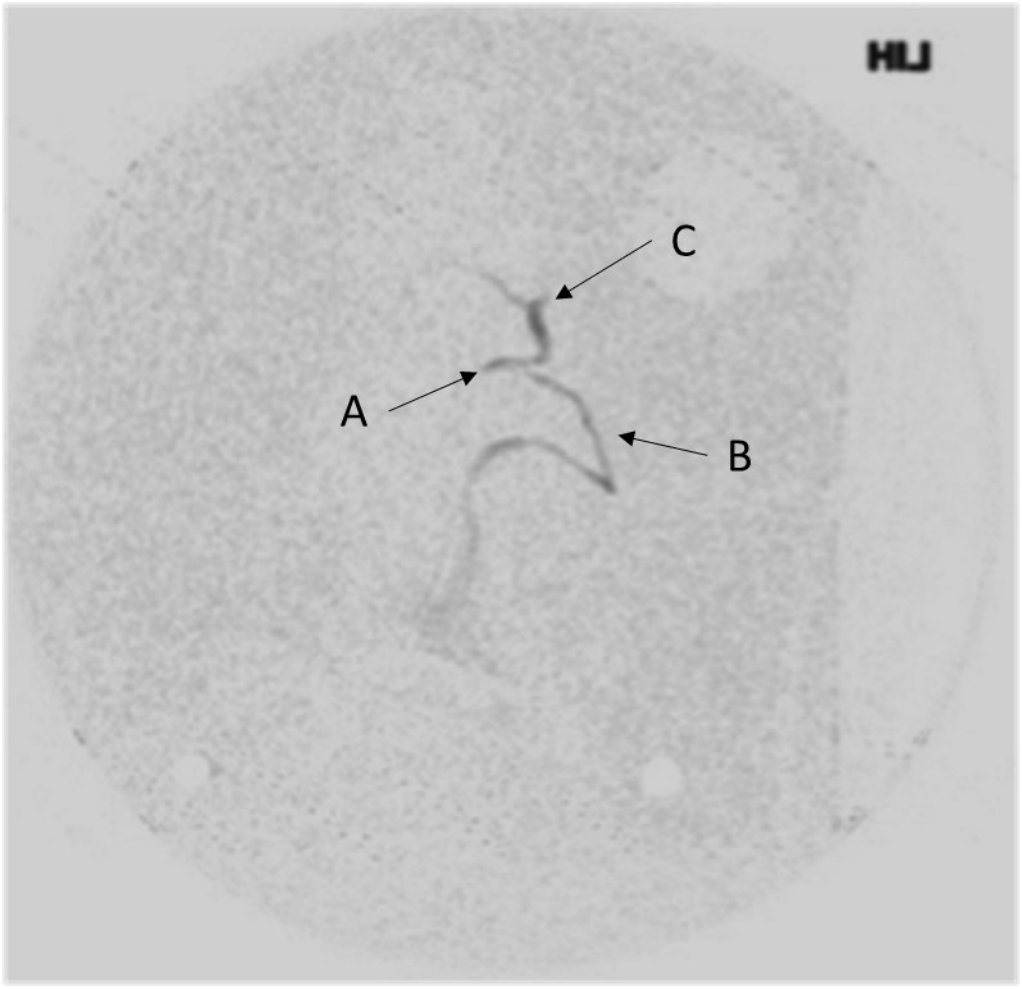

Figure 4-4 Digitally-subtracted-angiogram of a GKS-conjugate treated animal. This angiogram demonstrates flow from the anastomosed EJV (A) and stenosis with complete occlusion of the distal anastomosed EJV (C). There is distal flow via a preferential drainage of the contrast through an anomalous venous drainage pattern into the left subclavian vein (B) (Original image).

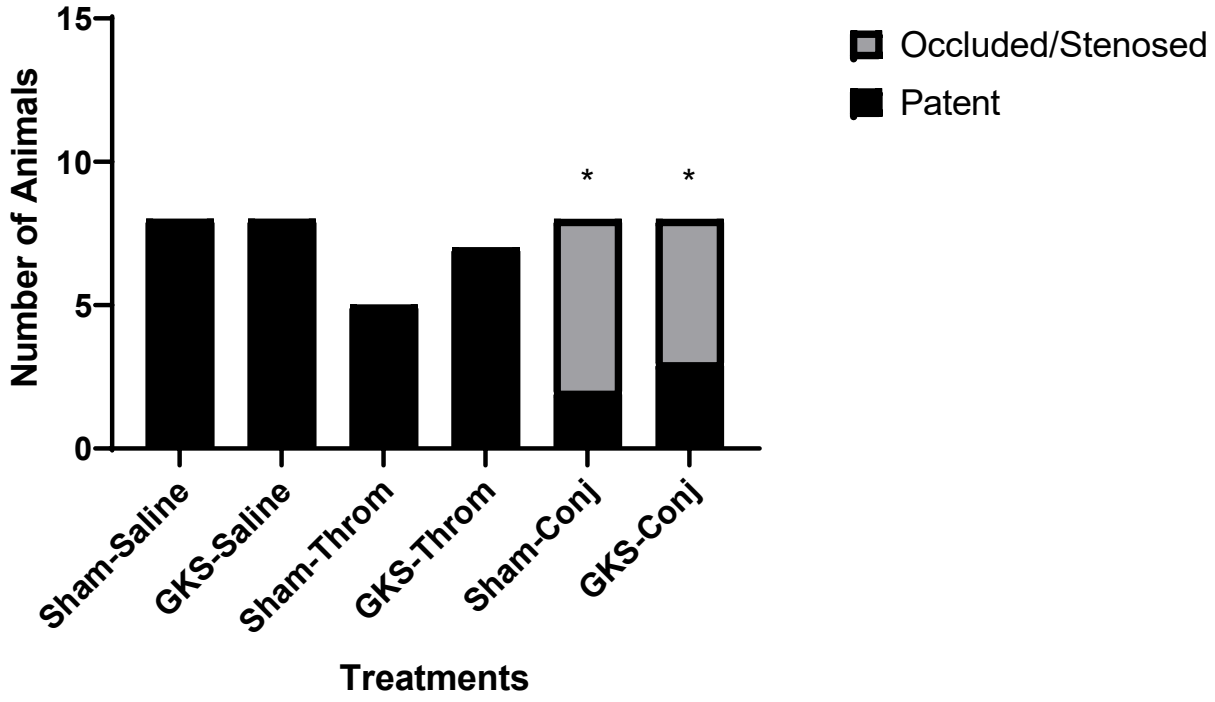

*Figure 4-5 Number of animals with occluded angiogram compared to patent vessels. Treatment groups included both sham-GKS and GKS with a marginal dose of 20 Gy to the model AVM and saline, thrombin (at 0.18 mg/kg) and annexin V/thrombin conjugate (at 0.77 mg/kg) treated animals. Patent angiograms included those angiograms with no evidence of stenosis or complete occlusion. Stenosed or occluded angiograms included those vessels with >50% stenosis in the course of the arterialised external jugular vein. * denotes statistical significance with $p<0.05$ (Fisher exact test - GraphPad Online calculator – GraphPad Quick Calcs Web site https://www.graphpad.com/quickcalcs, Graphpad Prism 8.2 version for Windows, GraphPad Software, La Jolla California USA).*

4.5.3 Flow Measurement

Flow measurement was performed in a number of animals at formation and at sacrifice. Mean values were 50 – 60 mL/min in all treatment groups in the arterialised left EJV with a mean increase ranging from 20 to 40 mL noted in EJV flow from formation to sacrifice (Figure 4-6). No statistically significant difference was observed between the treatment groups. Similar observations were made in the distal carotid flow with a mean flow ranging from -2 to -7 mL/min with wide variations between recording and differences between formation and sacrifice. No significant difference was noted between the treatment groups (Figure 4-7). Similar flow rates were observed in the proximal CCA and the contralateral right EJV and CCA.

Due to the difficulty of dissection and the risk of precipitating an on-table rupture of the AVM, it was decided to assess the preliminary results of the flow measurement to determine whether it was a useful outcome measure to be pursuing. The lack of change of flow in the left EJV group between animals with angiographic abnormalities may also be explained by the presence of anomalous venous drainage patterns that were noted in a number of animals (Figure 4-4).

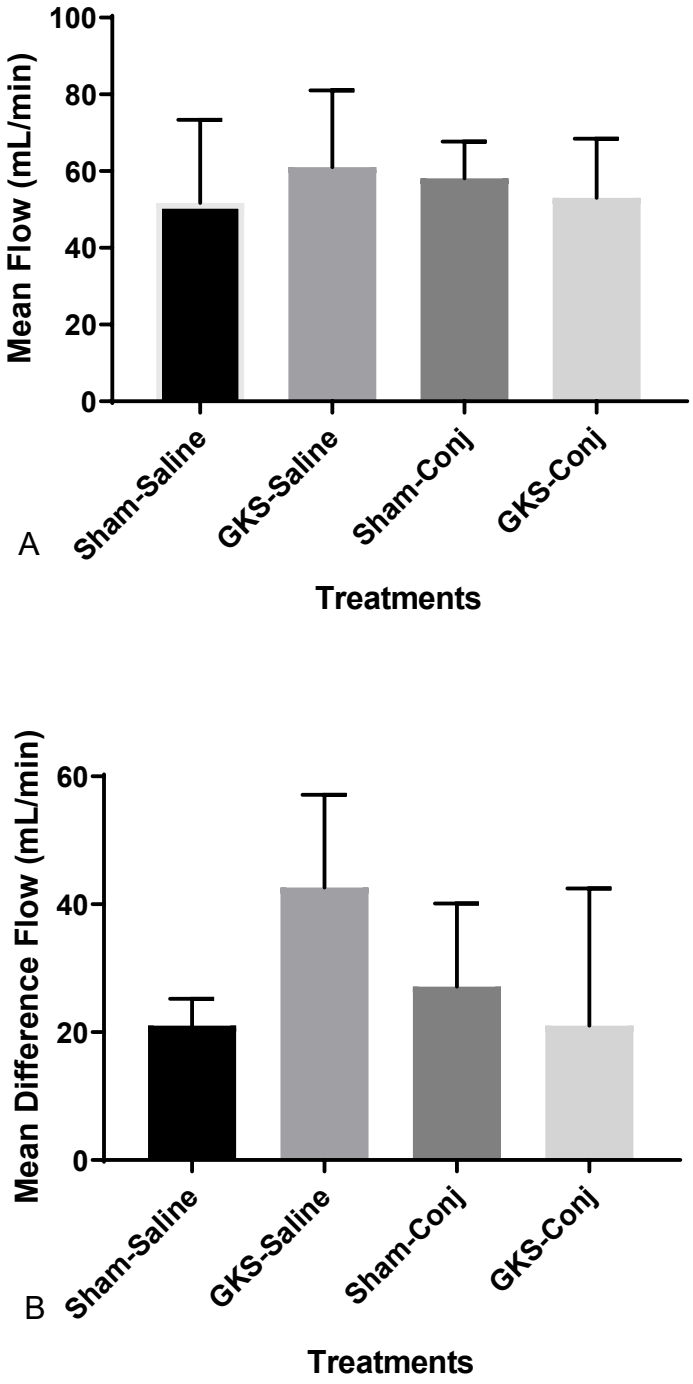

Figure 4-6 Graphs of flow in the left external jugular vein. Graph A demonstrates the mean flow (with SD) (mL/min) for both saline and conjugate GKS and sham-GKS groups in the left external jugular vein at sacrifice. Graph B demonstrates the difference between mean flow (mL/min) for each treatment group through the left external jugular vein determined by subtracting mean flow at sacrifice by mean flow at AVM creation (with SD). No significant difference was noted between treatment groups (Students t-test – Graphpad Prism 8.2 version for Windows, GraphPad Software, La Jolla California USA)).

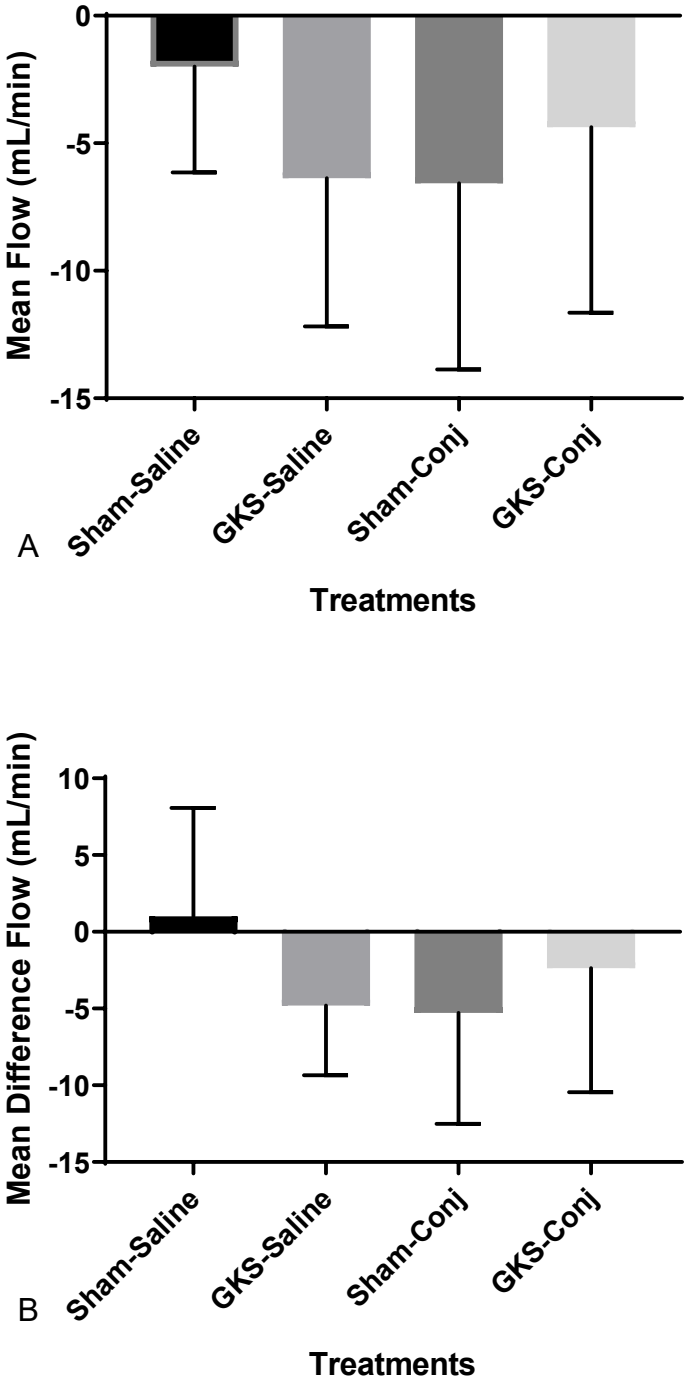

Figure 4-7 Graphs of flow in the left distal common carotid. Graph A demonstrates the mean flow (with SD) (mL/min) for both saline and conjugate GKS and sham-GKS groups. Graph B demonstrates the mean difference (with SD) in flow (mL/min) in the distal common carotid from the time of anastomosis formation to the point of sacrifice. No significant difference was noted between treatment groups with comparisons between sham-GKS saline against other treatment groups and GKS vs sham comparison group (Students t-test – GraphPad Online calculator – GraphPad Quick Calcs Web site https://www.graphpad.com/quickcalcs, Graphpad Prism 8.2 version for Windows, GraphPad Software, La Jolla California USA)).

4.5.4 Histological outcomes

All animals were perfused, and their tissue processed following both successful and unsuccessful attempts at angiogram and AVM flow measurement, hence the numbers of animals included for histological analysis were greater than those for angiographic and flow analysis. With the exception of the saline groups, all other treatment groups exhibited thrombus formation within both large and small microvessels.

4.5.4.1 EJV thrombus formation

Intraluminal EJV thrombus was identified in all treatment groups with the exception of the sham thrombin group where no animals (0%) demonstrated thrombus (n=5; 95% CI: 0 – 43%) (Figure 4-8, Figure 4-9). Approximately 15% of animals (n=13; 95% CI: 4.3 – 42%), in the sham saline group and 21% (n=14; 95% CI:7.6 – 48%) in the GKS saline group demonstrated EJV intraluminal thrombus on histology. In the GKS thrombin treatment group 86% of animals (n=7; 95% CI:49 – 97%) demonstrated thrombus formation within the EJV, this was statistically significant when compared to both sham salines, GKS saline and sham thrombin arms (p=0.004, p=0.02, and p=0.02 respectively).

Both conjugate treatment arms demonstrated higher proportions of EJV thrombus formation with 73% of animals, (n=11; 95% CI:43 – 90%), in the sham conjugate group and 50% of animals, (n=12; 95% CI:25 – 75%), of the GKS conjugate arm demonstrating EJV thrombus. The sham conjugate group demonstrated statistically significant proportions of EJV thrombus when compared to the sham saline arm (p=0.01), GKS saline arm (p=0.02), and the sham thrombin arm (p=0.03). Other comparisons with the sham conjugate group were not significant. The GKS conjugate group did not demonstrate a statistically significant difference favouring EJV thrombus formation over any other group.

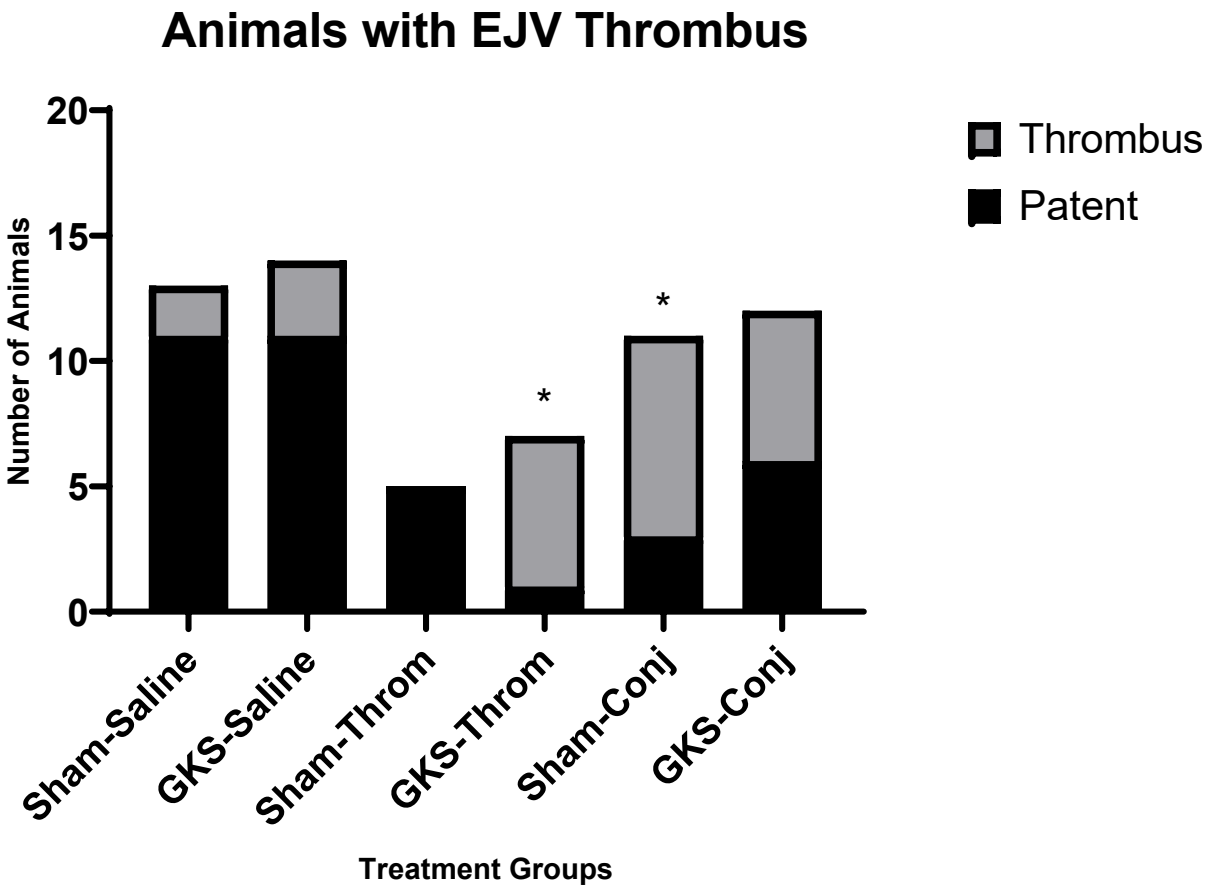

*Figure 4-8 Graph of number of animals with left EJV thrombus vs patent. GKS thrombin and sham GKS conjugate arms demonstrated statistical significance when compared to the saline control groups. * denotes P<0.05 when compared to the sham-GKS saline, GKS saline and sham-GKS thrombin arms (Fisher exact test - GraphPad Online calculator – GraphPad Quick Calcs Web site https://www.graphpad.com/quickcalcs, Graphpad Prism 8.2 version for Windows, GraphPad Software, La Jolla California USA).*

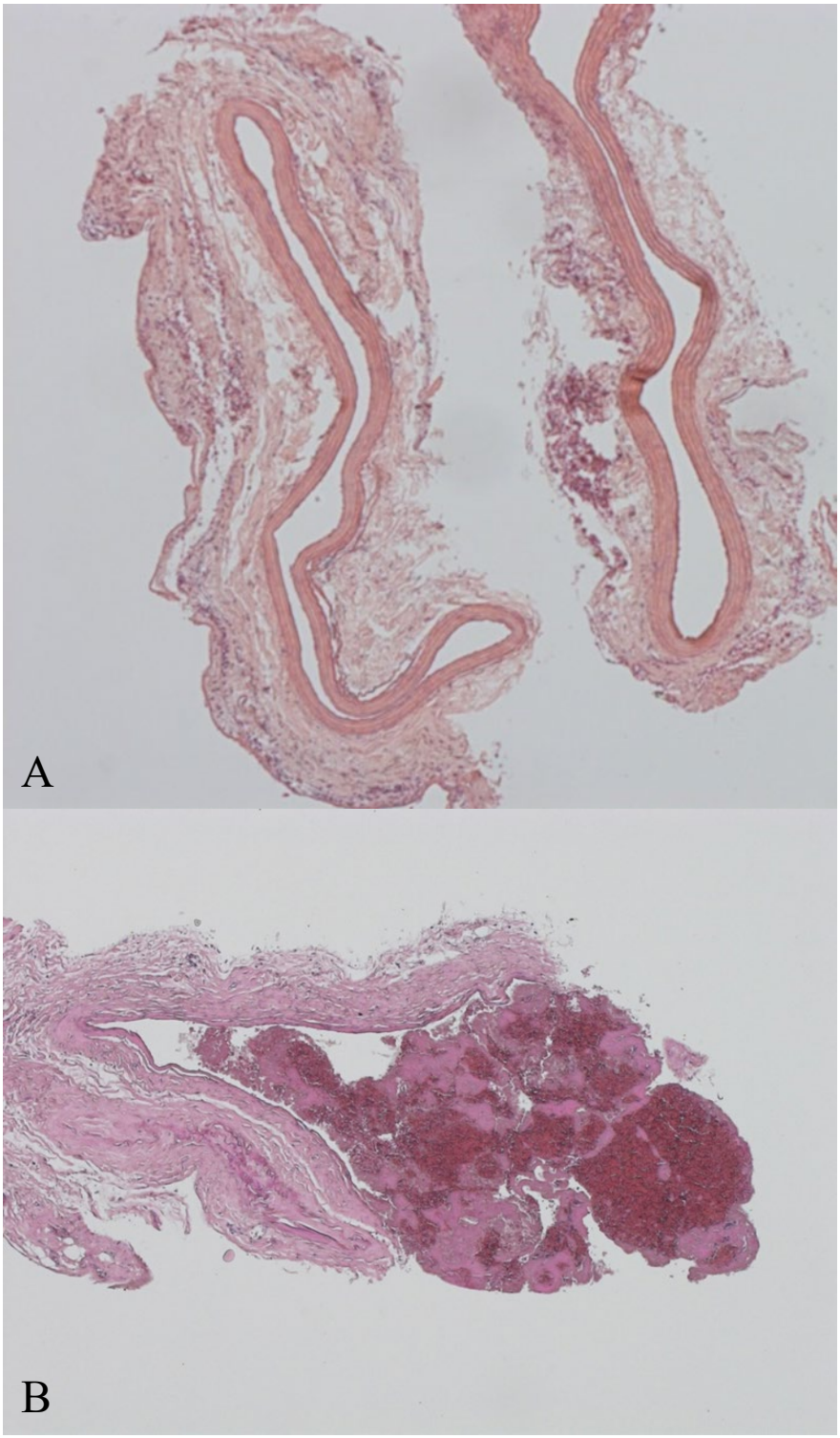

Figure 4-9 H and E stained axial section of a left EJV. Image A demonstrates an axial section of a sham-GKS treated animal. The vessel is patent with no evidence of thrombus. Image B is obtained from a GKS conjugate treated animal. The section demonstrates a large intraluminal established thrombus (Original image).

4.5.4.2 Nidus thrombus formation

No evidence of large vessel thrombus was observed in the niduses of either saline treatment arm (0%), (n=13; 95% CI:0 – 23%) and 0%, (n=14; 95% CI:0 – 22%) for sham saline and GKS saline respectively (Figure 4-10, Figure 4-11). Small rates of large vessel thrombi were observed in both of the thrombin treatment arms with 20% of animals, (n=5; 95% CI:3.6 – 62%), in the sham thrombin arm and 29% of animals, (n=7; 95% CI:8.2 – 64%), in the GKS thrombin arm.

Higher rates of large vessel thrombi were observed in both conjugate treatment arms with 50% animals, (n=8; 95% CI:22 – 78%), in the sham conjugate arm and 67% of animals, (n=12; 95% CI:39 – 86%), in the GKS conjugate treatment group demonstrating thrombi.

The sham conjugate arm demonstrated a statistically significant increase favouring large vessel thrombus formation when compared to sham saline (p=0.01), and GKS saline groups (p=0.01). The GKS conjugate group significantly favoured large vessel thrombus formation over the sham-GKS saline (p=0.0005), and GKS saline (p=0.0003) arms. The trend favouring large vessel thrombus formation in the GKS conjugate did not reach significance in the sham thrombin

(p=0.13), GKS thrombin (p=0.17) and sham conjugate (p=0.65) arms. No significant difference was observed with comparison to either thrombin treatment arms.

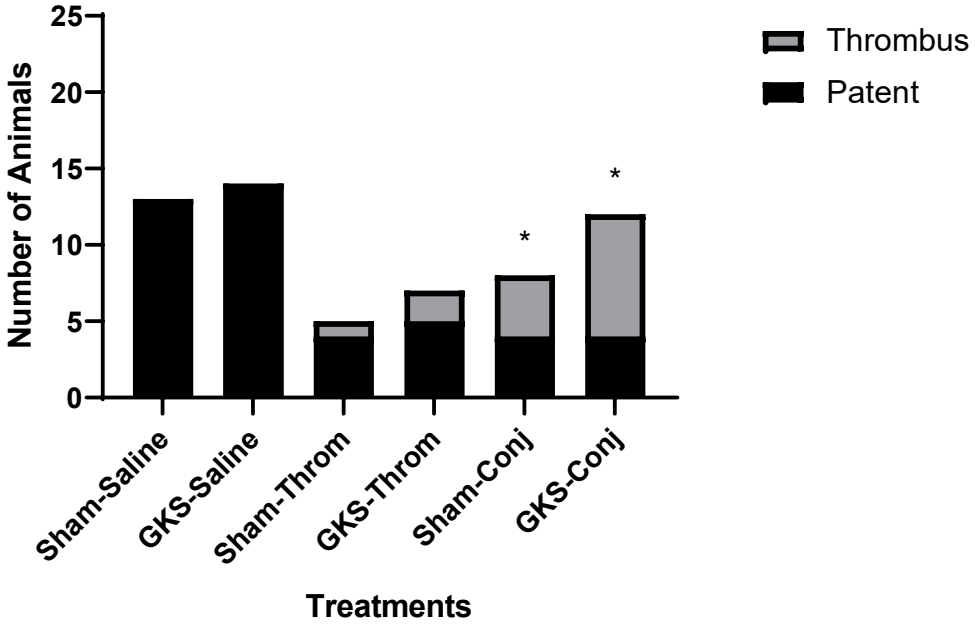

Figure 4-10 Graph of number of animals with large nidus vessel intraluminal thrombus. This demonstrates numbers for saline, thrombin and annexin V/thrombin conjugate-treated groups. Both conjugate treatment groups demonstrated 50 to 60% of animals with large nidus vessel thrombus. These proportions were statistically significant when compared to both saline control arms (denotes $p<0.05$ by Fisher exact test - GraphPad Online calculator – GraphPad Quick Calcs Web site https://www.graphpad.com/quickcalcs, Graphpad Prism 8.2 version for Windows, GraphPad Software, La Jolla California USA).*

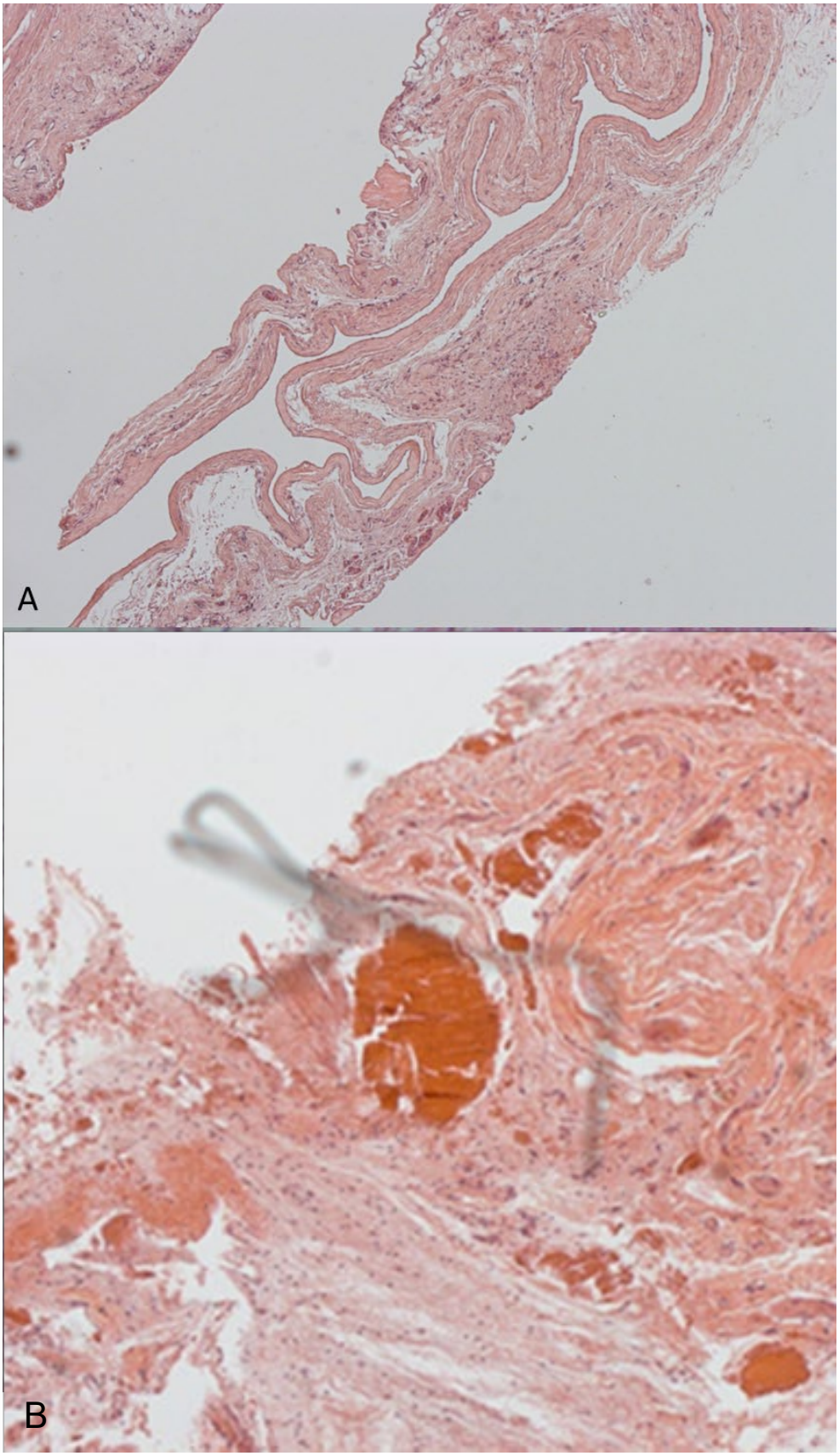

Figure 4-11 H and E stained sections from large nidus vessels. Image A demonstrates a large vessel from a sham-GKS saline treated animal that demonstrates complete patency of the vessel. Image B demonstrates a large vessel from the AVM nidus of an animal treated with GKS and annexin V/thrombin conjugate. It has an intraluminal established thrombus.

Microvessel thrombi were observed in all treatment groups with the exception of the sham-GKS saline treatment arm, (n=13; 0%; 95% CI:0 – 23%) (Figure 4-12, Figure 4-13). The GKS saline treatment arm exhibited micro-vessel thrombus in 57% of animals, (n=14; 95% CI:33 – 79%). This difference favouring the GKS saline treatment arm was noted to be statistically significant (p=0.002). Micro thrombi were present in the sham-GKS thrombin arm in 40% of animals (n=5; 95% CI:12 – 77%) and in the GKS thrombin arm in 86% of animals (n=7; 95% CI:49 – 97%). The sham-GKS thrombin arm was not statistically significant when compared to the sham-GKS saline arm, (p=0.07), whereas the GKS thrombin arm was observed to be statistically significant (p=0.0002).

Both conjugate treatment groups demonstrated micro thrombi within the AVM nidus with 63% animals, (n=8; 95% CI:30 – 86%), in the sham-GKS conjugate arm and 67% of animals, (n=12; 95% CI:39 – 86%), in the GKS conjugate arm. Both conjugate treatment arms favoured micro thrombi formation significantly when compared to sham-GKS saline (p=0.003 and p=0.0005 for sham-GKS conjugate and GKS conjugate respectively), but not to other thrombin treatment arms.

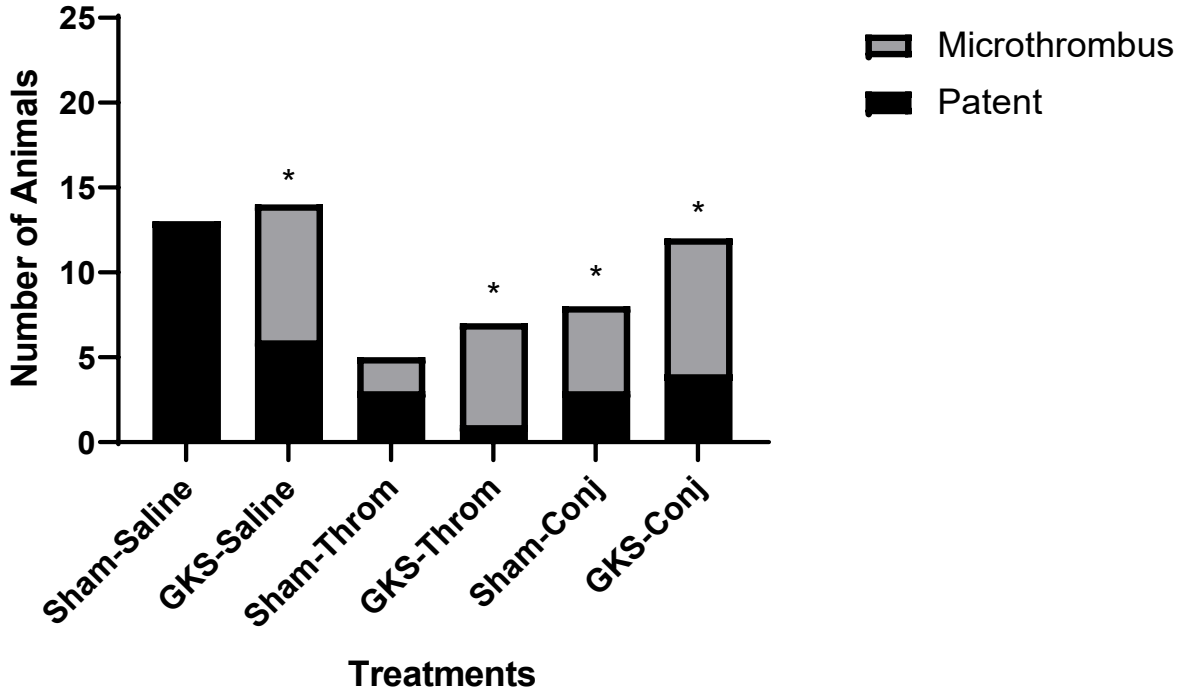

Figure 4-12 Graph of number of animals with nidus microvessel intraluminal thrombus. The groups with statistically significant numbers of animals were in both conjugate treatment groups, GKS thrombin and GKS saline groups. This was significant when compared to the sham GKS saline control arms (denotes p <0.05 compared with the sham-GKS saline treatment group – Fisher exact test - GraphPad Online calculator – GraphPad Quick Calcs Web site https://www.graphpad.com/quickcalcs, Graphpad Prism 8.2 version for Windows, GraphPad Software, La Jolla California USA).*

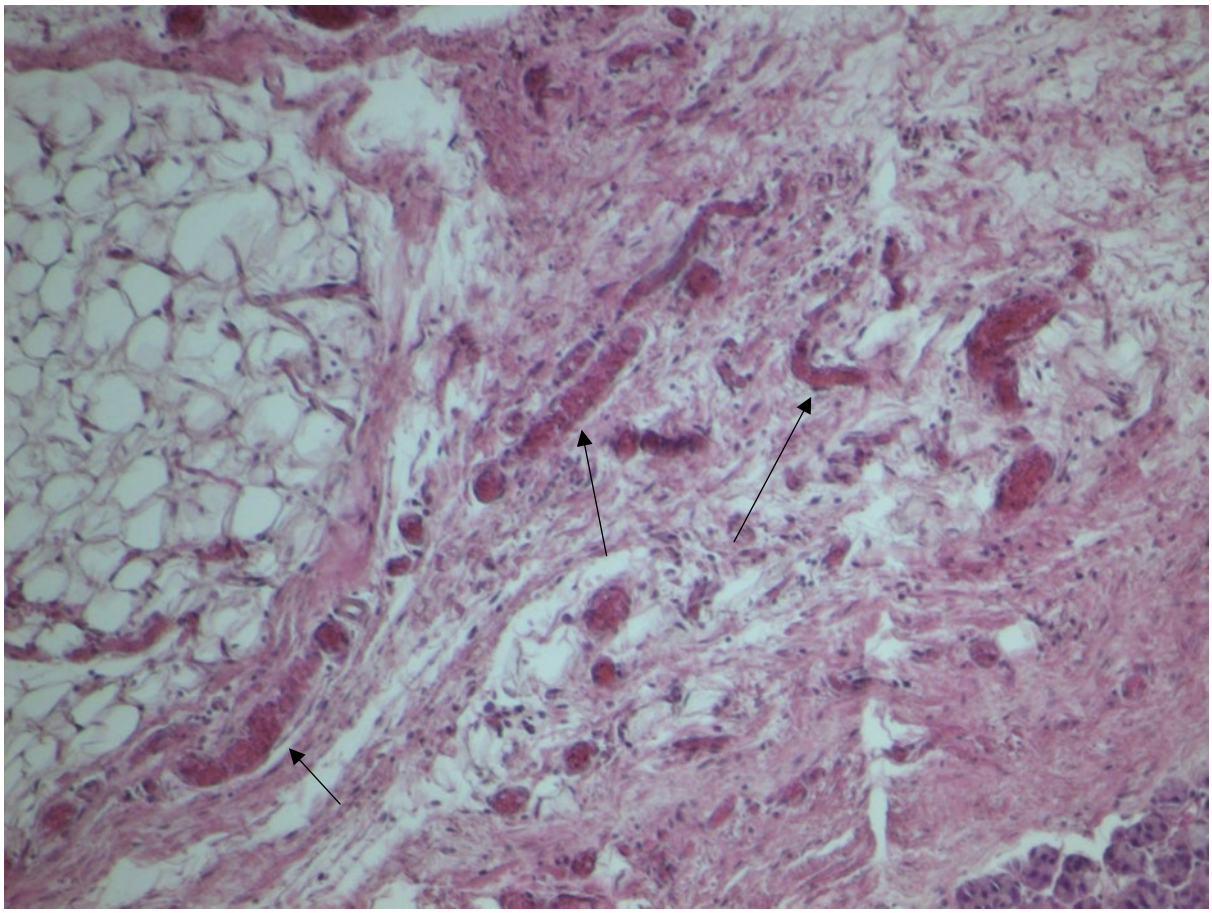

Figure 4-13 H and E stain of microvessels of the AVM nidus of a GKS, thrombin-treated animal. This example demonstrates the effect of both the radiation and prothrombotic compound with extensive microvessel thrombosis present in multiple small vessels (demonstrated by the arrows) (Original image).

4.6 Discussion

This study examines the use of a novel annexin V/thrombin conjugate in the treatment of a radiation-sensitised AVM rat model. To our knowledge, this study is the first to demonstrate the effective use of ligand vascular targeting of a biomarker in the setting of an AVM animal model. It is also the first study to demonstrate both large vessel thrombus formation and angiographic abnormalities from vascular targeting. Previous vascular targeting studies have only demonstrated microscopic vessel occlusion or thrombus formation in the *in vivo* setting [217].

The absence of death from injection or cardiorespiratory compromise in our conjugate group provides further evidence of the safety of the current dose compared to an equivalent dose of human thrombin. This would suggest that through conjugation of our annexin V to thrombin we reduce the chance of systemic thrombus formation with the exception of the targeted region of PS translocation.

The results of this study demonstrate angiographic occlusion or stenosis occurring only within the AVM vessels in the presence of conjugate. In the conjugate-treated groups, statistically significant rates of angiographic flow impairment could be observed in 60 to 75% of animals. The fact that angiographic abnormalities occurred only in those animals treated with our annexin V thrombin conjugate it would strongly support assurances that our conjugate binds to PS. This is supported in the literature where annexin V is used both in investigative work and as a therapeutic delivery mechanism in the setting of cancer vascular targeting research [344].

It is important to note that the angiographic and thrombotic effect of our treatment occurred independent of whether prior GKS-radiation sensitisation occurred or not. This effect in radiation naïve animals could be explained by the presence of baseline PS translocation that was observed in non-irradiated animals in earlier studies [193]. It is possible that our vascular targeting agent is targeting this baseline level of PS translocation in the non-irradiated animals. The finding of angiographic abnormalities is, however, promising, particularly as it demonstrates gross vascular abnormalities that are translatable to the clinical treatment of brain AVMs.

The histological outcomes further substantiate the angiographic findings. Micro-vessel thrombi were present in significant proportions in both the GKS, and all conjugate groups. This suggests that the formation of micro vessel thrombi occurs either as a result of the radiosurgery or alternatively as an effect of conjugate treatment. The effect of micro-vessel thrombi formation in the effect of GKS was not unexpected and believed to be occurring as a result of an early radiation effect.

It is well known that radiation induces a pro-coagulant state in the endothelium [467-473]. Under normal physiological circumstances the endothelium plays a critical role in maintaining an anti-thrombotic and anti-coagulant balance through the exertion of molecular control on the processes of platelet aggregation, coagulation and fibrinolysis [479]. The transmembrane glycoprotein TM is located on the luminal surface of endothelial cells and plays a critical role in this balance through its ability to form a complex with thrombin, changing its substrate specificity. Once bound to TM, thrombin no longer has the ability to convert fibrinogen to fibrin or activate protease-activated receptor-1. The TM, thrombin complex plays a role activating protein C, an important anti-coagulant and anti-inflammatory protein [472]. A deficiency of TM has been noted in irradiated microvasculature, and this has been suggested to cause a reduction in scavenging of thrombin and insufficient Protein C activation causing a pro-coagulant state [480]. This pro-coagulant state is advantageous for AVM thrombin-targeted treatment for a number of reasons. Firstly, the post irradiated AVM vessels provide a pro-coagulant state and a pro-coagulant surface for thrombin activity due to the TM deficiency. In addition to improving the pro-coagulant effect, the presence of TM in other systemic vascular regions would not support thrombus formation due the inherent inhibition of thrombin.

Larger vessel and EJV thrombus rates appear to mirror the angiographic findings, suggesting pro-coagulant changes in response to radiation alone are not sufficient to induce thrombosis in larger vessels, and providing further evidence suggesting the targeted thrombotic effect of our annexin V/thrombin conjugate. Although EJV thrombus rates did not reach statistical significance in the

GKS full-dose conjugate treatment group it is possible this was due to the small sample size in this study or due to selective sampling of the EJV for histological analysis, failing to gather the segment containing the thrombus.

It remains difficult to quantify the degree of thrombus formation histologically with our animal model. The histological structures within the nidus are varied and include submandibular salivary glands, adipose tissue and skeletal muscle. Because of this, the distribution of blood vessels is not uniform across the tissue and it is difficult to quantify the degree of macro and microvascular thrombus present within the nidus.

The left EJV also demonstrated thrombus formation in both saline treatment groups and also in the GKS thrombin arm in a statistically significant proportion. Although the greater proportion of EJV thrombus formation occurred in the conjugate-treated animals it is concerning that thrombus was present in these control groups. As for the most part, thrombus was found in both irradiated and non-irradiated animals, it is possible that the process of anastomosing the EJV and the required manipulation of the vessel causes injury to the tunica intima predisposing this vessel to spontaneous thrombus formation. This finding will need to be confirmed on a larger scale to determine a difference between conjugate and non-conjugate-treated animals.

In addition, the extent of thrombus may also be underestimated within the EJV due to the discrete nature of some thrombi and sampling error. The process of perfusion of our animal model may also have the potential to disrupt already established thrombus and therefore underestimating the extent of thrombus formation in both micro and macro vessels. Alternative outcome measures such as high frequency ultrasound imaging may better quantify the extent of large vessel thrombus formation than a quantitative histological method [481].

The use of the Doppler flow measurement device failed to demonstrate a significant difference in flow within the major associated vessels of our AVM model. No significant difference was noted in either the feeding arteries of the proximal CCA and distal CCA and neither the arterialised vein of the left EJV (Figure 4-6, Figure 4-7). This was also noted in our angiographically occluded

AVMs. While it is possible that this is because of persistent flow in our AVM model, an alternative explanation has been demonstrated in our occluded AVMs (Figure 4-4). In this example, the point of occlusion of the arterialised vein occurred distally at the transition point to the intracranial segment of the arterialised vein. Because of this distal location, the contrast flowed preferentially via an anomalous venous drainage pattern via a tributary to the left subclavian vein. In this example, due to this anomalous drainage pattern, flow in the proximal left EJV would be preserved and remain arterialised and it is unlikely that any difference of flow would be observed on Doppler.

Furthermore, the values recorded both at the time of anastomosis and at the final point of sacrifice were highly variable, positional and necessitated an average reading over 5 minutes. This would undoubtedly have introduced potential bias with assessing the flow in these vessels. The concept of inaccuracies and the operator-dependent nature of Doppler flow measurements has been described in the literature in the setting of transcranial Doppler measurements in the clinical setting of subarachnoid haemorrhage [477, 478]. Due to these reasons and the inaccuracies it is unlikely that the use of Doppler flow measurements will be of use as an outcome measurement tool in the AVM model. Alternative measurements such as the digital subtraction angiogram, MRI [484], or high frequency ultrasound [481], are likely to be of greater sensitivity in detecting flow changes and distal occlusion with the model AVM.

A second potential explanation for the reason for decreased thrombus formation in the GKS conjugate group may be that there is a dose-effect present, whereby increasing dosage of the targeting agent may result in less selective targeting and reduced efficacy of the treatment. The pro-drug combretastatin A-4 (CA-4P) is a microtubule targeting agent that has been extensively examined in the cancer setting of vascular targeting [480]. Concern had been raised that the efficacy of CA-4P and other vascular targeting agents only developed an anti-tumour vascular effect at doses that caused significant associated toxicity. Work by Dark et al. using human umbilical vein endothelial cells and an *in vivo* mouse model of human breast carcinoma and rat carcinosarcoma tumours demonstrated increased anti-tumour efficacy of the drug at 1/10th the

maximum tolerated dose [200]. This finding has been validated in other vascular targeting studies with vascular disrupting agents [198-204]. Furthermore, other more recent work has identified increased anti-tumour efficacy of CA-4P in a multiple dose regimen in a Hodgkin's lymphoma xenograft model [486]. It is possible that in the *in vivo* AVM we are observing a similar inverse dose-response effect with less selectivity of PS targeting. With the observation of angiographic abnormalities, it would be reasonable to proceed with dose modification studies to examine for improved selectivity of our targeting of PS with lower doses and multiple dose treatment regimens.

The use of PS as a potential target for vascular targeting technique is well established in the literature [482]. PS as the most abundant anionic phospholipid and one which is closely regulated by environmental conditions or cell injury and is an attractive choice for target in AVM targeted treatment [338, 483]. Research in the tumour setting of vascular targeting has suggested that vessels with externalised PS develop complexes with lipid binding proteins such as β2-glycoprotein I and remain patent despite the externalised PS [213]. Although this evidence would suggest PS would be an attractive choice of target for a vascular targeting technique there is other evidence to suggest that other sources of tissue injury may induce PS externalisation. This includes changes in the tissue microenvironment such as tissue hypoxia, inflammatory cytokines and an acidic pH [213, 484], as well as reactive oxygen species released by neutrophils or cancer cells may oxidise phospholipids and induce Ca2+ influx into the cytosol which induces PS externalisation [484-486]. PS externalisation has also been implicated in a large number of other cellular processes in addition to apoptosis including erythropoiesis, erythrocyte clearance, myoblast fusion, neuronal synaptic pruning, and as a consequence of viral infection [487-490]. This study has very promising findings regarding the use of PS as a target. It is, however, possible that other targets may be more selective and therefore more effective in treating AVMs. Although it is reassuring that there is no evidence of off-target systemic thrombotic effects of our conjugate (Chapter 3), other PS targeting research has not specifically examined for off-target effects and the presence of systemic vascular targeting. Furthermore, there was effectiveness of our conjugate

in animals that had not been exposed to radiation. Due to this fact and the evidence suggesting that PS may externalise under other injurious effects to the endothelium a better understanding of the distribution of externalised PS is needed.

An ideal biomarker would be one that is only upregulated in the presence of radiation sensitisation and only within AVM tissue. It is possible that an alternative or additional target may improve the selectivity and efficacy of this targeting technique and in line with this research has examined other targets using an *in vivo* technique of biotin-labelling of surface-accessible endothelial proteins and comparative proteomics. This work has established other potential targets for the development of further conjugates and is addressed further in Chapter 6 [326, 335].

The use of annexin V to target externalised PS in apoptotic cells is well established as a labelling agent [491-493]. The rat immunoglobulin M monoclonal antibody 9D2 is designed to bind to anionic phospholipids such as PS and has been shown to be indistinguishable from annexin V in a solid tumour murine model [344]. Other studies in vascular targeting have looked at targeting PS using a number of monoclonal antibodies such as 3G4, 2aG4 and bavituximab in the settings of non-small cell lung cancer, breast cancer and hepatitis [317, 334, 494-496]. These antibodies differ from annexin V and 9D2 as they require the presence of β2-glycoprotein 1 to be complexed with PS to bind effectively [317, 334, 497]. Despite the demonstration of efficacy of PS binding, these antibodies such as 9D2 and bavituximab are designed as immune modulators through PS blockade and have yet to be used for delivery of a treatment payload unlike our annexin V/thrombin conjugate [496, 498]. Although these antibodies have undergone phase III clinical trials they are yet to prove to be successful in the human clinical setting [499, 500]. This research with the annexin V/thrombin conjugate is unique in the use of a targeting agent to deliver a pro-thrombotic molecule directly to endothelium with externalised PS.

4.7 Conclusion

This study demonstrates that with the use of annexin V/thrombin conjugate, targeting of PS is effective in causing occlusion and thrombus formation in the model AVM. This has been

demonstrated using both angiographic evidences, but also confirmed with histological findings of nidus vessel thrombus in both microscopic and macroscopic vessels. These results are the first of their kind and are "proof of principle" that ligand vascular targeting may become a potential future treatment in brain AVMs and aid in the prevention of haemorrhagic stroke caused by these lesions. Although the thrombotic effect of the conjugate was noted, there was no significant difference between the GKS and sham-GKS conjugate groups. We postulate that this may be related to an inverse dose-effect which has been described in other targeting agents. Further work is needed to determine whether this dose-response exists, and if by using different treatment dosage approaches there is an increased efficacy in AVM occlusion.

Chapter 5 Dose Modification Increases Targeting Selectivity

5.1 Background

The previous chapter demonstrated the pro-thrombotic effects of the annexin V/thrombin conjugate in targeting PS translocation within the model AVM. Although this was successful in causing large vessel occlusion, no significant difference was noted between the GKS and sham-GKS conjugate-treated groups. Although this could be because of the previously observed baseline of PS translocation in non-irradiated model AVMs [193], it was postulated that a dose-response of the conjugate may exist, and that saturation of PS at high doses of annexin V caused this effect. This dose response has been observed with other vascular targeting agents, where increased efficacy was noted with lower doses and in multiple dose administration regimens [198, 501]. Thus, it was hypothesised that with reducing the dose or by using multiple low doses the thrombotic effectiveness and the selectivity of PS targeting of our annexin V/thrombin conjugate may be improved.

5.2 Hypothesis

Reducing the dose of annexin V/thrombin conjugate will increase PS selectivity and improve AVM occlusion in the rat AVM model.

5.3 Aims

- To examine the PS selectivity and thrombotic effectiveness of the annexin V/thrombin conjugate with a single ½-dose (0.38 mg/kg) administration.
- To examine the PS selectivity and thrombotic effectiveness of the annexin V/thrombin conjugate with multiple ½-dose administrations.
- To assess the safety of the proposed new treatment regimens.

5.4 Methods

5.4.1 Treatment Groups

The standard method for AVM creation was used in Sprague-Dawley rats in the same manner as described in the previous chapters (Section 2.1). Four treatment groups were included to assess both GKS and sham-GKS and the two conjugate dosage groups as follows, with an aim of 8 animals per treatment arm (n=8):

1. Sham GKS and ½-dose conjugate (0.38 mg/kg)
2. GKS and ½-dose conjugate (0.38 mg/kg)
3. Sham GKS and 2× ½-dose conjugate (2 x 0.38 mg/kg)
4. GKS and 2× ½-dose conjugate (2x 0.38 mg/kg)

5.4.2 Conjugate Administration

The administration occurred at the same initial time point at 3 weeks following GKS treatment, in line with the increase in PS translocation that was noted in earlier *in vivo* studies [193]. In the ½-dose group, a single dose of annexin V/thrombin conjugate was administered and standard post injection care of the animal was observed with 7 days of daily reviews and sacrifice and perfusion at 3 to 4 weeks following injection of the conjugate.

The multiple dose group treatment involved two separate doses administered to each animal at 0.38 mg/kg. The first dose was given at 3 weeks following GKS identical to the ½-dose group. The second dose was administered after 48 hours and was administered at the same dose of 0.38 mg/kg. The animals were then observed for 7 days following the second injection and they were monitored daily for 7 days before sacrifice and perfusion at 3 to 4 weeks following the final injection.

During each inhalational anaesthetic for the multiple dose group the animal was positioned supine and the anterior neck was shaved. A vascular ultrasound was performed and used to identify the

point of anastomosis and the horizontal segment of the anastomosed left EJV for qualitative assessment of the anastomosis.

5.4.3 Outcome Measures

Perfusion, sacrifice and angiogram methods were used in the method recorded in the previous chapter. Flow measurements were not taken in these animals either at AVM formation or at the time of sacrifice. It was felt that due to the lack of statistical significance noted in the previous chapter, the high variability of the outcome, and the high risk of AVM rupture during the dissection process required for the procedure that this outcome measure was not necessary.

Outcome measures included in this study were otherwise similar to the previous chapters. A positive angiographic finding was noted if there was evidence of stenosis or occlusion of contrast flow distal to the point of anastomosis of the left EJV.

5.5 Results

5.5.1 Overview

Three animals died within a 24-hour period following intraperitoneal anaesthetic and GKS (two in the sham GKS ½-dose group and 1 from the GKS ½-dose group). Necropsies were performed on each animal and they did not reveal any cause for death and the model AVM appeared patent and intact. Death was presumed to have occurred due to an anaesthetic-related complication and poor recovery.

Eight animals underwent the sham-GKS with ½-dose conjugate treatment and 5 animals underwent the GKS with ½-dose conjugate treatment. Seven animals underwent the sham-GKS with 2× ½-dose treatment and 9 animals underwent the GKS with 2× ½-dose conjugate treatment.

5.5.2 Angiographic Outcomes

Angiographic data were obtained in all surviving animals. The sham-GKS with ½-dose conjugate group had 13% of animals with evidence of stenosis or occlusion of the model AVM, (n=8; 95% CI: 2%-47%), with 80% animals in the GKS with ½-dose conjugate group with evidence of

impairment of contrast flow, (n=5; 95% CI: 38% to 96%), (Figure 5-1,Figure 5-2). This difference was noted to be statistically significant (p=0.03).

A similar difference was noted in the 2× ½-dose groups, with animals in the sham-GKS group having no evidence of angiographic flow impairment (0%), (n=7, 95% CI: 0 – 35%), and 78% of animals, (n=9, 95% CI: 45 – 94%), with evidence of stenosis or occlusion in the GKS group. This difference was also noted to be statistically significant (p=0.003). The difference between the GKS ½-dose and GKS 2× ½-dose groups was not statistically significant (p=1.0).

In addition, in one animal undergoing GKS with 2× ½-dose conjugate treatment there was complete occlusion of the proximal EJV with restoration of normal anatomical circulation in the distal CCA (Figure 5-1). On inspection of this vessel and subsequent histopathology it was found to be caused by a large calcified thrombus causing complete occlusion of the vessel lumen. This finding of complete occlusion within the prescribed GKS treatment field had not been demonstrated in prior experiments.

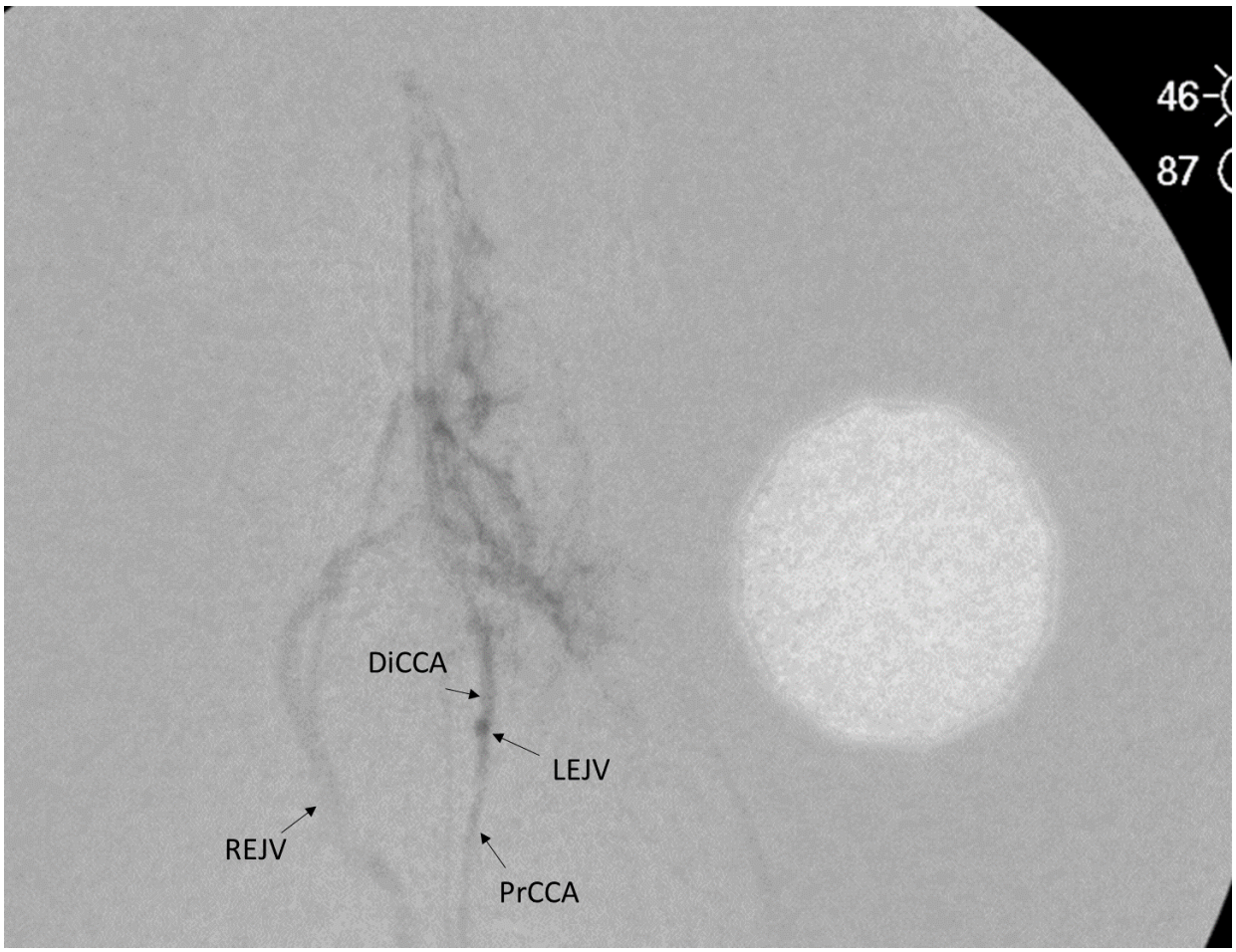

Figure 5-1 Digitally-subtracted angiogram of GKS with double 1/2-dose conjugate-treated animal following injection of proximal carotid artery. Similar to past angiograms in this manuscript the tip of the catheter is at the point of surgical anastomosis. Different to previous examples this angiogram demonstrates complete occlusion of anastomosed left external jugular vein (LEJV) with restoration of distal common carotid artery (diCCA) flow intracranially. Other abbreviations right external jugular vein (REJV), and proximal carotid artery (PrCCA)- (Original image).

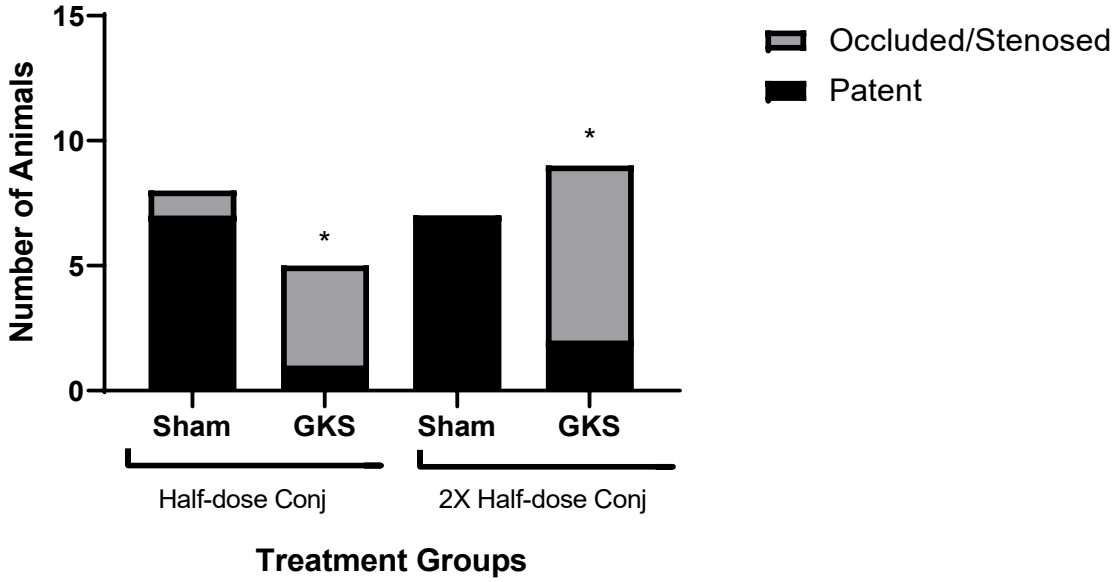

*Figure 5-2 Numbers of animals with occluded/stenosed vs patent angiogram in 1/2-dose and 2× 1/2 dose conjugate groups. Sham-GKS with ½-dose conjugate group had 13% of animals with evidence of stenosis or occlusion with 80% animals in the GKS with ½-dose conjugate group with evidence of impairment of contrast flow. A similar difference was noted in the 2× ½-dose groups, with animals in the sham-GKS group having no evidence of angiographic flow impairment (0%), and 78% of animals with evidence of stenosis or occlusion in the GKS group. * denotes $p<0.05$ for each GKS group compared to its comparison sham-GKS group (Fisher exact test - GraphPad Online calculator – GraphPad Quick Calcs Web site https://www.graphpad.com/quickcalcs, Graphpad Prism 8.2 version for Windows, GraphPad Software, La Jolla California USA).*

5.5.3 Histological outcomes

5.5.3.1 EJV thrombus formation

Intraluminal thrombi were observed in the EJV in all ½ dose conjugate groups and 2× ½ dose conjugate groups (Figure 5-3, Figure 5-4). Half of the animals (n=8; 95% CI:22 – 78%) were observed to have EJV thrombus in the sham-GKS ½ dose conjugate group, and 60% of animals (n=5; 95% CI:23 – 88%), in the GKS ½ dose conjugate group, (Figure 5-4).

Similar rates of EJV thrombus formation were observed in the 2× ½ dose conjugate groups with 57% of animals, (n=7; 95% CI:25 – 84%), in the sham-GKS arm and 44% of animals, (n=9; 95% CI:19 – 73%) in the GKS arm (Figure 5-3). No significant difference was observed favouring each ½-dose conjugate group against their respective comparison.

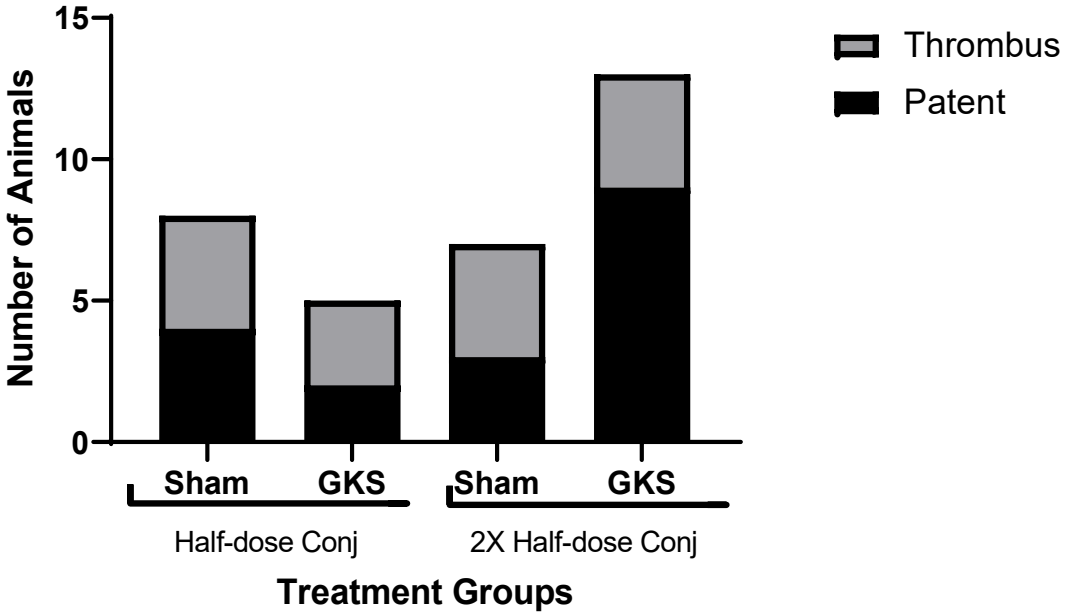

Figure 5-3 Numbers of animal with external jugular vein (EJV) thrombus in 1/2-dose and 2× 1/2-dose conjugate groups. Evidence of thrombus formation within the EJV was noted to be present in all treatment groups in a similar proportion. Differences between each GKS and their comparator group was not noted to be statistically significant (Fisher exact test - GraphPad Online calculator – GraphPad Quick Calcs Web site https://www.graphpad.com/quickcalcs, Graphpad Prism 8.2 version for Windows, GraphPad Software, La Jolla California USA).

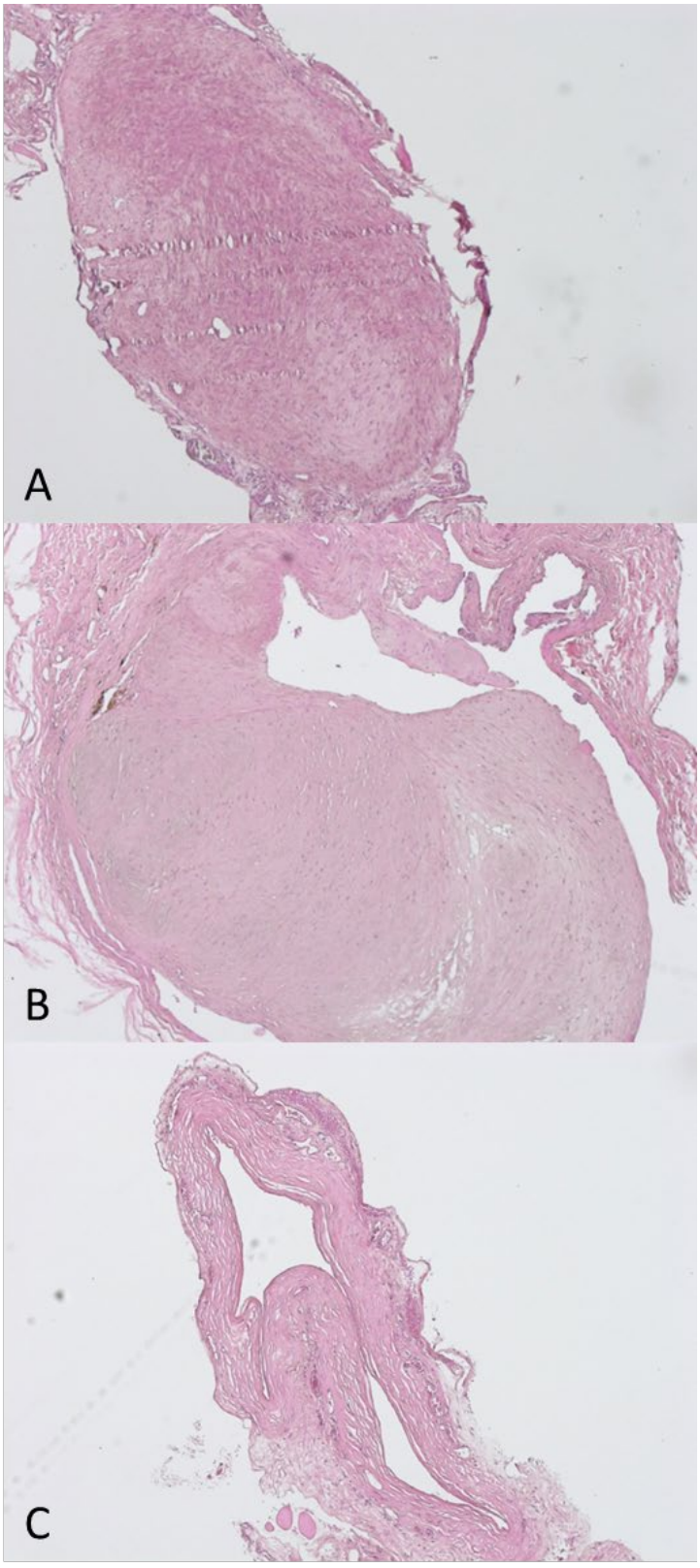

Figure 5-4 H and E stain of left external jugular vein (LEJV). A denotes an EJV in GKS double 1/2-dose conjugate treatment group demonstrating complete occlusion of vessel lumen by organised thrombus. B demonstrates al section of LEJV of sham GKS 1/2-dose conjugate treated animal with a large organised thrombus with small amounts of haemosiderin. Image C demonstrates a LEJV of GKS 1/2-dose conjugate treated animal. The section demonstrates complete patency of the EJV with no evidence of intraluminal thrombus.

5.5.3.2 Nidus thrombus formation

Large vessel thrombi were present in the nidi of all four ½-dose conjugate treatment arms. In 38% of animals (n=8; 95% CI:14 – 69%), and 80%of animals (n=5; 95% CI:38 – 96%), were observed to have large vessel thrombi in the sham-GKS ½-dose conjugate and GKS ½-dose conjugate arms, respectively, (Figure 5-5, Figure 5-6). This difference was not statistically significant (p=0.27).

Similar proportions of animals with large vessel thrombi were observed in both 2× ½ dose conjugate treatment arms with 57% of animals (n=7; 95% CI:25 – 84%), and 44% of animals (n=9; 95% CI:19 – 73%), in the sham-GKS 2× ½-dose conjugate and GKS 2× ½-dose conjugate treatment arms, respectively (Figure 5-5). No significant difference was observed between these treatment groups.

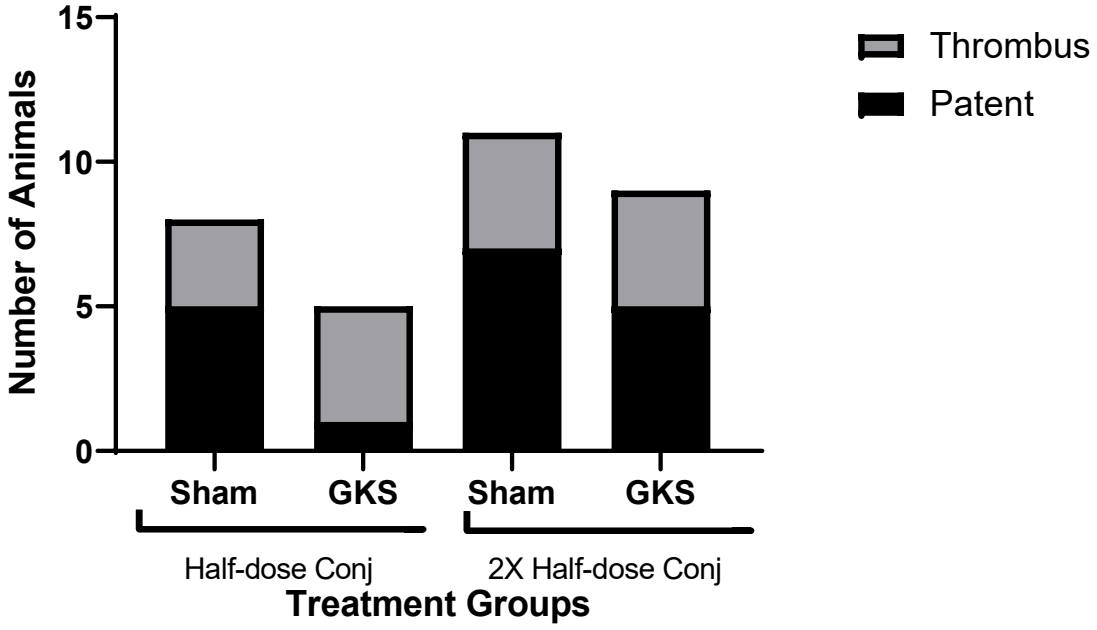

Figure 5-5 Number of animals with large vessel thrombi in 1/2-dose and 2×1/2-dose conjugate groups. Evidence of thrombus formation within large vessels in all treatment groups in a similar proportion. Differences between each GKS and their comparator group was not noted to be statistically significant (Fisher exact test - GraphPad Online calculator – GraphPad Quick Calcs Web site https://www.graphpad.com/quickcalcs, Graphpad Prism 8.2 version for Windows, GraphPad Software, La Jolla California USA).

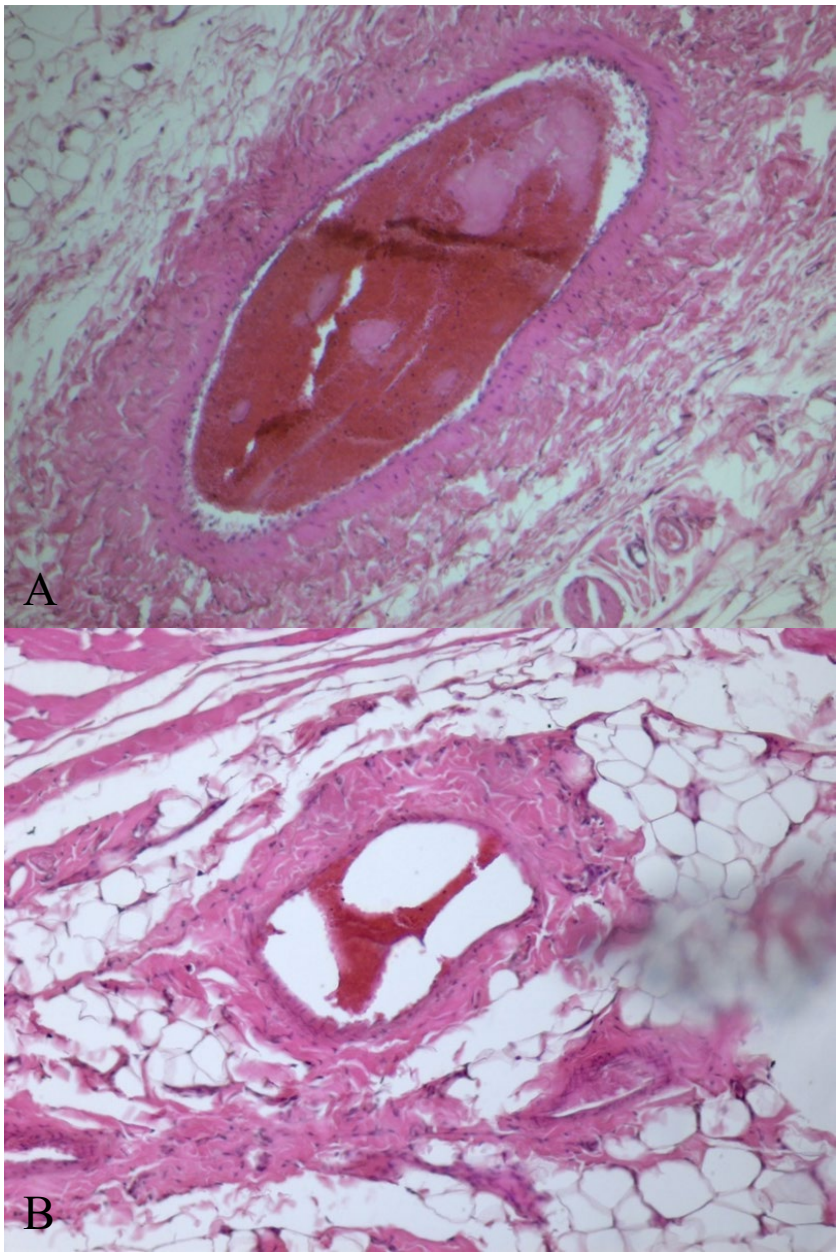

Figure 5-6 H and E stain of large AVM nidus vessels. A denotes an established thrombus in a GKS 1/2-dose conjugate treated animal. B denotes a large nidus vessel from a GKS 2× ½-dose conjugate treated animal with intraluminal acute blood but no evidence of thrombus formation

Micro-thrombi were present in the AVM nidus of all animals in the ½-dose and 2× ½-dose conjugate treatment arms (Figure 5-7, Figure 5-8). In the ½ dose conjugate arms, 7 of 8 animals (88%; 95% CI:53 – 98%), and 4 of 5 animals (80%; 95% CI:38 – 96%), had micro thrombi in the sham-GKS and GKS groups, respectively. In the 2× ½-dose conjugate group there was evidence of micro-vessel thrombus formation in 4 of 7 animals (57%; 95% CI:25 – 84%), and 7 of 9 animals (78%; 95% CI:45 – 94%), in the sham-GKS and GKS groups, respectively. All four groups demonstrated significant differences favouring micro-vessel thrombus formation when compared to the sham saline control arm and no differences between each group and its respective comparison.

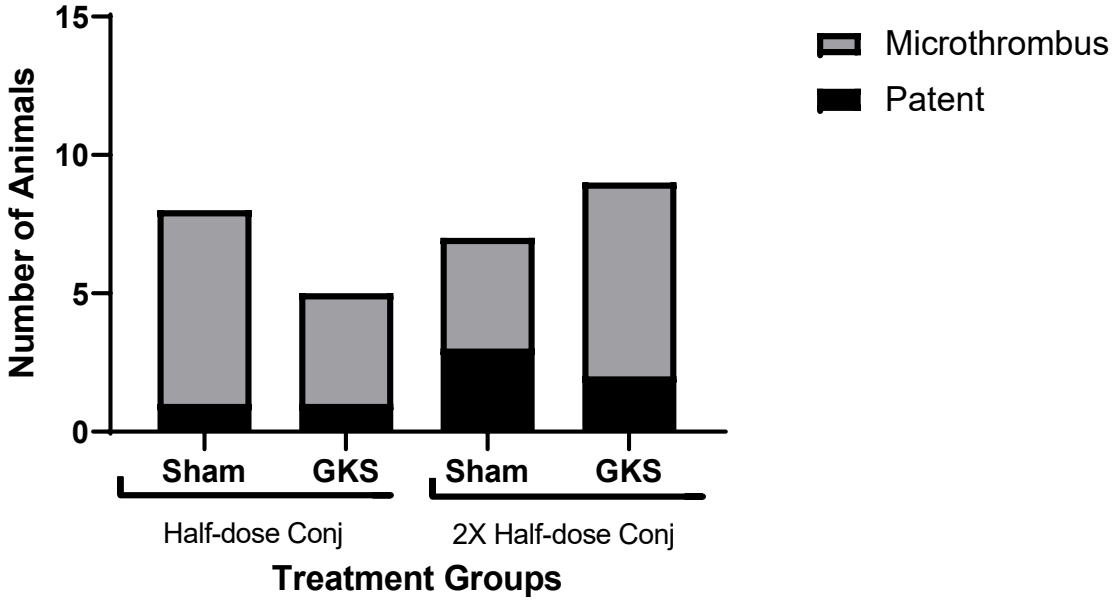

Figure 5-7 Number of animals with micro vessel thrombus in 1/2-dose and 2× 1/2-dose conjugate groups. Evidence of thrombus formation within microvasculature in all treatment groups in a similar proportion of 80% of animals. Differences between each GKS and their comparator group was not noted to be statistically significant (Fisher exact test - GraphPad Online calculator – GraphPad Quick Calcs Web site https://www.graphpad.com/quickcalcs, Graphpad Prism 8.2 version for Windows, GraphPad Software, La Jolla California USA).

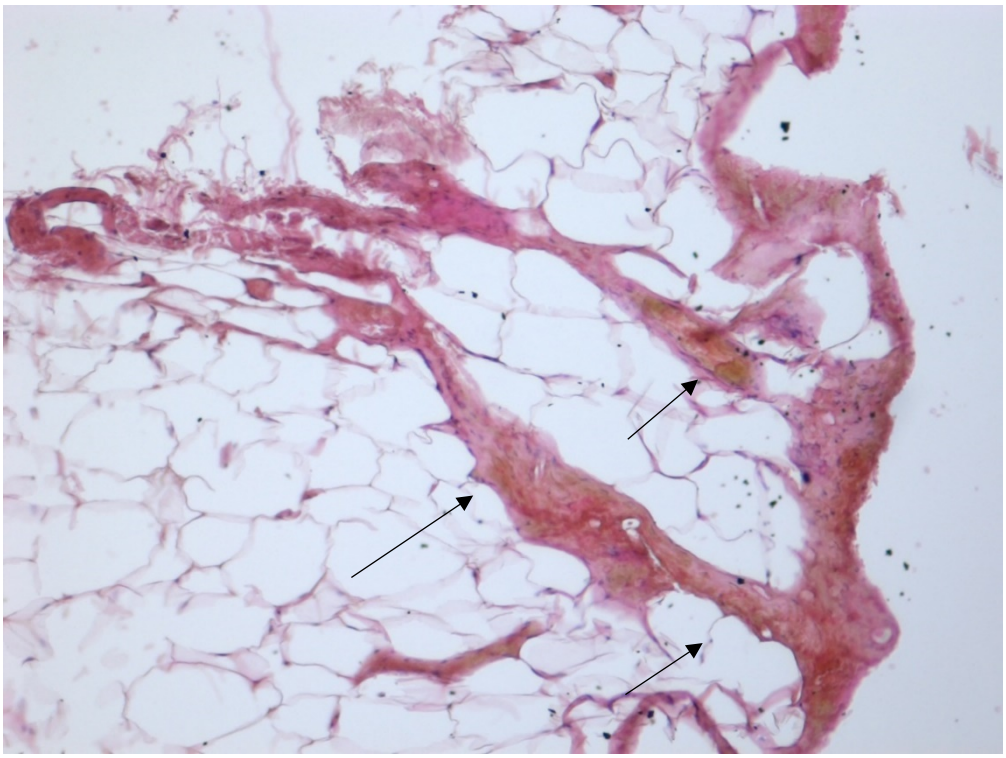

Figure 5-8 H and E stain of nidus microvessels in a GKS 2×1/2-dose conjugate treated animal. It demonstrates microvessel thrombus formation (denoted by arrows) with surrounding areas of fibrosis and haemosiderin

5.6 Discussion

This study examined the efficacy of dose modification of the annexin V/thrombin conjugate. It explored the hypothesis that by lowering the dose per weight and administering multiple doses the selectiveness and efficacy of the conjugate would be improved.

The results of this study demonstrated that by halving the dose of the annexin V/thrombin conjugate and by administering this in two doses there was a statistically significant improvement in rate of angiographic occlusion for each GKS group compared to its sham-GKS comparison arm. This finding aligns with other vascular targeting studies [198, 501], that suggest that using dose reduction and modifications to the dosage regimen could improve selectivity and reduce off-target effects.

This has now also been observed in the proposed AVM targeted treatment with our annexin V/thrombin conjugate where the maximum safe dose of conjugate may not be the most effective in causing targeted thrombus formation. It is therefore important when considering other potential targets and targeting conjugates that lower doses and multiple dose regimens are considered as they may improve the selectivity of targeting and improve AVM occlusion rates.

This finding also demonstrates the angiographic abnormalities in greater proportion within the GKS treated groups and provides evidence to support the use of GKS as a sensitising agent to create PS translocation within the AVM vessels. Although research by the Macquarie University AVM group has aimed to develop a vascular targeting technique for AVMs using radiation as a priming agent, this research is the first time that this priming technique has been demonstrated in the *in vivo* setting to a degree to cause curative occlusion of AVMs. This translocation of PS following radiation has been demonstrated in other vascular targeting research [317, 334]. Although this work established the presence of translocated PS in the *in vivo* setting in both lung cancer and glioblastoma animal models, this research (and the earlier work by Raoufi-Rad et al. [193]) with AVMs demonstrates the use of radiosurgery as a priming agent rather than conventional external beam radiotherapy. Such a focussed technique is necessary in AVM

treatment to target only pathological vessels to cause PS translocation without affecting surrounding normal brain. The previous chapter identified the effective use of the novel annexin V/thrombin conjugate to target externalised PS in AVM endothelium (Section 4). The results of this study demonstrate the effective targeting of PS using the conjugate only on irradiated endothelium.

The use of focussed irradiation as a sensitising agent to aid vascular targeting may have applications beyond the clinical setting of AVM treatment and the prevention of haemorrhagic stroke. To date, all investigation of the use of vascular targeting in conjunction with radiotherapy is in the setting of the treatment of malignant tumours both as a synergistic treatment agent [502-504], as well as a priming tool to aid in the presentation of potential targets [317, 334]. Currently, no other research examines the use of radiosurgery to sensitise tissue for vascular targeting. Our proposed treatment may find use in the treatment of tumours that previously were not able to be successfully treated with other vascular targeting techniques or that may have been difficult to treat with more conventional radiotherapy.

The histological outcomes remain difficult to interpret in this study. Thrombus formation was observed within the nidus in both large vessels and microvessels as well as in the horizontal segment of the EJV in all treatment groups irrespective of GKS exposure. The lack of a quantifiable histological outcome in this study makes it difficult to determine the significance of this finding. These results also suggest that it is challenging to estimate the extent of thrombus formation within the EJV from a single axial histological segment. It is possible that with this limited sampling of the vessel the thrombus may not be sampled and ultimately it may underestimate the degree of large vessel thrombus formation. In the future, studies that can encompass sectioning of the entire segment of the EJV with interval analysis should be performed to determine the extent of thrombus formation.

The presence of thrombus on histological examination suggests that the conjugate is successful in targeting baseline PS translocation even in non-irradiated animals, albeit not to a degree that causes

angiographic abnormality. It is postulated that outcomes can be viewed as a continuum, ranging from microvascular thrombus formation through to larger vessels, EJV, and ultimately to cause angiographic abnormalities and occlusion of the AVM. To cause durable thrombus formation of a sufficient size to cause changes in AVM haemodynamics within the model is very promising and suggests that vascular targeting may be a treatment translatable to human AVM treatment.

5.7 Conclusion

Dose modification with halving the dose and administering multiple doses of the annexin V/thrombin conjugate improves AVM occlusion rates and selectivity of targeting PS translocation following irradiation in the AVM animal model. The findings of this study suggest that PS may be a potential treatment target for AVMs, although further work is necessary to understand the basal expression in AVMs in the human setting. The use of radiosurgery may increase PS and in the combination with an optimal dosing strategy it is possible to achieve selective thrombosis in irradiated vessels and may demonstrate a potential treatment strategy for AVMs.

Chapter 6 Preliminary validation of novel radiation-induced vascular targets

6.1 Background

Findings in the previous chapters established in the AVM animal model the efficacy of an annexin V/thrombin conjugate targeting PS for inducing both histological thrombus formation and angiographic stenosis and occlusion. The targeting of PS is based on the premise that in the normal healthy physiological setting it is located on the internal leaflet of the phospholipid membrane and only translocates in response to certain stimuli [317, 334, 505, 506]. Although one of these stimuli is known to be radiation and well-studied, it is possible that other stimuli that induce apoptosis may give rise to potential off-target thrombosis in the vasculature of other organs. The observation of baseline PS translocation in non-irradiated animal model AVMs that may have occurred as a result of changes in haemodynamics suggests that vasculature under stress does have the potential for PS translocation [193]. This also raises the potential concern that baseline PS translocation may be present in normal arterial feeding vessels or the draining vein and therefore thrombotic targeting of such vessels may lead to adjacent areas of normal brain infarction or precipitate AVM haemorrhage.

In addition, although there is evidence to support PS translocation in animal model AVMs, whether this occurs in humans remains unknown. It is necessary to consider other targets that may more be more appropriate for use in radiation-sensitised AVMs.

Using a biotin-labelling approach combined with proteomic analysis to examine surface expressed proteins induced by radiation, a number of potential targets have previously been identified both *in vivo,* using the AVM model [335] (and L. McRobb, unpublished), and also using *in vitro* endothelial cell culture [326]. These proteomic studies provide a novel way of assessing large numbers of proteins for their changes in response to radiation but typically require further validation by other means. Although the previous work suggested that these targets are potentially surface expressed on endothelial cells, further work is needed to support this prior to *in vivo* assessment within the AVM model. The aim of this work was to provide further validation of the

radiation-stimulated expression of a series of these markers using immunohistochemistry and preliminary *in vivo* imaging studies to assess luminal localisation in response to radiation.

Two potential targets that were identified in the proteomic studies were the activated leukocyte cell adhesion molecule, CD166 (or ALCAM) (L. McRobb, unpublished), and the mitochondrial protein, pyruvate dehydrogenase complex subunit E2 (PDC-E2, alternatively named DLAT or ODP2) [326, 335].

CD166, otherwise known as ALCAM, is a membrane glycoprotein that is part of the immunoglobulin family [507]. Normally, this protein is located on epithelial and endothelial cells, where it is associated with intercellular junctions, forming an adhesive complex between adjacent cells to maintain tissue architecture [513]. It has also been implicated in trans-endothelial monocyte migration [508, 509]. It has also been identified in other tissues including other epithelia, lymphoid and myeloid cells, fibroblasts, neurons, hepatocytes, pancreas acinar and islet cells, and bone marrow [509-513]. The known surface distribution of this marker and localisation to the vascular endothelium would make this target a potential option for the development of future vascular targeting agents.

PDC-E2 is a mitochondrial enzyme protein that is part of a complex of enzymes that are responsible for the conversion of pyruvate to acetyl-CoA. As a mitochondrial protein, it is expected to be localised intracellularly but was previously identified as an upregulated endothelial surface protein in response to radiation in prior *in vivo* proteomics studies [326, 335](L .McRobb, unpublished) and an *in vitro* biotinylation study [326, 335]. This result was quite unexpected, but abnormal surface localisation of PDC-E2 in biliary epithelial cells is implicated in the pathogenesis of primary biliary cirrhosis, an autoimmune condition that is linked to the presence of circulating anti-PDC-E2 antibodies [514-516]. Although radiation exposure has not been directly causally linked to PDC-E2 surface localisation, it has been noted to cause an increased risk of developing primary biliary cirrhosis as evidenced in atomic bomb survivors in Japan [522]. The findings may implicate radiation exposure as a causal link in primary biliary cirrhosis and then the surface

localisation of PDC-E2 [326, 335], but further, suggest that PDC-E2 may indeed be a valid target on irradiated vessels.

6.2 Aims

- To qualitatively examine the localisation and temporal expression of PDCE2 and CD166 expression after radiation in *ex vivo* sections from the AVM animal model.
- To determine whether there is luminal up-regulation of target proteins in response to radiation in an AVM-naïve animal model.

6.3 Methods

6.3.1 Animal Model

All immunohistochemistry experiments were completed using specimens from animals which had AVM formation and GKS previously [326, 335](L. McRobb, unpublished). These experiments were conducted in a manner approved by the Animal Care and Ethics Committee (2014/051). AVM formation was completed in a manner identical to that described in Chapter 2 (Section 2.1) and as previously published [329]). Following AVM formation and a 6-week period of maturation, the animals underwent GKS (or sham GKS). Sacrifice occurred at multiple time points (3 days, 1 week, 3 weeks, 6 weeks) following irradiation with GKS (20 Gy) or sham irradiation. At sacrifice, animals were perfused with 500 mL PBS, (pH 7.4), and tissue was harvested from the AVM branches with contralateral vessels (CCA and EJV) used as comparison controls. Following tissue harvesting, the AVM samples were embedded in optimal cutting temperature compound, (OCT – 10.24% polyvinyl alcohol, 4.36% polyethylene glycol and 85.5% non-reactive ingredients), snap frozen in liquid nitrogen, and stored at -80 degrees Celsius.

6.3.2 Cryosectioning and immunostaining

Samples were cut at 10-micron thickness using a cryotome at -20 degrees Celsius and placed in groups of three on standard microscope slides. Slides were taken from frozen storage (-80 degrees Celsius) and samples were dried at 37 degrees Celsius in a drying oven. Following drying, the slides were immersed in two sequential pots of Phosphate buffered saline solution with Tween

0.1% (PBST) for 10 minutes each. Slides were then fixed in 50% ethanol/PBST for 20 minutes. Following fixing, the tissue segments were rounded with a liquid blocker hydrophobic paraffin pen (Liquid Blocker Super Pap Pen). The tissue segments were blocked in 5% donkey serum/1% bovine serum albumin (BSA) in PBST for a minimum of 1 hour with 30 to 40 µL of blocking solution added to each tissue segment.

After blocking, the blocking serum was removed, and the primary antibodies were added to each tissue segment. These included the antibodies to the targets PDC-E2 and CD166 (anti-PDC-E2, rabbit polyclonal antibody 200 µg/mL, H-160, Santa Cruz Biotech, SC – 32925; and anti-CD166, goat polyclonal antibody 200 µg/mL, Thermo Fisher Scientific, PA5-47083). An antibody to the endothelial cell marker, CD31 (Mouse anti-rat antibody, 0.5 mg/mL, BD Biosciences, Cat 555025), was also included to assist in identifying the endothelium during microscopy.

Both method and IgG controls were included for comparison purposes (rabbit IgG, Santa Cruz Biotechnologies; mouse IgG, BD Biosciences; or goat IgG, BD Biosciences). After the primary antibody solutions were added (30 – 40 µL per tissue section) the tissue samples were stored overnight at 4 degrees Celsius.

Following the refrigerated storage, the tissue specimens were inspected for evidence of tissue segments drying out and these were noted, due to the risk of high-background staining. The slides were washed in PBST for 2 periods of 10 minutes.

Species specific secondary antibodies were added (Anti-goat or anti-rabbit Alexa Fluor 647 (AF647) and anti-mouse Alexa Fluor 488 (AF488) – Life Technologies) in a 1/500 dilution in 1% BSA/PBST with 30 – 40 µL added to each tissue segment. The slides were covered to prevent fluorophore bleaching and were stored at room temperature for 1 hour.

The slides were washed in PBST for 5 minutes and nuclei were counterstained with DAPI (4',6-diamidino-2-phenylindole, 5 µg/mL) in 1% BSA/PBST. A volume of 30 to 40 µL of DAPI was added to each tissue segment and the slides were covered and stored for 2 minutes at room

temperature. The tissue segments were washed for a further 5 minutes in PBST and mounted in aqueous fluorescent mounting.

The slides were reviewed using a fluorescence microscope (Zeiss Axioimager Z2). Tissue segments were observed, and qualitative assessment of fluorescence was noted and recorded. CD31 fluorescence was noted to determine the location of the endothelium and co-localisation with other targets. Each target was assessed at multiple time points.

6.3.3 Animal Model and GKS for in vivo fluorescent optical imaging

A small pilot study was performed to examine potential target expression *in vivo* using *in vivo* fluorescent optical imaging. Ethics approval was obtained from the Macquarie University Animal Ethics Committee (ARA 2017/018). Sprague-Dawley male rats were obtained at 6 – 12 weeks of age with a weight range of 250 – 500 g (N=2). Animals did not undergo AVM creation surgery as in the previous experiments. The animals were anaesthetised with intraperitoneal ketamine and metatomidine injection and secured supine in the custom-made frame as per the methods detailed in Chapter 2. Planning for GKS was conducted with axial CT imaging with 3D reconstruction. Treatment was planned for a marginal dose of 20 Gy. As these animals were AVM naïve, the treatment field was centred on the position of the left EJV proximal to its union with the left subclavian vein (Figure 6-1). Following reversal of the anaesthetic with atipamazole and recovery as per the prior published method the animals were monitored for 1-week post GKS treatment.

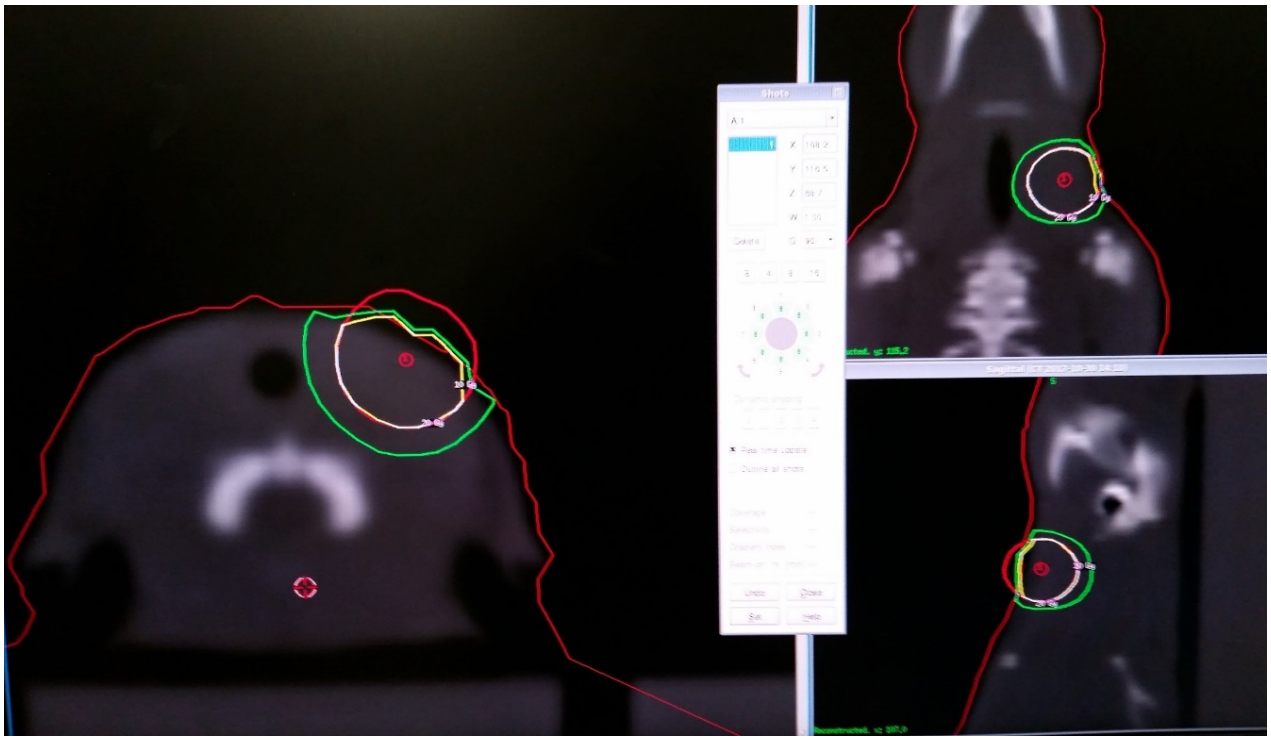

Figure 6-1 CT planning images for GKS in AVM naive animals. A marginal dose of 20 Gy was administered to the left EJV prior to union with the left subclavian vein. This treatment was identical in dose to the AVM model animals presented in earlier chapters but was targeted at the midpoint of the EJV within the animal's neck (Original image).

6.3.4 Near-infrared (NIR) dye preparation and NIR fluorescence optical *in vivo* imaging

In vivo fluorescence optical imaging was performed to localise the luminal expression of PDC-E2 [193]). The antibody-dye probe was created by conjugating the NIR dye, Xenolight C750 (Caliper Life Sciences Inc., MA, USA, PK1125674) to the antibody anti-PDC-E2 (Ab sc-32925 rabbit polyclonal, Santa Cruz). Conjugation was performed as per the manufacturer's instructions with a calculated degree of labelling (DOL) achieved of 0.8. The conjugate was run on an SDS-PAGE gel (as per Chapter 2, Section 2.7) to assess efficiency of the reaction and conjugate size (Figure 6-2).

The animals were anaesthetised with inhalation isoflurane (2%). On confirmation of adequate anaesthesia, the anterior neck was shaved, and the animal was positioned prone in a Kodak In Vivo Multispectral Imaging System FX cabinet (Carestream, NY, USA). The Xenolight 750-conjugated probes were injected via the tail vein over a 1-minute period, (drawn up to a volume of 400 µL) and followed by a 200 µL normal saline flush.

The animals were then imaged with a NIR fluorescence image, (excitation filter, 730 nm; emission filter, 790 nm; exposure time, 60 sec; f-stop = 2.5; field of view = 120 mm). Prior to injection with the NIR conjugate, an image was taken in the Xenolight 750 NIR fluorescence channel to provide a background comparison reading.

This study was a pilot study designed to determine the degree of upregulation and luminal distribution of PDC-E2 in irradiated AVM naïve animals. It was also designed to determine an optimal dosage and injection time for the NIR dye conjugate following radiation. Initial dosing was based on previously published work [313]. Two animals underwent radiation and conjugate injection at different conjugate dosage and injection time points: The first animal had 60 µg/kg PDCE2-CF750 conjugate injected 48 hours post GKS; the second had 120 µg/kg PDCE2-CF750 conjugate injected 72 hours post GKS.

Animals were imaged immediately following NIR dye injection and daily for 8 days following GKS and at a further time point of 15 days following GKS.

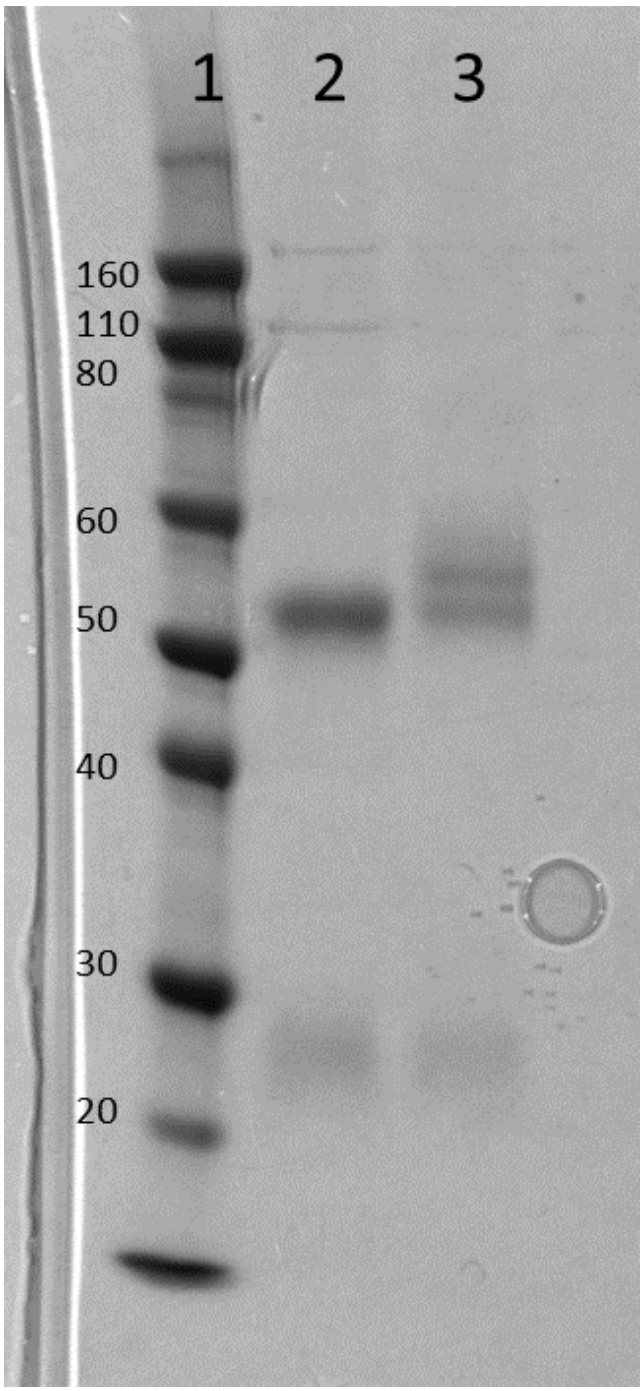

Figure 6-2 SDS-PAGE gel of PDCE-2 antibody conjugate for use in in vivo imaging. Lane 1 denotes the reference protein ladder demonstrating MW in kDa. Lane 2 denotes the PDCE2 Ab sc-32925 rabbit polyclonal and Lane 3 denotes the PDCE2-CF750 conjugate. The IgG heavy chain is denoted by the band at 50-55kDa MW and the IgG light chain at 25-28kDa MW

Primary outcome measures included the immunofluorescence signal noted in the anatomical region of the GKS treatment field. The contralateral, non-irradiated region acted as an internal control. Due to the small sample size and pilot-study design of this experiment the fluorescence was only qualitatively assessed.

6.4 Results

6.4.1 Immunolocalisation of PDC-E2 in rat AVM nidus in response to radiation

The targets mitochondrial PDC-E2 and CD166 were assessed across multiple treatment time points and in both GKS and sham GKS samples. Control sections incubated with IgG did not demonstrate any reactivity.

PDC-E2 was assessed for localisation and expression at all of the time points from 3 days post GKS treatment to 6 weeks in both GKS and control (Figure 6-3). Four animal AVM samples were included per treatment and time point (n=4), with the exception of three animal samples in the 3-day sham GKS group. At all-time points, general fluorescence was observed throughout the entire tissue irrespective of GKS status, consistent with the expected ubiquitous expression of PDC-E2 in the mitochondria of all cells. PDC-E2 was present in cells throughout the vessel wall with a segment that co-localised with CD31, providing evidence of endothelial PDC-E2 expression. At the 3-day timepoint, all four GKS samples demonstrated a slight increase in endothelial fluorescence that was not observed in the sham GKS at the same time point. Minimal fluorescence was observed at the 1 week and 3-week time points in either GKS treatment or the sham GKS control group. At 6 weeks there was an increase in general tissue fluorescence of PDC-E2 in both GKS and sham GKS group, relative to earlier time points, with some evidence of greater endothelial fluorescence in the GKS treated group. It was unclear why expression seemed significantly higher at this time point relative to earlier time points but may have represented a general change in expression in response to AVM creation or may have been associated with tissue preparation. Due to the limited evidence for significant induction of PDCE2 in response to radiation and the ubiquitous nature of the expression, further quantitation was not performed.

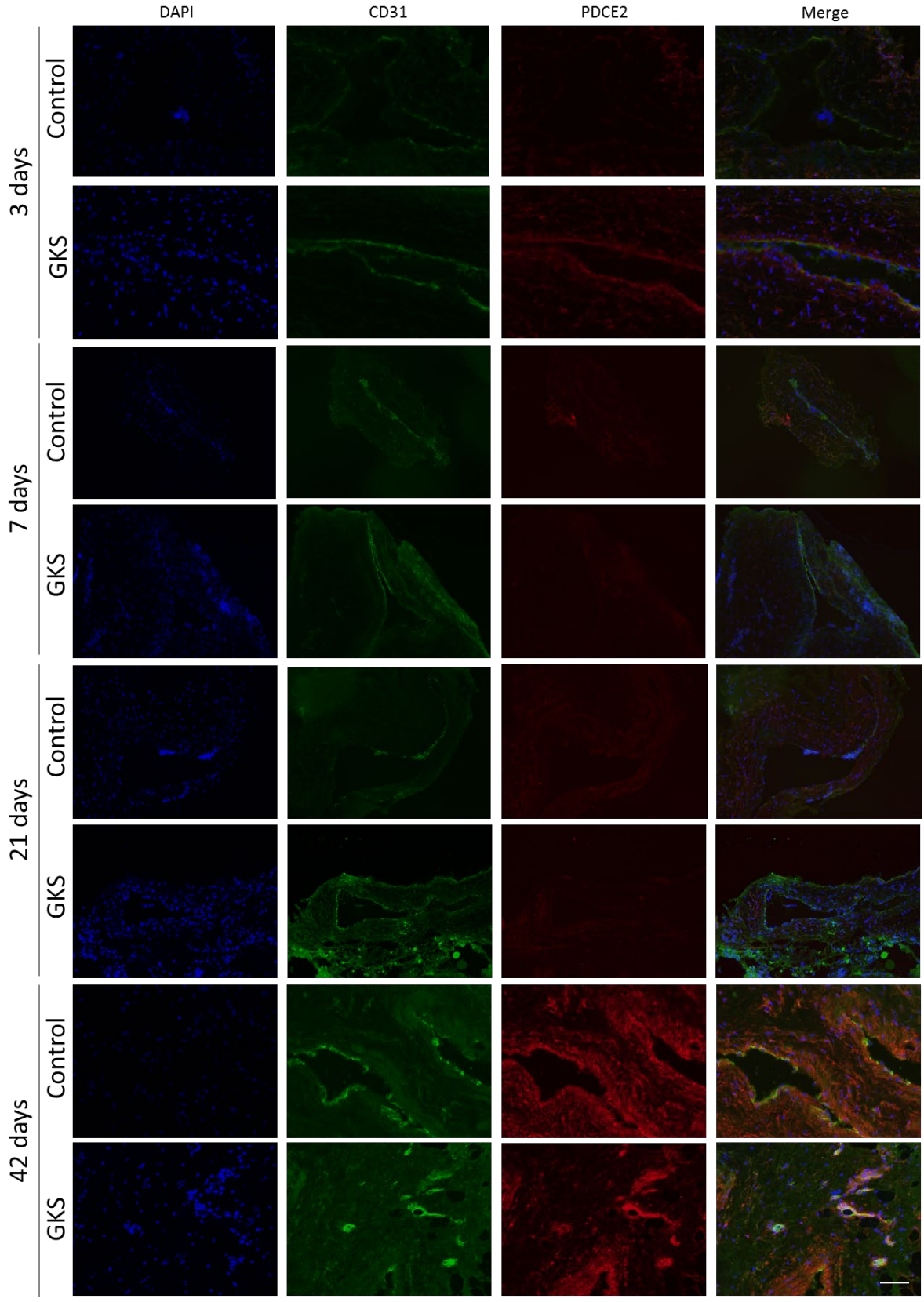

Figure 6-3 Immunohistochemical localisation of PDCE2 in the rat AVM. The surgically created AVMs were excised 3 days, 7 days, 21 days or 42 days following GKS (20 Gy) or sham GKS (control) treatment. Representative images of AVM nidus vessels stained with antibodies targeting PDCE2 (AF647, red); endothelial marker CD31 (AF488, green); nuclei were stained with DAPI (blue). Original magnification 200x, Scale bar – 100 µm. (Original image).

6.4.2 Immunolocalisation of CD166 in rat AVM nidus in response to radiation

CD166 was assessed at all of the time points and in both GKS and sham GKS samples with four animal samples used for each time point of GKS treatment and at 6 weeks with sham GKS, (n=4), and three animal samples used for the remaining sham GKS time points (n=3) (Figure 6-4). CD166 fluorescence was localised to the endothelium of both macro and microvessels as evident from co-localisation with the CD31 endothelial marker. Basal expression of CD166 was observed in the non-irradiated AVM samples and there did not appear to be any significant difference in either localisation or magnitude of expression between the GKS and sham GKS groups.

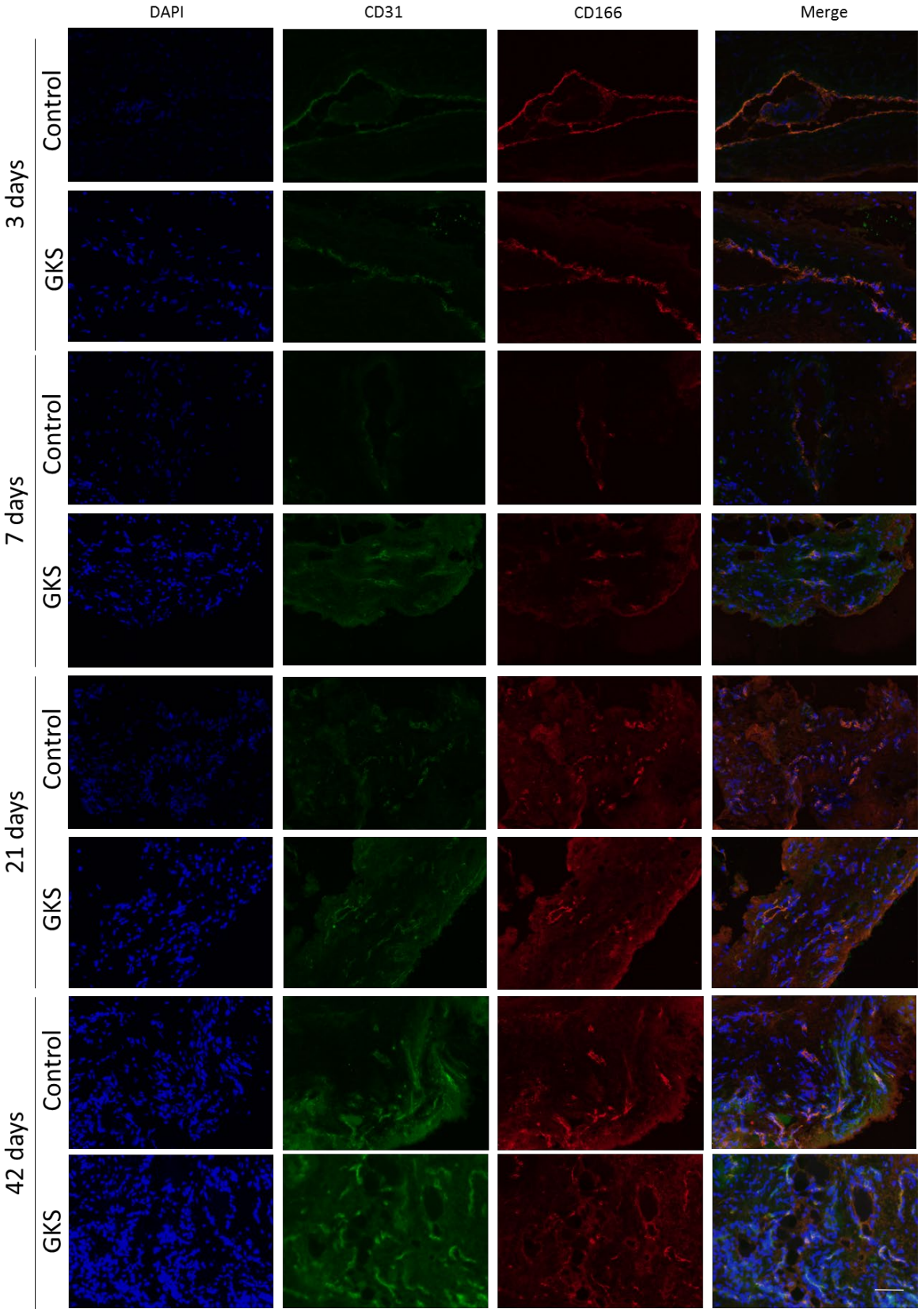

Figure 6-4 Immunohistochemical localisation of CD166 in the rat AVM. The surgically created AVMs were excised 3 days, 7 days, 21 days or 42 days following GKS (20 Gy) or sham GKS (control) treatment. Representative images of AVM nidus vessels stained with antibodies targeting CD166 (AF647, red); endothelial marker CD31 (AF488, green); nuclei were stained with DAPI (blue). Original magnification 200x, Scale bar – 100 µm. (Original image).

6.4.3 Results of *in vivo* imaging for PDCE2

The immunohistochemistry studies failed to reveal any significant upregulation of PDCE2 or CD166 in response to radiation. This may have been due to the high basal expression in cells in non-irradiated tissues. For CD166, the high basal level of expression was unexpected and further *in vitro* work (L. McRobb, unpublished) confirmed a relatively high basal level on cultured brain endothelial cells that may make this target inappropriate for further development. For PDC-E2, the high basal expression was not unexpected given the ubiquitous expression in the mitochondria, but due to the limitations of immunohistochemistry techniques, the exact location of the increase in PDC-E2 expression and specifically whether it is located on the luminal surface of the endothelium or intracellularly remains unknown. Further *in vitro* studies (L. McRobb, unpublished) continued to confirm a unique luminal localisation after irradiation and therefore PDC-E2 was considered for further validation using *in vivo* imaging to determine the location and degree of increase of protein expression similar to the previous experiments conducted on PS translocation and cellular adhesion molecules [193, 313].

Two animals underwent GKS and *in vivo* imaging with no complications and tolerated the injection of conjugate (Figure 6-5). Both animals demonstrated an area of fluorescence that corresponded to the anatomical location of the left EJV and the irradiated region. This appeared to increase in intensity over the 1-week period. Although, the intensity was present at the day 15 time point after GKS it was noted to have reduced signal intensity. The higher dose of 120 μg/kg appeared to elicit a higher and more diffuse level of binding relative to the 60 μg/kg dose. In contrast, no significant fluorescence was noted on the right contralateral, non-irradiated region, suggesting a specific accumulation in response to irradiation. Although care was taken to shave the anterior neck, significant autofluorescence was present from the animal fur, particularly on the flanks.

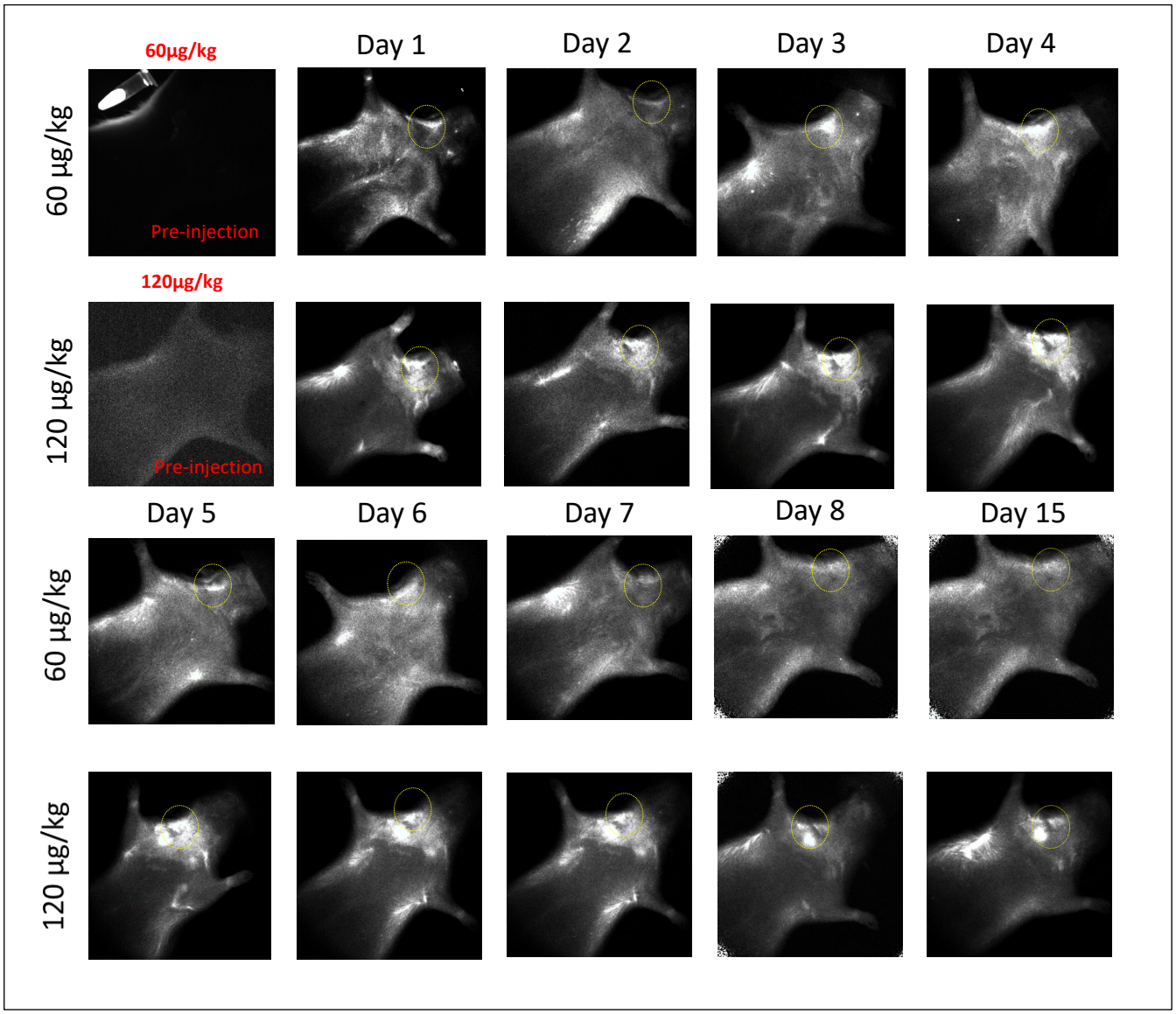

Figure 6-5 In vivo near-infrared fluorescent optical imaging of PDCE2 expression in response to GKS. A PDCE2-CF750 dye conjugate was administered to 2 rats at doses of 60 or 120 ug/kg by intravenous injection and monitored for 15 days. Irradiation was delivered by GKS at a dose of 20 Gy to the left EJV. The yellow ring denotes an approximate field of treatment for GKS (Original image).

6.5 Discussion

For vascular targeting in AVMs, an ideal target would be one that is localised to the endothelial luminal surface and only upregulated in the presence of radiation. The use of PS as a target, while looking promising, has potentially some limitations if there are flow-modulated effects in feeder vessels to an AVM as discussed earlier. Other recent studies have sought to identify novel radiation-induced targets expressed at the endothelial surface through the use of protein biotinylation and proteomic analysis [326, 335](L. McRobb, unpublished data). Targets identified in large scale proteomic studies are ideal for generating new hypothetical targets, but typically require further validation due to the potential for the generation of false hits. The current experiments demonstrate the use of immunohistochemistry and *in vivo* imaging to further validate potential novel markers that are upregulated by radiation at the surface for use as a potential target for vascular targeting with a pro-thrombotic compound in AVM treatment. Using this approach, the targets CD166 and PDC-E2 were assessed.

In this study, CD166 fluorescence was observed with a high level of basal expression in non-irradiated endothelium and in a similar intensity in irradiated tissue. This was strongly co-localised with the endothelial marker CD31 and not in other cell types, consistent with the literature. However, the high basal expression of CD166 may impede its use as a target within the radiation-sensitised targeting paradigm and the risk of off-target binding on normal endothelium may be high. CD166 has been used as a vascular target in the setting of prostate cancer with an internalising, single-chain variable fragment antibody, to good effect [518]. Furthermore, the success of PS targeting in the AVM model in the current studies suggests that even in high basal expression, a vascular target may still be a viable treatment option if there is an expression difference and dose is modulated.

Previous immunohistochemical studies performed on tissue extracted 24 hours after radiation suggested there was an increase in PDC-E2 expression in response to the radiation [326]. The findings from this study have identified a potential nominal increase in fluorescence within the

AVM samples from the irradiated time points of 3 days and 42 days, however this was not absolutely quantitated due to relatively low levels of expression as well as the heterogeneous nature of the tissue that makes quantitating endothelial expression difficult. The exact distribution of the fluorescence from PDC-E2 is difficult to interpret as it appears to be upregulated in a similar intensity across the entire tissue segment. This fluorescence does, however, co-localise with the endothelial marker CD31. This would suggest that in part the radiation-induced upregulation of PDC-E2 observed in these tissues involves the endothelial layer. In addition, while there is potential for endothelial upregulation in response to radiation, these findings do not determine whether the protein is surface expressed in the endothelium [326, 335]. To confirm the presence of PDC-E2 on the luminal surface of the endothelium in the AVM model in response to radiation and its absence at the surface on non-irradiated endothelium, further work with *in vivo* imaging was required to determine whether PDC-E2 is a viable target in AVMs.

The use of immunohistochemistry in collected AVM samples is useful for assessing the tissue qualitatively for evidence of upregulation of the target in question or for establishing localisation, however, it does not provide quantitative assessment. Furthermore, even with the use of CD31 co-localisation to provide an endothelial reference, the presence of fluorescence does not necessarily indicate surface expression of the target in this tissue segment. While for these targets, immunohistochemistry proved limited in its ability to assess radiation-induced changes in the vascular wall, its use in future for other more suitable targets, that is, those that may be completely absent on the endothelium in the absence of radiation, may still be appropriate. This sort of study has the advantage of using multiple animal AVM samples from multiple time points for the ready analysis of multiple targets which cannot be done readily in live imaging studies which require a series of individual animals for each protein target. Overall, the inconclusive results of the immunohistochemical studies suggested that both targets require further investigation in the form of *in vivo* imaging to better understand the biodistribution and magnitude of their upregulation within the AVM model. However, recent studies *in vitro* (L. McRobb, unpublished), suggested

that basal expression of CD166 on brain endothelial cells in the absence of radiation may be a continuing problem for off-target binding, while PDC-E2 remained a valid target with little to no expression on normal ECs, but a significant increase at the surface after irradiation. Hence the small pilot study using *in vivo* imaging was performed only for PDC-E2 analysis.

This pilot study was an initial project examining the upregulation and location of PDC-E2 in an AVM naïve rat using *in vivo* fluorescent optical imaging. The results of this study highlight an upregulation of PDC-E2 related fluorescence in the anatomical vicinity of the left EJV. The fluorescence accumulation appeared to increase over time with a peak at 7 days following antibody-dye injection with limited clearance by 15 days. The contralateral right side of the animal was used as an internal non-irradiated control, and minimal fluorescence was observed within this region at either dose. These findings are in line with findings from previous studies suggesting an upregulation and surface expression of PDC-E2 following radiation exposure in the AVM model [326, 335].

This study also demonstrates the ability of the anti-PDC-E2 Xenolight C750 conjugate to bind in the region whilst being delivered in the blood. Due to limited availability of PDCE2 antibodies commercially, a rabbit polyclonal was used. This however is not ideal, and the use of monoclonal antibodies would be preferred to reduce any off-target, non-specific binding. However, these preliminary results give support to further work and creation of a new antibody. Furthermore, the level of fluorescence obtained with each dose suggests for further studies that appropriate amounts of fluorescence indicating PDC-E2 upregulation may be achieved using the lower dose of 60 µg/kg, and perhaps testing of a subsequent lower dose may be useful. These findings will require further validation in larger trials.

It is important to highlight that this study is a pilot study and has been performed on a small sample size. Furthermore, this study was completed on AVM naïve animals using a non-arterialised left EJV. It is possible that with the addition of the altered haemodynamics of an AVM that the distribution or magnitude of PDC-E2 expression could be altered significantly. In addition, at this

stage there is no IgG control group or independent non-irradiated control (although the contralateral was used) to provide a comparison. Future work would need to include a larger sample size with both control groups.

6.6 Conclusion

Overall, the findings from this preliminary *in vivo* imaging work are promising and highlight a possibility that PDC-E2 is not only up-regulated following exposure to targeted radiotherapy, but also present on the luminal surface of the endothelium. This suggests that PDC-E2 may be a potential target for AVM targeted treatment following radiosurgery. To confirm this finding and to quantify the degree of upregulation of this target further work is necessary on our AVM model on a larger scale with the inclusion of appropriate control arms.

Chapter 7 General Discussions and Future Directions

7.1 Overview

AVMs, if left untreated, pose a life-long risk of stroke, neurological disability, and death. Although the current treatments of microsurgical resection, radiosurgery and endovascular embolisation are effective in certain subtypes, there are AVMs that have no effective treatment available. In particular, 90% of large, deep AVMs have no effective treatment and, in the case of the very young, have a high lifetime risk of haemorrhage [85].

An attractive potential treatment in AVMs is that of vascular targeting. This technique has demonstrated some success in the treatment of cancer and would allow the systemic administration of a targeting compound bound to a pro-thrombotic agent. The challenge in developing such a treatment in AVMs is complicated by the fact that, unlike tumour endothelium, the molecular differences expressed in AVM endothelium are not unique, therefore creating the potential to inappropriately target non-AVM sites and cause thrombosis elsewhere. It is for this reason that targeted radiation has been proposed as a priming agent, to evoke changes in the presentation of molecules on the luminal surface of the endothelium in the AVM volume. These molecules are then used to direct a targeting agent conjugated to a pro-thrombotic molecule.

Previous work using *in vivo* imaging has demonstrated translocation of PS within the luminal surface of the endothelium following irradiation in the AVM animal model [193]. PS is an attractive target due to its localisation to irradiated endothelium and its use as a potential vascular target in the setting of cancer. Previous use of a non-ligand approach to PS targeting with TF and LPS has demonstrated some success in causing small vessel thrombus formation in the animal model, but no thrombus was formed in large high-flow vessels [217].

The primary aim of this research was to examine the efficacy of a ligand-directed vascular targeting treatment technique within the AVM animal model. Through the use of an annexin V/thrombin conjugate, this study has now successfully demonstrated occlusion of high-flow

arterialised veins as well as microvasculature. Furthermore, with dose modification, this study has demonstrated selective AVM occlusion in GKS-treated AVMs. The rate of systemic thrombus formation from this treatment was low in this study. This research is "proof of principle" that a ligand-directed vascular targeting approach can be used effectively to cause occlusion of high-flow arterialised vessels that are analogous to the human AVM setting. These results agree with recent studies from the Macquarie University AVM Research Group performed preliminary research with the annexin V/thrombin conjugate in an *in vitro* setting. This method examined the conjugate in a parallel flow system using irradiated ECs exposed to high flow and whole blood with conjugate injected into the system. The results of this started demonstrated no off-target thrombosis on non-irradiated cells, but demonstrated a combinatorial effect of radiation dose and conjugate dose on the degree of thrombosis [519]. Although these findings did not demonstrate the dosage response that was observed in the *in vivo* work, the work is limited by the *in vitro* system which does not completely reflect the full physiological AVM model that is closer to the *in vivo* AVM animal model.

7.2 PS and Other targets

The use of PS as a target was prompted by its detection *in vivo* in the AVM model as a response to radiation [193], as well as its use in cancer research, where translocation has been noted as a response to cellular stress, reactive oxygen species exposure, and a relative hypoxic tumour environment [213, 334]. It is generally accepted that in healthy ECs, PS is maintained on the inner leaflet of the plasma membrane and translocates to the external surface only in response to cellular injury, either from disease or from an external source such as radiation [317, 334, 505, 506, 520].

Although, this would suggest that PS may be a useful target in the development of an AVM vascular targeted technique following radiosurgery, there are concerns in its use in the human setting. Earlier research concerning PS distribution following radiation has demonstrated PS externalisation both as a baseline in non-irradiated animals as well as an increase following radiosurgery within the model AVM [193]. The exact distribution of the translocation is difficult

to determine, whether it has propagated along feeding arteries or distally along the arterialised EJV. It is therefore possible, in administering this PS targeting treatment in human AVMs that inappropriate binding of the conjugate could occur in vessels located within the normal cerebral circulation exhibiting PS from the change in haemodynamics occurring within an AVM. This could result in occlusion of normal vessels and potentially adjacent infarction of normal brain tissue. It could also result in premature draining vein occlusion which is widely recognised as an important cause of spontaneous haemorrhage of brain AVMs during microsurgical resection [521].

The concern of possible off-target effects with distant sites of thrombus formation and potential ischaemia has been discussed within this thesis. Although in our model there was no evidence of systemic thrombus formation it is difficult to be certain whether PS translocation occurs in other non-AVM tissues. Although PS translocation is well recognised in the cancer literature it also can occur in other non-malignant processes such as hyperlipidaemia and atherosclerosis [344, 528]. Although this concern does need to be addressed prior to the translation of this treatment to the human setting it is likely not be of a practical concern due to most patients with AVMs being treated will be young and therefore unlikely to exhibit significant degrees of atherosclerotic disease.

Furthermore, although the AVM model has been demonstrated to be structurally and morphologically similar to human brain AVMs [280, 329], whether PS translocation occurs in human AVMs either as baseline or as a direct consequence of radiosurgery, remains unknown. Current *ex vivo* techniques of assessing microsurgically resected AVMs are not sufficient to localise the translocation to the apical surface of the AVM endothelium. It is possible to extrapolate cancer research that highlight PS translocation in tumour-associated endothelium [317, 334]. Moreover, apoptosis in AVMs has been recognised within AVM non-endothelial tissue, presumably as a direct consequence of the haemodynamic changes associated with the fistulous arteriovenous connection [528]. Therefore, as PS externalisation has an accepted role in apoptosis

it is possible that it is externalised in AVM endothelium before, and after radiation. Despite these extrapolations there is currently no clear evidence to support PS translocation in human AVMs.

It is because of these reasons that it is necessary to identify the presence of PS translocation in human AVMs both with, and following radiosurgery, as well as an accurate assessment of its distribution within the internal AVM anatomy prior to human translation of an AVM targeting treatment. Molecular *in vivo* imaging such as Positron emission tomography (PET) has the potential to identify our proposed targets and to provide assessment both prior to radiosurgery and at multiple time points following the treatment. Currently, a number of molecular probes are used to assess apoptosis *in vivo* through targeting of PS translocation, including technetium-labelled annexin V (^{99m}Tc-annexin-V) [529]. Although this technique has demonstrated some effect in atherosclerosis and head and neck cancers [524, 525], it is hampered by its high molecular weight and degraded image quality [532]. Alternative probes targeting PS have been proposed in the literature such as the C2A domain of synaptotagmin I [527, 528], however, these studies are still preliminary. Further work is necessary to identify a probe of sufficient quality to provide a high-quality image needed for this proposed research.

It is also possible that an alternative target may be a more efficacious and safer alternative to PS in AVM vascular targeting. Targets such as PDC-E2 and proteolytic targets of ADAM10 are upregulated following radiation in the AVM model [326, 335]. This research has demonstrated an increase in the model AVM of PDC-E2 using immunohistochemistry. Using a histological technique is limited due to the difficulty of quantifying the degree of upregulation and determining whether the target is luminally projected in the AVM endothelium. It is therefore necessary to further examine these potential targets using *in vivo* imaging techniques. Also included in this research are promising findings of a pilot study suggesting that PDC-E2 may be both upregulated 1 week following radiation in irradiated blood vessels and luminally projected and accessible by antibodies from the blood on the endothelial cells. These findings will need further validation on a larger scale and using the AVM rat model.

CD166 would seem at face-value to be an attractive potential target due to our knowledge that is expressed in the endothelium and its external location of the plasma membrane. Although this was identified within the endothelium of all of the sample AVMs using immunohistochemistry it was noted to have increased in the samples that had been exposed to radiation. Although, in theory, there could be a change in the proportion of CD166 that is expressed luminally these findings suggest that it would be unlikely to be a candidate in the development of a targeted AVM treatment.

More recent research using DNA sequencing techniques and polymerase chain reaction (PCR) analysis with tissue and blood samples of human AVMs has implicated *KRAS* mutations in approximately 50% of sporadic AVMs [399]. KRAS is an effector molecule that is involved in the activation of a range of cellular signalling systems including the MAPK-ERK signalling pathway and the phosphoinositide 3 kinase pathway [529]. *In vitro* testing of mutant *KRAS* in endothelial cells demonstrated increased expression of genes involved in angiogenesis and Notch signalling, with enhanced migratory behaviour [399]. These mutations are known to drive strong MAPK–ERK signalling [63], and have been implicated both in tumourigenesis [64], and in non-cancer settings such as endometriosis [530]. These findings and the high frequency of the mutations suggest that the mutations arise early in AVM development and may potentially be a primary event in their pathogenesis, supporting a genetic cause for AVMs [399].

This finding also has therapeutic implications as it may demonstrate a potential target for AVM treatments. Currently, there are no direct pharmacological inhibitors of KRAS but other agents targeting the downstream kinases such as small molecule MEK inhibitors may be useful. These inhibitors have been examined in the cancer setting both as single agents and in combination with cytotoxic chemotherapy and other targeted agents to some success, particularly in melanoma [68]. Further work is needed to understand the distribution of *KRAS* mutations in sporadic AVMs that may give rise to other targets, potentially without the need for radiation sensitisation.

Although the use of the novel annexin V/thrombin conjugate has demonstrated promising findings regarding targeting and occluding a rat model AVM, consideration of other combinations of ligands and effector agents, or the delivery method, may further improve the efficacy and safety of an AVM vascular targeting treatment.

Annexin V as a targeting ligand was chosen because of its high binding affinity to PS and its extensive use as a labelling agent [491-493]. This research has demonstrated effective targeting with annexin V at varying dosage regimens. It has demonstrated annexin V selectively targeting PS externalisation in the setting of lower dose per weight and in multiple dose preparations. It is, however, possible that the anticoagulation function of annexin V through the blockage of PS may be simultaneously inhibiting the procoagulant functions of PS [492, 531-533]. Despite this consideration, high rates of thrombus formation were noted in both macro and microvessels.

An alternative method of targeting PS may be through an antibody-targeting PS such as bavituximab. Bavituximab and its related antibodies 3G4 and 2aG4 differ in their action to annexin V as they do not bind directly to PS but rather to β2-glycoprotein 1 after it forms a complex with PS [317, 334, 497]. This particular antibody has undergone extensive animal studies, phase I, and II clinical trials in hepatocellular carcinoma, malignant melanoma, glioblastoma multiforme, and rectal cancer [317, 334, 494-496]. It has also been considered in the treatment of hepatitis C, in which it is undergoing Phase I and II clinical trials [540]. It is also undergoing phase III clinical trials in non-small cell lung cancer and breast cancer [499, 500]. The proposed use of PS targeting in this context is primarily as an immune modulator through PS blockade, rather than as a target for drug delivery [496, 498]. Despite this treatment proposal in cancer, it has been less effective in the breast cancer and non-small cell lung cancer settings where phase III trials have been discontinued on preliminary analyses due to the lack of improvement in overall survival. Despite this lack of efficacy, there may be a role of bavituximab or other PS targeting antibodies as part of

combination treatments with other immunotherapies or chemo-radiotherapy in cancer therapy [535].

Although bavituximab has demonstrated mixed results in cancer research, an alternative method of targeting of PS may still be a viable alternative to annexin V and as yet, its use in AVM targeted treatment remains unknown. It is also, however, possible that through the obscuration of PS by an antibody there may be an anticoagulant effect reducing AVM occlusion as was suggested with annexin V [492, 531-533].

Thrombin has been used as an effector agent in these targeting experiments to good effect. There are, however, other effector alternatives, such as truncated tissue factor tTF [454]. The use of tTF is an attractive alternative to thrombin for a number of reasons, firstly, as a human protein it should be devoid of antigenicity and it is also fully functional in rodent models similar to thrombin [217, 312, 360]. In addition, tTF is highly effective as a prothrombotic agent and activates a chain of coagulation factors with the potential to cause a magnified pro-thrombotic effect above that of thrombin which occupies a downstream role in the coagulation cascade. This could mean that an amplified cascade would involve multiple thrombin activations using tTF. Conversely, the amplified thrombotic response could, in AVMs, result in more extensive vessel occlusion that may result in thrombosis of feeding arteries or the draining vein precipitating brain infarct or AVM haemorrhage respectively.

The use of tTF has been well validated for use in cancer research where it has demonstrated widespread and durable thrombus formation [191, 217, 453]. There is also evidence to suggest that the presence of PS is essential for the coagulant activity of tTF [365]. In using annexin V, (or an alternative antibody to PS), it is possible to obscure it from tTF and this has the potential to reduce the thrombogenic quality of tTF. Conversely, however, if an alternative target was used, the known PS translocation in the model may further amplify the thrombotic effect of tTF effector conjugate. It may also have an improved safety profile than thrombin which does not require the presence of PS for activation of the coagulation cascade.

The goal in the treatment of brain AVMs remains complete occlusion of the fistulous connection. Due to the high velocity of blood flow and complex vascular networks involving multiple arterial feeding vessels, complete occlusion remains a theoretical challenge for a systemically administered treatment such as the proposed vascular targeting method. These considerations of both targeting and effector agent may demonstrate potential methods to improve both specificity and efficacy of the treatment.

7.4 Translation from animal model to the clinic

Prior to translation to human brain AVMs treatment it is necessary to understand the safety and efficacy of the vascular targeting treatment. The use of the rat AVM model has provided a comparatively inexpensive and reproducible model with which to test the annexin V/thrombin conjugate. This model has also been validated to be closely similar to human brain AVMs [280, 329]. However, this model is extracranial, and the differing rodent physiology would make it problematic to directly translate to the human setting. It is therefore necessary to consider alternative models that may aid this translation process.

Transgenic mouse models involving HHT-related mutations provide the only example of the spontaneous formation of brain AVMs. The example proposed by Walker et al. demonstrates brain AVMs formed in *ALK1* and *ENG* deficient mice with direct VEGF stimulation following injection directly into the brains of adult mice [417]. Although this method can produce spontaneous formation of brain AVMs it carries significant expense. Furthermore, the use of a transgenic model AVM has the potential to create AVMs with anatomical variability making standardised comparisons on variable AVM morphologies challenging. The use of small rodent model does not provide information regarding safety of the proposed conjugates due to the haemodynamic differences between mice and humans. Finally, the technical challenge of angiography and imaging to document effects of treatment due to the small nature of the mouse vascular system precludes the use of this model in the development of our AVM vascular targeting treatment.

The use of a large animal surgically formed AVM may provide an alternative model for translation. The choice of a large animal would provide important information regarding the safety of this vascular targeting treatment, particularly due to the physiological similarities with a human. The use of a swine RM AVM model through surgical anastomosis between the CCA and EJV may provide the most similar AVM to the human setting from a haemodynamic perspective [387]. However, this model is still extracranial and therefore carries some of the limitations of the extracranial rat AVM model. Despite this, the swine model remains the most useful from a safety perspective to monitor for evidence of systemic thromboembolism from the pro-thrombotic conjugate.

Following proven efficacy of this vascular targeting treatment in future research within the rat AVM model it will be necessary to translate this research to human testing. Prior to translation the use of large animal models such as the swine RM AVM model will provide the necessary safety information before proceeding to human clinical trials.

7.5 Conclusion

This research has demonstrated that using focused irradiation and the administration of a novel vascular targeting pro-thrombotic conjugate targeting PS translocation, it is possible to cause thrombus formation and ultimately occlusion of a model AVM. Furthermore, the use of multiple smaller dose preparations can improve the targeting selectivity and effectiveness of thrombosis of vascular targeting treatments. Although further work is required for translation to human studies, this study demonstrates a potential new treatment modality in the management of brain AVMs.

References

1. Abecassis, I.J., et al., *Natural history of brain arteriovenous malformations: a systematic review.* Neurosurg Focus, 2014. **37**(3): p. E7.
2. Steinheil, S.O., *Ueber einen Fall von Varix aneurysmaticus im Bereich der Gehirngefaesse*. 1895, Wuerzburg: F. Fromme.
3. McCormick, W.F., *The pathology of vascular ("arteriovenous") malformations.* J Neurosurg, 1966. **24**(4): p. 807-16.
4. McCormick, W.F., *Pathology of vascular malformations of the brain*, in *Intracranial Vascular Malformations*, C.B. Wilson and B.M. Stein, Editors. 1984, William & Wilkins: Baltimore. p. 44-63.
5. Fadok, V.A. and G. Chimini, *The phagocytosis of apoptotic cells.* Semin Immunol, 2001. **13**(6): p. 365-72.
6. Leventis, P.A. and S. Grinstein, *The distribution and function of phosphatidylserine in cellular membranes.* Annu Rev Biophys, 2010. **39**: p. 407-27.
7. Joint Writing Group of the Technology Assessment Committee American Society of, I., et al., *Reporting terminology for brain arteriovenous malformation clinical and radiographic features for use in clinical trials.* Stroke, 2001. **32**(6): p. 1430-42.
8. Al-Shahi, R., et al., *Prospective, population-based detection of intracranial vascular malformations in adults: the Scottish Intracranial Vascular Malformation Study (SIVMS).* Stroke, 2003. **34**(5): p. 1163-9.
9. Brown, R.D., et al., *Frequency of intracranial hemorrhage as a presenting symptom and subtype analysis: a population-based study of intracranial vascular malformations in Olmsted County, Minnesota.* J Neurosurg, 1996. **85**: p. 29-32.
10. Brown, R.D., et al., *Incidence and prevalence of intracranial vascular malformations in Olmsted County, Minnesota, 1965 to 1992.* Neurology, 1996. **46**: p. 949-952.
11. Gabriel, R.A., et al., *Ten-year detection rate of brain arteriovenous malformations in a large, multiethnic, defined population.* Stroke, 2010. **41**(1): p. 21-6.
12. Hillman, J., *Population-based analysis of arteriovenous malformation treatment.* J Neurosurg, 2001. **95**: p. 633-637.
13. Jessurun, G.A.J., et al., *Cerebral arteriovenous malformations in the Netherlands Antilles.* Clin Neurol Neurosurg, 1993. **95**: p. 193-198.
14. Stapf, C., et al., *The New York Islands AVM Study Design, Study Progress, and Initial Results.* Stroke, 2003. **34**: p. e29-e33.
15. Stapf, C., et al., *Epidemiology and natural history of arteriovenous malformations.* Neurosurg Focus, 2001. **11**(5): p. E1.
16. Ondra, S.L., et al., *The natural history of symptomatic arteriovenous malformations of the brain: a 24-year follow-up assessment.* J Neurosurg, 1990. **73**(3): p. 387-91.
17. Hofmeister, C., et al., *Demographic, morphological, and clinical characteristics of 1289 patients with brain arteriovenous malformation.* Stroke, 2000. **31**(6): p. 1307-10.
18. Stefani, M.A., et al., *Large and deep brain arteriovenous malformations are associated with risk of future hemorrhage.* Stroke, 2002. **33**(5): p. 1220-4.
19. Mohr, J.P., et al., *Medical management with or without interventional therapy for unruptured brain arteriovenous malformations (ARUBA): a multicentre, non-blinded, randomised trial.* The Lancet, 2014. **383**(9917): p. 614-621.
20. Gross, B.A. and R. Du, *Natural history of cerebral arteriovenous malformations: a meta-analysis.* J Neurosurg, 2013. **118**(2): p. 437-43.
21. Brown, R.D., Jr., et al., *The natural history of unruptured intracranial arteriovenous malformations.* J Neurosurg, 1988. **68**(3): p. 352-7.
22. Crawford, P.M., et al., *Arteriovenous malformations of the brain: natural history in unoperated patients.* J Neurol Neurosurg Psychiatry, 1986. **49**(1): p. 1-10.
23. Forster, D.M., L. Steiner, and S. Hakanson, *Arteriovenous malformations of the brain. A long-term clinical study.* J Neurosurg, 1972. **37**(5): p. 562-70.

24. Graf, C.J., G.E. Perret, and J.C. Torner, *Bleeding from cerebral arteriovenous malformations as part of their natural history.* J Neurosurg, 1983. **58**(3): p. 331-7.
25. Hernesniemi, J.A., et al., *Natural history of brain arteriovenous malformations: a long-term follow-up study of risk of hemorrhage in 238 patients.* Neurosurgery, 2008. **63**(5): p. 823-9; discussion 829-31.
26. Svien, H.J. and J.A. McRae, *Arteriovenous anomalies of the brain. Fate of patients not having definitive surgery.* J Neurosurg, 1965. **23**(1): p. 23-8.
27. Svien, H.J., I. Olive, and P. Angulo-Rivero, *The fate of patients who have cerebral arteriovenous anomalies without definitive surgical treatments.* J Neurosurg, 1956. **13**(4): p. 293-9.
28. Conger, A., et al., *Diagnosis and evaluation of intracranial arteriovenous malformations.* Surg Neurol Int, 2015. **6**: p. 76.
29. Kim, H., et al., *Untreated brain arteriovenous malformation: patient-level meta-analysis of hemorrhage predictors.* Neurology, 2014. **83**(7): p. 590-7.
30. Itoyama, Y., et al., *Natural course of unoperated intracranial arteriovenous malformations: study of 50 cases.* J Neurosurg, 1989. **71**(6): p. 805-9.
31. Kader, A., et al., *The influence of hemodynamic and anatomic factors on hemorrhage from cerebral arteriovenous malformations.* Neurosurgery, 1994. **34**(5): p. 801-7; discussion 807-8.
32. Spetzler, R.F., et al., *Relationship of perfusion pressure and size to risk of hemorrhage from arteriovenous malformations.* J Neurosurg, 1992. **76**(6): p. 918-23.
33. Stapf, C., et al., *Predictors of hemorrhage in patients with untreated brain arteriovenous malformation.* Neurology, 2006. **66**(9): p. 1350-5.
34. da Costa, L., et al., *The natural history and predictive features of hemorrhage from brain arteriovenous malformations.* Stroke, 2009. **40**(1): p. 100-5.
35. Brown, R.D., Jr., *Simple risk predictions for arteriovenous malformation hemorrhage.* Neurosurgery, 2000. **46**(4): p. 1024.
36. Kondziolka, D., M.R. McLaughlin, and J.R. Kestle, *Simple risk predictions for arteriovenous malformation hemorrhage.* Neurosurgery, 1995. **37**(5): p. 851-5.
37. Theodore, N., P.J. Apostolides, and R.F. Spetzler, *Simple risk predictions for arteriovenous malformation hemorrhage.* Neurosurgery, 1996. **38**(5): p. 1066-7.
38. Perret, G. and H. Nishioka, *Report on the Cooperative Study of Intracranial Aneurysms and Subarachnoid Hemorrhge. Section VI. Arteriovenous Malformations: An Analysis of 545 Cases of Cranio-Cerebral Arteriovenous Malformations and Fistulae Reported to the Cooperative Study.* J Neurosurg, 1966. **25**: p. 467-490.
39. Thomas, J.M., et al., *Genetic and epigenetic mechanisms in the development of arteriovenous malformations in the brain.* Clin Epigenetics, 2016. **8**: p. 78.
40. Nikolaev, S.I., J.E. Fish, and I. Radovanovic, *Somatic Activating KRAS Mutations in Arteriovenous Malformations of the Brain.* N Engl J Med, 2018. **378**(16): p. 1561-1562.
41. Al-Olabi, L., et al., *Mosaic RAS/MAPK variants cause sporadic vascular malformations which respond to targeted therapy.* J Clin Invest, 2018. **128**(4): p. 1496-1508.
42. Fuwa, I., H. Wada, and T. Matsumoto, *[Recurrence of AVM after disappearing on postoperative angiography--report of two cases].* No Shinkei Geka, 1988. **16**(7): p. 887-91.
43. Gabriel, E.M., J.H. Sampson, and R.H. Wilkins, *Recurrence of a cerebral arteriovenous malformation after surgical excision. Case report.* J Neurosurg, 1996. **84**(5): p. 879-82.
44. Hashimoto, N. and K. Nozaki, *Do cerebral arteriovenous malformations recur after angiographically confirmed total extirpation?* Crit Rev Neurosurg, 1999. **9**(3): p. 141-146.
45. Higuchi, M., et al., *[Marked growth of arteriovenous malformation 19 years after resection: a case report].* No Shinkei Geka, 1991. **19**(1): p. 75-8.
46. Hook, O. and C. Johanson, *Intracranial arteriovenous aneurysms; a follow-up study with particular attention to their growth.* AMA Arch Neurol Psychiatry, 1958. **80**(1): p. 39-54.

47. Kondziolka, D., et al., *Arteriovenous malformations of the brain in children: a forty year experience.* Can J Neurol Sci, 1992. **19**(1): p. 40-5.
48. Krayenbuhl, H.A., *Angiographic contribution to the problem of enlargement of cerebral arteriovenous malformations.* Acta Neurochir (Wien), 1977. **36**(3-4): p. 215-42.
49. Miller, B.A., D.I. Bass, and J.J. Chern, *Development of a de novo arteriovenous malformation after severe traumatic brain injury.* J Neurosurg Pediatr, 2014. **14**(4): p. 418-20.
50. Pabaney, A.H., et al., *Development of De Novo Arteriovenous Malformation Following Ischemic Stroke: Case Report and Review of Current Literature.* World Neurosurg, 2016. **96**: p. 608 e5-608 e12.
51. Shi, S., et al., *De novo AVM formation following venous sinus thrombosis and prior AVM resection in adults: report of 2 cases.* J Neurosurg, 2018. **128**(2): p. 506-510.
52. Parsa, A.T. and R.A. Solomon, *Vascular malformations affecting the nervous system*, in *Principles of neurosurgery*, S. Rengachary and G. Ellenbogen, Editors. 2005, Esevier Mosby: New York. p. 3-4.
53. Bayrak-Toydemir, P., et al., *Hereditary hemorrhagic telangiectasia: an overview of diagnosis and management in the molecular era for clinicians.* Genet Med, 2004. **6**(4): p. 175-91.
54. Berg, J.N., et al., *The activin receptor-like kinase 1 gene: genomic structure and mutations in hereditary hemorrhagic telangiectasia type 2.* Am J Hum Genet, 1997. **61**(1): p. 60-7.
55. Mouchtouris, N., et al., *Biology of cerebral arteriovenous malformations with a focus on inflammation.* J Cereb Blood Flow Metab, 2015. **35**(2): p. 167-75.
56. Sturiale, C.L., et al., *Single nucleotide polymorphisms associated with sporadic brain arteriovenous malformations: where do we stand?* Brain, 2013. **136**(Pt 2): p. 665-81.
57. Satomi, J., et al., *Cerebral vascular abnormalities in a murine model of hereditary hemorrhagic telangiectasia.* Stroke, 2003. **34**(3): p. 783-9.
58. Hashimoto, T., et al., *Gene microarray analysis of human brain arteriovenous malformations.* Neurosurgery, 2004. **54**(2): p. 410-23; discussion 423-5.
59. Couto, J.A., et al., *A somatic MAP3K3 mutation is associated with verrucous venous malformation.* Am J Hum Genet, 2015. **96**(3): p. 480-6.
60. Couto, J.A., et al., *Somatic MAP2K1 Mutations Are Associated with Extracranial Arteriovenous Malformation.* Am J Hum Genet, 2017. **100**(3): p. 546-554.
61. Ayturk, U.M., et al., *Somatic Activating Mutations in GNAQ and GNA11 Are Associated with Congenital Hemangioma.* Am J Hum Genet, 2016. **98**(6): p. 1271.
62. Couto, J.A., et al., *Endothelial Cells from Capillary Malformations Are Enriched for Somatic GNAQ Mutations.* Plast Reconstr Surg, 2016. **137**(1): p. 77e-82e.
63. Cagnol, S. and N. Rivard, *Oncogenic KRAS and BRAF activation of the MEK/ERK signaling pathway promotes expression of dual-specificity phosphatase 4 (DUSP4/MKP2) resulting in nuclear ERK1/2 inhibition.* Oncogene, 2013. **32**(5): p. 564-76.
64. Park, J.T., et al., *Differential in vivo tumorigenicity of diverse KRAS mutations in vertebrate pancreas: A comprehensive survey.* Oncogene, 2015. **34**(21): p. 2801-6.
65. Luke, J.J., P.A. Ott, and G.I. Shapiro, *The biology and clinical development of MEK inhibitors for cancer.* Drugs, 2014. **74**(18): p. 2111-28.
66. Zhao, Y. and A.A. Adjei, *The clinical development of MEK inhibitors.* Nat Rev Clin Oncol, 2014. **11**(7): p. 385-400.
67. Illi, B., et al., *Shear stress-mediated chromatin remodeling provides molecular basis for flow-dependent regulation of gene expression.* Circ Res, 2003. **93**(2): p. 155-61.
68. Tu, J., Y. Li, and Z. Hu, *Notch1 and 4 signaling responds to an increasing vascular wall shear stress in a rat model of arteriovenous malformations.* Biomed Res Int, 2014. **2014**: p. 368082.

69. Batjer, H.H., et al., *Evidence of redistribution of cerebral blood flow during treatment for an intracranial arteriovenous malformation.* Neurosurgery, 1989. **25**(4): p. 599-604; discussion 605.
70. Markl, M., et al., *Cerebral arteriovenous malformation: complex 3D hemodynamics and 3D blood flow alterations during staged embolization.* J Magn Reson Imaging, 2013. **38**(4): p. 946-50.
71. Hashimoto, T., et al., *Abnormal pattern of Tie-2 and vascular endothelial growth factor receptor expression in human cerebral arteriovenous malformations.* Neurosurgery, 2000. **47**(4): p. 910-8; discussion 918-9.
72. Kamiya, A. and T. Togawa, *Adaptive regulation of wall shear stress to flow change in the canine carotid artery.* Am J Physiol, 1980. **239**(1): p. H14-21.
73. Girerd, X., et al., *Remodeling of the radial artery in response to a chronic increase in shear stress.* Hypertension, 1996. **27**(3 Pt 2): p. 799-803.
74. Malek, A.M., S.L. Alper, and S. Izumo, *Hemodynamic shear stress and its role in atherosclerosis.* JAMA, 1999. **282**(21): p. 2035-42.
75. Chen, L.J., S.Y. Wei, and J.J. Chiu, *Mechanical regulation of epigenetics in vascular biology and pathobiology.* J Cell Mol Med, 2013. **17**(4): p. 437-48.
76. Noden, D.M., *Embryonic origins and assembly of blood vessels.* Am Rev Respir Dis, 1989. **140**(4): p. 1097-103.
77. Risau, W., *Mechanisms of angiogenesis.* Nature, 1997. **386**(6626): p. 671-4.
78. Chiu, J.J. and S. Chien, *Effects of disturbed flow on vascular endothelium: pathophysiological basis and clinical perspectives.* Physiol Rev, 2011. **91**(1): p. 327-87.
79. Hahn, C. and M.A. Schwartz, *Mechanotransduction in vascular physiology and atherogenesis.* Nat Rev Mol Cell Biol, 2009. **10**(1): p. 53-62.
80. Söderman, M., et al., *Management of patients with brain arteriovenous malformations.* European Journal of Radiology, 2003. **46**(3): p. 195-205.
81. Russin, J. and R. Spetzler, *Commentary: The ARUBA trial.* Neurosurgery, 2014. **75**(1): p. E96-7.
82. Spetzler, R.F. and N.A. Martin, *A proposed grading system for arteriovenous malformations.* J Neurosurg, 1986. **65**(4): p. 476-83.
83. Davidson, A.S. and M.K. Morgan, *How safe is arteriovenous malformation surgery? A prospective, observational study of surgery as first-line treatment for brain arteriovenous malformations.* Neurosurgery, 2010. **66**(3): p. 498-504; discussion 504-5.
84. Spetzler, R.F. and F.A. Ponce, *A 3-tier classification of cerebral arteriovenous malformations. Clinical article.* J Neurosurg, 2011. **114**(3): p. 842-9.
85. Han, P.P., F.A. Ponce, and R.F. Spetzler, *Intention-to-treat analysis of Spetzler-Martin grades IV and V arteriovenous malformations: natural history and treatment paradigm.* J Neurosurg, 2003. **98**(1): p. 3-7.
86. Lawton, M.T. and U.B.A.M.S. Project, *Spetzler-Martin Grade III arteriovenous malformations: surgical results and a modification of the grading scale.* Neurosurgery, 2003. **52**(4): p. 740-8; discussion 748-9.
87. Pandey, P., et al., *Multimodality management of Spetzler-Martin Grade III arteriovenous malformations.* J Neurosurg, 2012. **116**(6): p. 1279-88.
88. Lawton, M.T., et al., *Effect of presenting hemorrhage on outcome after microsurgical resection of brain arteriovenous malformations.* Neurosurgery, 2005. **56**(3): p. 485-93; discussion 485-93.
89. Du, R., et al., *The effects of diffuseness and deep perforating artery supply on outcomes after microsurgical resection of brain arteriovenous malformations.* Neurosurgery, 2007. **60**(4): p. 638-46; discussion 646-8.
90. Lawton, M.T., et al., *A supplementary grading scale for selecting patients with brain arteriovenous malformations for surgery.* Neurosurgery, 2010. **66**(4): p. 702-13; discussion 713.

91. Kim, H., et al., *Evaluating Performance of the Spetzler-Martin Supplemented Model in Selecting Patients With Brain Arteriovenous Malformation for Surgery.* Stroke, 2012. **43**(9): p. 2497-+.
92. Spears, J., et al., *A discriminative prediction model of neurological outcome for patients undergoing surgery of brain arteriovenous malformations.* Stroke, 2006. **37**(6): p. 1457-64.
93. Davidson, A.S. and M.K. Morgan, *How Safe Is Arteriovenous Malformation Surgery? A Prospective, Observational Study of Surgery As First-Line Treatment for Brain Arteriovenous Malformations* Neurosurgery, 2009. **66**(3): p. 498-505.
94. Bollet, M.A., et al., *Efficacy and morbidity of arc-therapy radiosurgery for cerebral arteriovenous malformations: a comparison with the natural history.* Int J Radiat Oncol Biol Phys, 2004. **58**(5): p. 1353-63.
95. Chang, J.H., et al., *Factors related to complete occlusion of arteriovenous malformations after gamma knife radiosurgery.* J Neurosurg, 2000. **93 Suppl 3**: p. 96-101.
96. Flickinger, J.C., et al., *A dose-response analysis of arteriovenous malformation obliteration after radiosurgery.* Int J Radiat Oncol Biol Phys, 1996. **36**(4): p. 873-9.
97. Inoue, H.K. and C. Ohye, *Hemorrhage risks and obliteration rates of arteriovenous malformations after gamma knife radiosurgery.* J Neurosurg, 2002. **97**(5 Suppl): p. 474-6.
98. Liscak, R., et al., *Arteriovenous malformations after Leksell gamma knife radiosurgery: rate of obliteration and complications.* Neurosurgery, 2007. **60**(6): p. 1005-14; discussion 1015-6.
99. Lunsford, L.D., et al., *Stereotactic radiosurgery for arteriovenous malformations of the brain.* J Neurosurg, 1991. **75**(4): p. 512-24.
100. Ogilvy, C.S., et al., *AHA Scientific Statement: Recommendations for the management of intracranial arteriovenous malformations: a statement for healthcare professionals from a special writing group of the Stroke Council, American Stroke Association.* Stroke, 2001. **32**(6): p. 1458-71.
101. Pollock, B.E., D.A. Gorman, and R.J. Coffey, *Patient outcomes after arteriovenous malformation radiosurgical management: results based on a 5- to 14-year follow-up study.* Neurosurgery, 2003. **52**(6): p. 1291-6; discussion 1296-7.
102. Pollock, B.E., et al., *The Mayo Clinic gamma knife experience: indications and initial results.* Mayo Clin Proc, 1999. **74**(1): p. 5-13.
103. Sasaki, T., et al., *Arteriovenous malformations in the basal ganglia and thalamus: management and results in 101 cases.* J Neurosurg, 1998. **88**(2): p. 285-92.
104. Shin, M., et al., *Retrospective analysis of a 10-year experience of stereotactic radio surgery for arteriovenous malformations in children and adolescents.* J Neurosurg, 2002. **97**(4): p. 779-84.
105. Shin, M., et al., *Analysis of nidus obliteration rates after gamma knife surgery for arteriovenous malformations based on long-term follow-up data: the University of Tokyo experience.* J Neurosurg, 2004. **101**(1): p. 18-24.
106. Steiner, L., et al., *Stereotactic radiosurgery in intracranial arterio-venous malformations.* Acta Neurochir (Wien), 1974. **Suppl 21**: p. 195-209.
107. Yamamoto, M., et al., *Gamma knife radiosurgery for arteriovenous malformations: long-term follow-up results focusing on complications occurring more than 5 years after irradiation.* Neurosurgery, 1996. **38**(5): p. 906-14.
108. Yen, C.P., et al., *Subtotal obliteration of cerebral arteriovenous malformations after gamma knife surgery.* J Neurosurg, 2007. **106**(3): p. 361-9.
109. Pollock, B.E. and J.C. Flickinger, *A proposed radiosurgery-based grading system for arteriovenous malformations.* J Neurosurg, 2002. **96**(1): p. 79-85.
110. Meder, J.F., et al., *Cerebral arteriovenous malformations: the value of radiologic parameters in predicting response to radiosurgery.* AJNR Am J Neuroradiol, 1997. **18**(8): p. 1473-83.

111. Porter, P.J., et al., *Surgery versus stereotactic radiosurgery for small, operable cerebral arteriovenous malformations: a clinical and cost comparison.* Neurosurgery, 1997. **41**(4): p. 757-64; discussion 764-6.
112. Flickinger, J.C., et al., *Development of a model to predict permanent symptomatic postradiosurgery injury for arteriovenous malformation patients. Arteriovenous Malformation Radiosurgery Study Group.* Int J Radiat Oncol Biol Phys, 2000. **46**(5): p. 1143-8.
113. Lax, I. and B. Karlsson, *Prediction of complications in gamma knife radiosurgery of arteriovenous malformation.* Acta Oncol, 1996. **35**(1): p. 49-55.
114. Karlsson, B., C. Lindquist, and L. Steiner, *Prediction of obliteration after gamma knife surgery for cerebral arteriovenous malformations.* Neurosurgery, 1997. **40**(3): p. 425-30; discussion 430-1.
115. Schwartz, M., et al., *Prediction of obliteration of arteriovenous malformations after radiosurgery: the obliteration prediction index.* Can J Neurol Sci, 1997. **24**(2): p. 106-9.
116. Andrade-Souza, Y.M., et al., *Testing the radiosurgery-based arteriovenous malformation score and the modified Spetzler-Martin grading system to predict radiosurgical outcome.* J Neurosurg, 2005. **103**(4): p. 642-8.
117. Andrade-Souza, Y.M., et al., *Radiosurgery for basal ganglia, internal capsule, and thalamus arteriovenous malformation: clinical outcome.* Neurosurgery, 2005. **56**(1): p. 56-63; discussion 63-4.
118. Cohen-Gadol, A.A. and B.E. Pollock, *Radiosurgery for arteriovenous malformations in children.* J Neurosurg, 2006. **104**(6 Suppl): p. 388-91.
119. Maruyama, K., et al., *Stereotactic radiosurgery for brainstem arteriovenous malformations: factors affecting outcome.* J Neurosurg, 2004. **100**(3): p. 407-13.
120. Maruyama, K., et al., *Gamma knife surgery for arteriovenous malformations involving the corpus callosum.* J Neurosurg, 2005. **102 Suppl**: p. 49-52.
121. Sirin, S., et al., *Prospective staged volume radiosurgery for large arteriovenous malformations: indications and outcomes in otherwise untreatable patients.* Neurosurgery, 2008. **62 Suppl 2**: p. 744-54.
122. Zabel-du Bois, A., et al., *Pediatric cerebral arteriovenous malformations: the role of stereotactic linac-based radiosurgery.* Int J Radiat Oncol Biol Phys, 2006. **65**(4): p. 1206-11.
123. Zabel-du Bois, A., et al., *Stereotactic linac-based radiosurgery in the treatment of cerebral arteriovenous malformations located deep, involving corpus callosum, motor cortex, or brainstem.* Int J Radiat Oncol Biol Phys, 2006. **64**(4): p. 1044-8.
124. Pollock, B.E. and J.C. Flickinger, *Modification of the radiosurgery-based arteriovenous malformation grading system.* Neurosurgery, 2008. **63**(2): p. 239-43; discussion 243.
125. Wegner, R.E., et al., *A modified radiosurgery-based arteriovenous malformation grading scale and its correlation with outcomes.* Int J Radiat Oncol Biol Phys, 2011. **79**(4): p. 1147-50.
126. Wong, G.K., et al., *Validation of the modified radiosurgery-based arteriovenous malformation score in a linear accelerator radiosurgery experience in Hong Kong.* J Clin Neurosci, 2012. **19**(9): p. 1252-4.
127. Starke, R.M., et al., *A practical grading scale for predicting outcome after radiosurgery for arteriovenous malformations: analysis of 1012 treated patients.* J Neurosurg, 2013. **119**(4): p. 981-7.
128. Ding, D., et al., *Radiosurgery for ruptured intracranial arteriovenous malformations.* J Neurosurg, 2014. **121**(2): p. 470-81.
129. Ding, D., et al., *Radiosurgery for Spetzler-Martin Grade III arteriovenous malformations.* J Neurosurg, 2014. **120**(4): p. 959-69.
130. Ding, D., et al., *Radiosurgery for low-grade intracranial arteriovenous malformations.* J Neurosurg, 2014. **121**(2): p. 457-67.

131. Ellis, T.L., et al., *Analysis of treatment failure after radiosurgery for arteriovenous malformations.* J Neurosurg, 1998. **89**(1): p. 104-10.
132. Gallina, P., et al., *Failure in radiosurgery treatment of cerebral arteriovenous malformations.* Neurosurgery, 1998. **42**(5): p. 996-1002; discussion 1002-4.
133. Pollock, B.E., et al., *Repeat stereotactic radiosurgery of arteriovenous malformations: factors associated with incomplete obliteration.* Neurosurgery, 1996. **38**(2): p. 318-24.
134. Flickinger, J.C., et al., *Radiosurgery-related imaging changes in surrounding brain: Multivariate analysis and model evaluation.* Radiosurgery, 1996. **1**: p. 229-236.
135. Flickinger, J.C., et al., *Analysis of neurological sequelae from radiosurgery of arteriovenous malformations: how location affects outcome.* Int J Radiat Oncol Biol Phys, 1998. **40**(2): p. 273-8.
136. Flickinger, J.C., et al., *Complications from arteriovenous malformation radiosurgery: multivariate analysis and risk modeling.* Int J Radiat Oncol Biol Phys, 1997. **38**(3): p. 485-90.
137. Flickinger, J.C., et al., *Radiosurgery and brain tolerance: an analysis of neurodiagnostic imaging changes after gamma knife radiosurgery for arteriovenous malformations.* Int J Radiat Oncol Biol Phys, 1992. **23**(1): p. 19-26.
138. Voges, J., et al., *Risk analysis of linear accelerator radiosurgery.* Int J Radiat Oncol Biol Phys, 1996. **36**(5): p. 1055-63.
139. Lo, E.H., *Linear accelerator radiosurgery of cerebral arteriovenous malformations: an update.* Neurosurgery, 1994. **35**(2): p. 342.
140. Pollock, B.E., et al., *Patient outcomes after stereotactic radiosurgery for "operable" arteriovenous malformations.* Neurosurgery, 1994. **35**(1): p. 1-7; discussion 7-8.
141. Friedman, W.A., et al., *The risk of hemorrhage after radiosurgery for arteriovenous malformations.* J Neurosurg, 1996. **84**(6): p. 912-9.
142. Maruyama, K., et al., *The risk of hemorrhage after radiosurgery for cerebral arteriovenous malformations.* N Engl J Med, 2005. **352**(2): p. 146-53.
143. Yen, C.P., et al., *Hemorrhage risk of cerebral arteriovenous malformations before and during the latency period after GAMMA knife radiosurgery.* Stroke, 2011. **42**(6): p. 1691-6.
144. Zabel-du Bois, A., et al., *Risk of hemorrhage and obliteration rates of LINAC-based radiosurgery for cerebral arteriovenous malformations treated after prior partial embolization.* Int J Radiat Oncol Biol Phys, 2007. **68**(4): p. 999-1003.
145. Yamamoto, M., et al., *Middle cerebral artery stenosis caused by relatively low-dose irradiation with stereotactic radiosurgery for cerebral arteriovenous malformations: case report.* Neurosurgery, 1997. **41**(2): p. 474-7; discussion 477-8.
146. Pollock, B.E., *Occlusive hyperemia: a radiosurgical phenomenon?* Neurosurgery, 2000. **47**(5): p. 1178-82; discussion 1182-4.
147. Yamamoto, M., et al., *A diffuse white matter ischemic lesion appearing 7 years after stereotactic radiosurgery for cerebral arteriovenous malformations: case report.* Neurosurgery, 1997. **41**(6): p. 1405-9.
148. Pollock, B.E. and R.D. Brown, Jr., *Management of cysts arising after radiosurgery to treat intracranial arteriovenous malformations.* Neurosurgery, 2001. **49**(2): p. 259-64; discussion 264-5.
149. Hara, M., et al., *Delayed cyst formation after radiosurgery for cerebral arteriovenous malformation: two case reports.* Minim Invasive Neurosurg, 1998. **41**(1): p. 40-5.
150. Kihlstrom, L., et al., *Magnetic resonance imaging of obliterated arteriovenous malformations up to 23 years after radiosurgery.* J Neurosurg, 1997. **86**(4): p. 589-93.
151. Kim, M.S., S.I. Lee, and J.H. Sim, *A case of very large cyst formation with Gamma Knife radiosurgery for an arteriovenous malformation.* Stereotact Funct Neurosurg, 1999. **72 Suppl 1**: p. 168-74.

152. Radanowicz-Harttmann, V., H. Bachli, and O. Gratzl, *Late complication of radiosurgery of AVMs with the gamma knife: a case report.* Acta Neurochir (Wien), 1998. **140**(2): p. 194-5.
153. Yamamoto, M., et al., *Late cyst convolution after gamma knife radiosurgery for cerebral arteriovenous malformations.* Stereotact Funct Neurosurg, 1998. **70 Suppl 1**: p. 166-78.
154. van Beijnum, J., et al., *Treatment of brain arteriovenous malformations: a systematic review and meta-analysis.* JAMA, 2011. **306**(18): p. 2011-9.
155. Saatci, I., et al., *Endovascular treatment of brain arteriovenous malformations with prolonged intranidal Onyx injection technique: long-term results in 350 consecutive patients with completed endovascular treatment course.* J Neurosurg, 2011. **115**(1): p. 78-88.
156. Mohlenbruch, M., M. Bendszus, and S. Rohde, *Comment on: Curative Embolization of Brain Arteriovenous Malformations with Onyx: Patient Selection, Embolization Technique, and Results.* Clin Neuroradiol, 2012. **22**(2): p. 181-2.
157. van Rooij, W.J., et al., *Curative embolization of brain arteriovenous malformations with onyx: patient selection, embolization technique, and results.* AJNR Am J Neuroradiol, 2012. **33**(7): p. 1299-304.
158. Debrun, G.M., et al., *Embolization of the nidus of brain arteriovenous malformations with n-butyl cyanoacrylate.* Neurosurgery, 1997. **40**(1): p. 112-20; discussion 120-1.
159. Hartmann, A., et al., *Risk of endovascular treatment of brain arteriovenous malformations.* Stroke, 2002. **33**(7): p. 1816-20.
160. Yuki, I., et al., *Treatment of brain arteriovenous malformations with high-flow arteriovenous fistulas: risk and complications associated with endovascular embolization in multimodality treatment. Clinical article.* J Neurosurg, 2010. **113**(4): p. 715-22.
161. Willinsky, R., et al., *Embolisation of Small (< 3 cm) Brain Arteriovenous Malformations. Correlation of Angiographic Results to a Proposed Angioarchitecture Grading System.* Interv Neuroradiol, 2001. **7**(1): p. 19-27.
162. Feliciano, C.E., et al., *A proposal for a new arteriovenous malformation grading scale for neuroendovascular procedures and literature review.* P R Health Sci J, 2010. **29**(2): p. 117-20.
163. Sanborn, M.R., et al., *Endovascular approaches to pial arteriovenous malformations.* Neurosurg Clin N Am, 2014. **25**(3): p. 529-37.
164. Kusske, J.A. and W.A. Kelly, *Embolization and reduction of the "steal" syndrome in cerebral arteriovenous malformations.* J Neurosurg, 1974. **40**(3): p. 313-21.
165. Luessenhop, A.J. and P.H. Mujica, *Embolization of segments of the circle of Willis and adjacent branches for management of certain inoperable cerebral arteriovenous malformations.* J Neurosurg, 1981. **54**(5): p. 573-82.
166. Behrens, L. and S. Rohde, *Comment on: treatment of brain arteriovenous malformations by double arterial catheterization with simultaneous injection of Onyx: retrospective series of 17 patients: Abud DG, Riva R, Nakiri GS, Padovani F, Khawaldeh M, Mounayer C. AJNR Am J Neuroradiol. 2011;32:152-158.* Clin Neuroradiol, 2011. **21**(2): p. 107-9.
167. Abud, D.G., et al., *Treatment of brain arteriovenous malformations by double arterial catheterization with simultaneous injection of Onyx: retrospective series of 17 patients.* AJNR Am J Neuroradiol, 2011. **32**(1): p. 152-8.
168. Yu, S.C., et al., *Complete obliteration of intracranial arteriovenous malformation with endovascular cyanoacrylate embolization: initial success and rate of permanent cure.* AJNR Am J Neuroradiol, 2004. **25**(7): p. 1139-43.
169. Radvany, M.G. and L. Gregg, *Endovascular treatment of cranial arteriovenous malformations and dural arteriovenous fistulas.* Neurosurg Clin N Am, 2012. **23**(1): p. 123-31.
170. Krings, T., et al., *Partial "targeted" embolisation of brain arteriovenous malformations.* Eur Radiol, 2010. **20**(11): p. 2723-31.

171. Le Feuvre, D. and A. Taylor, *Target Embolization of AVMs: Identification of Sites and Results of Treatment.* Interv Neuroradiol, 2007. **13**(4): p. 389-94.
172. Denekamp, J., *Endothelial cell proliferation as a novel approach to targeting tumour therapy.* Br J Cancer, 1982. **45**(1): p. 136-9.
173. Denekamp, J., *Review article: angiogenesis, neovascular proliferation and vascular pathophysiology as targets for cancer therapy.* Br J Radiol, 1993. **66**(783): p. 181-96.
174. Thorpe, P.E., *Vascular targeting agents as cancer therapeutics.* Clin Cancer Res, 2004. **10**(2): p. 415-27.
175. Burrows, F.J., Y. Watanabe, and P.E. Thorpe, *A murine model for antibody-directed targeting of vascular endothelial cells in solid tumors.* Cancer Res, 1992. **52**(21): p. 5954-62.
176. Burrows, F.J. and P.E. Thorpe, *Vascular targeting--a new approach to the therapy of solid tumors.* Pharmacol Ther, 1994. **64**(1): p. 155-74.
177. Burrows, F.J. and P.E. Thorpe, *Eradication of large solid tumors in mice with an immunotoxin directed against tumor vasculature.* Proc Natl Acad Sci U S A, 1993. **90**(19): p. 8996-9000.
178. Hill, S.A., et al., *Vinca alkaloids: anti-vascular effects in a murine tumour.* Eur J Cancer, 1993. **29A**(9): p. 1320-4.
179. Hill, S.A., et al., *The effect of vinca alkaloids on tumour blood flow.* Adv Exp Med Biol, 1994. **345**: p. 417-22.
180. Landuyt, W., et al., *Vascular targeting of solid tumours: a major 'inverse' volume-response relationship following combretastatin A-4 phosphate treatment of rat rhabdomyosarcomas.* Eur J Cancer, 2000. **36**(14): p. 1833-43.
181. Thorpe, P.E., D.J. Chaplin, and D.C. Blakey, *The first international conference on vascular targeting: meeting overview.* Cancer Res, 2003. **63**(5): p. 1144-7.
182. Denekamp, J., *Vascular attack as a therapeutic strategy for cancer.* Cancer Metastasis Rev, 1990. **9**: p. 267-282.
183. Denekamp, J. and B. Hobson, *Endothelial-cell proliferation in experimental tumours.* Br J Cancer, 1982. **46**(5): p. 711-20.
184. Neri, D. and R. Bicknell, *Tumour vascular targeting.* Nat Rev Cancer, 2005. **5**(6): p. 436-46.
185. Burrows, F.J., et al., *Up-regulation of endoglin on vascular endothelial cells in human solid tumors: implications for diagnosis and therapy.* Clin Cancer Res, 1995. **1**(12): p. 1623-34.
186. Seon, B.K., *Expression of endoglin (CD105) in tumor blood vessels.* Int J Cancer, 2002. **99**(2): p. 310-1; author reply 312.
187. Brekken, R.A. and P.E. Thorpe, *Vascular endothelial growth factor and vascular targeting of solid tumors.* Anticancer Res, 2001. **21**(6B): p. 4221-9.
188. Veenendaal, L.M., et al., *In vitro and in vivo studies of a VEGF121/rGelonin chimeric fusion toxin targeting the neovasculature of solid tumors.* Proc Natl Acad Sci U S A, 2002. **99**(12): p. 7866-71.
189. Arap, W., R. Pasqualini, and E. Ruoslahti, *Cancer treatment by targeted drug delivery to tumor vasculature in a mouse model.* Science, 1998. **279**(5349): p. 377-80.
190. Brooks, P.C., R.A. Clark, and D.A. Cheresh, *Requirement of vascular integrin alpha v beta 3 for angiogenesis.* Science, 1994. **264**(5158): p. 569-71.
191. Nilsson, F., et al., *Targeted delivery of tissue factor to the ED-B domain of fibronectin, a marker of angiogenesis, mediates the infarction of solid tumors in mice.* Cancer Res, 2001. **61**(2): p. 711-6.
192. Chang, S.S., et al., *Prostate-specific membrane antigen is produced in tumor-associated neovasculature.* Clin Cancer Res, 1999. **5**(10): p. 2674-81.
193. Raoufi Rad, N., et al., *Phosphatidylserine Translocation after Radiosurgery in an Animal Model of Arteriovenous Malformation.* Radiat Res, 2017. **187**(6): p. 701-707.

194. Siemann, D.W., D.J. Chaplin, and M.R. Horsman, *Vascular-targeting therapies for treatment of malignant disease.* Cancer, 2004. **100**(12): p. 2491-9.
195. Nihei, Y., et al., *Evaluation of antivascular and antimitotic effects of tubulin binding agents in solid tumor therapy.* Jpn J Cancer Res, 1999. **90**(12): p. 1387-95.
196. Baguley, B.C., et al., *Inhibition of growth of colon 38 adenocarcinoma by vinblastine and colchicine: evidence for a vascular mechanism.* Eur J Cancer, 1991. **27**(4): p. 482-7.
197. Chaplin, D.J., G.R. Pettit, and S.A. Hill, *Anti-vascular approaches to solid tumour therapy: evaluation of combretastatin A4 phosphate.* Anticancer Res, 1999. **19**(1A): p. 189-95.
198. Dark, G.G., et al., *Combretastatin A-4, an agent that displays potent and selective toxicity toward tumor vasculature.* Cancer Res, 1997. **57**(10): p. 1829-34.
199. Li, L., A. Rojiani, and D.W. Siemann, *Targeting the tumor vasculature with combretastatin A-4 disodium phosphate: effects on radiation therapy.* Int J Radiat Oncol Biol Phys, 1998. **42**(4): p. 899-903.
200. Blakey, D.C., et al., *Antitumor activity of the novel vascular targeting agent ZD6126 in a panel of tumor models.* Clin Cancer Res, 2002. **8**(6): p. 1974-83.
201. Horsman, M.R., et al., *The effect of combretastatin A-4 disodium phosphate in a C3H mouse mammary carcinoma and a variety of murine spontaneous tumors.* Int J Radiat Oncol Biol Phys, 1998. **42**(4): p. 895-8.
202. Hori, K., et al., *Antitumor effects due to irreversible stoppage of tumor tissue blood flow: evaluation of a novel combretastatin A-4 derivative, AC7700.* Jpn J Cancer Res, 1999. **90**(9): p. 1026-38.
203. Siemann, D.W. and M.R. Horsman, *Enhancement of radiation therapy by vascular targeting agents.* Curr Opin Investig Drugs, 2002. **3**(11): p. 1660-5.
204. Tozer, G.M., et al., *Combretastatin A-4 phosphate as a tumor vascular-targeting agent: early effects in tumors and normal tissues.* Cancer Res, 1999. **59**(7): p. 1626-34.
205. Dowlati, A., et al., *A phase I pharmacokinetic and translational study of the novel vascular targeting agent combretastatin a-4 phosphate on a single-dose intravenous schedule in patients with advanced cancer.* Cancer Res, 2002. **62**(12): p. 3408-16.
206. Rustin, G.J., et al., *Phase I clinical trial of weekly combretastatin A4 phosphate: clinical and pharmacokinetic results.* J Clin Oncol, 2003. **21**(15): p. 2815-22.
207. Pettit, G.R., et al., *Isolation and structure of the strong cell growth and tubulin inhibitor combretastatin A-4.* Experientia, 1989. **45**(2): p. 209-11.
208. Beauregard, D.A., et al., *Magnetic resonance imaging and spectroscopy of combretastatin A4 prodrug-induced disruption of tumour perfusion and energetic status.* Br J Cancer, 1998. **77**(11): p. 1761-7.
209. Malcontenti-Wilson, C., et al., *Combretastatin A4 prodrug study of effect on the growth and the microvasculature of colorectal liver metastases in a murine model.* Clin Cancer Res, 2001. **7**(4): p. 1052-60.
210. Hill, S.A., et al., *Preclinical evaluation of the antitumour activity of the novel vascular targeting agent Oxi 4503.* Anticancer Res, 2002. **22**(3): p. 1453-8.
211. Natsume, T., et al., *Enhanced antitumor activities of TZT-1027 against TNF-alpha or IL-6 secreting Lewis lung carcinoma in vivo.* Cancer Chemother Pharmacol, 2002. **49**(1): p. 35-47.
212. Kobayashi, M., et al., *Antitumor activity of TZT-1027, a novel dolastatin 10 derivative.* Jpn J Cancer Res, 1997. **88**(3): p. 316-27.
213. Ran, S., A. Downes, and P.E. Thorpe, *Increased exposure of anionic phospholipids on the surface of tumor blood vessels.* Cancer Res, 2002. **62**(21): p. 6132-40.
214. Bucki, R., et al., *Involvement of phosphatidylinositol 4,5-bisphosphate in phosphatidylserine exposure in platelets: use of a permeant phosphoinositide-binding peptide.* Biochemistry, 2001. **40**(51): p. 15752-61.
215. Reddy, R., et al., *Durable thrombosis in a rat model of arteriovenous malformation treated with radiosurgery and vascular targeting.* J Neurosurg, 2014. **120**(1): p. 113-9.

216. Storer, K., et al., *Coadministration of low-dose lipopolysaccharide and soluble tissue factor induces thrombosis after radiosurgery in an animal arteriovenous malformation model.* Neurosurgery, 2007. **61**(3): p. 604-10; discussion 610-1.
217. Huang, X., et al., *Tumor infarction in mice by antibody-directed targeting of tissue factor to tumor vasculature.* Science, 1997. **275**(5299): p. 547-50.
218. Kirszberg, C., et al., *Simultaneous tissue factor expression and phosphatidylserine exposure account for the highly procoagulant pattern of melanoma cell lines.* Melanoma Res, 2009. **19**(5): p. 301-8.
219. Friede, R.L., *Developmental Neuropathology: Dysplasias of Cerebral Vasculature*. 1975, New York: Springer-Verlag.
220. Hamby, W.B., *The pathology of supratentorial angiomas.* J Neurosurg, 1958. **15**(1): p. 65-75.
221. Isoda, K., et al., *Arteriovenous malformation of the brain -- histological study and micrometric measurement of abnormal vessels.* Acta Pathol Jpn, 1981. **31**(5): p. 883-93.
222. Kaplan, H.A., S.M. Aronson, and E.J. Browder, *Vascular malformatons of the brain. An anatomical study.* J Neurosurg, 1961. **18**: p. 630-5.
223. Sadoshima, S. and K. Tanaka, *[Clinicopathological study of cerebral arteriovenous malformation (author's transl)].* No To Shinkei, 1978. **30**(4): p. 437-42.
224. Stein, B.M., *Arteriovenous malformations of the cerebral convexities*, in *Intracranial Vascular Malformations*, C.B. Wilson and B.M. Stein, Editors. 1984, William & Wilkins: Baltimore. p. 156-183.
225. Penfield, W. and A. Ward, *Calcifying epileptogenic lesions; hemangioma calcificans; report of a case.* Arch Neurol Psychiatry, 1948. **60**(1): p. 20-36.
226. Alexander, W.S., *Cerebral calcification epilepsy; report of a case of epilepsy caused by a calcified hamartoma of the brain.* J Neurosurg, 1953. **10**(1): p. 69-74.
227. Arieti, S. and E.W. Gray, *Progressive multiform angiosis.* Arch Neurol Psychiatry, 1944. **51**: p. 182-189.
228. Russell, D.S. and L.J. Rubinstein, *Pathology of tumours of the nervous system*. 1959, London: Edward Arnold.
229. Wolf, A. and S. Brock, *The pathology of cerebral angiomas.* Bull Neurol Inst N.Y., 1935. **4**: p. 144-176.
230. Neumann, M.A., *Combined amyloid vascular changes and argyrophilic plaques in the central nervous system.* J Neuropathol Exp Neurol, 1960. **19**: p. 370-82.
231. Peterson, E.W. and D.M. Schulz, *Amyloid in vessels of a vascular malformation in brain.* Arch Pathol, 1961. **72**: p. 480-3.
232. Williams, A.W., *Ossifying haemangioma of the cerebrum.* Br J Surg, 1950. **38**(150): p. 245-6.
233. Antoni, N., *Spinal vascular malformations (angiomas) and myelomalacia.* Neurology, 1962. **12**: p. 795-804.
234. Sato, S., et al., *Perinidal dilated capillary networks in cerebral arteriovenous malformations.* Neurosurgery, 2004. **54**(1): p. 163-8; discussion 168-70.
235. Attia, W., et al., *Microvascular pathological features of immediate perinidal parenchyma in cerebral arteriovenous malformations: giant bed capillaries.* J Neurosurg, 2003. **98**(4): p. 823-7.
236. Kinoshita, A., et al., *Analysis of vessels located around the nidus of arteriovenous malformations.* Surg Cerebral Stroke, 1990. **18**: p. 283-286.
237. Ohtake, T., et al., *Computer-assisted complete three-dimensional reconstruction of the mammary ductal/lobular systems: implications of ductal anastomoses for breast-conserving surgery.* Cancer, 2001. **91**(12): p. 2263-72.
238. Suzuki, M., et al., *The development and extension of hepatohilar bile duct carcinoma. A three-dimensional tumor mapping in the intrahepatic biliary tree visualized with the aid of a graphics computer system.* Cancer, 1989. **64**(3): p. 658-66.

239. Drake, C.G., *Cerebral arteriovenous malformations: considerations for and experience with surgical treatment in 166 cases.* Clin Neurosurg, 1979. **26**: p. 145-208.
240. Solomon, R.A., et al., *Management of residual dysplastic vessels after cerebral arteriovenous malformation resection: implications for postoperative angiography.* Neurosurgery, 2000. **46**(5): p. 1052-60; discussion 1060-2.
241. Takemae, T., S. Kobayashi, and K. Sugita, *Perinidal hypervascular network on immediate postoperative angiogram after removal of large arteriovenous malformations located distant from the arterial circle of Willis.* Neurosurgery, 1993. **33**(3): p. 400-5; discussion 405-6.
242. Tu, J., et al., *Ultrastructure of perinidal capillaries in cerebral arteriovenous malformations.* Neurosurgery, 2006. **58**(5): p. 961-70; discussion 961-70.
243. Wong, J.H., I.A. Awad, and J.H. Kim, *Ultrastructural pathological features of cerebrovascular malformations: a preliminary report.* Neurosurgery, 2000. **46**(6): p. 1454-9.
244. Sekhon, L.H., M.K. Morgan, and I. Spence, *Normal perfusion pressure breakthrough: the role of capillaries.* J Neurosurg, 1997. **86**(3): p. 519-24.
245. Ikeda, E., I. Flamme, and W. Risau, *Developing brain cells produce factors capable of inducing the HT7 antigen, a blood-brain barrier-specific molecule, in chick endothelial cells.* Neurosci Lett, 1996. **209**(3): p. 149-52.
246. Storer, K.P., et al., *Thrombotic molecule expression in cerebral vascular malformations.* J Clin Neurosci, 2007. **14**(10): p. 975-80.
247. Storer, K.P., et al., *Inflammatory molecule expression in cerebral arteriovenous malformations.* J Clin Neurosci, 2008. **15**(2): p. 179-84.
248. Robinson, J.R., Jr., et al., *Expression of basement membrane and endothelial cell adhesion molecules in vascular malformations of the brain: preliminary observations and working hypothesis.* Neurol Res, 1995. **17**(1): p. 49-58.
249. Kilic, T., et al., *Expression of structural proteins and angiogenic factors in cerebrovascular anomalies.* Neurosurgery, 2000. **46**(5): p. 1179-91; discussion 1191-2.
250. Garbisa, S. and A. Negro, *Macromolecular organization and functional architecture of basement membranes.* Appl Pathol, 1984. **2**(4): p. 217-22.
251. Krum, J.M., N.S. More, and J.M. Rosenstein, *Brain angiogenesis: variations in vascular basement membrane glycoprotein immunoreactivity.* Exp Neurol, 1991. **111**(2): p. 152-65.
252. Liakka, A., et al., *Distribution of laminin and types IV and III collagen in fetal, infant and adult human spleens.* Cell Tissue Res, 1991. **263**(2): p. 245-52.
253. Navaratnam, V., *Organisation and reorganisation of blood vessels in embryonic development.* Eye (Lond), 1991. **5 (Pt 2)**: p. 147-50.
254. Dejana, E., et al., *Fibrinogen induces endothelial cell adhesion and spreading via the release of endogenous matrix proteins and the recruitment of more than one integrin receptor.* Blood, 1990. **75**(7): p. 1509-17.
255. Merei, F.T., F. Gallyas, and Z. Horvath, *Elastic elements in the media and adventitia of human intracranial extracerebral arteries.* Stroke, 1980. **11**(4): p. 329-36.
256. Risau, W. and V. Lemmon, *Changes in the vascular extracellular matrix during embryonic vasculogenesis and angiogenesis.* Dev Biol, 1988. **125**(2): p. 441-50.
257. Rutka, J.T., et al., *The extracellular matrix of the central and peripheral nervous systems: structure and function.* J Neurosurg, 1988. **69**(2): p. 155-70.
258. Takahashi, K., et al., *Cellular markers that distinguish the phases of hemangioma during infancy and childhood.* J Clin Invest, 1994. **93**(6): p. 2357-64.
259. Herman, I.M., *Endothelial cell matrices modulate smooth muscle cell growth, contractile phenotype and sensitivity to heparin.* Haemostasis, 1990. **20 Suppl 1**: p. 166-77.
260. Mulliken, J.B., B.R. Zetter, and J. Folkman, *In vitro characteristics of endothelium from hemangiomas and vascular malformations.* Surgery, 1982. **92**(2): p. 348-53.

261. Shovlin, C.L. and J. Scott, *Inherited diseases of the vasculature.* Annu Rev Physiol, 1996. **58**: p. 483-507.
262. Lane, N.J., T.S. Reese, and B. Kachar, *Structural domains of the tight junctional intramembrane fibrils.* Tissue Cell, 1992. **24**(2): p. 291-300.
263. Nehls, V., E. Schuchardt, and D. Drenckhahn, *The effect of fibroblasts, vascular smooth muscle cells, and pericytes on sprout formation of endothelial cells in a fibrin gel angiogenesis system.* Microvasc Res, 1994. **48**(3): p. 349-63.
264. Stone, J., et al., *Development of retinal vasculature is mediated by hypoxia-induced vascular endothelial growth factor (VEGF) expression by neuroglia.* J Neurosci, 1995. **15**(7 Pt 1): p. 4738-47.
265. Dvorak, H.F., et al., *Vascular permeability factor/vascular endothelial growth factor, microvascular hyperpermeability, and angiogenesis.* Am J Pathol, 1995. **146**(5): p. 1029-39.
266. Gille, J., R.A. Swerlick, and S.W. Caughman, *Transforming growth factor-alpha-induced transcriptional activation of the vascular permeability factor (VPF/VEGF) gene requires AP-2-dependent DNA binding and transactivation.* EMBO J, 1997. **16**(4): p. 750-9.
267. Rothbart, D., et al., *Expression of angiogenic factors and structural proteins in central nervous system vascular malformations.* Neurosurgery, 1996. **38**(5): p. 915-24; discussion 924-5.
268. Sonstein, W.J., et al., *Expression of vascular endothelial growth factor in pediatric and adult cerebral arteriovenous malformations: an immunocytochemical study.* J Neurosurg, 1996. **85**(5): p. 838-45.
269. Hatva, E., et al., *Tie endothelial cell-specific receptor tyrosine kinase is upregulated in the vasculature of arteriovenous malformations.* J Neuropathol Exp Neurol, 1996. **55**(11): p. 1124-33.
270. Hatva, E., et al., *Vascular growth factors and receptors in capillary hemangioblastomas and hemangiopericytomas.* Am J Pathol, 1996. **148**(3): p. 763-75.
271. Uranishi, R., et al., *Expression of endothelial cell angiogenesis receptors in human cerebrovascular malformations.* Neurosurgery, 2001. **48**(2): p. 359-67; discussion 367-8.
272. Mohri, H., *Acquired von Willebrand syndrome: features and management.* Am J Hematol, 2006. **81**(8): p. 616-23.
273. Ruggeri, Z.M. and T.S. Zimmerman, *von Willebrand factor and von Willebrand disease.* Blood, 1987. **70**(4): p. 895-904.
274. Esmon, C.T., N.L. Esmon, and K.W. Harris, *Complex formation between thrombin and thrombomodulin inhibits both thrombin-catalyzed fibrin formation and factor V activation.* J Biol Chem, 1982. **257**(14): p. 7944-7.
275. Esmon, C.T. and W.G. Owen, *Identification of an endothelial cell cofactor for thrombin-catalyzed activation of protein C.* Proc Natl Acad Sci U S A, 1981. **78**(4): p. 2249-52.
276. Daly, C., et al., *Angiopoietins bind thrombomodulin and inhibit its function as a thrombin cofactor.* Sci Rep, 2018. **8**(1): p. 505.
277. Noshiro, S., et al., *Biological relevance of tissue factor and IL-6 in arteriovenous malformations.* Neurosurg Rev, 2017. **40**(3): p. 359-367.
278. Bach, R.R., *Initiation of coagulation by tissue factor.* CRC Crit Rev Biochem, 1988. **23**(4): p. 339-68.
279. Mackman, N., *The role of tissue factor and factor VIIa in hemostasis.* Anesth Analg, 2009. **108**(5): p. 1447-52.
280. Tu, J., et al., *Comparison of an animal model of arteriovenous malformation with human arteriovenous malformation.* J Clin Neurosci, 2010. **17**(1): p. 96-102.
281. Tu, J., et al., *Responses of arteriovenous malformations to radiosurgery: ultrastructural changes.* Neurosurgery, 2006. **58**(4): p. 749-58; discussion 749-58.
282. Cheung, K., et al., *CD31 signals confer immune privilege to the vascular endothelium.* Proc Natl Acad Sci U S A, 2015. **112**(43): p. E5815-24.

283. Lertkiatmongkol, P., et al., *Endothelial functions of platelet/endothelial cell adhesion molecule-1 (CD31).* Curr Opin Hematol, 2016. **23**(3): p. 253-9.
284. Liu, L. and G.P. Shi, *CD31: beyond a marker for endothelial cells.* Cardiovasc Res, 2012. **94**(1): p. 3-5.
285. Privratsky, J.R. and P.J. Newman, *PECAM-1: regulator of endothelial junctional integrity.* Cell Tissue Res, 2014. **355**(3): p. 607-19.
286. Woodfin, A., M.B. Voisin, and S. Nourshargh, *PECAM-1: a multi-functional molecule in inflammation and vascular biology.* Arterioscler Thromb Vasc Biol, 2007. **27**(12): p. 2514-23.
287. Kansas, G.S., *Selectins and their ligands: current concepts and controversies.* Blood, 1996. **88**(9): p. 3259-87.
288. Luo, J., G. Paranya, and J. Bischoff, *Noninflammatory expression of E-selectin is regulated by cell growth.* Blood, 1999. **93**(11): p. 3785-91.
289. Fox, S.B., et al., *The increased expression of adhesion molecules ICAM-3, E- and P-selectins on breast cancer endothelium.* J Pathol, 1995. **177**(4): p. 369-76.
290. Ye, C., et al., *Expression of E-selectin on endothelial cells of small veins in human colorectal cancer.* Int J Cancer, 1995. **61**(4): p. 455-60.
291. Labow, M.A., et al., *Characterization of E-selectin-deficient mice: demonstration of overlapping function of the endothelial selectins.* Immunity, 1994. **1**(8): p. 709-20.
292. Klisch, J., et al., *The two-in-one model: a new variation of the arteriovenous malformation model in swine.* Neuroradiology, 2001. **43**(5): p. 393-7.
293. Qian, Z., et al., *A simplified arteriovenous malformation model in sheep: feasibility study.* AJNR Am J Neuroradiol, 1999. **20**(5): p. 765-70.
294. Berger, G., D.W. Hartwell, and D.D. Wagner, *P-Selectin and platelet clearance.* Blood, 1998. **92**(11): p. 4446-52.
295. Hsu-Lin, S., et al., *A platelet membrane protein expressed during platelet activation and secretion. Studies using a monoclonal antibody specific for thrombin-activated platelets.* J Biol Chem, 1984. **259**(14): p. 9121-6.
296. Berman, C.L., et al., *A platelet alpha granule membrane protein that is associated with the plasma membrane after activation. Characterization and subcellular localization of platelet activation-dependent granule-external membrane protein.* J Clin Invest, 1986. **78**(1): p. 130-7.
297. Mayadas, T.N., et al., *Leukocyte rolling and extravasation are severely compromised in P selectin-deficient mice.* Cell, 1993. **74**(3): p. 541-54.
298. Frenette, P.S., et al., *Platelets roll on stimulated endothelium in vivo: an interaction mediated by endothelial P-selectin.* Proc Natl Acad Sci U S A, 1995. **92**(16): p. 7450-4.
299. Elstad, M.R., et al., *The interaction of leukocytes with platelets in blood coagulation.* Curr Opin Hematol, 1995. **2**(1): p. 47-54.
300. Subramaniam, M., et al., *Defects in hemostasis in P-selectin-deficient mice.* Blood, 1996. **87**(4): p. 1238-42.
301. Larsen, E., et al., *PADGEM protein: a receptor that mediates the interaction of activated platelets with neutrophils and monocytes.* Cell, 1989. **59**(2): p. 305-12.
302. Rinder, H.M., et al., *Progressive platelet activation with storage: evidence for shortened survival of activated platelets after transfusion.* Transfusion, 1991. **31**(5): p. 409-14.
303. Storer, K.P., et al., *Expression of endothelial adhesion molecules after radiosurgery in an animal model of arteriovenous malformation.* Neurosurgery, 2010. **67**(4): p. 976-83; discussion 983.
304. Marui, N., et al., *Vascular cell adhesion molecule-1 (VCAM-1) gene transcription and expression are regulated through an antioxidant-sensitive mechanism in human vascular endothelial cells.* J Clin Invest, 1993. **92**(4): p. 1866-74.
305. Cybulsky, M.I. and M.A. Gimbrone, Jr., *Endothelial expression of a mononuclear leukocyte adhesion molecule during atherogenesis.* Science, 1991. **251**(4995): p. 788-91.

306. Elices, M.J., et al., *VCAM-1 on activated endothelium interacts with the leukocyte integrin VLA-4 at a site distinct from the VLA-4/fibronectin binding site.* Cell, 1990. **60**(4): p. 577-84.
307. Bochner, B.S., et al., *Adhesion of human basophils, eosinophils, and neutrophils to interleukin 1-activated human vascular endothelial cells: contributions of endothelial cell adhesion molecules.* J Exp Med, 1991. **173**(6): p. 1553-7.
308. Carlos, T., et al., *Human monocytes bind to two cytokine-induced adhesive ligands on cultured human endothelial cells: endothelial-leukocyte adhesion molecule-1 and vascular cell adhesion molecule-1.* Blood, 1991. **77**(10): p. 2266-71.
309. Oppenheimer-Marks, N., et al., *Differential utilization of ICAM-1 and VCAM-1 during the adhesion and transendothelial migration of human T lymphocytes.* J Immunol, 1991. **147**(9): p. 2913-21.
310. Burkly, L.C., et al., *Signaling by vascular cell adhesion molecule-1 (VCAM-1) through VLA-4 promotes CD3-dependent T cell proliferation.* Eur J Immunol, 1991. **21**(11): p. 2871-5.
311. Roy, J., M. Audette, and M.J. Tremblay, *Intercellular adhesion molecule-1 (ICAM-1) gene expression in human T cells is regulated by phosphotyrosyl phosphatase activity. Involvement of NF-kappaB, Ets, and palindromic interferon-gamma-responsive element-binding sites.* J Biol Chem, 2001. **276**(18): p. 14553-61.
312. Noraz, N., et al., *Cell surface phenotypic changes induced in H9 T cells chronically infected with HTLV type I or HIV type 1 or coinfected with the two viruses.* AIDS Res Hum Retroviruses, 1995. **11**(1): p. 145-54.
313. Raoufi-Rad, N., et al., *In vivo imaging of endothelial cell adhesion molecule expression after radiosurgery in an animal model of arteriovenous malformation.* PLoS One, 2017. **12**(9): p. e0185393.
314. van de Stolpe, A. and P.T. van der Saag, *Intercellular adhesion molecule-1.* J Mol Med (Berl), 1996. **74**(1): p. 13-33.
315. van de Stolpe, A., et al., *Fibrinogen binding to ICAM-1 on EA.hy 926 endothelial cells is dependent on an intact cytoskeleton.* Thromb Haemost, 1996. **75**(1): p. 182-9.
316. Roebuck, K.A. and A. Finnegan, *Regulation of intercellular adhesion molecule-1 (CD54) gene expression.* J Leukoc Biol, 1999. **66**(6): p. 876-88.
317. He, J., T.A. Luster, and P.E. Thorpe, *Radiation-enhanced vascular targeting of human lung cancers in mice with a monoclonal antibody that binds anionic phospholipids.* Clin Cancer Res, 2007. **13**(17): p. 5211-8.
318. Garcia-Barros, M., et al., *Tumor response to radiotherapy regulated by endothelial cell apoptosis.* Science, 2003. **300**(5622): p. 1155-9.
319. Schneider, B.F., D.A. Eberhard, and L.E. Steiner, *Histopathology of arteriovenous malformations after gamma knife radiosurgery.* J Neurosurg, 1997. **87**(3): p. 352-7.
320. Szeifert, G.T., et al., *Histopathological changes in cerebral arteriovenous malformations following Gamma Knife radiosurgery.* Prog Neurol Surg, 2007. **20**: p. 212-9.
321. Chang, S.D., et al., *Stereotactic radiosurgery of arteriovenous malformations: pathologic changes in resected tissue.* Clin Neuropathol, 1997. **16**(2): p. 111-6.
322. Szeifert, G.T., et al., *The potential role of myofibroblasts in the obliteration of arteriovenous malformations after radiosurgery.* Neurosurgery, 1997. **40**(1): p. 61-5; discussion 65-6.
323. Szeifert, G.T., et al., *Morphological observations in brain arteriovenous malformations after gamma knife radiosurgery.* Prog Neurol Surg, 2013. **27**: p. 119-29.
324. Kashba, S.R., et al., *Angiographic, hemodynamic, and histological changes in an animal model of brain arteriovenous malformations treated with Gamma Knife radiosurgery.* J Neurosurg, 2015: p. 1-7.
325. De Salles, A.A., et al., *Arteriovenous malformation animal model for radiosurgery: the rete mirabile.* AJNR Am J Neuroradiol, 1996. **17**(8): p. 1451-8.

326. McRobb, L.S., et al., *Ionizing radiation reduces ADAM10 expression in brain microvascular endothelial cells undergoing stress-induced senescence.* Aging (Albany NY), 2017. **9**(4): p. 1248-1268.
327. Nilsson, A., et al., *Stereotactic gamma irradiation of basilar artery in cat. Preliminary experiences.* Acta Radiol Oncol Radiat Phys Biol, 1978. **17**(2): p. 150-60.
328. Kamiryo, T., et al., *Occlusion of the anterior cerebral artery after Gamma Knife irradiation in a rat.* Acta Neurochir (Wien), 1996. **138**(8): p. 983-90; discussion 990-1.
329. Yassari, R., et al., *Angiographic, hemodynamic and histological characterization of an arteriovenous fistula in rats.* Acta Neurochir (Wien), 2004. **146**(5): p. 495-504.
330. Szeifert, G.T., O. Major, and A.A. Kemeny, *Ultrastructural changes in arteriovenous malformations after gamma knife surgery: an electron microscopic study.* J Neurosurg, 2005. **102 Suppl**: p. 289-92.
331. Hashimoto, T., et al., *Coexpression of angiogenic factors in brain arteriovenous malformations.* Neurosurgery, 2005. **56**(5): p. 1058-65; discussion 1058-65.
332. Jabbour, M.N., et al., *Aberrant angiogenic characteristics of human brain arteriovenous malformation endothelial cells.* Neurosurgery, 2009. **64**(1): p. 139-46; discussion 146-8.
333. Liu, S., et al., *Molecular responses of brain endothelial cells to radiation in a mouse model.* J Clin Neurosci, 2012. **19**(8): p. 1154-8.
334. He, J., et al., *Antiphosphatidylserine antibody combined with irradiation damages tumor blood vessels and induces tumor immunity in a rat model of glioblastoma.* Clin Cancer Res, 2009. **15**(22): p. 6871-80.
335. McRobb, L.S., et al., *Radiosurgery Alters the Endothelial Surface Proteome: Externalized Intracellular Molecules as Potential Vascular Targets in Irradiated Brain Arteriovenous Malformations.* Radiat Res, 2017. **187**(1): p. 66-78.
336. Zwaal, R.F., P. Comfurius, and E.M. Bevers, *Surface exposure of phosphatidylserine in pathological cells.* Cell Mol Life Sci, 2005. **62**(9): p. 971-88.
337. Zwaal, R.F. and E.M. Bevers, *Platelet phospholipid asymmetry and its significance in hemostasis.* Subcell Biochem, 1983. **9**: p. 299-334.
338. Zwaal, R.F. and A.J. Schroit, *Pathophysiologic implications of membrane phospholipid asymmetry in blood cells.* Blood, 1997. **89**(4): p. 1121-32.
339. Devaux, P.F. and A. Zachowski, *Maintenance and consequences of membrane phospholipid asymmetry.* Chemistry and Physics of Lipids, 1994. **73**: p. 107-120.
340. Schroit, A.J. and R.F. Zwaal, *Maintenance and consequences of membrane phospholipid asymmetry.* Biochemica et Biophysica Acta, 1991. **1071**: p. 313-329.
341. Heemskerk, J.W., E.M. Bevers, and T. Lindhout, *Platelet activation and blood coagulation.* Thromb Haemost, 2002. **88**(2): p. 186-93.
342. Ran, S. and P.E. Thorpe, *Phosphatidylserine is a marker of tumor vasculature and a potential target for cancer imaging and therapy.* International Journal of Radiation Oncology*Biology*Physics, 2002. **54**(5): p. 1479-1484.
343. Henninger, D.D., et al., *Cytokine-induced VCAM-1 and ICAM-1 expression in different organs of the mouse.* J Immunol, 1997. **158**(4): p. 1825-32.
344. Norris, P.G., et al., *Adhesion molecule expression in polymorphic light eruption.* J Invest Dermatol, 1992. **99**(4): p. 504-8.
345. Poston, R.N., et al., *Expression of intercellular adhesion molecule-1 in atherosclerotic plaques.* Am J Pathol, 1992. **140**(3): p. 665-73.
346. Molla, M., et al., *Relative roles of ICAM-1 and VCAM-1 in the pathogenesis of experimental radiation-induced intestinal inflammation.* Int J Radiat Oncol Biol Phys, 2003. **57**(1): p. 264-73.
347. Henseleit, U., et al., *Expression of murine VCAM-1 in vitro and in different models of inflammation in vivo: correlation with immigration of monocytes.* Exp Dermatol, 1994. **3**(6): p. 249-56.

348. Myers, C.L., et al., *Induction of ICAM-1 by TNF-alpha, IL-1 beta, and LPS in human endothelial cells after downregulation of PKC.* Am J Physiol, 1992. **263**(4 Pt 1): p. C767-72.
349. Panes, J., et al., *Regional differences in constitutive and induced ICAM-1 expression in vivo.* Am J Physiol, 1995. **269**(6 Pt 2): p. H1955-64.
350. Gaugler, M.H., et al., *Late and persistent up-regulation of intercellular adhesion molecule-1 (ICAM-1) expression by ionizing radiation in human endothelial cells in vitro.* Int J Radiat Biol, 1997. **72**(2): p. 201-9.
351. Gaugler, M.H., et al., *Characterization of the response of human bone marrow endothelial cells to in vitro irradiation.* Br J Haematol, 1998. **103**(4): p. 980-9.
352. Van Der Meeren, A., et al., *Differential regulation by IL-4 and IL-10 of radiation-induced IL-6 and IL-8 production and ICAM-1 expression by human endothelial cells.* Cytokine, 1999. **11**(11): p. 831-8.
353. Heckmann, M., et al., *Vascular activation of adhesion molecule mRNA and cell surface expression by ionizing radiation.* Exp Cell Res, 1998. **238**(1): p. 148-54.
354. Haubner, F., et al., *Effects of radiation on the expression of adhesion molecules and cytokines in a static model of human dermal microvascular endothelial cells.* Clin Hemorheol Microcirc, 2013. **54**(4): p. 371-9.
355. Sharp, C.D., et al., *Gamma knife irradiation increases cerebral endothelial expression of intercellular adhesion molecule 1 and E-selectin.* Neurosurgery, 2003. **53**(1): p. 154-60; discussion 160-1.
356. Hallahan, D., J. Kuchibhotla, and C. Wyble, *Cell adhesion molecules mediate radiation-induced leukocyte adhesion to the vascular endothelium.* Cancer Res, 1996. **56**(22): p. 5150-5.
357. Molla, M., et al., *Influence of dose-rate on inflammatory damage and adhesion molecule expression after abdominal radiation in the rat.* Int J Radiat Oncol Biol Phys, 1999. **45**(4): p. 1011-8.
358. Quarmby, S., R.D. Hunter, and S. Kumar, *Irradiation induced expression of CD31, ICAM-1 and VCAM-1 in human microvascular endothelial cells.* Anticancer Res, 2000. **20**(5B): p. 3375-81.
359. Howard, M., et al., *Vascular targeting of nanocarriers: perplexing aspects of the seemingly straightforward paradigm.* ACS Nano, 2014. **8**(5): p. 4100-32.
360. Ran, S., et al., *Infarction of solid Hodgkin's tumors in mice by antibody-directed targeting of tissue factor to tumor vasculature.* Cancer Res, 1998. **58**(20): p. 4646-53.
361. Muro, S. and V.R. Muzykantov, *Targeting of antioxidant and anti-thrombotic drugs to endothelial cell adhesion molecules.* Curr Pharm Des, 2005. **11**(18): p. 2383-401.
362. Howard, M.D., et al., *Nanocarriers for vascular delivery of anti-inflammatory agents.* Annu Rev Pharmacol Toxicol, 2014. **54**: p. 205-26.
363. Kalogeris, T.J., et al., *Differential monocyte adhesion and adhesion molecule expression in venous and arterial endothelial cells.* Am J Physiol, 1999. **276**(1 Pt 1): p. L9-L19.
364. Hallahan, D.E., J. Kuchibhotla, and C. Wyble, *Sialyl Lewis X mimetics attenuate E-selectin-mediated adhesion of leukocytes to irradiated human endothelial cells.* Radiat Res, 1997. **147**(1): p. 41-7.
365. Prabhakarpandian, B., et al., *Expression and functional significance of adhesion molecules on cultured endothelial cells in response to ionizing radiation.* Microcirculation, 2001. **8**(5): p. 355-64.
366. Hallahan, D.E. and S. Virudachalam, *Ionizing radiation mediates expression of cell adhesion molecules in distinct histological patterns within the lung.* Cancer Res, 1997. **57**(11): p. 2096-9.
367. Xu, M., H. Xu, and Z. Qin, *Animal Models in Studying Cerebral Arteriovenous Malformation.* Biomed Res Int, 2015. **2015**: p. 178407.
368. Spetzler, R.F., et al., *Normal perfusion pressure breakthrough theory.* Clin Neurosurg, 1978. **25**: p. 651-72.

369. Sakaki, T., et al., *Perfusion pressure breakthrough threshold of cerebral autoregulation in the chronically ischemic brain: an experimental study in cats.* J Neurosurg, 1992. **76**(3): p. 478-85.
370. Miyasaka, Y., et al., *The effects of a carotid-jugular fistula on cerebral blood flow in the cat: an experimental study in the acute period.* Surg Neurol, 1994. **41**(5): p. 396-8.
371. Tokiwa, K., et al., *The effects of a carotid-jugular fistula on cerebral blood flow in the cat: an experimental study in the chronic period.* Neurol Res, 1995. **17**(4): p. 297-300.
372. Morgan, M.K., R.E. Anderson, and T.M. Sundt, Jr., *A model of the pathophysiology of cerebral arteriovenous malformations by a carotid-jugular fistula in the rat.* Brain Res, 1989. **496**(1-2): p. 241-50.
373. Morgan, M.K., R.E. Anderson, and T.M. Sundt, Jr., *The effects of hyperventilation on cerebral blood flow in the rat with an open and closed carotid-jugular fistula.* Neurosurgery, 1989. **25**(4): p. 606-11; discussion 611-2.
374. Irikura, K., et al., *Impaired autoregulation in an experimental model of chronic cerebral hypoperfusion in rats.* Stroke, 1996. **27**(8): p. 1399-404.
375. Meyer, B., et al., *Norepinephrine in the rat cortex before and after occlusion of chronic arteriovenous fistulae: a microdialysis study in an animal model of cerebral arteriovenous malformations.* Neurosurgery, 2002. **51**(3): p. 771-9; discussion 779-80.
376. Mut, M., et al., *Effects of ionizing radiation on brain tissue surrounding arteriovenous malformations: an experimental study in a rat caroticojugular fistula model.* Neurosurg Rev, 2004. **27**(2): p. 121-7.
377. Bederson, J.B., et al., *Intracranial venous hypertension and the effects of venous outflow obstruction in a rat model of arteriovenous fistula.* Neurosurgery, 1991. **29**(3): p. 341-50.
378. Hai, J., et al., *A new rat model of chronic cerebral hypoperfusion associated with arteriovenous malformations.* J Neurosurg, 2002. **97**(5): p. 1198-202.
379. Hai, J., et al., *Chronic cerebral hypoperfusion and reperfusion injury of restoration of normal perfusion pressure contributes to the neuropathological changes in rat brain.* Brain Res Mol Brain Res, 2004. **126**(2): p. 137-45.
380. Hai, J., et al., *The pre-treatment effect on brain injury during restoration of normal perfusion pressure with hemodilution in a new rat model of chronic cerebral hypoperfusion.* Neurol Res, 2007. **29**(6): p. 583-7.
381. Scott, B.B., et al., *Vascular dynamics of an experimental cerebral arteriovenous shunt in the primate.* Surg Neurol, 1978. **10**(1): p. 34-8.
382. Numazawa, S., et al., *Experimental model of intracranial arteriovenous shunting in the acute stage.* Neurol Med Chir (Tokyo), 2005. **45**(6): p. 288-92; discussion 292-3.
383. Lee, D.H., et al., *Evaluation of three embolic agents in pig rete.* AJNR Am J Neuroradiol, 1989. **10**(4): p. 773-6.
384. Brothers, M.F., et al., *n-Butyl 2-cyanoacrylate--substitute for IBCA in interventional neuroradiology: histopathologic and polymerization time studies.* AJNR Am J Neuroradiol, 1989. **10**(4): p. 777-86.
385. Lylyk, P., et al., *Use of a new mixture for embolization of intracranial vascular malformations. Preliminary experimental experience.* Neuroradiology, 1990. **32**(4): p. 304-10.
386. Chaloupka, J.C., et al., *An in vivo arteriovenous malformation model in swine: preliminary feasibility and natural history study.* AJNR Am J Neuroradiol, 1994. **15**(5): p. 945-50.
387. Massoud, T.F., et al., *An experimental arteriovenous malformation model in swine: anatomic basis and construction technique.* AJNR Am J Neuroradiol, 1994. **15**(8): p. 1537-45.
388. Massoud, T.F., et al., *Histopathologic characteristics of a chronic arteriovenous malformation in a swine model: preliminary study.* AJNR Am J Neuroradiol, 2000. **21**(7): p. 1268-76.

389. Murayama, Y., T.F. Massoud, and F. Vinuela, *Hemodynamic changes in arterial feeders and draining veins during embolotherapy of arteriovenous malformations: an experimental study in a swine model.* Neurosurgery, 1998. **43**(1): p. 96-104; discussion 104-6.
390. Murayama, Y., et al., *Nonadhesive liquid embolic agent for cerebral arteriovenous malformations: preliminary histopathological studies in swine rete mirabile.* Neurosurgery, 1998. **43**(5): p. 1164-75.
391. Becker, T.A., et al., *In vivo assessment of calcium alginate gel for endovascular embolization of a cerebral arteriovenous malformation model using the Swine rete mirabile.* Neurosurgery, 2002. **51**(2): p. 453-8; discussion 458-9.
392. Akin, E.D., E. Perkins, and I.B. Ross, *Surgical handling characteristics of an ethylene vinyl alcohol copolymer compared with N-butyl cyanoacrylate used for embolization of vessels in an arteriovenous malformation resection model in swine.* J Neurosurg, 2003. **98**(2): p. 366-70.
393. Becker, T.A., et al., *Calcium alginate gel as a biocompatible material for endovascular arteriovenous malformation embolization: six-month results in an animal model.* Neurosurgery, 2005. **56**(4): p. 793-801; discussion 793-801.
394. Wakhloo, A.K., et al., *Acute and chronic swine rete arteriovenous malformation models: hemodynamics and vascular remodeling.* AJNR Am J Neuroradiol, 2005. **26**(7): p. 1702-6.
395. Jahan, R., et al., *An arteriovenous malformation model for stereotactic radiosurgery research.* Neurosurgery, 2007. **61**(1): p. 152-9; discussion 159.
396. Siekmann, R., et al., *Modification of a previously described arteriovenous malformation model in the swine: endovascular and combined surgical/endovascular construction and hemodynamics.* AJNR Am J Neuroradiol, 2000. **21**(9): p. 1722-5.
397. Pawlikowska, L., et al., *Polymorphisms in genes involved in inflammatory and angiogenic pathways and the risk of hemorrhagic presentation of brain arteriovenous malformations.* Stroke, 2004. **35**(10): p. 2294-300.
398. Shenkar, R., et al., *Differential gene expression in human cerebrovascular malformations.* Neurosurgery, 2003. **52**(2): p. 465-77; discussion 477-8.
399. Nikolaev, S.I., et al., *Somatic Activating KRAS Mutations in Arteriovenous Malformations of the Brain.* N Engl J Med, 2018. **378**(3): p. 250-261.
400. Morgan, M. and M. Winder, *Haemodynamics of arteriovenous malformations of the brain and consequences of resection: a review.* J Clin Neurosci, 2001. **8**(3): p. 216-24.
401. Pietila, T.A., et al., *Animal model for cerebral arteriovenous malformation.* Acta Neurochir (Wien), 2000. **142**(11): p. 1231-40.
402. Lawton, M.T., et al., *The transgenic arteriovenous fistula in the rat: an experimental model of gene therapy for brain arteriovenous malformations.* Neurosurgery, 2004. **54**(6): p. 1463-71; discussion 1471.
403. Lawton, M.T., et al., *Radiation arteriopathy in the transgenic arteriovenous fistula model.* Neurosurgery, 2008. **62**(5): p. 1129-38; discussion 138-9.
404. Konya, D., et al., *Testing the angiogenic potential of cerebrovascular malformations by use of a rat cornea model: usefulness and novel assessment of changes over time.* Neurosurgery, 2005. **56**(6): p. 1339-45; discussion 1345-6.
405. Akakin, A., et al., *Endovascular treatment increases but gamma knife radiosurgery decreases angiogenic activity of arteriovenous malformations: an in vivo experimental study using a rat cornea model.* Neurosurgery, 2010. **66**(1): p. 121-9; discussion 129-30.
406. Kim, H., et al., *Genetic considerations relevant to intracranial hemorrhage and brain arteriovenous malformations.* Acta Neurochir Suppl, 2008. **105**: p. 199-206.
407. Corti, P., et al., *Interaction between alk1 and blood flow in the development of arteriovenous malformations.* Development, 2011. **138**(8): p. 1573-82.
408. Urness, L.D., L.K. Sorensen, and D.Y. Li, *Arteriovenous malformations in mice lacking activin receptor-like kinase-1.* Nat Genet, 2000. **26**(3): p. 328-31.

409. Sorensen, L.K., et al., *Loss of distinct arterial and venous boundaries in mice lacking endoglin, a vascular-specific TGFbeta coreceptor.* Dev Biol, 2003. **261**(1): p. 235-50.
410. Bourdeau, A., D.J. Dumont, and M. Letarte, *A murine model of hereditary hemorrhagic telangiectasia.* J Clin Invest, 1999. **104**(10): p. 1343-51.
411. Oh, S.P., et al., *Activin receptor-like kinase 1 modulates transforming growth factor-beta 1 signaling in the regulation of angiogenesis.* Proc Natl Acad Sci U S A, 2000. **97**(6): p. 2626-31.
412. Srinivasan, S., et al., *A mouse model for hereditary hemorrhagic telangiectasia (HHT) type 2.* Hum Mol Genet, 2003. **12**(5): p. 473-82.
413. Xu, B., et al., *Vascular endothelial growth factor induces abnormal microvasculature in the endoglin heterozygous mouse brain.* J Cereb Blood Flow Metab, 2004. **24**(2): p. 237-44.
414. Hao, Q., et al., *Increased tissue perfusion promotes capillary dysplasia in the ALK1-deficient mouse brain following VEGF stimulation.* Am J Physiol Heart Circ Physiol, 2008. **295**(6): p. H2250-6.
415. Hao, Q., et al., *VEGF Induces More Severe Cerebrovascular Dysplasia in Endoglin than in Alk1 Mice.* Transl Stroke Res, 2010. **1**(3): p. 197-201.
416. Chen, W., W.L. Young, and H. Su, *Induction of Brain Arteriovenous Malformation in the Adult Mouse*, in *Cerebral Angiogrenesis: Methods and Protocols*, R. Milner, Editor. 2014. p. 305-316.
417. Walker, E.J., et al., *Arteriovenous malformation in the adult mouse brain resembling the human disease.* Ann Neurol, 2011. **69**(6): p. 954-62.
418. Choi, E.J., et al., *Minimal homozygous endothelial deletion of Eng with VEGF stimulation is sufficient to cause cerebrovascular dysplasia in the adult mouse.* Cerebrovasc Dis, 2012. **33**(6): p. 540-7.
419. Park, S.O., et al., *Real-time imaging of de novo arteriovenous malformation in a mouse model of hereditary hemorrhagic telangiectasia.* J Clin Invest, 2009. **119**(11): p. 3487-96.
420. Choi, E.J., et al., *Novel brain arteriovenous malformation mouse models for type 1 hereditary hemorrhagic telangiectasia.* PLoS One, 2014. **9**(2): p. e88511.
421. Park, S.O., et al., *ALK5- and TGFBR2-independent role of ALK1 in the pathogenesis of hereditary hemorrhagic telangiectasia type 2.* Blood, 2008. **111**(2): p. 633-42.
422. Chen, W., et al., *De novo cerebrovascular malformation in the adult mouse after endothelial Alk1 deletion and angiogenic stimulation.* Stroke, 2014. **45**(3): p. 900-2.
423. Mahmoud, M., et al., *Pathogenesis of arteriovenous malformations in the absence of endoglin.* Circ Res, 2010. **106**(8): p. 1425-33.
424. Milton, I., et al., *Age-dependent lethality in novel transgenic mouse models of central nervous system arteriovenous malformations.* Stroke, 2012. **43**(5): p. 1432-5.
425. Murphy, P.A., et al., *Endothelial Notch signaling is upregulated in human brain arteriovenous malformations and a mouse model of the disease.* Lab Invest, 2009. **89**(9): p. 971-82.
426. Murphy, P.A., et al., *Endothelial Notch4 signaling induces hallmarks of brain arteriovenous malformations in mice.* Proc Natl Acad Sci U S A, 2008. **105**(31): p. 10901-6.
427. Krebs, L.T., et al., *Haploinsufficient lethality and formation of arteriovenous malformations in Notch pathway mutants.* Genes Dev, 2004. **18**(20): p. 2469-73.
428. Krebs, L.T., et al., *Notch1 activation in mice causes arteriovenous malformations phenocopied by ephrinB2 and EphB4 mutants.* Genesis, 2010. **48**(3): p. 146-50.
429. Murphy, P.A., et al., *Constitutively active Notch4 receptor elicits brain arteriovenous malformations through enlargement of capillary-like vessels.* Proc Natl Acad Sci U S A, 2014. **111**(50): p. 18007-12.

430. Yao, Y., et al., *Reducing Jagged 1 and 2 levels prevents cerebral arteriovenous malformations in matrix Gla protein deficiency.* Proc Natl Acad Sci U S A, 2013. **110**(47): p. 19071-6.
431. Nielsen, C.M., et al., *Deletion of Rbpj from postnatal endothelium leads to abnormal arteriovenous shunting in mice.* Development, 2014. **141**(19): p. 3782-92.
432. Kashba, S.R., et al., *Angiographic, hemodynamic, and histological changes in an animal model of brain arteriovenous malformations treated with Gamma Knife radiosurgery.* J Neurosurg, 2015. **123**(4): p. 954-60.
433. Lendrum, A.C., et al., *Studies on the character and staining of fibrin.* J Clin Pathol, 1962. **15**: p. 401-13.
434. Bode, W., *Structure and interaction modes of thrombin.* Blood Cells Mol Dis, 2006. **36**(2): p. 122-30.
435. Davie, E.W. and J.D. Kulman, *An overview of the structure and function of thrombin.* Semin Thromb Hemost, 2006. **32 Suppl 1**: p. 3-15.
436. Coughlin, S.R., *Protease-activated receptors in hemostasis, thrombosis and vascular biology.* J Thromb Haemost, 2005. **3**(8): p. 1800-14.
437. Li, Y.T., T. Nishikawa, and Y. Kaneda, *Platelet-cytokine Complex Suppresses Tumour Growth by Exploiting Intratumoural Thrombin-dependent Platelet Aggregation.* Sci Rep, 2016. **6**: p. 25077.
438. Aleman-Garcia, M.A., R. Orbach, and I. Willner, *Ion-responsive hemin-G-quadruplexes for switchable DNAzyme and enzyme functions.* Chemistry, 2014. **20**(19): p. 5619-24.
439. Mogami, H., et al., *Effect of thrombin on human amnion mesenchymal cells, mouse fetal membranes, and preterm birth.* J Biol Chem, 2014. **289**(19): p. 13295-307.
440. Zheng, C., et al., *System-level multi-target drug discovery from natural products with applications to cardiovascular diseases.* Mol Divers, 2014. **18**(3): p. 621-35.
441. Tait, J.F., et al., *Chromosomal localization of the human gene for annexin V (placental anticoagulant protein I) to 4q26----q28.* Cytogenet Cell Genet, 1991. **57**(4): p. 187-92.
442. Tait, J.F. and D. Gibson, *Phospholipid binding of annexin V: effects of calcium and membrane phosphatidylserine content.* Arch Biochem Biophys, 1992. **298**(1): p. 187-91.
443. Eilertsen, K.E. and B. Osterud, *Tissue factor: (patho)physiology and cellular biology.* Blood Coagul Fibrinolysis, 2004. **15**(7): p. 521-38.
444. Comfurius, P., et al., *Assembly of the prothrombinase complex on lipid vesicles depends on the stereochemical configuration of the polar headgroup of phosphatidylserine.* Biochemistry, 1994. **33**(34): p. 10319-24.
445. Ravassa, S., et al., *Annexin A5 down-regulates surface expression of tissue factor: a novel mechanism of regulating the membrane receptor repertoir.* J Biol Chem, 2005. **280**(7): p. 6028-35.
446. Koopman, G., et al., *Annexin V for flow cytometric detection of phosphatidylserine expression on B cells undergoing apoptosis.* Blood, 1994. **84**(5): p. 1415-20.
447. Boersma, H.H., et al., *Past, present, and future of annexin A5: from protein discovery to clinical applications.* J Nucl Med, 2005. **46**(12): p. 2035-50.
448. Guillen, K.P., et al., *Annexin V-Directed Enzyme Prodrug Therapy Plus Docetaxel for the Targeted Treatment of Pancreatic Cancer.* Pancreas, 2015. **44**(6): p. 945-52.
449. Van Rite, B.D., et al., *Enzyme prodrug therapy designed to target L-methioninase to the tumor vasculature.* Cancer Lett, 2011. **301**(2): p. 177-84.
450. Krais, J.J., O. De Crescenzo, and R.G. Harrison, *Purine nucleoside phosphorylase targeted by annexin v to breast cancer vasculature for enzyme prodrug therapy.* PLoS One, 2013. **8**(10): p. e76403.
451. Cederholm, A. and J. Frostegard, *Annexin A5 as a novel player in prevention of atherothrombosis in SLE and in the general population.* Ann N Y Acad Sci, 2007. **1108**: p. 96-103.
452. Cederholm, A. and J. Frostegard, *Annexin A5 multitasking: a potentially novel antiatherothrombotic agent?* Drug News Perspect, 2007. **20**(5): p. 321-6.

453. Kessler, T., et al., *Inhibition of tumor growth by RGD peptide-directed delivery of truncated tissue factor to the tumor vasculature.* Clin Cancer Res, 2005. **11**(17): p. 6317-24.
454. Jahanban-Esfahlan, R., K. Seidi, and N. Zarghami, *Tumor vascular infarction: prospects and challenges.* Int J Hematol, 2017. **105**(3): p. 244-256.
455. Quick, A.J., et al., *Occult intravascular clotting by means of intravenous injection of thrombin.* Am J Physiol, 1959. **197**: p. 791-4.
456. Lee, L., *Reticuloendothelial clearance of circulating fibrin in the pathogenesis of the generalized Shwartzman reaction.* J Exp Med, 1962. **115**: p. 1065-82.
457. Siller-Matula, J.M., et al., *An experimental model to study isolated effects of thrombin in vivo.* Thromb Res, 2010. **126**(5): p. 454-61.
458. Bates, S.M. and J.I. Weitz, *Coagulation assays.* Circulation, 2005. **112**(4): p. e53-60.
459. Lee, H.B. and M.D. Blaufox, *Blood volume in the rat.* J Nucl Med, 1985. **26**(1): p. 72-6.
460. Maddox, D.A., D.C. Price, and F.C. Rector, Jr., *Effects of surgery on plasma volume and salt and water excretion in rats.* Am J Physiol, 1977. **233**(6): p. F600-6.
461. Wang, L., *Plasma volume, cell volume, total blood volume and F cells factor in the normal and splenectomized Sherman rat.* Am J Physiol, 1959. **196**(1): p. 188-92.
462. Lippman, R.W., *Blood, plasma, and drawn blood volumes in the rat.* Proc Soc Exp Biol Med, 1947. **66**(1): p. 188-91.
463. Garcia, J.F., *Changes in blood, plasma and red cell volume in the male rat, as a function of age.* Am J Physiol, 1957. **190**(1): p. 19-24.
464. Tait, J.F., C. Smith, and F.G. Blankenberg, *Structural requirements for in vivo detection of cell death with Tc-99m-annexin V.* Journal of Nuclear Medicine, 2005. **46**(5): p. 807-815.
465. Arbustini, E., et al., *Immunohistochemical characterization of coronary thrombi in allograft vascular disease.* Transplantation, 2000. **69**(6): p. 1095-101.
466. Galindo, M., et al., *Immunohistochemical detection of intravascular platelet microthrombi in patients with lupus nephritis and anti-phospholipid antibodies.* Rheumatology (Oxford), 2009. **48**(8): p. 1003-7.
467. Baker, D.G. and R.J. Krochak, *The response of the microvascular system to radiation: a review.* Cancer Invest, 1989. **7**(3): p. 287-94.
468. Hopewell, J.W., et al., *Microvasculature and radiation damage.* Recent Results Cancer Res, 1993. **130**: p. 1-16.
469. Jaenke, R.S., et al., *Capillary endothelium. Target site of renal radiation injury.* Lab Invest, 1993. **68**(4): p. 396-405.
470. Lyubimova, N. and J.W. Hopewell, *Experimental evidence to support the hypothesis that damage to vascular endothelium plays the primary role in the development of late radiation-induced CNS injury.* Br J Radiol, 2004. **77**(918): p. 488-92.
471. Rezvani, M., J.W. Hopewell, and M.E. Robbins, *Initiation of non-neoplastic late effects: the role of endothelium and connective tissue.* Stem Cells, 1995. **13 Suppl 1**: p. 248-56.
472. Wang, J., et al., *Deficiency of microvascular thrombomodulin and up-regulation of protease-activated receptor-1 in irradiated rat intestine: possible link between endothelial dysfunction and chronic radiation fibrosis.* Am J Pathol, 2002. **160**(6): p. 2063-72.
473. Fajardo, L.F., *The pathology of ionizing radiation as defined by morphologic patterns.* Acta Oncol, 2005. **44**(1): p. 13-22.
474. Pearson, J.D., *Endothelial cell function and thrombosis.* Baillieres Best Pract Res Clin Haematol, 1999. **12**(3): p. 329-41.
475. Richter, K.K., et al., *Is the loss of endothelial thrombomodulin involved in the mechanism of chronicity in late radiation enteropathy?* Radiother Oncol, 1997. **44**(1): p. 65-71.
476. van Raaij, M.E., et al., *Functional micro-ultrasound imaging of rodent cerebral hemodynamics.* Neuroimage, 2011. **58**(1): p. 100-8.

477. Bhuiyan, M.R., et al., *The effect of formal training on the clinical utility of transcranial Doppler ultrasound monitoring in patients with aneurysmal subarachnoid haemorrhage.* J Clin Neurosci, 2012. **19**(9): p. 1255-60.
478. Deb, S., et al., *The role of transcranial Doppler ultrasound monitoring in patients with aneurysmal subarachnoid haemorrhage.* J Clin Neurosci, 2012. **19**(7): p. 950-5.
479. Millon, A., et al., *Animal models of atherosclerosis and magnetic resonance imaging for monitoring plaque progression.* Vascular, 2014. **22**(3): p. 221-37.
480. Greene, L.M., M.J. Meegan, and D.M. Zisterer, *Combretastatins: more than just vascular targeting agents?* J Pharmacol Exp Ther, 2015. **355**(2): p. 212-27.
481. Nabha, S.M., et al., *Evaluation of combretastatin A-4 prodrug in a non-Hodgkin's lymphoma xenograft model: preclinical efficacy.* Anticancer Drugs, 2001. **12**(1): p. 57-63.
482. Ran, S., et al., *Antitumor effects of a monoclonal antibody that binds anionic phospholipids on the surface of tumor blood vessels in mice.* Clin Cancer Res, 2005. **11**(4): p. 1551-62.
483. Balasubramanian, K. and A.J. Schroit, *AMINOPHOSPHOLIPIDASYMMETRY: A Matter of Life and Death.* Annual Review of Physiology, 2003. **65**(1): p. 701-734.
484. Zulueta, J.J., et al., *Release of hydrogen peroxide in response to hypoxia-reoxygenation: role of an NAD(P)H oxidase-like enzyme in endothelial cell plasma membrane.* Am J Respir Cell Mol Biol, 1995. **12**(1): p. 41-9.
485. Soares, F.A., et al., *Quantification and morphologic demonstration of reactive oxygen species produced by Walker 256 tumor cells in vitro and during metastasis in vivo.* Lab Invest, 1994. **71**(4): p. 480-9.
486. Shaughnessy, S.G., et al., *Walker carcinosarcoma cells damage endothelial cells by the generation of reactive oxygen species.* Am J Pathol, 1989. **134**(4): p. 787-96.
487. Bevers, E.M. and P.L. Williamson, *Getting to the Outer Leaflet: Physiology of Phosphatidylserine Exposure at the Plasma Membrane.* Physiol Rev, 2016. **96**(2): p. 605-45.
488. Kay, J.G. and S. Grinstein, *Phosphatidylserine-Mediated Cellular Signalling*, in *Lipid-mediated Protein Signalling*, D.G.S. Capelluto, Editor. 2013, Springer: New York. p. 177-193.
489. Cheshenko, N., C. Pierce, and B.C. Herold, *Herpes simplex viruses activate phospholipid scramblase to redistribute phosphatidylserines and Akt to the outer leaflet of the plasma membrane and promote viral entry.* PLoS Pathog, 2018. **14**(1): p. e1006766.
490. Morizono, K. and I.S. Chen, *Role of phosphatidylserine receptors in enveloped virus infection.* J Virol, 2014. **88**(8): p. 4275-90.
491. Van den Eijnde, S.M., et al., *Phosphatidylserine plasma membrane asymmetry in vivo: a pancellular phenomenon which alters during apoptosis.* Cell Death Differ, 1997. **4**(4): p. 311-6.
492. Schutte, B., et al., *Annexin V binding assay as a tool to measure apoptosis in differentiated neuronal cells.* J Neurosci Methods, 1998. **86**(1): p. 63-9.
493. van Engeland, M., et al., *Annexin V-affinity assay: a review on an apoptosis detection system based on phosphatidylserine exposure.* Cytometry, 1998. **31**(1): p. 1-9.
494. Gerber, D.E., et al., *Phase I safety and pharmacokinetic study of bavituximab, a chimeric phosphatidylserine-targeting monoclonal antibody, in patients with advanced solid tumors.* Clin Cancer Res, 2011. **17**(21): p. 6888-96.
495. Shtivelband S, et al., *Randomized, blinded, placebo-controlled phase II trial of docetaxel and bavituximab as second-line therapy in locally advanced or metastatic non-squamous non-small cell lung cancer*, in *J Clin Oncol. 2013 ASCO Annual Meeting Abstracts.* 2013. p. 18.
496. Yin, Y., et al., *Phosphatidylserine-targeting antibody induces M1 macrophage polarization and promotes myeloid-derived suppressor cell differentiation.* Cancer Immunol Res, 2013. **1**(4): p. 256-68.

497. Luster, T.A., et al., *Plasma protein beta-2-glycoprotein 1 mediates interaction between the anti-tumor monoclonal antibody 3G4 and anionic phospholipids on endothelial cells.* J Biol Chem, 2006. **281**(40): p. 29863-71.
498. Kenis, H. and C. Reutelingsperger, *Targeting phosphatidylserine in anti-cancer therapy.* Curr Pharm Des, 2009. **15**(23): p. 2719-23.
499. DeRose, P., P.E. Thorpe, and D.E. Gerber, *Development of bavituximab, a vascular targeting agent with immune-modulating properties, for lung cancer treatment.* Immunotherapy, 2011. **3**(8): p. 933-44.
500. Huang, X., M. Bennett, and P.E. Thorpe, *A monoclonal antibody that binds anionic phospholipids on tumor blood vessels enhances the antitumor effect of docetaxel on human breast tumors in mice.* Cancer Res, 2005. **65**(10): p. 4408-16.
501. Li, L., A.M. Rojiani, and D.W. Siemann, *Preclinical evaluations of therapies combining the vascular targeting agent combretastatin A-4 disodium phosphate and conventional anticancer therapies in the treatment of Kaposi's sarcoma.* Acta Oncol, 2002. **41**(1): p. 91-7.
502. Siemann, D.W. and A.M. Rojiani, *Enhancement of radiation therapy by the novel vascular targeting agent ZD6126.* Int J Radiat Oncol Biol Phys, 2002. **53**(1): p. 164-71.
503. Murata, R., et al., *Improved tumor response by combining radiation and the vascular-damaging drug 5,6-dimethylxanthenone-4-acetic acid.* Radiat Res, 2001. **156**(5 Pt 1): p. 503-9.
504. Wilson, W.R., et al., *Enhancement of tumor radiation response by the antivascular agent 5,6-dimethylxanthenone-4-acetic acid.* Int J Radiat Oncol Biol Phys, 1998. **42**(4): p. 905-8.
505. Zhang, L., et al., *Phosphatidylserine-targeted bimodal liposomal nanoparticles for in vivo imaging of breast cancer in mice.* J Control Release, 2014. **183**: p. 114-23.
506. Hanshaw, R.G., et al., *Fluorescent detection of apoptotic cells by using zinc coordination complexes with a selective affinity for membrane surfaces enriched with phosphatidylserine.* Chembiochem, 2005. **6**(12): p. 2214-20.
507. Bowen, M.A., et al., *Cloning, mapping, and characterization of activated leukocyte-cell adhesion molecule (ALCAM), a CD6 ligand.* J Exp Med, 1995. **181**(6): p. 2213-20.
508. Swart, G.W., *Activated leukocyte cell adhesion molecule (CD166/ALCAM): developmental and mechanistic aspects of cell clustering and cell migration.* Eur J Cell Biol, 2002. **81**(6): p. 313-21.
509. Bruder, S.P., et al., *Mesenchymal stem cell surface antigen SB-10 corresponds to activated leukocyte cell adhesion molecule and is involved in osteogenic differentiation.* J Bone Miner Res, 1998. **13**(4): p. 655-63.
510. Patel, D.D., et al., *Identification and characterization of a 100-kD ligand for CD6 on human thymic epithelial cells.* J Exp Med, 1995. **181**(4): p. 1563-8.
511. Uchida, N., et al., *The characterization, molecular cloning, and expression of a novel hematopoietic cell antigen from CD34+ human bone marrow cells.* Blood, 1997. **89**(8): p. 2706-16.
512. Stephen, J.P., et al., *Distribution and function of the adhesion molecule BEN during rat development.* Dev Biol, 1999. **212**: p. 264-277.
513. Konno, A., et al., *Tissue distribution of CD6 and CD6 ligand in cattle: expression of the CD6 ligand (CD166) in the autonomic nervous system of cattle and the human.* J Leukoc Biol, 2001. **69**(6): p. 944-50.
514. Sasaki, M., et al., *Increased expression of mitochondrial proteins associated with autophagy in biliary epithelial lesions in primary biliary cirrhosis.* Liver Int, 2013. **33**(2): p. 312-20.
515. Joplin, R., et al., *Membrane dihydrolipoamide acetyltransferase (E2) on human biliary epithelial cells in primary biliary cirrhosis.* Lancet, 1992. **339**(8785): p. 93-4.

516. Sasaki, M., et al., *Infiltration of inflammatory cells expressing mitochondrial proteins around bile ducts and in biliary epithelial layer may be involved in the pathogenesis in primary biliary cirrhosis.* J Clin Pathol, 2014. **67**(6): p. 470-6.
517. Ohba, K., et al., *Primary biliary cirrhosis among atomic bomb survivors in Nagasaki, Japan.* J Clin Epidemiol, 2001. **54**(8): p. 845-50.
518. Roth, A., et al., *Anti-CD166 single chain antibody-mediated intracellular delivery of liposomal drugs to prostate cancer cells.* Mol Cancer Ther, 2007. **6**(10): p. 2737-46.
519. Subramanian, S., et al., *Stable thrombus formation on irradiated microvascular endothelial cells under pulsatile flow: Pre-testing annexin V-thrombin conjugate for treatment of brain arteriovenous malformations.* Thromb Res, 2018. **167**: p. 104-112.
520. Zhao, Z., et al., *Live-cell imaging to detect phosphatidylserine externalization in brain endothelial cells exposed to ionizing radiation: implications for the treatment of brain arteriovenous malformations.* J Neurosurg, 2016. **124**(6): p. 1780-7.
521. Torne, R., A. Rodriguez-Hernandez, and M.T. Lawton, *Intraoperative arteriovenous malformation rupture: causes, management techniques, outcomes, and the effect of neurosurgeon experience.* Neurosurg Focus, 2014. **37**(3): p. E12.
522. Chen, G., et al., *Macrophage migration inhibitory factor reduces apoptosis in cerebral arteriovenous malformations.* Neurosci Lett, 2012. **508**(2): p. 84-8.
523. Reshef, A., et al., *Small-molecule biomarkers for clinical PET imaging of apoptosis.* J Nucl Med, 2010. **51**(6): p. 837-40.
524. Wolters, S.L., et al., *Cardiovascular molecular imaging of apoptosis.* Eur J Nucl Med Mol Imaging, 2007. **34 Suppl 1**: p. S86-98.
525. Hoebers, F.J., et al., *99mTc Hynic-rh-Annexin V scintigraphy for in vivo imaging of apoptosis in patients with head and neck cancer treated with chemoradiotherapy.* Eur J Nucl Med Mol Imaging, 2008. **35**(3): p. 509-18.
526. Blankenberg, F.G., *In vivo detection of apoptosis.* J Nucl Med, 2008. **49 Suppl 2**: p. 81S-95S.
527. Niu, G. and X. Chen, *Apoptosis imaging: beyond annexin V.* J Nucl Med, 2010. **51**(11): p. 1659-62.
528. Wang, F., et al., *Imaging paclitaxel (chemotherapy)-induced tumor apoptosis with 99mTc C2A, a domain of synaptotagmin I: a preliminary study.* Nucl Med Biol, 2008. **35**(3): p. 359-64.
529. Simanshu, D.K., D.V. Nissley, and F. McCormick, *RAS Proteins and Their Regulators in Human Disease.* Cell, 2017. **170**(1): p. 17-33.
530. Anglesio, M.S., et al., *Cancer-Associated Mutations in Endometriosis without Cancer.* N Engl J Med, 2017. **376**(19): p. 1835-1848.
531. Raynal, P. and H.B. Pollard, *Annexins: the problem of assessing the biological role for a gene family of multifunctional calcium- and phospholipid-binding proteins.* Biochim Biophys Acta, 1994. **1197**(1): p. 63-93.
532. Swairjo, M.A. and B.A. Seaton, *Annexin structure and membrane interactions: a molecular perspective.* Annu Rev Biophys Biomol Struct, 1994. **23**: p. 193-213.
533. van Heerde, W.L., P.G. de Groot, and C.P. Reutelingsperger, *The complexity of the phospholipid binding protein Annexin V.* Thromb Haemost, 1995. **73**(2): p. 172-9.
534. Ahn, J. and S.L. Flamm, *Hepatitis C therapy: other players in the game.* Clin Liver Dis, 2011. **15**(3): p. 641-56.
535. Gray, M.J., et al., *Phosphatidylserine-targeting antibodies augment the anti-tumorigenic activity of anti-PD-1 therapy by enhancing immune activation and downregulating pro-oncogenic factors induced by T-cell checkpoint inhibition in murine triple-negative breast cancers.* Breast Cancer Res, 2016. **18**(1): p. 50.